



# Development and Characterization of Cementitious Waste Forms for Immobilization of Granular Activated Carbon, Silver Mordenite, and HEPA Filter Media Solid Secondary Waste

**September 2020**

RM Asmussen  
SA Saslow  
J Neeway  
AL Fujii Yamagata  
A Bourchy  
T Varga  
Z Zhu

KA Rod  
CE Lonergan  
BR Johnson  
JA Silverstein  
JH Westsik, Jr.  
GL Smith

## DISCLAIMER

This report was prepared as an account of work sponsored by an agency of the United States Government. Neither the United States Government nor any agency thereof, nor Battelle Memorial Institute, nor any of their employees, makes **any warranty, express or implied, or assumes any legal liability or responsibility for the accuracy, completeness, or usefulness of any information, apparatus, product, or process disclosed, or represents that its use would not infringe privately owned rights.** Reference herein to any specific commercial product, process, or service by trade name, trademark, manufacturer, or otherwise does not necessarily constitute or imply its endorsement, recommendation, or favoring by the United States Government or any agency thereof, or Battelle Memorial Institute. The views and opinions of authors expressed herein do not necessarily state or reflect those of the United States Government or any agency thereof.

PACIFIC NORTHWEST NATIONAL LABORATORY  
*operated by*  
BATTELLE  
*for the*  
UNITED STATES DEPARTMENT OF ENERGY  
*under Contract DE-AC05-76RL01830*

Printed in the United States of America

Available to DOE and DOE contractors from the  
Office of Scientific and Technical Information,  
P.O. Box 62, Oak Ridge, TN 37831-0062;  
ph: (865) 576-8401  
fax: (865) 576-5728  
email: reports@adonis.osti.gov

Available to the public from the National Technical Information Service  
5301 Shawnee Rd., Alexandria, VA 22312  
ph: (800) 553-NTIS (6847)  
email: [orders@ntis.gov](mailto:orders@ntis.gov) <<http://www.ntis.gov/about/form.aspx>>  
Online ordering: <http://www.ntis.gov>

# **Development and Characterization of Cementitious Waste Forms for Immobilization of Granular Activated Carbon, Silver Mordenite, and HEPA Filter Media Solid Secondary Waste**

September 2020

RM Asmussen  
SA Saslow  
J Neeway  
AL Fujii Yamagata  
A Bourchy  
T Varga  
Z Zhu

KA Rod  
CE Lonergan  
BR Johnson  
JA Silverstein  
JH Westsik, Jr.  
GL Smith

Prepared for  
the U.S. Department of Energy  
under Contract DE-AC05.76RL01830

Pacific Northwest National Laboratory  
Richland, Washington 99354

## Executive Summary

At the Department of Energy's Hanford site, over 53 million gallons of chemically complex and radioactive wastes have been stored in 177 underground tanks. The Hanford Tank Waste Treatment and Immobilization Plant (WTP) is under construction and is designed to treat and immobilize these wastes. During operations of WTP, solid secondary wastes (SSWs) will be generated as a result of waste treatment, vitrification, off-gas management, and supporting process activities. SSW treatment processes and resulting disposal pathways for the final disposition form of the SSW are needed to support direct feed low activity waste (DFLAW) operations and facilitate continued operation of WTP. The SSWs produced through WTP operations are expected to include used process equipment, contaminated tools and instruments, decontamination wastes, high-efficiency particulate air (HEPA) filters, carbon absorption beds (granular activated carbon, GAC), silver mordenite (AgM) and spent ion-exchange resins. These waste streams are planned to be immobilized in a cementitious waste form and disposed of either as stabilized/blended (non-debris) or encapsulated (debris) in a cementitious waste form. Accordingly, cementitious waste forms from these streams were included in the 2017 Integrated Disposal Facility (IDF) Performance Assessment (PA). The input data used to represent these SSW forms in the 2017 IDF PA involved many assumptions and associated uncertainties. This data limitation was due to the lack of material- and site-specific data available for representative SSW materials in cementitious matrices. ***To verify the assumed values used in the IDF PA and fill this limitation in available data, Washington River Protection Solutions, LLC (WRPS), has initiated a program targeted toward gathering site specific data relevant to Hanford SSW disposal.*** The work within this report is a continuation of this ongoing program.

The objectives of this work were to supply information related to (1) the sorption/desorption behavior of key contaminants (technetium, iodide, iodate, mercury) expected to be found in Hanford SSW (GAC, AgM, HEPA) in simulated grout pore water conditions; (2) the leaching behavior of iodide from stabilized/blended GAC/AgM in oxidized and reduced grout; (3) the ability of two down-selected grout mixes to stabilize GAC/AgM upon curing; and (4) providing additional solid characterization data on candidate grout mixes to immobilize SSW. Two grout formulations were selected for this work to represent an oxidized environment (similar to Hanford grout mix 5, HGM-5) and a reduced environment (formulation similar to that used to create the Cast Stone waste form). The grout selections of a reduced and oxidized formulation for the testing in this report will inform selection of a grout formulation for GAC and AgM by showing if the presence of slag (reduced grout) improves/impedes iodine retention. As well, reduced grouts will oxidize with time. Having a comparison data set between an oxidized and reduced grout can facilitate modeling of a reduced grout that oxidizes with time. A third formulation, a mortar, known as Hanford grout mix 3 (HGM-3) containing dry sand, was also evaluated for hydraulic properties to provide a comparative case against the other two aggregate-free systems.

To meet these objectives, testing involved the sorption/desorption of Tc, iodide, iodate, and mercury to the SSW materials and the grouts (ASTM C1733-17a to determine the distribution coefficient,  $K_d$ ), evaluation of the fresh grout properties (flowability, set time, free liquids, and heat of hydration), cured grout properties (compressive strength, saturated hydraulic conductivity, and water characteristic curve), and the interaction between the GAC/AgM and grout matrix (microscopy and imaging and leach testing (EPA Method 1315)).

The major findings of this work are given below. Three summary tables, Tables ES.1, ES.2 and ES.3, present a comparison between the data present in the SSW data package using best available assumptions and the site- and system-specific results from this work.

- *GAC/AgM Stabilization*: both grout mixes were able to incorporate and suspend the GAC and AgM. The GAC showed complete adherence to the hardened matrix in both formulations. The AgM appeared to be involved in some degree of reaction during curing, and Ag was observed to migrate into the hardened grout matrix.
- *Sorption/Desorption*:
  - *Iodide*: The  $K_d$  for iodide sorption to the oxidized grout (HGM-5) was comparable to the data package (Flach et al. 2016) “best” value and previous work, while the reduced grout (Cast Stone) had a nonzero value, different from the zero  $K_d$  in the data package. For sorption to the GAC material itself, the measured  $K_d$  values were lower than the data package values, likely a result of competition from high concentration salt components in the grout pore water. Iodide  $K_d$  values for sorption to AgM were extremely high, with little desorption observed. The HEPA filter media had a nonzero  $K_d$  for iodide and an expanded testing matrix would be required to reduce the uncertainty on the small  $K_d$  values measured to be  $<10$ .
  - *Iodate*: Iodate values were not included in the SSW data package (Flach et al 2016) but were included in this work due to the lack of knowledge of iodine speciation throughout the WTP flowsheet and recent identification of the prevalence of iodate in the Hanford subsurface. Iodate  $K_d$  values were comparable to iodide in all material cases except for a larger  $K_d$  value was measured for the GAC in HGM-5 pore water.
  - *Technetium*: The  $K_d$  values for sorption of Tc to the oxidizing grout were similar to the SSW data package values (Flach et al. 2016). For the reduced grout, the measured values were lower; however, this is a result of the test method used, in which a reducing grout was added to the solution and was likely unable to reduce the Tc to its lower oxidation state. The reduced-grout data package values assume Tc is added to the waste form from the time of curing, where the Tc can be reduced directly. High Tc  $K_d$  values were measured for GAC, showing promise for GAC to be used as Tc barrier material either in a waste form or in the disposal facility, while nonzero  $K_d$  values were measured for the AgM and HEPA filter media.
  - *Mercury*: The  $K_d$  values for sorption of Hg to the oxidized grout were slightly below the minimum value used in the SSW data package (Flach et al. 2016), higher in the reduced grout system, and highest for the contact with the GAC.
- *Leaching*: The iodide observed diffusivity ( $D_{obs}$ ) values in both deionized water (DIW) and simulated Hanford vadose zone pore water (VZPW) for the neat (no SSW material included) grout mixes were comparable to the optimistic  $D_{eff}$  value for both grout and paste suggested in the SSW data package (Flach et al. 2016). For the stabilized GAC in oxidized (HGM-5) and reduced (Cast Stone) grout, the iodide observed diffusivities were below the optimistic value reported for a mobile species from a mortar in the SSW data package. The stabilized AgM grout samples in the oxidized system (HGM-5) did not produce measurable iodide in the leachates, and only maximum  $D_{obs}$  values could be reported. These  $D_{obs}$  values are more than four orders of magnitude lower than the mobile species value in the data package and diffusivity of a mobile species from neat Cast Stone. In the reduced grout, some measurable iodide was present in the leachates due to interferences present in the reduced grout. It is suggested that an oxidized grout system be used to immobilize AgM.
- *Fresh Properties*: The HGM-5 and Cast Stone grouts had similar properties to those in previous reports where down-selections to these formulations were made (Nichols et al. 2017).
- *Cured Properties*: Compressive strength values for the neat grouts were comparable to previous work (Nichols et al. 2017). Upon the introduction of GAC to the grout (up to 30 vol%) the compressive strength decreased. This was an expected result due to the 30% volume material replacement of the grout with a lower strength material (GAC). However, these samples still met projected waste acceptance criteria limits ( $> 500$  psi, Ramirez, 2008).

- *Hydraulic Properties:* The saturated hydraulic conductivity ( $K_{sat}$ ) and van Genuchten parameters of the neat grouts were similar to those suggested in the SSW data package and reported elsewhere (Flach et al. 2016). Upon addition of GAC or AgM to the grout, the  $K_{sat}$  values ranged from  $(5.7 \pm 3.9) \times 10^{-9}$  cm/s –  $(5.8 \pm 2.8) \times 10^{-10}$  cm/s for Cast Stone, HGM-5 and HGM-3. The reported hydraulic conductivity value range can be used in an updated IDF PA calculation for SSW. The origin of the high  $K_{sat}$  values measured in FY18 at 30 vol% GAC loading are still unknown and the values within this revision supersede the prior release. Recent grout simulations in the IDF have shown that orders of magnitude increase in  $K_{sat}$  only correlate to  $\approx 2\times$  increase in contaminant release, thus the  $K_{sat}$  range reported herein is unlikely to significantly influence contaminant release from SSW waste forms in the IDF (Asmussen et al. 2019). The need for a consensus method or test suite to evaluate hydraulic conductivity of nuclear waste form/barrier cementitious materials and associated precision and bias is again evident.

The data presented in this report can be used in future updates of the IDF PA related to SSW and can be used to inform grout formulation selection for SSW disposal. Significant difference between the data package values and measured values in this report were found for the  $K_{sat}$  of the GAC-containing grouts (increased porosity and channels), the  $K_d$  for the sorption of Tc to reduced grout (method), and the  $K_d$  for the sorption of iodide to GAC (ionic competition). Further work may be required to confirm the nature of these variances.

This work advances the WRPS SSW testing program and only minor additional investigations are suggested related to GAC and AgM stabilization. Future work should focus on the behavior of encapsulated HEPA filters and the release of Tc and iodine. As well, low porosity/permeable grout mixes such as ultra-high performance cement composites (UHPC) may be useful in retarding the migration of contaminants from stabilized/encapsulated systems.

**Table ES.1** – Comparison of the sorption distribution coefficients ( $K_d$ ) given in the data package (Flach et al 2016) and those measured in simulated grout porewater in this work.

Distribution Coefficient ( $K_d$ )					
		Iodide Data Package (Flach et al. 2016) (mL/g)	Iodide Sorption $K_d$ This Work (mL/g)	Technetium Data Package (Flach et al. 2016) (mL/g)	Technetium Sorption $K_d$ This Work (mL/g)
<b>Oxidized Grout</b>	HGM-5		$2.5 \pm 1.4$		$1.4 \pm 0.7$
	Nichols et al. 2018 Mix 1 <sup>a</sup>		$3.03 \pm 0.23$		$2.39 \pm 0.50$
	Flach et al. 2016 Max <sup>b</sup>	10		2	
	Best	4		0.8	
	Min	0		0	
<b>Reduced Grout</b>	Cast Stone		$2.1 \pm 0.9^*$		$1.5 \pm 2.2$
	Nichols et al. 2018 Mix 13 <sup>a</sup>		$2.33 \pm 0.10$		$2.59 \pm 0.90$
	Flach et al. 2016 Max <sup>c</sup>	0		2000	
	Best	0		1000	
	Min	0		100	
<b>GAC</b>	In HGM-5 Pore Water		$16 \pm 22$		
	In Cast Stone Pore Water		$100 \pm 60$		
	Flach et al. 2016 Max <sup>d</sup>	2000			
	Best	600			
	Min	100			
<b>HEPA Filter Media</b>	In HGM-5 Pore Water		$0.39 \pm 0.34$		$0.32 \pm 0.05$
	In Cast Stone Pore Water		$0.077 \pm 0.058$		$0.36 \pm 0.48$
	Flach et al. 2016 Max <sup>c</sup>	0.2		0	
	Best	0		0	
	Min	0		0	

\*Note: the  $K_d$  values for Tc to the neat grouts represent the sorption of Tc to the grout. In the 2017 IDF PA the  $K_d$  values used for reducing grout were selected to represent the ability of a reducing grout to sequester Tc by reducing it from its mobile oxidized form to an immobile low solubility state. In this experimental design the Tc is most likely not reduced during the test.

**Table ES.2** – Comparison of the saturated hydraulic conductivity ( $K_{sat}$ ) given in the SSW data package (Flach et al 2016) and those measured for a GAC containing system in this work.

	Data Package (Flach et al. 2016) (cm/s)	This Work, $K_{sat}$ (cm/s)
Hydraulic Conductivity (measured between 1 vol% and 30 vol% GAC)	$1.2 \times 10^{-8} - 6.3 \times 10^{-9}$	$(5.7 \pm 3.9) \times 10^{-9} - (5.8 \pm 2.8) \times 10^{-10}$

**Table ES.3** – Comparison of the effective diffusivities for mobile species given in the SSW data package (Flach et al 2016) and the observed diffusivities for iodide measured in this work in DIW. *Italicized* values represented maximum values as no measurable iodide was found in the leachates.

	<b>Effective/Observed Diffusivity (cm<sup>2</sup>/s)</b>
Optimistic Mortar Mobile Species Effective Diffusivity (Flach et al. 2016)	$6.3 \times 10^{-9}$
Suggested Mobile Species Effective Diffusivity – Cast Stone (Cantrell et al. 2016)	$5.8 \times 10^{-9}$
Neat Cast Stone (Reduced)- Iodide	$1.3 \times 10^{-11}$
Neat HGM-5 (Oxidized) - Iodide	$1.3 \times 10^{-10}$
GAC in Cast Stone (Reduced) - Iodide	$9.7 \times 10^{-10}$
GAC in HGM-5 (Oxidized) - Iodide	$1.1 \times 10^{-9}$
AgM in Cast Stone (Reduced) - Iodide	<i><math>5.0 \times 10^{-13}</math></i>
AgM in HGM-5 (Oxidized) - Iodide	<i><math>4.6 \times 10^{-13}</math></i>

# Change History, Rev.1

Revision 1 of this document includes an update of saturated hydraulic conductivity measurements of GAC containing cementitious waste form samples of different waste loadings. A third formulation was evaluated in the effort, Hanford grout mix 3, a mortar. Minor grammatical changes were made and figure/table numberings were updated. Descriptions of the main changes are provided below:

Table ES.1: was updated to include a footnote describing experimental differences of the Tc measurements versus how the  $K_d$  is handled in the IDF PA.

Section 1.1: was updated to include the additional work scope.

Section 2.2: Table 2.1 was updated to include the HGM-3 formulation.

Section 2.2.3: was added to include a description of the HGM-3 formulation.

Section 3.1: Table 3-1 was updated to include the additional formulation tested.

Section 3.3.3: was updated to include Table 3.3 of the samples made specifically for  $K_{sat}$  measurements.

Section 3.3.5.6: was added to describe ToF-SIMS measurements.

Section 4.1: Table 4.1 was updated to include the flowability of the HGM-3.

Section 4.2: Table 4.2 was updated to include the set time of the HGM-3.

Section 4.4: was updated to include the free liquids analysis of the HGM-3 and Table 4.3 was added.

Section 5.3: was updated to include a discussion of the updated hydraulic conductivity measurements and Table 5-3 was updated.

Section 5.5: was updated to include Figure 5-4, an XRD pattern of HGM-3.

Section 5.6.1: was updated to include data and images for the HGM-3 analyzed with XCT.

Section 5.6.2: was updated to include optical images of HGM-3.

Section 5.6.3: was updated with electron microscopy images of the HGM-3.

Section 8.0: was updated to include the updated observations.

## Acknowledgments

The authors are grateful to Elvie Brown, Dave Swanberg and Ridha Mabrouki at Washington River Protection Solutions, LLC, Richland, Washington, for the project funding and programmatic guidance. We also thank Charlie Bonham, Viviana Gervasio, and Mark Rhodes in the Radiological Materials group at Pacific Northwest National Laboratory for their assistance in conducting the waste form characterization testing. We also acknowledge Amanda Lawter, Nancy Avalos, Michelle Valenta Snyder, Ian Leavy, and Steven Baum in the Subsurface Science and Technology group at PNNL for their analytical and laboratory support. We thank Anil Battu and Loren Reno for XRD interpretations and XCT reconstructions. We would also like to thank Guzel Tartakovsky for calculation reviews and Kirk Cantrell, Sebastien Kerisit, Gary Smith, David MacPherson, Elvie Brown, Dan Kaplan, Pat Lee, Rodney Skeen, Ridha Mabrouki and DaBrisha Smith for their technical reviews. We would like to acknowledge Maura Zimmerschied and Susan Tackett for editing this report.

This research used resources of the Advanced Photon Source (APS), a U.S. Department of Energy (DOE) Office of Science User Facility operated for the DOE Office of Science by Argonne National Laboratory under Contract No. DE-AC02-06CH11357. The authors would like to thank Dale Brewé and the staff at APS BL 20-ID for their assistance collecting micro X-ray fluorescence data.

Pacific Northwest National Laboratory is a multi-program national laboratory operated by Battelle for the U.S. Department of Energy.

## Acronyms and Abbreviations

3D	three dimensional
AgI	silver iodide
AgM	silver mordenite
ANS	American Nuclear Society
ANSI	American National Standards Institute
ASME	American Society of Mechanical Engineers
ASTM	ASTM International (West Conshohocken, PA)
BFS	blast furnace slag
BSE	backscattered electron
CS	Cast Stone
C-S-H	calcium silicate hydrate
CST	crystalline silicotitanate
CWF	cementitious waste form
DDI	double deionized water (ASTM Type I)
DFLAW	Direct Feed Low-Activity Waste
DIW	deionized water (ASTM Type II)
$D_{obs}$	observed diffusivity
DOE	U.S. Department of Energy
EBSD	electron backscatter diffraction
EDS	energy-dispersive spectroscopy
EPA	U.S. Environmental Protection Agency
EQL	Estimated Quantitation Limit
FA	fly ash
FEG	field emission gun
FY	fiscal year
GAC	granular activated carbon
HEME	high-efficiency mist eliminators
HEPA	high-efficiency particulate air
HGM-3	Hanford Grout Mix 3
HGM-5	Hanford Grout Mix 5
HLW	high-level waste
ICP-MS	inductively coupled plasma mass spectrometry
ICP-OES	inductively coupled plasma optical emission spectroscopy
IDF	Integrated Disposal Facility
$K_d$	distribution coefficient
$K_{sat}$	saturated hydraulic conductivity

LAW	low-activity waste (Hanford)
LAWPS	Low Activity Waste Pretreatment System
LLC	Limited Liability Company
LV	low vacuum
MC	moisture content
ND	not detected
NQA	Nuclear Quality Assurance
OPC	ordinary portland cement
PA	performance assessment
PNNL	Pacific Northwest National Laboratory
QA	quality assurance
R&D	research and development
SBS	submerged bed scrubber
SDD	silicon drift detector
SE	secondary electron
SEM	scanning electron microscopy
SiC	silicon carbide
sRF	spherical resorcinol formaldehyde
SRNL	Savannah River National Laboratory
SSW	solid secondary waste
SWCS	secondary waste Cast Stone
ToF-SIMS	time of flight secondary ion mass spectroscopy
TSCR	Tank Side Cesium Removal
v/v	volume fraction
VZPW	vadose zone pore water
w/dm	free water-to-dry-mix (ratio, g/g)
WESP	wet electrostatic precipitator
WESP-SBS	wet electrostatic precipitator–submerged bed scrubber
WRPS	Washington River Protection Solutions, LLC
WTP	Hanford Tank Waste Treatment and Immobilization Plant
WWFTP	WRPS waste form testing program
XCT	X-ray computed tomography
XRD	x-ray diffraction

# Contents

Executive Summary .....	ii
Change History, Rev.1 .....	vii
Acknowledgments.....	viii
Acronyms and Abbreviations .....	ix
1.0 Introduction .....	1.7
1.1 Objectives.....	1.8
1.2 Report Organization .....	1.8
1.3 Quality Assurance .....	1.8
2.0 Material Descriptions .....	2.1
2.1 Solid Secondary Waste Types.....	2.1
2.1.1 Non-Debris Waste .....	2.2
2.1.2 Debris Wastes.....	2.4
2.2 Cementitious Waste Form Formulations.....	2.5
2.2.1 Oxidized System: Mix 1 – Fly Ash + Cement “Hanford Grout Mix 5”.....	2.6
2.2.2 Reduced System: Mix 2 – Fly Ash + Cement + Blast Furnace Slag “Cast Stone” .....	2.6
2.2.3 Mortar System: Mix 3– Fly Ash+Cement+Fine Sand “Hanford Grout Mix 3” .....	2.6
3.0 Characterization and Analysis Methods .....	3.1
3.1 Waste Form Preparation.....	3.1
3.2 Waste Form Set/Curing Properties.....	3.2
3.2.1 Grout Flow .....	3.2
3.2.2 Set Time .....	3.2
3.2.3 Heat of Hydration.....	3.3
3.2.4 Free Liquids.....	3.4
3.3 Solidified Waste Form Physical Properties.....	3.4
3.3.1 Compressive Strength Measurement.....	3.4
3.3.2 Density and Porosity .....	3.5
3.3.3 Saturated Hydraulic Conductivity .....	3.6
3.3.4 Water Characteristic Curve .....	3.7
3.3.5 Chemical and Mineralogical Composition.....	3.7
3.4 Sorption and Desorption Characteristics.....	3.10
3.4.1 Grout Pore Water and Contaminant Spike Preparation.....	3.10
3.4.2 Sorption Tests.....	3.12
3.4.3 Desorption Tests.....	3.13
3.4.4 Calculation of Sorption $K_d$ and Desorption $K_d$ Tests.....	3.14
3.5 Leaching of Solidified Waste Forms.....	3.15
3.5.1 Iodide Loading .....	3.15

3.5.2	Sample and Test Preparation.....	3.15
4.0	Cementitious Waste Form Set/Curing Properties.....	4.1
4.1	Grout Flow .....	4.1
4.2	Set Time .....	4.1
4.3	Heat of Hydration.....	4.2
4.4	Free Liquids .....	4.2
5.0	Solidified Cementitious Waste Form Properties .....	5.1
5.1	Compressive Strength .....	5.1
5.2	Density, Permeable Pore Space, and Moisture Content .....	5.1
5.3	Saturated Hydraulic Conductivity.....	5.2
5.4	Water Characteristic Curve and van Genuchten Parameters.....	5.5
5.5	Mineralogy .....	5.6
5.6	X-Ray Imaging and Microscopy .....	5.8
5.6.1	X-ray Computed Tomography .....	5.8
5.6.2	Optical Microscopy .....	5.11
5.6.3	SEM/EDS.....	5.13
5.6.4	Microprobe X-ray Fluorescence ( $\mu$ XRF) Mapping.....	5.31
6.0	Technetium, Iodine, and Mercury Sorption and Desorption Behavior.....	6.1
6.1	Sorption/Desorption Characteristics of Secondary Waste Materials .....	6.2
6.1.1	Tests to Determine Equilibrium Time.....	6.2
6.1.2	Sorption and Desorption $K_d$ Values.....	6.2
6.1.3	GAC .....	6.2
6.1.4	Silver Mordenite.....	6.6
6.1.5	HEPA Filter Media.....	6.7
6.2	Sorption/Desorption Characteristics of Neat Grouts.....	6.7
6.3	$K_d$ Summary and Discussion .....	6.8
7.0	EPA Method 1315 Leach Testing of Stabilized GAC and Ag-Mordenite .....	7.1
7.1	Iodide Loading .....	7.1
7.2	EPA Method 1315.....	7.1
7.3	Leach Testing Discussion and Summary .....	7.4
8.0	Summary.....	8.1
9.0	References .....	9.1
	Appendix A – Scanning Electron Micrographs of GAC and AgM Materials .....	A.1
	Appendix B – Initial $K_d$ Tests .....	B.1
	Appendix C – Sorption $K_d$ .....	C.1
	Appendix D – Desorption $K_d$ .....	D.1
	Appendix E – EPA 1315 Leach Test Data.....	E.1

# Figures

Figure 2-1. Schematic Showing a Representation of Cementitious Waste Forms to be Used for SSW .....	2.2
Figure 2-2. Kombisorb BAT 37 Composed of the Inert Material (chunks) and Activated Carbon (cylinder).....	2.3
Figure 2-3. AgM Spheres Used in this Work.....	2.4
Figure 2-4. HEPA Filter Material Used in this Work.....	2.5
Figure 3-1. Vicat Needle Apparatus Showing Complete Penetration of the 1-mm Diameter Needle Such That the Rod Has Made an Indentation in the Specimen Surface in Previously Tested Areas .....	3.3
Figure 3-2. MTS Model 312.31 Servohydraulic Frame with a 55 kip Actuator and Load Cell Used for Compressive Strength Measurements.....	3.5
Figure 4-1. Isothermal Calorimetry Data Shown as Heat Flow Versus Time for Sand (black), HGM-5 (red), and Cast Stone (blue) at 30 °C .....	4.2
Figure 4-2. Residual Free Liquids Present at the Surface of HGM-5 and Cast Stone Neat Grouts Immediately After Fabrication, and After 1, 2, and 8 Days of Curing. An example HGM-3 sample containing 1vol% GAC is also shown at 2 h, 3 h and 5 days. The 8-day HGM-5 sample is not shown because the HGM-5 sample absorbed all free liquids after ~2 days. ....	4.3
Figure 5-1 - Plot of Water Characteristic Data and Model for Cast Stone and HGM-5 .....	5.6
Figure 5-2 XRD Pattern Collected for a Bulk Specimen Collected from Neat Cast Stone Monolith from Test Batch 2 .....	5.7
Figure 5-3 XRD Pattern Collected for a Bulk Specimen Collected from Neat HGM-5 Monolith from Test Batch 1 .....	5.7
Figure 5-4 XRD Pattern Collected for a Bulk Specimen Collected from Neat HGM-3.....	5.8
Figure 5-5 XCT Micrographs of the AgM and GAC in Cast Stone, HGM-5 and HGM-3 showing the distribution of these particles. ....	5.9
Figure 5-6 - Rendered 3D XCT images of Cast Stone, HGM-5 and HGM-3 formulation sub-sections containing AgM and GAC particles. Images used to calculate volume fractions of the cement and SSW components.....	5.10
Figure 5-7 - Optical images of HGM-5 a) Test Batch 1 the neat grout, b) Test Batch 3 with GAC added, c) Test Batch 5 with AgM added and d) magnified view of the image in c). The white arrow indicating a possible region of Ag.....	5.12
Figure 5-8 - Optical images of Cast Stone a) Test Batch 2 the neat grout, b) Test Batch 4 with GAC added, c) Test Batch 6 with AgM added and d) HGM-3 with AgM added .....	5.13
Figure 5-9 - Collage of SEM BSE micrographs of AgM granules (arrowed) in the Cast Stone Matrix from Test Batch 6. Successively higher magnifications of the AgM-Cast Stone interface are shown in A-C; D is a higher magnification micrograph of the Cast Stone matrix; the red arrow points to a spherical fly ash particle (imaged in both panel B and D) and the dashed arrow to a slag particle. ....	5.14
Figure 5-10 - SEM BSE (A) micrograph and elemental EDS dot map (B) showing the interface between an AgM granule and Cast Stone .....	5.15

Figure 5-11 - SEM EDS elemental maps showing the spatial distributions of Al, Si, Ca, and Ag for AgM in Cast Stone. The intensity of the color is an indication of the relative concentration. (Note: The field of view is the same as shown in Figure 5.9).....	5.15
Figure 5-12 - EDS sum spectrum of AgM in Cast Stone extracted from the EDS dot map in Figure 5.10 B .....	5.16
Figure 5-13 - SEM BSE micrograph of fly ash particles in the AgM-Cast Stone sample from test batch 6 showing the hydration progress around the fly ash.....	5.16
Figure 5-14 - Collage of SEM BSE micrographs showing the same region with AgM particles (seen in the top, bottom and right of image A) in the cured HGM-5 Matrix at A) 100×, B) 250×, C) 500× and D) 750× magnification. The AgM granules are the very large light-gray features at the edges of the micrographs. ....	5.17
Figure 5-15 - SEM BSE (A) and EDS elemental dot map (B) of an AgM granule in HGM-5 matrix.....	5.18
Figure 5-16 - SEM EDS elemental maps showing the spatial distributions of Al, Si, Ca, and Ag for AgM in HGM-5. The intensity of the color is an indication of the relative concentration. (NOTE: The field of view is the same as shown in the Figure 5.14 EDS elemental dot map. ....	5.18
Figure 5-17 - EDS sum spectrum of AgM in HGM-5 extracted from the EDS dot map in Figure 5-15. ....	5.19
Figure 5-18 - Higher magnification SEM BSE micrographs showing the interface between GAC and the Cast Stone matrix at A) 1000 ×, B) 2500 ×, C 5000 × and D) 10000× magnification. The GAC is the dark region at the bottom of the micrographs denoted with the white arrow. The red arrow denotes cracking around the unreacted particles in the paste (e.g. fly ash).....	5.20
Figure 5-19 - SEM BSE micrograph (A) of GAC in Cast Stone and (B) the associated EDS elemental dot map from the same area. The GAC particle is marked with a white arrow. ....	5.21
Figure 5-20 - EDS elemental maps showing the spatial distributions of Al, Si, Ca, and C for GAC in Cast Stone. The intensity of the color is an indication of the relative concentration. (NOTE: The field of view is the same as shown in Figure 5.18 elemental dot map. ....	5.21
Figure 5-21. EDS sum spectrum of AgM in HGM-5 extracted from the EDS dot map in Figure 5.19. ....	5.22
Figure 5-22. SEM BSE micrographs from a polished cross-section of GAC in HGM-5. Note: The black spherical shapes (yellow arrows) at the interface were pores that filled with epoxy. A large GAC particle is in the lower left of the image. ....	5.23
Figure 5-23. SEM BSE micrograph (A) of GAC in HGM-5 and the associated EDS elemental dot map from the same area (B).....	5.24
Figure 5-24. EDS sum spectrum of GAC in HGM-5 extracted from the EDS elemental map in Figure 5.22. ....	5.25
Figure 5-25. SEM EDS elemental maps showing the spatial distributions of Al, Si, Ca, and C for GAC in HGM-5. The intensity of the colors was intensified to illustrate where the elements were located in relation to each other; the intensity is NOT correlated to concentration. (Note: The field of view is the same as shown in Figure 5.22. ....	5.26
Figure 5-26 - SEM BSE micrographs of increasing magnification from a polished cross-section of GAC in HGM-3. (Note: The GAC is the black area in the upper right of the micrographs. The yellow box in the micrographs highlights the region that is magnified in the subsequent image). ....	5.27
Figure 5-27 - EDS sum spectrum of GAC in HGM-5 extracted from the EDS elemental map in Figure 5.27. ....	5.28

Figure 5-28 - SEM EDS elemental maps showing the spatial distributions of Al, Si, Ca, and C for GAC in HGM-3. The intensity of the colors was intensified to illustrate where the elements were located in relation to each other; the intensity is NOT correlated to concentration. ....	5.29
Figure 5-29 - SEM BSE micrographs of the AgM in HGM-3. (Note: The AgM is the region in the bottom left of the image.).....	5.30
Figure 5-30 - SEM EDS elemental maps showing the spatial distributions of Al, Si, Ca, and C for AgM in HGM-3. The intensity of the colors was intensified to illustrate where the elements were located in relation to each other; the intensity is NOT correlated to concentration. ....	5.30
Figure 5-31 - $\mu$ XRF maps for S, Ag, I, Si, Ca, and Al distributed within a specimen fragment taken from Cast Stone impregnated with iodine contacted AgM and leached in DIW.. Brighter areas indicate higher concentrations of the element of interest. The concentration gradient (color scale) is specific to individual elements. ....	5.31
Figure 5-32 - $\mu$ XRF maps for S, Ag, I, Si, Ca, and Al distributed within a second fragment taken from Cast Stone impregnated with iodine contacted AgM and leached in DIW.. Brighter areas indicate higher concentrations of the element of interest. The concentration gradient (color scale) is specific to individual elements. ....	5.32
Figure 5-33 – TOF-SIMS iodine images of HGM5-AgM samples after A) 90 day leaching in DIW and B) 2 year leaching in VZPW and Cast Stone-AgM samples after C) 90 day leaching in VZPW and D) 2 year leaching in DIW. Brighter regions correspond to high concentrations of iodine.....	5.33
Figure 7-1. The Iodide Observed Diffusivities for the Two Neat Mixes, HGM-5 and Cast Stone, following Leach Testing in (a) DIW and (b) VZPW .....	7.2
Figure 7-2. The Iodide Observed Diffusivities for the HGM-5 and Cast Stone Mixes Used to Stabilize AgM following Leach Testing in a) DIW and b) VZPW .....	7.3
Figure 7-3. The Iodide Observed Diffusivities for the HGM-5 and Cast Stone Mixes Used to Stabilize GAC following Leach Testing in a) DIW and b) VZPW .....	7.4

# Tables

Table 2-1 List of Down-Selected Formulations for Further SSW Testing from Previous Work .....	2.6
Table 3-1. Summary of the Test Batches Prepared in This Work .....	3.2
Table 3-2. Mixture Amounts for Preparation of HGM-5 and Cast Stone Formulations for Heat of Hydration Measurements .....	3.4
Table 3-3. Chemical Composition of the Non-Spiked Initial Pore Water Solutions .....	3.12
Table 3-4. Matrix Showing the Set of Sorption $K_d$ Tests Performed with Each Waste Material and Pore Water Solution Combination. A “+” indicates a solid:analyte combination where an initial test was also performed without replicates to determine test duration. An “x” indicates that the triplicate batch sorption $K_d$ test was performed. A “-” indicates that no tests were performed with the solid:analyte combination. Analyte concentrations are averaged and the standard deviations of the concentrations were measured from sorption tests performed without solids. ....	3.13
Table 3-5. Matrix Showing the Set of Batch Desorption $K_d$ Tests Performed with Each Waste Material and Pore Water Solution Combination. An “x” indicates that the $K_d$ test was performed in duplicate, whereas a “-” indicates that the test was not performed. ....	3.14
Table 3-6. Test Batches and Initial Iodide Concentrations ( $C_0$ ) for Leach Testing. The GAC values were adjusted to account for the nominal iodide in the GAC material. ....	3.16
Table 4-1. Grout Flowability Measurements .....	4.1
Table 4-2. Neat Grout Set Time Results using ASTM C191-13 .....	4.2
Table 4-3 – Comparison of the Free Liquids Measurements of HGM-3 and HGM-5 Containing Varying Loadings of GAC. ....	4.4
Table 5-1. Compressive Strength of Select Non-Rad Neat Specimens .....	5.1
Table 5-2. Density Measurements for Neat Grout Specimens .....	5.2
Table 5-3 – Prior FY18 neat mix $K_{sat}$ values and the average $K_{sat}$ values from FY20 determined from the average of all sample intervals measured along with the lowest and highest $K_{sat}$ measured at individual intervals. ....	5.4
Table 5-4. van Genuchten Functional Form Model Parameters and Model Fit Coefficient .....	5.6
Table 5-5. Bulk Mineralogical Composition of Neat Cast Stone and HGM-5 Formulations Determined by XRD .....	5.7
Table 5-6. Volume Fraction of AgM and GAC in CWF Specimens as Determined by XCT* .....	5.11
Table 6-1 - Sorption $K_d$ Values for the Specified Combination of Analytes and Waste Materials. ....	6.4
Table 6-2. Desorption $K_d$ Values for the Specified Combination of Analyte and Waste Materials .....	6.5
Table 6-3. Comparison of Iodine Species Sorption and Desorption Distribution Coefficients ( $K_d$ ), mL/g .....	6.10
Table 6-4. Comparison of Technetium Sorption and Desorption Distribution Coefficients ( $K_d$ ), mL/g .....	6.11
Table 6-5. Comparison of Mercury Sorption and Desorption Distribution Coefficients ( $K_d$ ), mL/g .....	6.12
Table 7-1 - Vadose Zone Pore Water Recipe Listed in Order of Addition of Each Component .....	7.2
Table 7-2. A comparison between the suggested effective diffusivity values for a mobile species from the 2017 IDF PA Data Packages for SSW and the iodine observed diffusivities from this work .....	7.6

# 1.0 Introduction

At the Department of Energy's Hanford site, over 53 million gallons of chemically complex and radioactive wastes are stored in 177 underground tanks. The Hanford Tank Waste Treatment and Immobilization Plant (WTP) is under construction and is designed to treat and immobilize these wastes. WTP comprises a high-level waste (HLW) vitrification facility, low-activity waste (LAW) vitrification facility, and supporting facilities. During operations of WTP, solid secondary waste (SSW) will be generated as a result of waste treatment, vitrification, off-gas management, and supporting process activities. The first stage of WTP operations will be direct feed LAW (DFLAW), which, at the time of this report, is scheduled to begin LAW vitrification in 2023 and continue for at least a decade.

Treatment processes for SSW and resulting disposal pathways for the final disposition form of the SSW are needed to support DFLAW operations and facilitate continued operation of the WTP. The SSW produced through WTP operations is expected to include used process equipment, contaminated tools and instruments, decontamination wastes, high-efficiency particulate air (HEPA) filters, carbon absorption beds, silver mordenite (AgM), and spent ion-exchange resins. Accordingly, waste forms from these streams were included in the 2017 Integrated Disposal Facility (IDF) Performance Assessment (PA) (Washington River Protection Solutions, 2018).

Modeling work for the 2017 IDF PA has been conducted using the parameters and data from a literature review compiled in the 2016 SSW data package (Flach et al. 2016). At the time of this data package development, no specific formulations for SSW solidification or encapsulation had been identified, and thus no direct experimental data existed for SSW form performance in the IDF. Recommendations were made for values to be used in the 2017 IDF PA for cured cementitious material properties, release of contaminants from the SSW materials, and transport of contaminants within the cured cementitious waste forms. The recognized limitations of the 2016 SSW data package became the basis for the SSW testing program initiated by Washington River Protection Solutions, LLC.

Through initial PA modeling efforts, the waste streams of primary interest were identified to be the ion-exchange resins (spherical resorcinol formaldehyde, sRF), HEPA filters, AgM, and granulated activated carbon (GAC) bed media. The results of the initial IDF PA modeling were used to prioritize the initial program testing efforts for fiscal year (FY) 2017, which covered the development and testing of SSW form grout (general grout formulation applicable to both debris and non-debris SSW) for encapsulating ion-exchange resin (Nichols et al. 2017). Thirteen mixes were tested in Phase 1 of the work, and a down-selection to three formulations was made. Also, an initial demonstration of the solidification of sRF resin was performed.

The Phase 1 work was followed by analysis of stabilized sRF resin using the three down-selected formulations (Nichols et al. 2018). The down-selected formulations include an oxidized system containing ordinary portland cement (OPC, 25 wt%) and class F fly ash (FA, 75 wt%) and two blast furnace slag (BFS) containing formulations (45 wt% and 75 wt% BFS). Initial data on the sorption of Tc and sorption/desorption of iodine (as iodide and iodate) to the neat grout mixes was also reported. In all, the results presented in Nichols et al. (2018) were either comparable to the recommendations in the data package, or showed the data package values to be conservative (i.e. the values in the data package would underestimate the retention of contaminants by the waste form after disposal).

Recently, a change in the DFLAW flowsheet has moved filtration and Cs removal from the LAW streams by the Low Activity Waste Pretreatment System (LAWPS), which would use sRF resin, to a Tank Side Cesium Removal (TSCR) process, which will use crystalline silicotitanate ion exchange material (CST) (Pease et al. 2019). As a result, the sRF resin inventory to be disposed of at the IDF will be far lower

while projected inventories of GAC, AgM and HEPA filters will remain unchanged. The CST disposition pathway has yet to be determined. This report describes the work of the SSW testing program to provide laboratory data representative of the eventual waste forms to be used for GAC, AgM, and HEPA filters.

## 1.1 Objectives

The general objectives of this work scope are to provide two types of information:

- data to support the maintenance activities of the IDF PA related to  $^{129}\text{I}$  and Hg retention on GAC and AgM, and  $^{99}\text{Tc}$  and  $^{129}\text{I}$  retention on HEPA filters; and,
- processing and formulation information for the stabilization and immobilization of SSW that will be generated during the operation of DFLAW or the full operation of WTP.

Specifically, the report will present data to measure:

- 1) The flowability, set time, free liquids and heat of hydration of the slurries for two grout mixes;
- 2) The compressive strength, hydraulic conductivity, water characteristic curves, mineralogy and microstructure of two cementitious waste forms; the microstructure and hydraulic conductivity of a third cementitious waste form, HGM-3, was also evaluated;
- 3) The sorption and desorption distribution coefficients ( $K_d$ ) of Tc, I,  $\text{IO}_3^-$  and  $\text{Hg}^+$  to GAC, AgM, HEPA filters, Cast Stone and HGM-5 in simulated grout porewaters;
- 4) The observed diffusivity of iodide from the two neat grout mixes (spiked with iodide) and the grout mixes containing AgM or GAC (with the AgM/GAC loaded with iodide).

## 1.2 Report Organization

This report is divided into multiple sections. Section 2 provides a description of the SSW materials including the GAC, AgM, and HEPA filter media; and a description of the grout compositions selected. Section 3 describes the characterization and analysis methods used in the report. Section 4 gives the results of characterization of the cementitious waste form set and curing properties including grout flow, set time, heat of hydration, and residual free water. Section 5 presents the measured solidified cementitious waste form properties, including compressive strength, density, permeable pore space, moisture content, saturated hydraulic conductivity, water characteristic curve and van Genuchten parameters, and mineralogy and microscopy. Section 6.0 describes the technetium, iodide, iodate, and mercury sorption and desorption behavior on the GAC, AgM, HEPA filter media, and the neat grouts (i.e. no SSW material included). Section 7.0 presents the results for leaching of iodine from the neat grouts and from AgM and GAC encapsulated in the two grout formulations. The summary in Section 8.0 includes conclusions and recommendations. References are provided in Section 9.0.

## 1.3 Quality Assurance

This work was funded by WRPS under contract 36436.161, *Secondary Waste Cast Stone Formulation and Waste Form Qualification*. The work was conducted as part of Pacific Northwest National Laboratory (PNNL) Project 72180, Solid Secondary Waste Form Development.

All research and development (R&D) work at PNNL was performed in accordance with PNNL's Laboratory-level Quality Management Program, which is based on a graded application of NQA-1-2000, *Quality Assurance Requirements for Nuclear Facility Applications* (ASME 2000), to R&D activities. In addition to the PNNL-wide quality assurance (QA) controls, the QA controls of the WRPS Waste Form

Testing Program (WWFTP) QA program were also implemented for the work. The WWFTP QA program consists of the WWFTP Quality Assurance Plan (QA-WWFTP-001) and associated QA-NSLW-numbered procedures that provide detailed instructions for implementing NQA-1 requirements for R&D work. The WWFTP QA program is based on the requirements of NQA-1-2008, *Quality Assurance Requirements for Nuclear Facility Applications*, and NQA-1a-2009, *Addenda to ASME NQA-1-2008 Quality Assurance Requirements for Nuclear Facility Applications*, graded on the approach presented in NQA-1-2008, Part IV, Subpart 4.2, “Guidance on Graded Application of Quality Assurance (QA) for Nuclear-Related Research and Development.”

Performance of this work and preparation of this report were assigned the technology level “Applied Research” by PNNL and were conducted in accordance with WWFTP procedure QA-NSLW-1102, *Scientific Investigation for Applied Research*. All staff members contributing to the work have technical expertise in the subject matter and received QA training before performing quality-affecting work. The “Applied Research” technology level provides adequate controls to make sure that the activities were performed correctly. Use of both the PNNL-wide and WWFTP QA controls made sure that all client QA expectations were addressed in performing the work.

## 2.0 Material Descriptions

This section provides descriptions of the solid secondary waste types including the GAC, AgM, and HEPA filter media. It also provides information on the HGM-5 and Cast Stone cementitious waste form formulations.

### 2.1 Solid Secondary Waste Types

Within the WTP, off-gas treatment systems are used to collect off-gases from the pretreatment and vitrification processes and remove radioactive and hazardous chemical species before releasing the gases to the environment. Included in the off-gas system are HEPA filters for removing particulates, activated carbon beds for removing Hg, and AgM columns for removing halides (I, Cl, and F). The spent HEPA filters, GAC, and AgM become SSW streams requiring immobilization for disposal. Each waste material is described in more detail below. In addition to the HEPA filters, GAC, and AgM, ion-exchange resins are to be included in another expected SSW form to be generated at the WTP. Nichols et al. (2018) describe work at Savannah River National Laboratory (SRNL) to develop and characterize cementitious waste forms for the immobilization of spherical resorcinol ion-exchange resins to be generated from cesium separation processes.

The SSW materials described in this report fall into two classes: non-debris waste and debris waste. Both waste streams are projected to be immobilized in a cementitious matrix prior to disposal at the IDF. Non-debris waste would be stabilized (or blended) as a loose particulate material into the cementitious matrix. Debris waste would be encapsulated in the core of a cementitious monolith. A visualization of the two immobilization approaches is shown in Figure 2-1. It should be noted that other waste form types for SSW could also be used, and a summary of these alternative approaches was recently provided (Seitz 2017).

Expected concentrations of radionuclides and contaminants on these three SSW materials has been reported previously (Brown et al. 2017). Based on these reports used in the 2017 IDF PA, the I-containing SSWs produced at WTP were primarily AgM (62%) and GAC (36%). Both waste streams are targeted for stabilization in a cementitious waste form. The suggestion for stabilized material in the 2016 SSW data package (Flach et al. 2016) was to assume behavior similar to a mortar (cement paste with a large aggregate). The HEPA filter inventory is the most risk-significant source term for <sup>99</sup>Tc in the 2017 IDF PA, with a disposal configuration as a compacted inventory of HEPA filters encapsulated in a cementitious waste form. As stated in Section 1.0, the values representing these waste streams has uncertainty built into the recommendations used for the 2017 IDF PA.

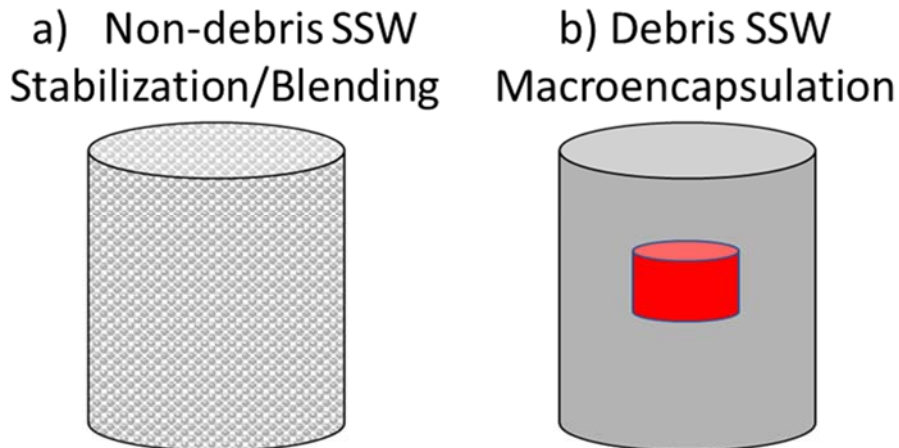


**Figure 2-1.** Schematic Showing a Representation of Cementitious Waste Forms to be Used for SSW, Showing (a) Stabilization/Blending for Non-Debris Waste and (b) Macro-Encapsulation for Debris Waste

## 2.1.1 Non-Debris Waste

### 2.1.1.1 Granular Activated Carbon

The carbon adsorber beds (containing GAC) are the first component of the secondary off-gas treatment system immediately following the HEPA filters; they come before the AgM columns in the HLW vitrification facility and before the catalytic oxidizer/reducer skid within the LAW vitrification facility. Carbon bed adsorbers are also included in the WTP pretreatment facility flowsheet. Their primary function is to remove elemental Hg vapors from the off-gas by sorption onto sulfur-impregnated GAC. The activated carbon beds may also remove halides (including iodine) and certain volatile organic compounds. GAC is a material with a very high specific surface area (600–1,500 m<sup>2</sup>/g) that is effective in removing contaminants from gaseous and liquid streams. The specific GAC formulation may be impregnated with other chemical species besides carbon to remove other chemicals that could poison downstream catalysts. Specific additives and compositions are often proprietary.

Following ~ 24 months in service the GAC material within the activated carbon adsorber beds will be removed by gravity flow from the bed into collection containers for handling and transport to the solids handling facility for immobilization. It is anticipated that the GAC material will be stabilized by blending into the grout mix, which is placed in containers to solidify and cure before disposal.

For the testing at PNNL, Donau Carbon U.S. provided ~1 kg of their Kombisorb<sup>®</sup> BAT 37 activated carbon. Kombisorb BAT 37, has a particle size of 3 to 5 mm and is composed of 70 vol% activated carbon cylinders and 30 vol% granular inert material, has been identified as the material to be used in the carbon adsorber bed (Taylor 2010). The BAT 37 is shown in Figure 2-2. At the end of its service life, the carbon absorbed bed material will contain appreciable amounts of Hg and radioiodine that need to be managed for disposal.



**Figure 2-2.** Kombisorb BAT 37 Composed of the Inert Material (chunks) and Activated Carbon (cylinder)

### 2.1.1.2 Silver Mordenite

Silver zeolites has long been investigated and used for the capture of radioiodine in reprocessing and vitrification off-gas management systems (Scheele et al. 2002). Silver mordenite (AgM) columns are to be used in the WTP HLW vitrification facility as part of the secondary off-gas treatment system. The AgM cartridges are downstream of the activated carbon beds and upstream of the selective catalytic oxidizer and reducer, with a primary function to remove radioiodine from the off-gas. The final product upon iodine capture is AgI. Other halides, including chlorine, fluorine, and nonradioactive iodine isotopes, may be captured as well. The planned AgM is in the form of small 1/16.inch (0.158 cm) spherical particles that are loaded into cylindrical 316L stainless steel cartridges. The cartridges would be placed in the airflow stream in a manner that the gases flow through the cartridges, thereby contacting the AgM. The spent AgM would be replaced by removing the cartridges and replacing them with cartridges containing fresh AgM. The AgM would then be removed by gravity and placed in collection containers. It is anticipated that the spent AgM will be blended into the grout mix, which is placed in containers to solidify and cure before disposal. Previous work has investigated the use of grout for the disposal of AgM at Hanford (Scheele et al. 2002). Other research efforts are ongoing under separate DOE programs to develop waste forms for spent iodine-loaded materials, including hot isostatic pressing of AgM (Jubin et al. 2017). In this work, AgM spherical pellets (0.8 mm, 20 mesh) from Sigma Aldrich<sup>®</sup> were used; an image of the particles is shown in Figure 2-3.

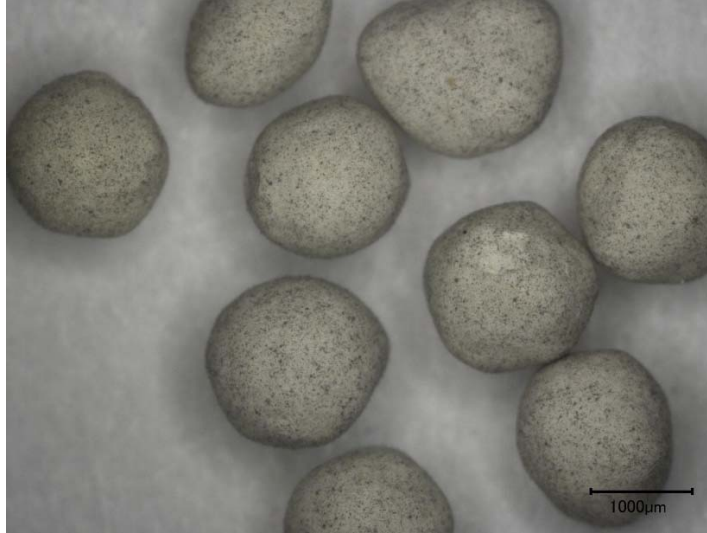


**Figure 2-3.** AgM Spheres Used in this Work. The Black Flecks are Areas of Reduced Ag.

## **2.1.2 Debris Wastes**

### **2.1.2.1 High Efficiency Particulate Air Filters**

HEPA filters are the final component of the primary off-gas treatment systems in the HLW and LAW vitrification facilities and are used to remove particulates and aerosols from the melter off-gas and vessel vent systems. They follow the submerged bed scrubber (SBS), wet electrostatic precipitator (WESP), and high-efficiency mist eliminators (HEMEs), and precede the activated carbon beds within the secondary off-gas treatment system. HEPA filters will also be used at other locations throughout WTP. The HEPA filters are composed of a borosilicate glass filter medium supported within a 316L stainless steel housing. At the end of service life, spent HEPA filters would be removed from the off-gas treatment line, packaged in 55-gallon drums to contain the contamination, and transferred to the solid-waste processing facility. Within the solid-waste processing facility, the HEPA filters will be compacted into pucks (volume reduction between 5× and 10×). The pucks will be consolidated and will then be placed in larger containers and encapsulated in a grout for disposal. The HEPA filter material used in this work was a borosilicate nuclear grade HEPA filter (cylinder) received from Parker Hanafin. The HEPA filter medium was size reduced prior to use; an image is shown in Figure 2-4.

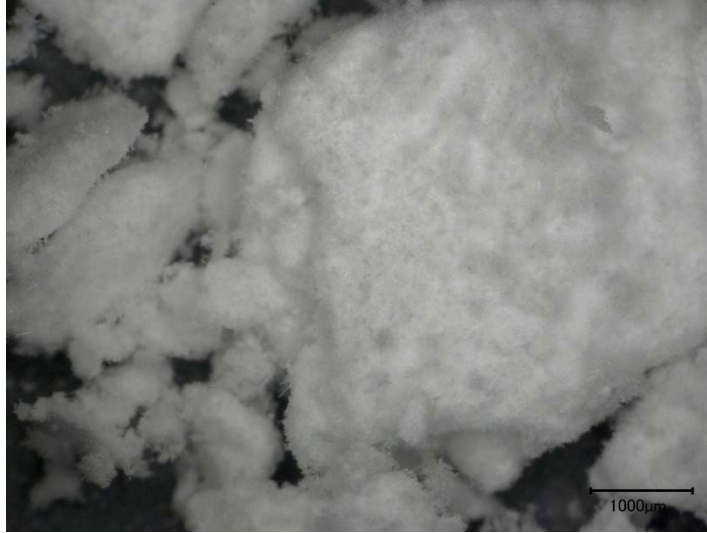


**Figure 2-4.** HEPA Filter Material Used in this Work

## **2.2 Cementitious Waste Form Formulations**

Based on initial work performed at SRNL (Nichols et al. 2017), a down-selection was made to grout formulations meeting the requirements needed to solidify SSW. Two formulations, Mix 1 (referred to in this report as Hanford Grout Mix 5, HGM-5) and Mix 2 (referred to in this report as Cast Stone) were used in the present testing, and are listed in Table 2-1. These formulations were selected to compare an oxidized system (HGM-5, Mix 1), which is used in burial applications at the Hanford site, to a formulation with reducing capacity (Cast Stone, Mix 2). A third formulation, Mix 3 (referred to as Hanford Grout Mix 3, HGM-3) was tested in FY20 for saturated hydraulic conductivity to represent a mortar. The formulation is similar to Mix 12 of Nichols et al. (2017) with the only difference being the sand used in this work was fully dried whereas the sand used in the previous work had an unknown moisture content. This difference will allow for comparisons in performance to be made relative to excess water introduced from wet sand.

**Table 2-1** List of Down-Selected Formulations for Further SSW Testing from Previous Work (Nichols et al. 2017).

Mix	H <sub>2</sub> O:CM <sup>a</sup> (w/w) <sup>c</sup>	FA/OPC/BFS <sup>b</sup> (w/w/w) <sup>c</sup>	Max. Waste Loading (v/v) <sup>d</sup>	Comment
1	0.29	75/25/0	0.30	American Rock Products 4257020 Grout also known as Hanford Grout Mix 5 used in burial ground, Oxidized System.
2	0.45	45/8/47	0.30	Similar composition to previously tested Cast Stone waste forms for liquid wastes. A ratio of 45/45/10 was used in Nichols et al. 2017. Reduced System.
3	0.42	14/14/72	0.30	American Rock Products 4100023 Grout also known as Hanford Grout Mix 3 a mortar. Mix 12 in Nichols et al. 2017 and Table 6-1, Flach et al. 2016

<sup>a</sup>CM = cementitious mix

<sup>b</sup>FA = class F fly ash, OPC = ordinary portland cement, BFS = blast furnace slag

<sup>c</sup>w/w and w/w/w refer to weight ratios

<sup>d</sup>v/v refers to volume ratios

### 2.2.1 Oxidized System: Mix 1 – Fly Ash + Cement “Hanford Grout Mix 5”

Two formulations were used in this testing and are listed in Table 2-1. Mix 1 (75 wt% class F FA and 25 wt% OPC) is similar to Mix 5 used on site at the Hanford burial ground, and from here on will be referred to as HGM-5. This formulation was named “Mix 1” in previous SSW-development reports and was made with a target water-to-dry-mix (w:dm) ratio of 0.29 (Nichols et al. 2017). Due to the clumping observed in previous work, polypropylene fibers were not added to the mix.

### 2.2.2 Reduced System: Mix 2 – Fly Ash + Cement + Blast Furnace Slag “Cast Stone”

Mix 2 (45 wt% class F fly ash, 8 wt% OPC, and 47 wt% BFS) is a formulation identical to that used to make “Cast Stone” waste forms in Hanford-focused testing and will be referred to as Cast Stone from here on. This mix is close in composition to “Mix 13” in previous SSW development work. The minor composition change was done to be consistent with previous Hanford related grout development work at PNNL. A w:dm ratio of 0.45 was used. A recent report on SSW development (Nichols et al. 2018) suggested that initial data showed that a w:dm ratio of 0.45 yielded a mix that was too wet; however, that report was not available at the time of planning and the 0.45 ratio was used in this work.

A mix with BFS was included because of BFS’s ability to reduce porosity of the cured grout. The BFS content of Cast Stone is at an intermediate level (47 wt%) compared to the third down-selected mix (Mix 5 in Nichols et al. 2017), which had 75 wt% BFS. The intermediate content was selected because any interference observed at 47 wt% BFS may be enhanced at 75 wt% and may be difficult to discern if a midrange slag content would alleviate the interference.

### 2.2.3 Mortar System: Mix 3– Fly Ash+Cement+Fine Sand “Hanford Grout Mix 3”

Hanford Grout Mix 3 (HGM3) was also included for hydraulic conductivity measurements. HGM3 was selected to provide data on a mortar formulation (containing fine aggregate) relevant to disposal at

Hanford. It is also known commercially as American Rock Products 4100023 Grout and is also suited for waste encapsulation (Flach et al. 2016, Nichols et al. 2017). The sand used in the most recent report, Nichols et al. 2017, was moist to an unknown degree and influenced the flowability, porosity and hydraulic conductivity of the mix, The sand used in this effort was fully dried as is common practice. This work presents a valuable data point on the influence of dry sand on HGM-3 properties to compare with the moist sand reported previously.

## 3.0 Characterization and Analysis Methods

This section describes how the solidified SSW waste forms were prepared, methods for characterizing the waste form setting and curing properties, the solidified waste form physical properties, and the methods for measuring the sorption and leaching characteristics of the waste materials and cementitious waste forms.

### 3.1 Waste Form Preparation

The monolith samples were prepared following the previously reported procedure for cementitious sample fabrication used in the WRPS testing programs (Asmussen et al. 2016a, Saslow et al. 2018, Westsik et al. 2013). All slurries were mixed for 15 minutes following the start of addition of the dry mix. The dry mix addition was completed within 5 minutes. The samples were cured in 2" inner diameter (ID) × 4" long or 2" ID × 5" long plastic forms with a perforated cap at >95% relative humidity for 28 days before analysis and testing. The following variations to the method were used for specific samples.

- For samples containing GAC/AgM – the GAC/AgM particles were added to the deionized water (DIW, conforming to ASTM Type II standards, ASTM D1193-06(2018)), while being stirred, immediately prior to addition of the dry mix. The addition approach was selected to be consistent with the fabrication of stabilized sRF resin used previously (Nichols et al. 2017). The amount of mix water was adjusted to account for the water taken up by the GAC/AgM.
- For fresh property evaluation – upon completion of the mixing time, the slurry was transferred to a separate mold for the slump test, set time, or free-liquids evaluation.
- For samples to be used in EPA Method 1315 testing – the GAC/AgM (Test Batches 3–6) were loaded with iodide prior to waste form fabrication through aqueous batch contact. The neat mixes (Test Batches 1 and 2) were made with iodide-spiked water. The loading of the iodide is discussed in Section 3.5.1.
- In all, thirteen test batches were prepared; they are listed in Table 3-1.

**Table 3-1.** Summary of the Test Batches Prepared in This Work

Test Batch	Mix	Added Material and Target Amount	Loading of GAC/AgM
1	HGM-5	N/A	Iodide solution spike for leach test samples
2	Cast Stone	N/A	Iodide solution spike for leach test samples
3	HGM-5	GAC – 30 vol%	Iodide, a sample from this batch was measured for $K_{sat}$ after ~3 years of leaching.
4	Cast Stone	GAC – 30 vol%	Iodide
5	HGM-5	AgM – 30 vol%	Iodide
6	Cast Stone	AgM – 30 vol%	Iodide
7	HGM-5	GAC – 30 vol%	N/A
8	Cast Stone	GAC – 30 vol%	N/A
9	HGM-3	N/A	N/A
10	HGM-3	GAC – 1 vol% - 30 vol%	For $K_{sat}$
11	HGM-5	GAC – 1 vol% - 30 vol%	For $K_{sat}$
12	HGM-3	AgM – 10%	For $K_{sat}$
13	HGM-5	AgM – 10%	For $K_{sat}$

## 3.2 Waste Form Set/Curing Properties

The freshly prepared wet paste of waste form specimens was characterized for properties relevant to the mixing, pouring, flow, and free liquid content during the initial curing stage. This work was performed to assure consistency with previous tests of the neat grout mixes.

### 3.2.1 Grout Flow

Select waste form specimens were measured for grout flow using modified ASTM D6103-17, *Standard Test Method for Flow Consistency of Controlled Low Strength Material*, with modifications given in Harbour et al. (2005). The slurry was transferred to an open-ended cylinder (83 cm height and 48 cm inner diameter, ~150 cm<sup>3</sup>, consistent for each measurement) on a steel plate and leveled at the top. The cylinder was removed, and the grout flowed into a pancake-like shape. At 1 min and 3 min following removal of the cylinder, the diameter and height of the pancake were measured.

### 3.2.2 Set Time

Set time was measured on the two neat mixes (Test Batch 1 and 2) according to the procedure outlined in ASTM C191-13, *Standard Test Methods for Time of Setting of Hydraulic Cement by Vicat Needle*, to provide an indication of cure progression at a given point in time and confirm consistency with previous work. This method can also be used to determine the time required between pours to prevent excessive hydraulic head on the vault walls and to provide a calculated estimate on material at risk for deflagration (Westsik et al. 2013).

After the specimens used for grout flowability tests in Section 3.2.1 were collected, each was used to evaluate waste form set time according to the procedure outlined in ASTM C191-13. Each grout slurry specimen was poured into an ~8-cm diameter × 6-cm tall cup until the cup was full. Any excess material was wiped from the surface so that the grout was level with the top of the sample holder, and then the specimen was weighed. Care was taken during this process not to compress the specimen. Once prepared, the specimen was placed under the Vicat needle apparatus (shown in Figure 3-1) to determine the penetration of the 1-mm diameter needle into the grout material and, ultimately, the waste form set time.

Set time measurements were collected at 1-hour intervals during normal working hours. To perform a measurement, the 1-mm needle was lowered until it rested on the surface of the material. The apparatus set screw was then tightened and the indicator at the top of the scale was set to zero. The rod holding the needle was then released by loosening the set screw, and the needle was allowed to settle for 30 seconds before the penetration depth, date, and measurement time were recorded. For each penetration measurement, the needle was positioned at least 5 mm away from any previous measurement and at least 10 mm from the edge of the sample ring. Measurements continued at 1-hour intervals until the needle rod no longer left a cylindrical mark on the sample surface. If the grout material was slow to set, the measurement intervals were allowed to increase above 1-hour. Samples were capped with a lid between measurements to maintain humid conditions and prevent water loss via evaporation.



**Figure 3-1.** Vicat Needle Apparatus Showing Complete Penetration of the 1-mm Diameter Needle Such That the Rod Has Made an Indentation in the Specimen Surface in Previously Tested Areas. The sample shown is not associated with the samples discussed in this report.

### 3.2.3 Heat of Hydration

The heat of hydration for select monoliths was measured using isothermal calorimetry as outlined in standard procedure ASTM C1679-17, *Standard Practice for Measuring Hydration Kinetics of Hydraulic Cementitious Mixtures Using Isothermal Calorimetry* modified for a 7-day measurement.

Heat of hydration was measured on grout mixtures using a TAM Air three-channel calorimeter by TA Instruments, Inc. Both neat mixes (Test Batches 1 and 2) were evaluated.

Samples were prepared using the method described in Section 3.1. After mixing, the slurries were transferred to 125-mL glass ampoules. The ampoules were sealed and placed into the calorimeter within 5 minutes of the completion of mixing. To provide stability of the system, the samples were equilibrated for 45 minutes after adding the ampoules. Sample references were empty glass ampoules placed in the calorimeter at the same time as the samples of interest. A third ampoule of sand (Lane Mountain Sand Co., #125) was also analyzed as a control.

**Table 3-2.** Mixture Amounts for Preparation of HGM-5 and Cast Stone Formulations for Heat of Hydration Measurements

Test Batch	Mass of Slurry Poured into Glass Ampoule for Testing (g)
<b>Neat-HGM-5</b>	193.7
<b>Neat-Cast Stone</b>	197.4
<b>Sand (dry)</b>	164.4

### 3.2.4 Free Liquids

This section describes observations made while monitoring individual waste forms for residual free liquids over the 28-day curing period. Per *Hanford Site Solid Waste Acceptance Criteria* (Ramirez 2008), free liquids must not exceed 1% of the total waste volume for a waste form to qualify for on-site disposal.

One half-filled specimen from the two neat grout mixes (Test Batches 1 and 2) were monitored for the presence of free liquids during the 28-day cure period, following the American Nuclear Society (ANS) method ANS/ANSI 55.1. Observations were made every day for the first 7 days after production of monolith specimens, and at least twice a week until the 28-day cure period was reached or until no free liquids remained. Visual inspection identified free liquids from curing waste form specimens. Visual observations of a few drops of liquid or less on the surface are considered less than 1% of the total waste volume.

## 3.3 Solidified Waste Form Physical Properties

After curing, select waste form specimens were characterized with respect to chemical and mineralogical composition, compressive strength, porosity, density, hydraulic conductivity, and water characteristic curve.

### 3.3.1 Compressive Strength Measurement

Compressive strengths were measured for select waste form specimens after the 28-day curing period. Prepared cylinders were subjected to the ASTM C39-18 *Standard Test Method for Compressive Strength of Cylindrical Concrete Specimens*.

After curing for at least 28 days, specimens (Test Batches 1, 2, 7 and 8, see Table 3-1) were selected for compressive strength analysis according to ASTM C39/C39M-18. Selected monoliths were cured in 2"

ID × 5" long (5 cm × 12.7 cm) plastic forms because the 4" (10.16 cm) long forms do not meet the desired specimen length for analysis. Once cured, the monoliths' flat ends were cut with a saw, while using a miter gauge to keep the sample ends parallel. The final length of the specimen was no less than 4" (10.16 cm) and was achieved for all specimens. The reported specimen length and diameter in Table 5-1 are the averages of three measurements: the diameter of the specimen was measured at the bottom, middle, and top of the monolith, and the specimen length was measured at three rotational orientations mutually separated by ~120 degrees from an arbitrary starting location using a caliper.

Once each specimen was cut and measured, it was loaded into the testing apparatus (MTS model 312.31 servohydraulic frame with a 55 kip actuator and load cell, Figure 3-2). An adapter, adequate to stabilize a 2" ID object, was placed on each end of the monolith specimen, which was then situated between the two compression platens so that the monolith axis was aligned with the center of thrust. The compression platens were then adjusted so that each was in contact with the adapters, securing the monolith specimen, but without applying a compressive load. The load indicator was set to zero, and then a load was applied to the specimen without shock at a stress rate of  $0.25 \pm 0.05$  MPa/s ( $36 \pm 7$  psi/s). Sample loading continued until specimen failure, e.g., a well-defined fracture in the monolith specimen. This maximum compressive load was recorded and then used to calculate the compressive strength of the monolith specimen. The results of this analysis are summarized in Table 5-1.

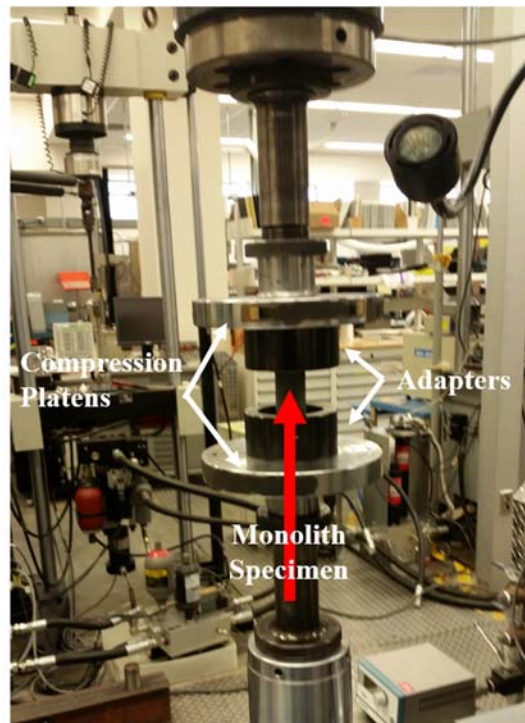


**Figure 3-2.** MTS Model 312.31 Servohydraulic Frame with a 55 kip Actuator and Load Cell Used for Compressive Strength Measurements

### 3.3.2 Density and Porosity

One specimen from Test Batches 1 and 2 (HGM-5 and Cast Stone) was measured for cured density and permeable pore space according to the procedure outlined in ASTM C642-13, *Standard Test Method for Density, Absorption, and Voids in Hardened Concrete*. The specimen size was a 2" diameter × ~2" height right circular cylinder. To summarize this procedure, each monolith specimen was first weighed in a

moisture tin, then dried in an oven set to  $110^{\circ}\text{C} \pm 10^{\circ}\text{C}$  for at least 24 hours. After 24 hours, the specimen was removed from the oven and allowed to cool briefly before the dry specimen mass was recorded. The specimen was then returned to the oven and this drying procedure repeated until the difference in successive dry mass values was less than 0.5% of the smallest mass value. The final sample mass was recorded as the “Mass of Oven-Dried Sample in Air” (Table 5-2). The moisture content of each partial monolith was then determined by the difference in mass between those of the monolith sample before and after drying at  $110 \pm 10^{\circ}\text{C}$  using Equation 3.1:

$$\text{MC (\%)} = [(M_{\text{wet}} - M_{\text{dry}})/M_{\text{wet}}] \times 100 \quad (3.1)$$

where

- MC = moisture content
- $M_{\text{wet}}$  = initial wet mass of monolith (g);
- $M_{\text{dry}}$  = next-to-last dry mass of monolith after drying (g).

After oven drying, specimens were immersed in approximately  $21^{\circ}\text{C}$  DIW for at least 48 h and then removed, blotted with a towel to remove excess water, and weighed. Specimen immersion and weighing were repeated for an immersion period of at least 24 h and deemed complete when the difference in successive mass measurements was less than 0.5% of the smallest value. The final mass of the specimen was recorded as “Mass of Surface-Dry Sample in Air After Immersion.”

Finally, each specimen was submerged in boiling DIW for 5 h before being removed and allowed to cool to room temperature by natural loss of heat for no less than 14 h. The specimen was surface dried by blotting the surface with an absorbent towel to remove excess liquid, and the mass was recorded as “Mass of Surface-Dry Sample in Air After Immersion and Boiling.” These measurements, along with the specimen volume (calculated from average monolith diameter and length), were then used to calculate the specimen density after each drying or immersion step in the procedure and finally the permeable pore space volume for each specimen. The equation used to determine the permeable pore space as given in ASTM C642-13 (2013) is as follows:

$$\text{Pore Space(\%)} = \frac{(g_2 - g_1)}{g_2} \times 100 \quad (3.2)$$

where

- $g_2$  = apparent density in  $\text{Mg/m}^3$  determined from the mass of the oven dried sample divided by the difference between the mass of the oven dried sample and the apparent mass of the sample following water immersion and boiling. This ratio is then multiplied by the density of water.
- $g_1$  = bulk density in  $\text{Mg/m}^3$  determined from the mass of the oven dried sample divided by the difference between the mass of the surface dried sample and the mass of the sample after water immersion. This ratio is multiplied by the density of water.

### 3.3.3 Saturated Hydraulic Conductivity

Hydraulic conductivity of intact, cured monoliths was measured using ASTM D5084-16a, *Standard Test Methods for Measurement of Hydraulic Conductivity of Saturated Porous Materials Using a Flexible Wall Permeameter*.

Two representative samples were selected from Test Batches 1, 2, 7 and 8 for analysis of  $K_{\text{sat}}$  (Table 3-1). Only the GAC-containing grouts (Test Batches 7 and 8) were included in these measurements due to time

constraints. The  $K_{sat}$  of the AgM-containing samples should be measured in the future. The samples had similar average diameters ranging from 4.91–4.93 cm, and the samples were cut to a length of 4.92–6.54 cm using a rock saw. After being cut, the samples were quickly rinsed of particulates and allowed to saturate in tap water under vacuum to displace air and help saturate the samples. Ordinary tap water was selected for saturating samples and for conducting the  $K_{sat}$  test since using DIW can be problematic (ASTM D5084-16a). As stated in ASTM D5084-16a the use of DIW can lead to chemical interactions in the porous media and as a result lead to underestimated  $K_{sat}$  values. Because of this either a representative solution or tap water is recommended by ASTM D5084. To maintain consistency of water used between cement formulations the recommended use of tap water was chosen. The saturation bath period was 1 week, and testing time was >2 weeks. Because this testing period is relatively short, material leaching (saturation) was not expected to affect the  $K_{sat}$ . Samples were removed from the saturation bath and immediately placed in a flexible wall permeameter (Tri-Flex 2 Permeability Test Cell, ELE International). The sample was placed between two end caps in the permeameter and surrounded by a rubber membrane held in place with O-rings. Once the sample was loaded, the permeameter was filled with water and pressurized with a confining pressure of 150 psi. The influent water pressure was maintained at 100–130 psi dependent on sample. Each regulated pressure was controlled by calibrated precision controllers (Alicat Scientific Inc.). Initial water breakthrough took more than 1 d and included water filling the dead space in the instrument. Measurements started as soon as the first effluent was observed. Testing was deemed complete once conductivity was determined to provide a steady  $K_{sat}$  (approximately three to seven measurements).

### 3.3.4 Water Characteristic Curve

Two representative samples were selected from test batches for Cast Stone and HGM-5. These samples were each fragmented and sieved, collecting the 1–2 mm fraction. This fraction was then rinsed to remove fine particulates, leaving the coarse fraction. Samples were then subdivided into 10 retaining dishes (~2 g each). Moisture was added using tap water until it reached the top surface of each of the subsamples. Water characteristic properties were measured using a Meter WP4C chilled mirror hygrometer following the testing procedure in ASTM D 6836-16 *Standard Test Methods for Determination of the Soil Water Characteristic Curve for Desorption Using Hanging Column, Pressure Extractor, Chilled Mirror Hygrometer, or Centrifuge*. This same method was used to evaluate moisture retention characteristics of SSW grout formulations by Nichols et al. (2017). Recorded pressure was measured by the WP4C instrument, and weights and densities (Table 5-2) were used to calculate gravimetric and volumetric water contents. This data is summarized in Table 5-4.

### 3.3.5 Chemical and Mineralogical Composition

Solids characterization was performed on the waste form specimens after curing and/or leach testing to identify interactions between the waste materials and the grout.

#### 3.3.5.1 Optical Microscopy

Optical images were obtained using a Keyence VHX-2000 Digital Microscope. Samples were imaged before polishing to analyze the as-reacted surfaces prior to preparation for microscopy. The Depth-Up feature of the digital microscope was used to allow for images containing surfaces of varying heights to have all points of interest in focus.

### 3.3.5.2 Scanning Electron Microscopy

Scanning electron microscopy (SEM) was conducted on selected specimens using a JEOL 7001F TTLS/LV instrument (JEOL USA, Inc.; Peabody, MA). This microscope was configured with a field emission gun (FEG) and was capable of imaging uncoated, nonconductive specimens in low vacuum (LV) mode. This SEM was equipped with a 60 mm<sup>2</sup> silicon drift detector (SDD) energy dispersive spectrometer (EDS; Bruker Quantax 6|60; Bruker Nano GmbH, Berlin, Germany), which is used to determine the elements present in a specimen. This SEM also has an electron backscatter diffraction detector (EBSD; Bruker e-Flash HR; Bruker Nano GmbH, Berlin, Germany), which is used to determine the crystal structure and orientation of the different phases in a specimen.

Specimens were prepared for SEM analysis by impregnating them with an ultralow-viscosity epoxy resin (L.R. White). The goal was to have the epoxy infiltrate all of the pore space to hold the microstructure intact during cutting and polishing. Because hydrated materials are saturated with water, it is very difficult to impregnate hydrated cementitious materials with hydrophobic epoxy compounds. Thus, a series of sequential solvent exchange steps were used to exchange the water in the specimen with alcohol, and then exchange the alcohol in the specimen with the ultralow-viscosity epoxy. A series of soaking steps were used, each lasting several days, starting with 100% ethanol and ending with 100% L.R. White epoxy resin. After the specimen had soaked in L.R. White resin for several days, the epoxy was cured in an oven at approximately 60°C and held at that temperature for 24–48 hours. After the specimens were fully impregnated with epoxy and cured, they were mechanically polished with silicon carbide (SiC) abrasive papers, using successively finer grits, eventually moving to diamond suspension, and ending with vibratory polishing with colloidal silica.

Specimen microstructures were typically examined uncoated, in LV mode. Typical imaging conditions were 15 kV, <1 nA of beam current, and <5 mm working distance. Microstructures were analyzed by collecting micrographs using both secondary electron (SE) detectors and backscattered electron (BSE) detectors. Images collected using SE detectors show enhanced details about topology of the specimen's surface. This is because edges tend to yield more SEs than flat surfaces, and thus appear brighter. BSE detectors, however, emphasize differences in composition. This is because the production of BSEs is roughly proportional to the average atomic number. Thus, the dominant contrast mechanisms in BSE micrographs is based on differences in average atomic number, where higher-atomic-number features are brighter than those features with lower atomic numbers.

Elemental analysis was conducted on selected specimens using EDS. Specimens were coated with approximately 5 nm of carbon using a carbon rod evaporator (Quorum, EMST150 ES, Quorum Technologies, Ltd., Laughton, East Sussex, England). This was done to create a conductive coating on the surface of the sample to allow dissipation of electric charge deposited by the electron beam of the SEM. The conductive coating enabled the specimens to be imaged in high vacuum mode with high beam currents, which improves the accuracy and quality of the EDS data. Typical EDS conditions were 20 kV, 5–6 nA, and 10 mm working distance. Spectra were collected point by point over a given field of view to create an elemental map that showed the spatial distribution of elements in that area. From this elemental map, a sum spectrum could be collected, showing the relative concentrations of the different elements present in that field of view.

### 3.3.5.3 X-ray Diffraction

The bulk mineralogy of neat grouts from Test Batches 1 and 2 (HGM-5 and Cast Stone) was determined after compressive strength testing using a Rigaku Miniflex II X-ray diffraction (XRD) unit equipped with a Cu K $\alpha$  radiation ( $\lambda = 1.5418 \text{ \AA}$  with 30 kV and 15 mA) source. To prepare the XRD samples, chips of material were collected and pulverized to a powder using a mortar and pestle. Following size reduction, a

~300 mg subsample was weighed and added to a separate (tared) collection vial (e.g., 7 mL glass sample vial). To this ~300 mg aliquot, ~30 mg of rutile TiO<sub>2</sub> (Aldrich, CAS# 1316.80-2) was added as an internal standard and the sample homogenized using the mortar and pestle. Samples were then loaded into zero-background quartz sample holders for analysis. Patterns were collected over the course of ~11 h in fixed time mode from 3–100° 2 $\theta$ . The scan step size was 0.05°, and the step count time was 20 s.

Mineral identification was performed using Jade software (Materials Data Incorporated, California) with the International Centre for Diffraction Data XRD database. Quantification was performed by the whole pattern fitting (Rietveld refinement) method using Topas software (v5, Bruker AXS, Germany), with the pattern for each phase calculated from published crystal structures (Inorganic Crystal Structure Database, Fachinformationszentrum Karlsruhe, Germany).

#### **3.3.5.4 X-ray Computed Tomography**

Select monoliths from Test Batches 3, 4, 5 and 6 following leach testing were scanned using a high-resolution microfocus X-ray computed tomography (XCT) scanner (Nikon XTH 320/225, Nikon Metrology, Inc, Brighton, MI) to visualize the 3D distribution and volume fractions of AgM and GAC inclusions. Scans were performed at 90 kV voltage and 350  $\mu$ A beam current from a tungsten target. The samples were rotated continuously during the scans with momentary stops to collect each projection (shuttling mode) to minimize ring artifacts. A total of 1500 projections were collected over 360° with 0.5 s exposure time and two frames per projection with an isotropic voxel size of 55.1  $\mu$ m. The images were reconstructed to obtain 3D volume data using the software CT Pro 3D (version XT 2.2, Nikon Metrology, Inc). Segmentation of AgM and GAC phases from the cement matrix was carried out in the software Avizo (version 9.5.0, Thermo Fisher Scientific, Waltham, MA). Volume analysis of the AgM beads and GAC inclusions was also calculated by Avizo.

#### **3.3.5.5 Microprobe X-ray Fluorescence ( $\mu$ XRF) Mapping**

A sample from Test Batch 6 following leaching was analyzed using synchrotron  $\mu$ XRF mapping to determine the distribution of key elements within the specimen. The selected specimen was prepared as two thin sections (1 mm thick and ~10–15 mm in diameter), which were cut after a specimen fragment containing AgM material in epoxy (Struers EpoFix Resin<sup>®</sup>) had been secured. Measurements were performed at the Advanced Photon Source (APS) at Argonne National Laboratory on beamline 20-ID.  $\mu$ XRF maps were collected for S, Ag, I, Si, Ca, and Al with a beam size of 5  $\mu$ m  $\times$  5  $\mu$ m and at an energy above the Fe K edge (7112 eV). Maps were collected with a step size of 5  $\mu$ m for a selected sub-area 1500  $\mu$ m  $\times$  1500  $\mu$ m in size.

#### **3.3.5.6 Time of Flight Secondary Ion Mass Spectroscopy (ToF-SIMS)**

Time of Flight Secondary Ion Mass Spectroscopy (ToF-SIMS) measurement was performed at the Environmental Molecular Sciences Laboratory, which located at PNNL. A TOF.SIMS5 instrument (IONTOF GmbH, Münster, Germany) was used. A 25 keV pulsed Bi<sub>3</sub><sup>+</sup> beam was used as the analysis beam to collect SIMS data. The Bi<sub>3</sub><sup>+</sup> beam was focused to be ~5  $\mu$ m diameter and scanned over a 500  $\times$  500  $\mu$ m<sup>2</sup> area with 128  $\times$  128 pixels. The current of the pulsed Bi<sub>3</sub><sup>+</sup> beam (10 kHz) was about 0.59 pA. Mass resolution was in a range of 3000-5000, varying from sample to sample due to sample roughness. A low energy (10 eV) electron flood gun was used for charge compensation in all measurement

### 3.4 Sorption and Desorption Characteristics

Distribution coefficients ( $K_d$ s) were measured using ASTM C1733-17a, *Standard Test Method for Distribution Coefficients of Inorganic Species by the Batch Method*.  $K_d$  is used to assess the degree to which a chemical species will be removed from solution (permanently or temporarily) as it contacts a solid material and is determined by the concentration of the adsorbate on the solid material divided by the concentration of the adsorbate in solution. The  $K_d$  value is a simplification of a number of processes including complexation, precipitation, and co-precipitation and may vary depending on the chemistry of the contacting solution and available surface area of the solid.

Two sets of  $K_d$  tests were performed: (1)  $K_d$  for the sorption of Tc, I (as iodide and iodate) and Hg to SSW materials (AgM, GAC, and HEPA filters) in grout-contacted water and (2)  $K_d$  for the sorption of Tc and I to grout samples from Test Batches 1 and 2 (HGM-5 and Cast Stone). Following the  $K_d$  sorption test, the solids were recovered with filtration and placed in double deionized water (DDI, 18.2 M $\Omega$ -cm, conforming to ASTM Type I classification, ASTM D1193-06(2018)) to monitor the desorption of Tc and I over a 30 d period in oxic conditions. The collected time-dependent leachates from sorption and desorption testing were analyzed for Tc and I concentration using inductively coupled plasma mass spectroscopy (ICP-MS).

The tests were designed to be more representative of actual disposal conditions, however, there are some limitations as to how representative they can be. For instance, the grout materials would not be crushed, and the sorption process may not occur in saturated conditions. In addition, the sorption of the analyte for each material may not occur in a saturated solution but rather from a vapor phase. Thus there are some limitations on the  $K_d$  values presented here but they can be used to provide guidance for source term modeling in PA calculations.

#### 3.4.1 Grout Pore Water and Contaminant Spike Preparation

Grout pore water starting solutions of either the reduced (Cast Stone) or oxidized (HGM-5) grouts were prepared by contacting a sized-reduced, cured, neat grout of < 2 mm size fraction with DDI for 7 days. The < 2-mm size fraction was obtained by passing crushed grout material through an appropriate sieve. The crushed grout/DDI mixtures prepared to a mass ratio of 1:4 were placed on a shaker for 7 d. At the end of the 7-d contact period, the solutions were decanted into a separate container. The separated pore water solutions were used as is or spiked with different contaminants for use in the sorption and desorption tests described below. The composition of the initial grout pore water solutions and spikes were analyzed by inductively coupled plasma optical emission spectroscopy (ICP-OES) and ICP-MS (see Table 4.3). All tests were performed in open atmosphere.  $E_h$  was ~ +105 mV (vs. the standard hydrogen electrode) for the Cast Stone contacted solution and + 305 mV (vs. the standard hydrogen electrode) for the HGM-5 solution.

Spiked test solutions containing the desired analyte at 50 ppm were prepared with the Cast Stone and HGM-5 pore water solutions. The choice of 50 ppm for each analyte was based on practical analytical decisions in regards to ensuring measurable concentrations in the high ionic strength pore water solutions. Actual loading values for the various waste materials can be found elsewhere (Brown et al. 2017). The 50-ppm solutions were prepared by adding 1 mL of a 10,000 ppm spike solution to 200 g of the pore water solution. The starting individual spike solutions of 10,000 ppm Tc, I, IO<sub>3</sub><sup>-</sup>, and Hg<sup>1</sup> were prepared

---

<sup>1</sup> Tc is likely TcO<sub>4</sub><sup>-</sup> and Hg is likely Hg<sup>2+</sup> in solution but, for simplicity, these species will be referred to as Tc and Hg, respectively. On the other hand, iodine (I) and iodate (IO<sub>3</sub><sup>-</sup>) are referred to as their target species in order to avoid confusion.

by adding requisite masses of  $\text{NH}_4\text{TcO}_4$ ,  $\text{NaI}$ ,  $\text{NaIO}_3$ , and  $\text{Hg}(\text{NO}_3)_2 \cdot x\text{H}_2\text{O}$  ( $x=1-2$ ) to DDI, respectively. In addition to the individual 50-ppm spiked solutions, two additional solutions of 50 ppm Hg and  $\text{I}^-$  and 50 ppm Hg,  $\text{I}^-$ ,  $\text{IO}_3^-$ , and Tc (denoted as ALL from hereafter) were also prepared. In all solutions containing  $\text{I}^-$  and  $\text{IO}_3^-$ , nonradioactive iodine-127 chemicals were used. Measured concentrations, which are used as  $C_{\text{blank}}$  values in  $K_d$  calculations, are provided in Table 3-4. Thus, for each pore water solution, six analyte solutions were made. We note that when Hg and  $\text{I}^-$  were added to the Cast Stone pore water, the solution changed to a yellowish color and a black precipitate formed at the bottom of the container. Thus, the initial aqueous Hg concentration for this test was only 8.3 ppm.

**Table 3-3.** Chemical Composition of the Non-Spiked Initial Pore Water Solutions (concentrations in mg/L)

Analyte	Cast Stone	HGM-5	Method
Al	11.7	3.0	ICP-OES
Ba	3.6	15.7	ICP-OES
Ca	205	274	ICP-OES
Fe	0.1	<0.1	ICP-OES
Mg	<0.03	<0.03	ICP-OES
K	182	203	ICP-OES
Si	1.9	1.0	ICP-OES
Na	129	374	ICP-OES
Sr	10.6	38.0	ICP-OES
S	19.1	2.1	ICP-OES
pH	12.3	12.5	ICP-MS
I	0.0073	0.0016	ICP-MS
Hg	0.26	0.089	ICP-MS
Tc	<3.3×10 <sup>-4</sup>	<3.3×10 <sup>-4</sup>	ICP-MS

### 3.4.2 Sorption Tests

Distribution coefficient ( $K_d$ ) values were determined for Tc, I, and  $\text{IO}_3^-$  to GAC, AgM, a HEPA filter material and the samples from Test Batches 1 and 2 (HGM-5 and Cast Stone). The GAC and AgM were used in their as-received form. The GAC consisted of cylindrical activated carbon and randomly-shaped inert pieces, see Figure 2-2. The cylinders were identified to contain native iodide, and this may have contributed to some of the observations that will be discussed further in the results section. The HEPA material was shredded with scissors and tweezers to a < 5 mm size and separated with a sieve. The grout materials were the < 2 mm size fraction neat grouts. Tests with neat grouts were only conducted with the corresponding pore water solution (e.g., Cast Stone solid material with Cast Stone pore water).

Tests were performed in triplicate with 0.5 g solid and 12.5 g solution. The full list of sorption tests is given in Table 3-4. The 1:25 solid:solution ratio is the same as given in ASTM C1733-17a. All batch sorption tests were performed on a shaker (100 rpm) in open atmosphere at room temperature. At the end of experiment, and after allowing 30 minutes for the solids to settle, a subsample was collected from each bottle and filtered through a 0.45  $\mu\text{m}$  syringe filter. The subsamples were submitted for analysis by ICP-MS, ICP-OES, or both. From the triplicate tests, two sets of separated solids were transferred to another vial for batch desorption  $K_d$  tests and the other set was set aside for solids characterization.

Prior to initiation of the set of batch sorption tests provided in Table 3-4, a smaller, initial set of scoping tests were performed with no replicates. This set of initial tests was used to examine the time required for equilibrium between the contaminant and solid material. These initial tests were conducted only with the HGM-5 pore water and with the single analyte spikes for a total of 14 tests. The combination of solids and solutions for these tests are provided in Table 3-4. The test protocol was identical to the tests described in the previous paragraph except 2 g of solid were contacted with 50 g of solution and 0.5 mL solution aliquot was collected at 1- to 2-d intervals. After 14 d and a total of 10 aliquots, the scoping tests were terminated. Results, provided in Appendix A, showed that typically less than one week was required to achieve an apparent equilibrium between the solid and solution.

**Table 3-4.** Matrix Showing the Set of Sorption  $K_d$  Tests Performed with Each Waste Material and Pore Water Solution Combination. A “+” indicates a solid:analyte combination where an initial test was also performed without replicates to determine test duration. An “x” indicates that the triplicate batch sorption  $K_d$  test was performed. A “-” indicates that no tests were performed with the solid:analyte combination. Analyte concentrations are averaged and the standard deviations of the concentrations were measured from sorption tests performed without solids.

Neat Grout Porewater:	Material	Contacting Analyte						
		No Spike	Tc	I <sup>-</sup>	IO <sub>3</sub> <sup>-</sup>	Hg	Hg/I <sup>-</sup>	ALL <sup>(1)</sup>
HGM-5	GAC	x	+/x	+/x	+/x	+/x	x	-
	AgM	x	+/x	+/x	+/x	-	-	-
	HEPA	x	+/x	+/x	+/x	-	-	-
	HGM-5	x	+/x	+/x	+/x	+/x	x	x
	No Solid	-	x	x	x	x	x	x
Cast Stone	GAC	x	x	x	x	x	x	-
	AgM	x	x	x	x	-	-	-
	HEPA	x	x	x	x	-	-	-
	Cast Stone	x	x	x	x	x	x	x
	No Solid	-	x	x	x	x	x	x
		Analyte Concentration (mg/L) <sup>(2)</sup>						
HGM-5		-	69.3±9.4	48.1±0.5	34.6±0.3	54.7±1.2	Hg: 38.3±0.2	Hg: 35.6±0.4
							I: 42.3±0.6	I: 71.0±3.4
								Tc: 53.9±2.8
Cast Stone		-	65.5±2.0	47.9±0.1	35.1±0.9	3.9±0.7	Hg: 20.1±1.4	Hg: 8.3±0.3
							I: 38.3±0.6	I: 73.1±0.7
								Tc: 53.8±2.2

<sup>(1)</sup>Tests were spiked with I<sup>-</sup> and IO<sub>3</sub><sup>-</sup> but analyte concentration is just for total iodine

<sup>(2)</sup>Values are total elemental concentrations and are not species specific

### 3.4.3 Desorption Tests

The analyte-loaded solids from the batch sorption  $K_d$  tests were collected and subjected to batch desorption  $K_d$  tests with fresh pore water. Desorption  $K_d$  tests were performed in duplicate in open atmosphere by placing the loaded solids in the pore water for 10 to 14 days on a shaker set at 100 rpm. A solid:solution ratio of 1:25 was used where the solid mass was the wet mass of the material after the batch sorption  $K_d$  test. At the end of the tests a solution aliquot from each bottle was filtered through a 0.45  $\mu$ m syringe filter and submitted for analysis with ICP-MS, ICP-OES, or both. Certain material combinations were not used for the batch desorption  $K_d$  tests when the amount of analyte sorption on the solid was negligible.

**Table 3-5.** Matrix Showing the Set of Batch Desorption  $K_d$  Tests Performed with Each Waste Material and Pore Water Solution Combination. An “x” indicates that the  $K_d$  test was performed in duplicate, whereas a “-” indicates that the test was not performed.

Neat Grout Porewater:	Material	Contacting Analyte					
		Tc	I <sup>-</sup>	IO <sub>3</sub> <sup>-</sup>	Hg	Hg/I	ALL <sup>(1)</sup>
<b>HGM-5</b>	GAC	x	-	-	x	x	-
	AgM	-	x	x	-	-	-
	HEPA	x	-	-	-	-	-
	HGM-5	x	x	x	x	x	-
<b>Cast Stone</b>	GAC	x	x	x	x	x	-
	AgM	x	x	x	-	-	-
	HEPA	x	x	x	-	-	-
	Cast Stone	x	x	x	x	x	x

### 3.4.4 Calculation of Sorption $K_d$ and Desorption $K_d$ Tests

The sorption  $K_d$  [ $K_{d(adsorb)}$ ] values were calculated with equation 3.3 (ASTM C1733-17a):

$$K_{d(adsorb)} = \left[ \frac{C_{blank,i} - C_i}{C_i} \right] \times \frac{V_{l,ads}}{m_s} \quad (3.3)$$

where

- $C_{blank,i}$  = the concentration of the analyte  $i$  in solution for the sorption test with no solid at contact time,  $t$  ( $\mu\text{g/mL}$ )
- $C_i$  = the concentration of the analyte  $i$  in solution for the sorption test with the waste material solid at contact time  $t$  ( $\mu\text{g/mL}$ )
- $V_{l,ads}$  = the volume of spiked solution contacting the solid at time  $t$  during the sorption test (mL)
- $m_s$  = the mass of the dry waste material used in the test (g)

The desorption  $K_d$  [ $K_{d(desorb)}$ ] values were calculated with equation 3.4:

$$K_{d(desorb)} = \frac{[(C_i \times V_{res}) + (C_{blank,i} - C_i) \times V_{l,ads}] - [C_{desorb,i} \times V_{l,desorb}]}{C_{desorb,i} \times m_{s,wet}} \quad (3.4)$$

where

- $C_{desorb,i}$  = the concentration of the analyte  $i$  in solution for the desorption test with the waste material solid at contact time  $t$  ( $\mu\text{g/mL}$ )
- $V_{l,desorb}$  = the volume of pore water solution contacting the solid for desorption test, respectively (mL)
- $V_{res}$  = the volume of the residual spiked sorption solution remaining in the tube at the end of the sorption test (mL)
- $m_{s,wet}$  = the mass of wet waste material used. (g)

The first term in square brackets in the numerator of Equation 3.4 is the mass of analyte in the tube at the end of the sorption test. The term in the second set of brackets in the numerator is the mass in the desorption solution. Some calculations have a negative second term in the desorption  $K_d$  numerator, which

is physically impossible as long as the waste material does not contribute additional analyte into the solution. This negative value can be caused by measurement of the two concentrations,  $C_{blank}$  and  $C_{sol}$ , which may be nearly the same value and dominated by analytical variability. It was also assumed that there is no significant container wall adsorption in the blank tubes and the analyte in solution is stable (i.e., not precipitating or volatilizing). In the cases where a negative  $K_d$  was calculated a zero is reported.

### 3.5 Leaching of Solidified Waste Forms

Specimens of solidified GAC and AgM were subjected to the EPA Method 1315, *Mass Transfer Rates of Constituents in Monolithic or Compacted Granular Materials Using a Semi-Dynamic Tank Leaching Procedure*. Test Batches 1, 2, 3, 4, 5 and 6 were used in the leach testing. The specimens were prepared with non-radioactive I-127 loaded GAC and AgM. DIW and vadose zone pore water (VZPW) were used as the leachants. Moisture contents and geometric surface areas that are needed to calculate observed diffusion coefficients were measured concurrently with the leach tests. The surface area of each monolith will be based on the geometric surface area of the specimen.

#### 3.5.1 Iodide Loading

Aqueous batch contacts were used to load the GAC/AgM with iodide. While the capture of iodine by these materials in WTP will be from the vapor phase, the final form on the material will be similar. The GAC will have physi-sorbed iodine and whose speciation is not well characterized. The AgM capture of iodine produces AgI (Jubin et al. 2017) and AgI is the product of the aqueous capture as well. The main difference between the GAC/AgM loaded with vapor phase capture vs. aqueous capture is a higher water content following the aqueous contact. The iodide concentration in the contact solution was measured before and after contact with the GAC/AgM to determine the loading to the materials. Due to scheduling constraints, vapor phase iodine loading was not feasible. I-129 levels are expected to be  $2.3 \times 10^{-4}$  Ci/m<sup>3</sup> on GAC and  $4.3 \times 10^{-3}$  Ci/m<sup>3</sup> on AgM (Brown et al. 2017). This was equivalent to 1.3 g I-129/m<sup>3</sup> and 24.3 g I-129/m<sup>3</sup> for the GAC and AgM respectively. The target loading of each material was  $10 \times$  of these values to improve the likelihood of measurable data in the leach tests. Initial iodide content has little impact on the magnitude of the measured observed diffusivity based on previous tests that compared loadings between 0.16 mg I/kg-dry waste form and 77 mg I/kg-dry waste form (Serne et al. 2015). Each monolith sample had a volume of  $\sim 205$  cm<sup>3</sup>. With an expected target waste loading expected of 30%, (see Table 3-1), the GAC/AgM will comprise  $\sim 62$  cm<sup>3</sup> of the monolith. Following the aqueous contact the water was decanted from the solid material and left to air dry for 24 h. No heat treatment was applied to the I-loaded GAC or AgM to prevent loss of the loaded I. Therefore, residual water was present in the materials before fabrication of the leach testing monolith samples and was taken into account for the mass of GAC/AgM added. It is possible that this residual water could contain some iodide, however it is calculated to be a maximum of 0.2% of the overall iodide loaded to the GAC/AgM and would not impact the overall leach results.

#### 3.5.2 Sample and Test Preparation

The leachability of iodine (as iodide) from the stabilized GAC and AgM was evaluated using EPA Method 1315 (EPA 2013). Six test batches were prepared for the leach testing as shown in Table 3-6.

**Table 3-6.** Test Batches and Initial Iodide Concentrations ( $C_0$ ) for Leach Testing. The GAC values were adjusted to account for the nominal iodide in the GAC material.

Test Batch	Formulation	Iodide Type	Measured $C_0$ for Iodide (mg I/kg waste form dry)
1	HGM-5	Direct spike as NaI	56.2
2	Cast Stone	Direct spike as NaI	80.0
3	HGM-5	Loaded on GAC	70.9 (adjusted)
4	Cast Stone	Loaded on GAC	71.0 (adjusted)
5	HGM-5	Loaded on AgM	51.7
6	Cast Stone	Loaded on AgM	45.5

After curing the cylindrical monolith were measured and the surface area used to determine the leachant volume at a ratio of 9 mL/cm<sup>2</sup>. The monoliths were placed in holders that exposed > 98% of the surface area and an initial mass taken for the monolith and holder. The monoliths were then placed in the leachant for a defined interval length. At the end of each interval the monolith was removed from the leachate, weighed, photographed and placed into a fresh leachant. The previous interval leachate was collected and analyzed for pH and concentration of iodine using ICP-MS. The test intervals followed the EPA method with samplings after a total test duration of 2 h, 1 d, 2 d, 7 d, 14 d, 28 d, 42 d, 49 d, and 63 d. The sixth interval exchange occurred at 29 d instead of 28 d due to staffing conflicts.

The resulting calculation from the measured leachate concentrations is an observed diffusivity for iodine,  $D_{obs}$ . A smaller  $D_{obs}$  represents a lower release rate of that species from the monolith. Previous works have identified that observed diffusivities and effective diffusivities are near identical terms (Cantrell et al. 2016). The  $D_{obs}$  was determined using the equation for simple radial diffusion from a cylinder into an infinite bath, as described in EPA Method 1315 (EPA 2013). The equation used is based on Fick's 2<sup>nd</sup> law is shown here, equation 3.5:

$$D_{obs} = \pi \left[ \frac{M_{t_i}}{2\rho C_0 (\sqrt{t_i} - \sqrt{t_{i-1}})} \right]^2 \quad (3.5)$$

where

- $D_{obs}$  = observed diffusivity of a specific constituent for leaching interval,  $i$  (m<sup>2</sup>/s)
- $M_{t_i}$  = mass of specific constituent released during leaching interval (mg/m<sup>2</sup>)
- $t_i$  = cumulative contact time at the end current leach interval,  $i$  (s)
- $t_{i-1}$  = cumulative contact time after previous leaching interval,  $i-1$  (s)
- $C_0$  = initial concentration of constituent in the dry Cast Stone mix (mg/kg<sub>dry</sub>) calculated using the theoretical initial constituent concentration in the simulant based on additions made in simulant preparation
- $\rho$  = Cast Stone dry bulk density (kg<sub>dry</sub>/m<sup>3</sup>).

It should be noted that the common units for effective or observed diffusion coefficients in transport modeling activities is cm<sup>2</sup>/s, in which case the value resulting from equation 3.2 is multiplied by 10<sup>4</sup> to convert from m<sup>2</sup>/s to cm<sup>2</sup>/s. The initial concentration ( $C_0$ ) of individual species was calculated based on iodide concentration difference before and after the batch contact to load the GAC/AgM. The higher iodide loading in Test Batches 1 and 2 (HGM-5 and Cast Stone) were selected to be on the same order of magnitude as the AgM samples. Both test batches had the starting water spiked to equal molar amounts of iodide and due to the difference in w:dm this resulted in differing  $C_0$  values between the two test batches.

## 4.0 Cementitious Waste Form Set/Curing Properties

### 4.1 Grout Flow

The results of the grout flowability tests performed on specimens from Test Batches 1 and 2 (neat grouts) and Test Batches 7 and 8 (containing 30 vol% GAC) are summarized in Table 4-1. Due to the higher water content of the Cast Stone recipe,  $w/dm = 0.45$ , the grout slurry rapidly flowed out of the cylinder (83 cm height and 48 cm inner diameter,  $\sim 150 \text{ cm}^3$  volume of slurry) and across the stainless-steel plate to cover a larger area (larger pancake diameter). With a  $w/dm$  ratio = 0.29, the HGM-5 specimen spreads to a diameter almost half the diameter of the Cast Stone formulation. As a result, the height measured for the HGM-5 specimen is two to three times larger than the Cast Stone specimen's height after one and three minutes. When 30 vol% GAC was added, similar flow was observed for the HGM-5, while flow for the Cast Stone was lowered by  $\sim 35\%$ . According to the procedure adapted from Nichols et al. (2017), a grout with a diameter  $\geq 120 \text{ mm}$  is considered acceptable for this work. Both neat Cast Stone and HGM-5 formulations pass the criteria. The HGM-3 formulation measured a diameter of 97.20 mm after one minute and 100.46 mm after three minutes, below the threshold of 120 mm. This flow is lower than that reported in Nichols et al (2017), however this difference is due to the sand used in the mix. The sand used in this effort was fully dried prior to use. Whereas in the previous work the sand supplied was moist and noticeable thinning was observed upon its addition to the slurry, pg. 24 of Nichols et al (2017). This work presents a valuable data point on the influence of dry sand on HGM-3 flowability. It should be noted that despite its lower flow, the HGM-3 was still workable and able to suspend the GAC and AgM during fabrication.

**Table 4-1.** Grout Flowability Measurements

Elapsed Time <i>Measurement</i>	One Minute		Three Minutes	
	<i>Dia. (mm)</i>	<i>Height (mm)</i>	<i>Dia.(mm)</i>	<i>Height (mm)</i>
HGM-5 (Test Batch 1)	121.71	13.46	121.92	12.66
Cast Stone (Test Batch 2)	221.59	4.93	225.33	3.21 (halfway to edge) 5.81 (center)
HGM-5 + 30% GAC (Test Batch 7)	126.88	14.92	126.88	14.92
Cast Stone + 30% GAC (Test Batch 8)	149.65	11.76	149.68	11.75
HGM-3	98.95	32.82	100.46	30.58

### 4.2 Set Time

Sample details and initial and final set time measurements for each specimen analyzed from neat test batches 1 and 2 (HGM-5 and Cast Stone) are provided in Table 4-2. Overall, minimal sample mass ( $<0.3 \text{ wt}\%$ ) was lost over the course of testing due to water evaporation. For the HGM-5 specimen, the set time of 22.4 hours is similar to the previously reported set time of less than 24 hours by Nichols et al. (2017). For the Cast Stone specimen, set time (69.7 hours) was comparable to those set times reported for other Cast Stone formulations used to solidify liquid secondary wastes (Saslow et al. 2018; Cozzi and McCabe 2016). The increase in Cast Stone set time is attributed to the higher  $w/dm$  ratio (0.45) relative to the HGM-5 formulation ( $w/dm = 0.29$ ). For HGM-3 specimen, the slurry was set after 5.1 h.

**Table 4-2.** Neat Grout Set Time Results using ASTM C191-13

Test Batch	Cast Stone	HGM-5	HGM-3
Initial Specimen Weight (g)	394.59	431.02	576.15
Final Specimen Weight (g)	393.36	430.36	576.15
Total Set Time (days)	2.9	0.9	0.2
Total Set Time (hours)	69.7	22.4	5.1

### 4.3 Heat of Hydration

Isothermal calorimetry was used to measure the heat of hydration for the Cast Stone matrix as well as the HGM-5 formulation to assess consistency with previous reports. The resulting data from the measurement is shown in Figure 4-1 along with sand, which was included as a reference.

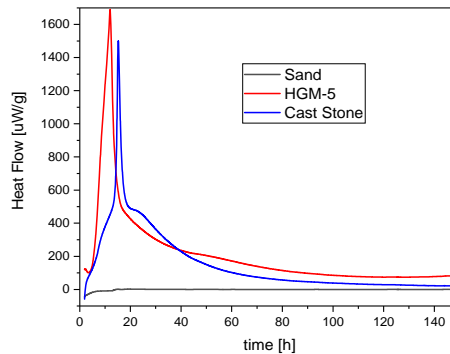


**Figure 4-1.** Isothermal Calorimetry Data Shown as Heat Flow Versus Time for Sand (black), HGM-5 (red), and Cast Stone (blue) at 30 °C

The curves shown in Figure 4-1 are thermal power curves for each material. The peak energy was 1691  $\mu\text{W/g}$  for the HGM-5 (compared with 1981 in  $\mu\text{W/g}$  reported in Nichols et al, 2017) and 1500  $\mu\text{W/g}$  for the Cast Stone (compared with 2365  $\mu\text{W/g}$  for the similar Mix 13 in Nichols et al 2017). Samples were monitored for 7 days (168 hours) since this is approximately the amount of time required for the heat flow signature to equilibrate near zero for both formulations.

It is interesting to note the significant differences between the curves for HGM-5 and Cast Stone. The peak energy for HGM-5 was greater during the reactions than Cast Stone but the main hydration peak for Cast Stone has more features. HGM-5 has a faster setting time, arriving at 50% max height of the main hydration peak by 7 hours, whereas the Cast Stone matrix took closer to 12 hours. Both results show that hydration reactions primarily occurring in the first 24 h, which correlates to observations made during set time and free liquids tests.

### 4.4 Free Liquids

The presence of free liquids was monitored on one monolith selected from Test Batches 1 and 2 (HGM-5 and Cast Stone). On each observation day, a photo was taken to document the presence of free liquids.

Photos taken on the production day, and after 1, 2, and 8 days of curing are provided for each monolith observed in Figure 4-2. The time required for free liquids to reduce to less than 1% of the total waste volume is shown in **Table 4-3**. Due to the elevated water content in the Cast Stone formulation, the observed monolith required up to 8.1 days to reabsorb residual free liquids to within <1% of the total waste volume. Comparatively, HGM-5, with a lower formulation water content, only required up to 1.8 days to reabsorb all residual free liquids. These results are comparable to measurements reported in Nichols et al 2017 for Mix 5 (HGM-5) and Mix 13 (similar to Cast Stone), where each took approximately one and three days, respectively, to reabsorb free liquids. When GAC was added to the mix a decrease in free liquids absorption time was observed with increasing GAC content as the GAC may assist in water uptake early in life, Table 4.3.

The residual free liquid results discussed here are based on observations collected for one specimen from each test batch. Replicate sample observations are needed to confirm these assessments. Once confirmed, the results of this work can be used to select formulations for scale-up tests and to provide baseline guidance for the time required before waste forms meet common waste acceptance criteria (<1 vol% free liquids).

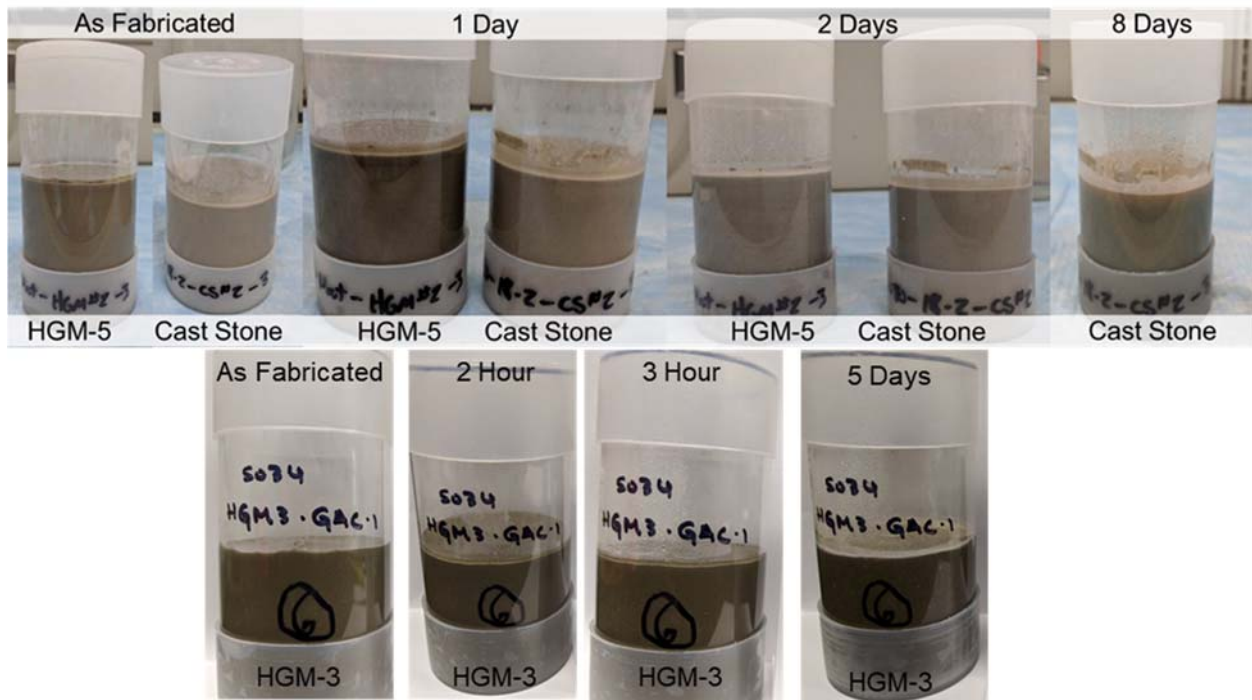


**Figure 4-2.** Residual Free Liquids Present at the Surface of HGM-5 and Cast Stone Neat Grouts Immediately After Fabrication, and After 1, 2, and 8 Days of Curing. An example HGM-3 sample containing 1 vol% GAC is also shown at 2 h, 3 h and 5 days. The 8-day HGM-5 sample is not shown because the HGM-5 sample absorbed all free liquids after ~2 days.

**Table 4-3** – Comparison of the Free Liquids Measurements of HGM-3 and HGM-5 Containing Varying Loadings of GAC.

Formulation	GAC Loading (vol %)	Free Liquid Retention Time (Days)
HGM-3	10	< 2 h
	7.5	< 6 h
	1	< 5 days
	0	<2 days
HGM-5	10	< 1 h
	7.5	< 2 h
	1	< 2h
	0	< 2 days

## 5.0 Solidified Cementitious Waste Form Properties

### 5.1 Compressive Strength

Compressive strength results are summarized in Table 5-1 for the four neat grout specimens analyzed from Test Batches 1 and 2 (HGM-5 and Cast Stone) and Test Batches 7 and 8 containing 30 vol% GAC. The AgM-containing samples were not planned for analysis and time constraints prevented their analysis. The average compressive strength for each test batch was determined from the compressive strength of two specimens from each formulation. A decrease in compressive strength was observed upon the inclusion of 30 vol% GAC from  $2662 \pm 271$  psi for the Cast Stone to  $1654 \pm 138$  psi when the GAC was added; and from  $3128 \pm 44$  psi for the HGM-5 to  $2501 \pm 46$  psi when the GAC was included. However, all monolith specimens met the minimum compressive strength of 500 psi (Siskind and Cowgill 1992).

**Table 5-1.** Compressive Strength of Select Non-Rad Neat Specimens

Formulation	Cast Stone		Cast Stone + 30% GAC		HGM-5		HGM-5 + 30% GAC	
	Test Batch 2		Test Batch 8		Test Batch 1		Test Batch 7	
Specimen Number	A	B	A	B	A	B	A	B
Average Monolith Height (mm)	113.27	116.22	118.70	119.50	121.40	119.20	119.30	119.60
Average Monolith Diameter (mm)	49.20	49.20	49.00	49.00	49.00	49.00	49.00	49.00
Specimen Length to Diameter Ratio	2.30	2.36	2.42	2.44	2.48	2.43	2.43	2.44
Cross-Sectional Area (mm <sup>2</sup> )	1901	1901	1886	1886	1886	1886	1886	1886
Cross-Sectional Area (in <sup>2</sup> )	2.95	2.95	2.92	2.92	2.92	2.92	2.92	2.92
Maximum Compressive Load (lbf)	8,410	7,280	4,549	5,122	9,052	9,233	7,407	7,215
Compressive Strength (psi)	2,853	2,470	1,556	1,735	3,097	3,159	2,534	2,468
Formulation Average Compressive Strength (psi)	$2,662 \pm 271$		$1,654 \pm 138$		$3,128 \pm 44$		$2,501 \pm 46$	

### 5.2 Density, Permeable Pore Space, and Moisture Content

Density measurements were performed using specimens from Test Batches 1 and 2 (HGM-5 and Cast Stone, specimen size was a 2" diameter  $\times$  ~2" height right circular cylinder.), the results of which are summarized in Table 5-2. The apparent density for the Cast Stone formulation is  $2.54 \text{ g/cm}^3$  (or  $\text{Mg/m}^3$ ) and  $2.52 \text{ Mg/m}^3$  (or  $\text{g/cm}^3$ ) for the HGM-5 formulation. However, using the approach outlined in ASTM C642-13 for calculating the volume of permeable pore space, the difference in permeable pore space between Cast Stone (47.22%) and HGM-5 specimens (33.99%) was significant. These values were comparable to those reported previously for HGM-5 (35%, Mix 1) and the formulation similar to Cast Stone (48%, Mix 13) (Nichols et al. 2017). Furthermore, the Cast Stone formulation had a moisture content value of 25.90% that supports the increase in permeable pore space when compared to the HGM-5 specimen with a moisture content of 15.64%.

**Table 5-2.** Density Measurements for Neat Grout Specimens

Formulation		Cast Stone	HGM-5	Variable in ASTM C642-13
Test Batch		2	1	
Specimen		3	3	
Initial Specimen Mass	g	179.6039	216.8059	
Mass of Oven-Dried Sample in Air	g	133.0886	182.9029	A
Moisture Content	%	25.90	15.64	
Mass of Surface-Dry Sample in Air After Immersion	g	179.3828	219.7850	B
Mass of Surface-Dry Sample in Air After Immersion and Boiling	g	179.9852	220.28	C
Specimen Volume	cm <sup>3</sup>	99.31	109.97	
Apparent Mass of Sample in Water After Immersion and Boiling	g	80.67	110.31	D
Bulk Density, Dry	g/cm <sup>3</sup>	1.34	1.66	g <sub>1</sub>
Bulk Density after Immersion	g/cm <sup>3</sup>	1.81	2.00	
Bulk Density after Immersion and Boiling	g/cm <sup>3</sup>	1.81	2.00	
Apparent Density	g/cm <sup>3</sup>	2.54	2.52	g <sub>2</sub>
Volume of Permeable Pore Space (voids)	%	47.22	33.99	

### 5.3 Saturated Hydraulic Conductivity

Hydraulic conductivity is a coefficient used to describe the ease with which a fluid can be transmitted through a porous matrix. Typically, the fluid measured is water and the fluid properties such as density, viscosity, and surface tension can influence how a fluid is transmitted. The coefficient K depends on the geometry of porous media, where large connected pores transmit water rapidly and small, poorly connected pores transmit water slowly. Because of the degree of water saturation can also influence the value for K, it is typical to use the measurement of K under hydraulically saturated conditions ( $K_{sat}$ ) to allow for objective comparison of samples.

The  $K_{sat}$  results from FY18 for each neat specimen evaluated are provided in **Table 5-3Error! Reference source not found.**, including the initial, final, and average  $K_{sat}$  values. The measured average  $K_{sat}$  for the HGM-5 neat samples was  $2.8 \times 10^{-9} \text{ cm s}^{-1}$  and  $1.8 \times 10^{-9} \text{ cm s}^{-1}$ . These values are slightly higher than the previously reported HGM-5  $K_{sat}$  value of  $< 4.0 \times 10^{-10} \text{ cm s}^{-1}$  (Nichols et al. 2017). In the neat Cast Stone specimens, the average  $K_{sat}$  value was  $2.1 \times 10^{-9} \text{ cm s}^{-1}$  and  $1.8 \times 10^{-10} \text{ cm s}^{-1}$ .

In the initial analysis in Rev.0 of this report high  $K_{sat}$  values were measured on two samples containing 30 vol% GAC in Cast Stone ( $\sim 10^{-5} \text{ cm s}^{-1}$ ) and HGM-5 of ( $\sim 10^{-6} \text{ cm s}^{-1}$ ) as compared with the neat mixes. Additional samples were prepared in FY20 to determine the influence of decreasing GAC content on  $K_{sat}$  and from the addition of Ag-M. It was observed that lower  $K_{sat}$  values were measured for the FY20 samples that aligned more with the neat mixes measuring a range between  $(5.7 \pm 3.9) \times 10^{-9} \text{ cm/s}$  –  $(5.8 \pm 2.8) \times 10^{-10} \text{ cm/s}$ , Table 5-3. Samples from FY18 was re-run after  $\sim 2$  years of leaching and the measured  $K_{sat}$  was in line with the FY20 values (sample 30% GAC Leach for both HGM-5 and Cast Stone). Updated batches at 30% GAC were also similar to the neat mixes. Analysis of Ag-M containing HGM-3

and HGM-5 also showed comparable  $K_{sat}$  values to the FY20 dataset. The FY18 values are therefore superseded by the updated measurements in Table 5-3. The origin of the discrepancy is unknown.

The  $K_{sat}$  measured for the neat HGM-3 was lower than reported by Nichols et al (2017). However, this difference is likely a direct result of the use of dry sand in this work compared to a moist sand with unknown water content, which would increase pore space.

Finally, due to some of the low  $K_{sat}$  values measured here, future  $K_{sat}$  measurements on similar high-performing materials might consider the procedure modifications suggested in ASTM D5084-16a for specimens with  $K_{sat}$  values lower than  $1 \times 10^{-9} \text{ cm s}^{-1}$  ( $1 \times 10^{-11} \text{ m s}^{-1}$ ), the recommended lower limit of the ASTM D5084-16a procedure. This is common in waste immobilization grouts. A standard test method for waste grouts should be specified and defined to ensure consistency moving forward. The ASTM D5084-16a procedure should also be updated to include a precision and bias statement relevant to immobilization and barrier cementitious materials.

**Table 5-3** – Prior FY18 neat mix  $K_{sat}$  values and the average  $K_{sat}$  values from FY20 determined from the average of all sample intervals measured along with the lowest and highest  $K_{sat}$  measured at individual intervals.

<b>FY18 Neat Mix Data</b>					
<b>Formulation</b>	<b>SSW Component Loading (vol %)</b>	<b>Test Time (d)</b>	<b>Hydraulic Conductivity</b>		
			<b>Initial</b>	<b>Final</b>	<b>Average</b>
			<b>(cm s<sup>-1</sup>)</b>	<b>(cm s<sup>-1</sup>)</b>	<b>(cm s<sup>-1</sup>)</b>
Cast Stone	N/A	7	$9.8 \times 10^{-10}$	$1.9 \times 10^{-9}$	$2.1 \times 10^{-9}$
Cast Stone	N/A	12	$1.4 \times 10^{-10}$	$2.1 \times 10^{-10}$	$1.8 \times 10^{-10}$
HGM-5	N/A	7	$3.4 \times 10^{-9}$	$1.7 \times 10^{-9}$	$2.8 \times 10^{-9}$
HGM-5	N/A	9	$1.3 \times 10^{-9}$	$1.9 \times 10^{-9}$	$1.8 \times 10^{-9}$
<b>FY20 Updated Results</b>					
<b>Formulation</b>	<b>SSW Component Loading (vol%)</b>	<b>Test Time (d)</b>	<b>Hydraulic Conductivity (<math>K_{sat}</math>)</b>		
			<b>Low</b>	<b>High</b>	<b>Average (cm s<sup>-1</sup>)</b>
			<b>(cm s<sup>-1</sup>)</b>	<b>(cm s<sup>-1</sup>)</b>	
HGM-5	30% GAC	14	$1.3 \times 10^{-10}$	$3.8 \times 10^{-9}$	$(2.4 \pm 1.0) \times 10^{-9}$
HGM-5	30% GAC Leach	9	$5.4 \times 10^{-10}$	$6.4 \times 10^{-9}$	$(3.1 \pm 1.9) \times 10^{-9}$
HGM-5	15% GAC	10	$1.1 \times 10^{-9}$	$5.9 \times 10^{-9}$	$(2.9 \pm 1.4) \times 10^{-9}$
HGM-5	10% GAC	4	$4.9 \times 10^{-10}$	$7.3 \times 10^{-10}$	$(6.2 \pm 1.2) \times 10^{-10}$
HGM-5	7.5% GAC	16	$3.6 \times 10^{-10}$	$6.0 \times 10^{-9}$	$(3.4 \pm 2.0) \times 10^{-9}$
HGM-5	1% GAC	4	$2.4 \times 10^{-10}$	$1.9 \times 10^{-9}$	$(1.1 \pm 0.8) \times 10^{-9}$
HGM-3	N/A	5 – 10	$2.5 \times 10^{-10}$	$1.2 \times 10^{-9}$	$(5.8 \pm 2.8) \times 10^{-10}$
HGM-3	30% GAC	6	$2.9 \times 10^{-10}$	$2.0 \times 10^{-9}$	$(1.2 \pm 0.5) \times 10^{-9}$
HGM-3	10% GAC	3 – 7	$1.6 \times 10^{-10}$	$1.7 \times 10^{-9}$	$(8.1 \pm 4.8) \times 10^{-10}$
HGM-3	7.5% GAC	12	$2.1 \times 10^{-10}$	$3.2 \times 10^{-9}$	$(1.8 \pm 0.8) \times 10^{-9}$
HGM-3	1% GAC	2 - 7	$7.7 \times 10^{-11}$	$1.9 \times 10^{-9}$	$(1.0 \pm 0.7) \times 10^{-9}$
Cast Stone	30% GAC Leach	13	$7.5 \times 10^{-10}$	$3.8 \times 10^{-9}$	$(2.5 \pm 0.9) \times 10^{-9}$
HGM-3	15% AgM	12	$1.1 \times 10^{-10}$	$1.1 \times 10^{-9}$	$(6.9 \pm 2.5) \times 10^{-10}$
HGM-5	15% AgM	20	$6.8 \times 10^{-10}$	$1.2 \times 10^{-8}$	$(5.7 \pm 3.9) \times 10^{-9}$

The influence of using a higher  $K_{sat}$  value for a grout waste form inventory in the IDF is expected to be minimal and two cases exist to support this hypothesis. In the 2017 IDF PA (USDOE 2018), the  $K_{sat}$  was varied in a sensitivity case for SSW with values ranging from  $1.7 \times 10^{-9}$  cm/s up to  $3.6 \times 10^{-8}$  cm/s (see Section 5.1.3.3 of the 2017 IDF PA). As quoted from the PA “*the effect of  $K_{sat}$  range is relatively small, indicating diffusion-dominated release*”. A series of simulations were also performed in FY19 related to the release of contaminants from a grouted supplemental low-activity waste inventory in the IDF where

the  $K_{sat}$  was varied from  $1.5 \times 10^{-9}$  cm/s up to  $1 \times 10^{-5}$  cm/s (see Table 3-3 of Asmussen et al. 2019). Despite the orders of magnitude increase in  $K_{sat}$  included, the total iodine release from the IDF (the contaminant tracked in the simulation) only increased  $1.8 \times$ . Therefore,  $K_{sat}$  values in sensitivity cases are not expected to impact PA simulation and the representation of an immobilized SSW inventory will use the values in Table 5-3 and the probability ranges from the SSW data package.

## 5.4 Water Characteristic Curve and van Genuchten Parameters

Water characteristic curves provide information which relates to the geometry of porous matrix. The pore diameters and their connectivity determine the shape of each curve. Experimental data was modeled with the van Genuchten functional form (van Genuchten 1980) using RETC software (van Genuchten 1991; Table 5-4, Figure 5-1):

$$S_e = \left[ \frac{1}{1+(\alpha h)^n} \right]^{(1-1/n)} \quad [5.1]$$

$$S_e = \frac{\theta_v - \theta_r}{\theta_s - \theta_r} \quad [5.2]$$

where:

$S_e$  = normalized water content (dimensionless);

$\alpha$  = model coefficient related to inverse of air entry pressure ( $\text{cm}^{-1}$  water);

$h$  = pressure head (cm water);

$n$  = model coefficient related to pore size distribution (dimensionless);

$\theta_v$  = volumetric water content ( $\text{cm}^3 \text{ cm}^{-3}$ );

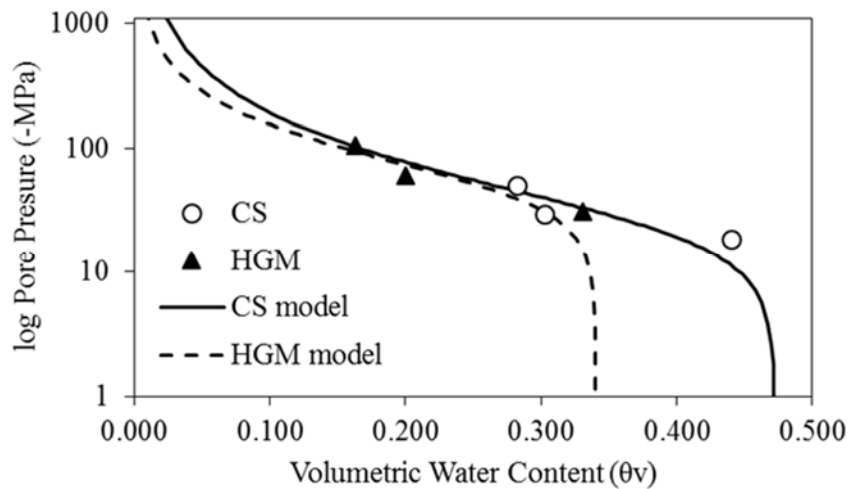
$\theta_r$  = residual water content ( $\text{cm}^3 \text{ cm}^{-3}$ );

$\theta_s$  = saturated water content ( $\text{cm}^3 \text{ cm}^{-3}$ ).

Based on empirical formulas (Jury and Horton 2004), pressures can be related to pore diameters of the porous matrix measured producing an estimated pore diameters 3 to 300 nm from the pressures measured ranging from -100 to -1 MPa. The larger well-connected pores drain first, followed by increasingly smaller and less well-connected pores. Initial air entry occurs at the point when the volumetric water content is less than 1.0, which occurs below -10 MPa for both the HGM-5 (Test Batch 1) and Cast Stone (Test Batch 2) material (Figure 5.1). As water continues to drain, smaller pores require more energy to overcome capillary forces and drain. The air entry and slope of water characteristic curves (Figure 5.1) of both materials are similar, which is reflected in similarities of their hydraulic conductivities (Table 5.3). The model coefficients derived from the model were similar to comparative analyses from Nichols et al. (2018; Table 5-4). The coefficient “n” is generally larger for a matrix with narrower pore size distributions. From these tests it is notable that the Cast Stone has a wider pore size distribution than HGM-5 (Table 5-4) but it also has higher measured porosity (Table 5.2). This higher porosity may represent poorly connected larger voids in the Cast Stone sample measured compared to the HGM-5 sample (Table 5-2). The van Genuchten parameters were also measured for a HGM-5 sample containing 30 vol% GAC and the neat GAC material. The addition of GAC to the HGM led to lower van Genuchten parameters ( $\alpha, n$ ) to the neat HGM-5.

**Table 5-4.** van Genuchten Functional Form Model Parameters and Model Fit Coefficient

Sample ID	$\theta_s$	$\theta_r$	$\alpha$	$n$	Model fit ( $r^2$ )
Cast Stone	0.4722	0	$<10^{-5}$	1.82642	0.87
HGM	0.3399	0	$<10^{-5}$	2.20099	0.92
HGM with 30% GAC	0.38792	0	0.00002	1.28931	0.90
GAC	0.5	0	0.00017	1.36624	0.93

**Figure 5-1** - Plot of Water Characteristic Data and Model for Cast Stone and HGM-5

## 5.5 Mineralogy

XRD patterns were collected for Test Batch 2 (Cast Stone, Figure 5-2), Test Batch 1 (HGM-5, Figure 5-3 XRD Pattern Collected for a Bulk Specimen Collected from Neat HGM-5 Monolith from Test Batch 1) and HGM-3 (**Figure 5-4**) to determine their mineralogical composition after curing for 28 days. From the XRD patterns, both Cast Stone and HGM-5 formulations primarily consist of an amorphous phase, likely calcium-silica-hydrate (C-S-H), with Cast Stone producing ~ 10 wt % less amorphous material than HGM-5, 63.8 wt% vs. 74.3 wt% respectively. The remaining material consisted of crystalline mineral phases including portlandite [ $\text{Ca}(\text{OH})_2$ ], ettringite [ $\text{Ca}_6\text{Al}_2(\text{SO}_4)_3(\text{OH})_{12} \cdot 26\text{H}_2\text{O}$ ], calcite [ $\text{CaCO}_3$ ], larnite [ $\text{Ca}_2\text{SiO}_4$ ], hydrocalumite [ $\text{Ca}_2\text{Al}(\text{OH})_7 \cdot 3\text{H}_2\text{O}$ ], and quartz [ $\text{SiO}_2$ ]. The presence of rutile/anatase [ $\text{TiO}_2$ ] is due to the internal  $\text{TiO}_2$  standard added before XRD analysis and is included for the purpose of determining the relative weight percent of each mineral phase. The HGM-3 contained higher amounts of portlandite and ettringite likely due to the higher OPC ratio in the slurry.

Between the Cast Stone and HGM-5 formulations, similar mineralogical fractions were determined for ettringite (3.1 – 3.7 wt%) and hydrocalumite (1.3 – 1.6 wt %) phases. However, the differences in calcite, larnite, quartz, and possibly portlandite fractions, all of which contain primarily Ca and Si, are likely influenced by the production of the C-S-H amorphous phase. With more C-S-H produced in the HGM-5 specimen, fewer resources remain to produce crystalline phases.

**Table 5-5.** Bulk Mineralogical Composition of Neat Cast Stone and HGM-5 Formulations Determined by XRD

Sample	Portlandite	Ettringite	Calcite	Larnite	Hydrocalumite	Quartz	Rutile + Anatase (Internal Standard)	Amorph. [e.g., C-S-H]	Other Minor Phases
	wt %	wt %	wt %	wt %	wt %	wt %	wt %	wt %	wt%
Cast Stone (Test Batch 2)	2.3	3.7	1.4	6.3	1.3	7.5	13.0 + 0.7	63.8	-
HGM-5 (Test Batch 1)	-	3.1	4.5	4.0	1.6	3.4	8.7 + 0.4	74.3	-
HGM-3	7.0	16.7	2.4	-	-	10.6	8.1	43.8	11.4

Portlandite,  $\text{Ca}(\text{OH})_2$ ; Ettringite,  $\text{Ca}_6\text{Al}_2(\text{SO}_4)_3(\text{OH})_{12} \cdot 26\text{H}_2\text{O}$ ; Calcite,  $\text{CaCO}_3$ ; Larnite,  $\text{Ca}_2\text{SiO}_4$ ; Hydrocalumite,  $\text{Ca}_2\text{Al}(\text{OH})_7 \cdot 3\text{H}_2\text{O}$ ; Quartz,  $\text{SiO}_2$ ; Rutile + Anatase (Internal Standard),  $\text{TiO}_2$ .

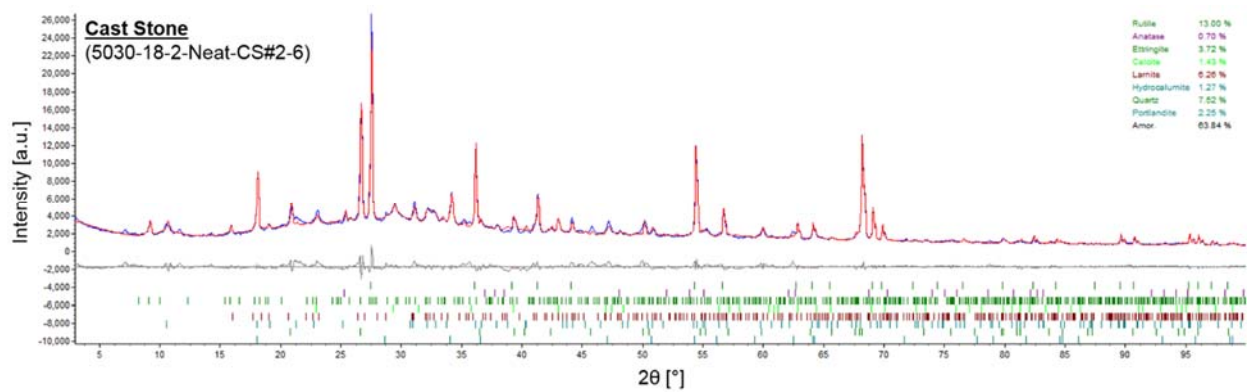


**Figure 5-2** XRD Pattern Collected for a Bulk Specimen Collected from Neat Cast Stone Monolith from Test Batch 2

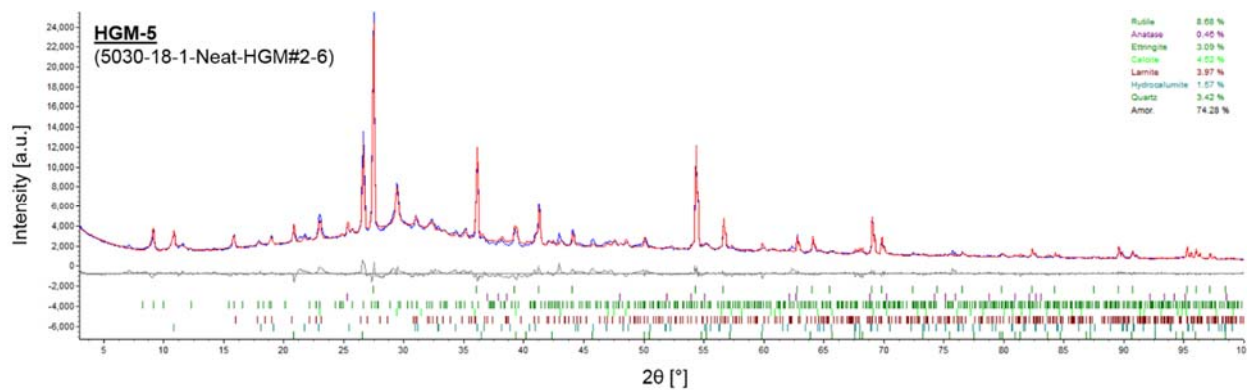


**Figure 5-3** XRD Pattern Collected for a Bulk Specimen Collected from Neat HGM-5 Monolith from Test Batch 1

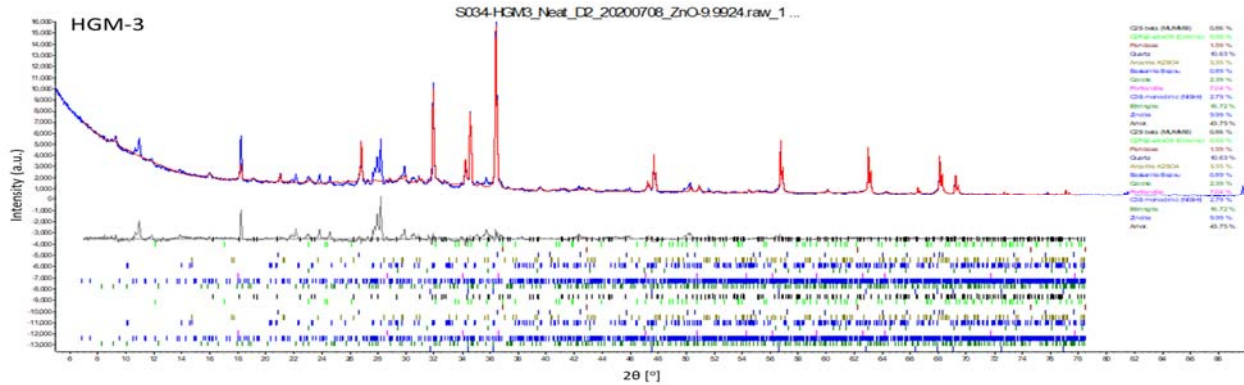


**Figure 5-4** XRD Pattern Collected for a Bulk Specimen Collected from Neat HGM-3

## 5.6 X-Ray Imaging and Microscopy

### 5.6.1 X-ray Computed Tomography

X-ray computed tomography (XCT) was used to determine the distribution of AgM and GAC particles dispersed within cured Cast Stone and HGM-5 samples from test batches 3 through 6 following EPA Method 1315 leach testing in DIW (Figure 5-5) and the cured HGM-3 samples containing GAC and AgM. All mixes were able to suspend and distribute the GAC and AgM within the hardened grout matrix. The larger GAC particles showed some heterogeneity in their distribution and in the Cast Stone specimen a higher number of particles were visible near the top of the monolith.

The XCT volume data collected for select specimens were cropped to rectangular sub-sections with an approximate volume of 77,000 mm<sup>3</sup>, and segmented for two components, cement matrix and AgM or GAC inclusions, depending on sample (Figure 5-6). These segmented volumes were used to calculate the fraction of cement and SSW material. The results of these measurements (FOR INFORMATION PURPOSES ONLY, this analysis is considered qualitative and has not met QA requirements for use as a quantitative measurement) are summarized in Table 5-6. For Cast Stone, HGM-5 and HGM-3 specimens containing GAC particles, the distribution of cement (0.78 – 0.79 v/v) and GAC (0.21 and 0.24 v/v) volume fractions are nearly identical. Similarly, for AgM immobilized using Cast Stone and HGM-5, cement accounts for 0.74 v/v of the specimen analyzed and AgM accounts for the rest, 0.26 v/v, on both formulations studied.

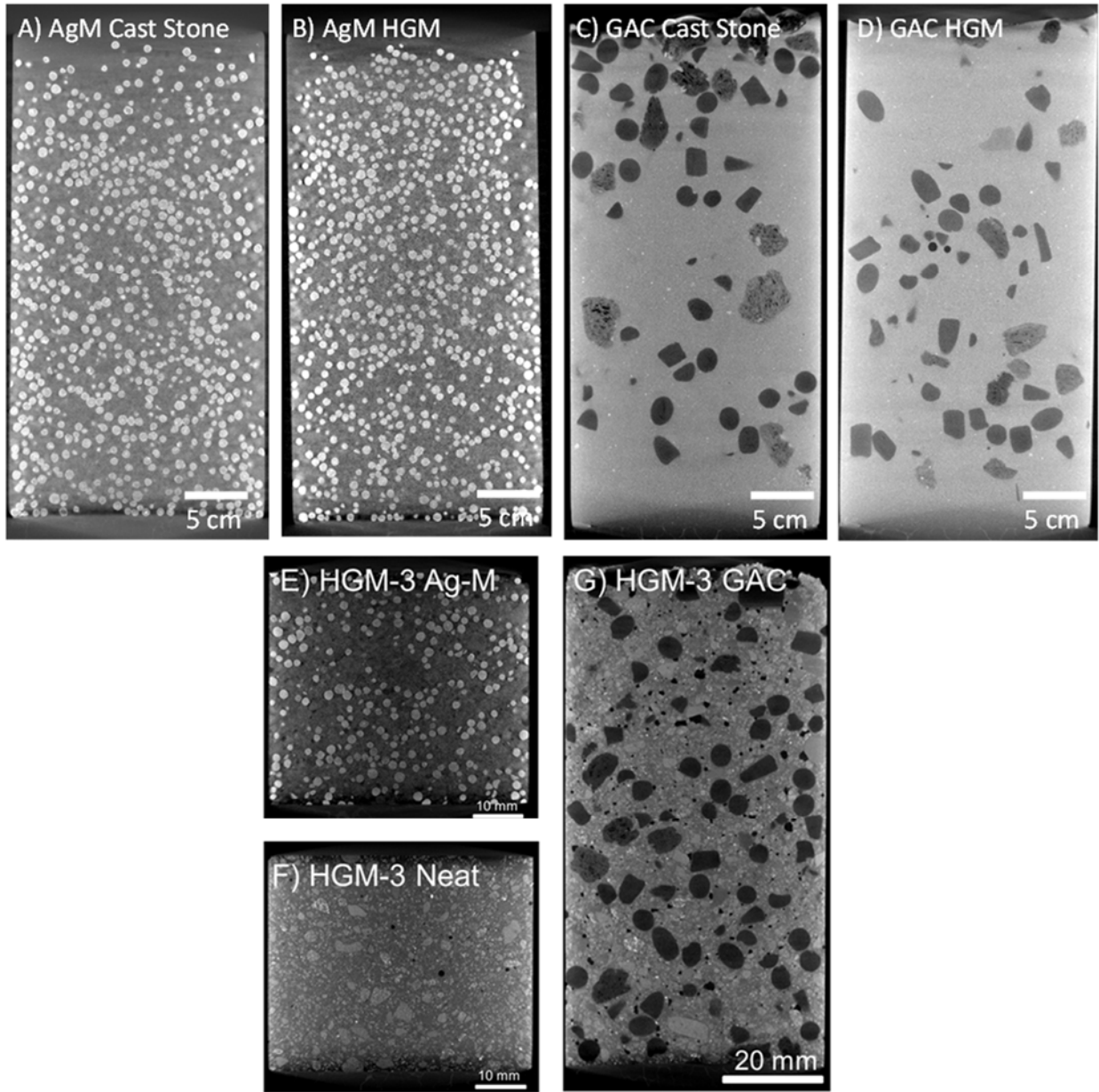


**Figure 5-5** XCT Micrographs of the AgM and GAC in Cast Stone, HGM-5 and HGM-3 showing the distribution of these particles.

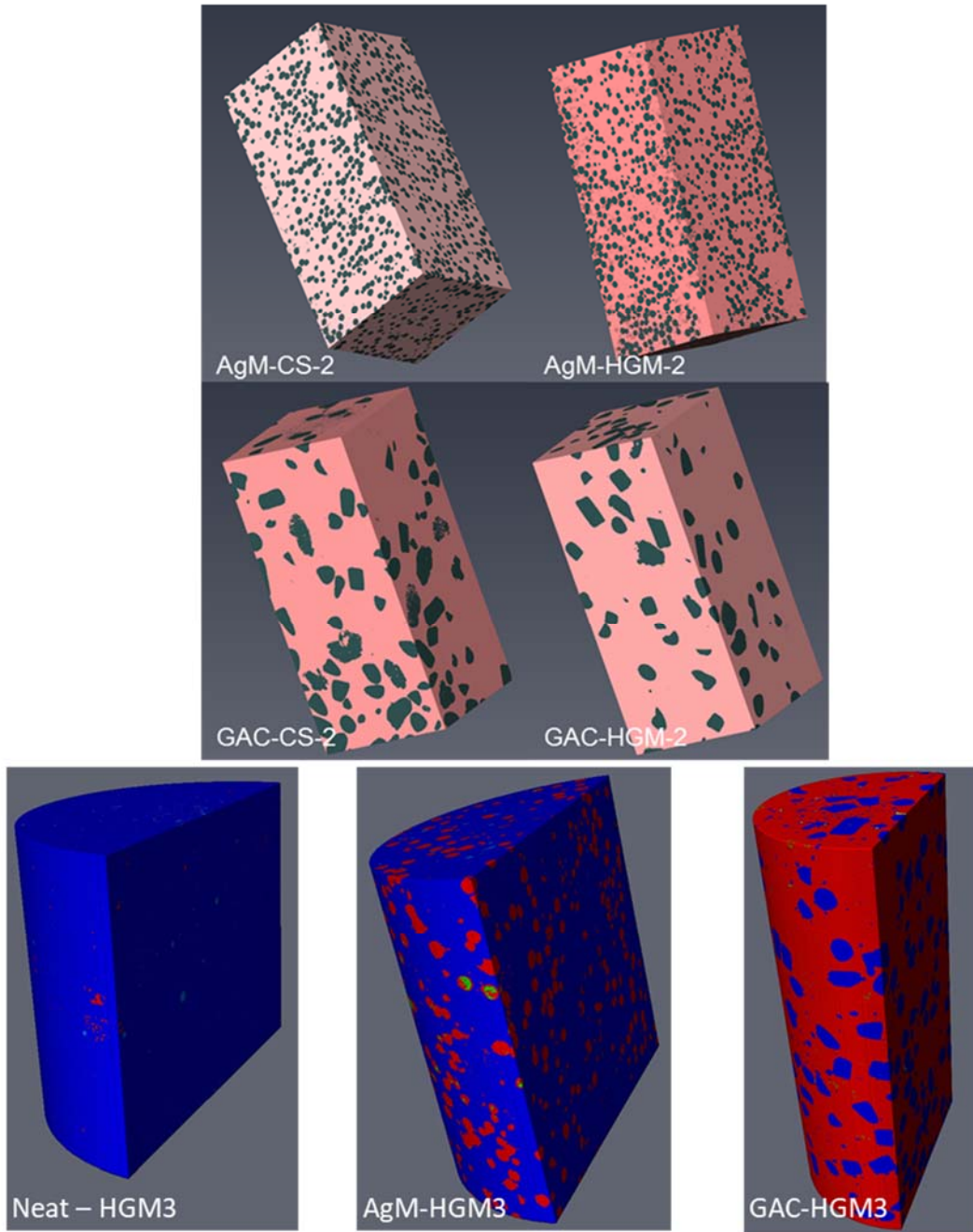


**Figure 5-6** - Rendered 3D XCT images of Cast Stone, HGM-5 and HGM-3 formulation sub-sections containing AgM and GAC particles. Images used to calculate volume fractions of the cement and SSW components.

**Table 5-6.** Volume Fraction of AgM and GAC in CWF Specimens as Determined by XCT\*

Sample	SSW Material	Formulation	Leachant	Cement Volume Fraction	AgM/GAC Volume Fraction
Test Batch 6	AgM	Cast Stone	DIW	0.74	0.26
Test Batch 5	AgM	HGM-5	DIW	0.74	0.26
Test Batch 4	GAC	Cast Stone	DIW	0.78	0.21
Test Batch 3	GAC	HGM-5	DIW	0.79	0.21
HGM3-GAC-30	GAC	HGM-3	N/A	0.74	0.24
HGM3-AgM-15	AgM	HGM-3	N/A	0.83	0.16
HGM3-Neat	N/A	HGM-3	N/A	0.99	N/A

\*For information purposes only

Cement and SSW Material fractions were determined from a 77,000 mm<sup>3</sup> sub-section of each specimen.

### 5.6.2 Optical Microscopy

Optical images of the HGM-5 and Cast Stone samples containing GAC/AgM were obtained. The images below show the neat HGM-5 grout material (Figure 5-7 a) as well as the HGM-5 with GAC (Figure 5-7 b), AgM (Figure 5-7 c) and a magnified view of the AgM (Figure 5-8 d). The AgM particles appeared to have reaction rings around the AgM particles. In the magnified view, a region of metallic-appearance material can be seen, possibly Ag.

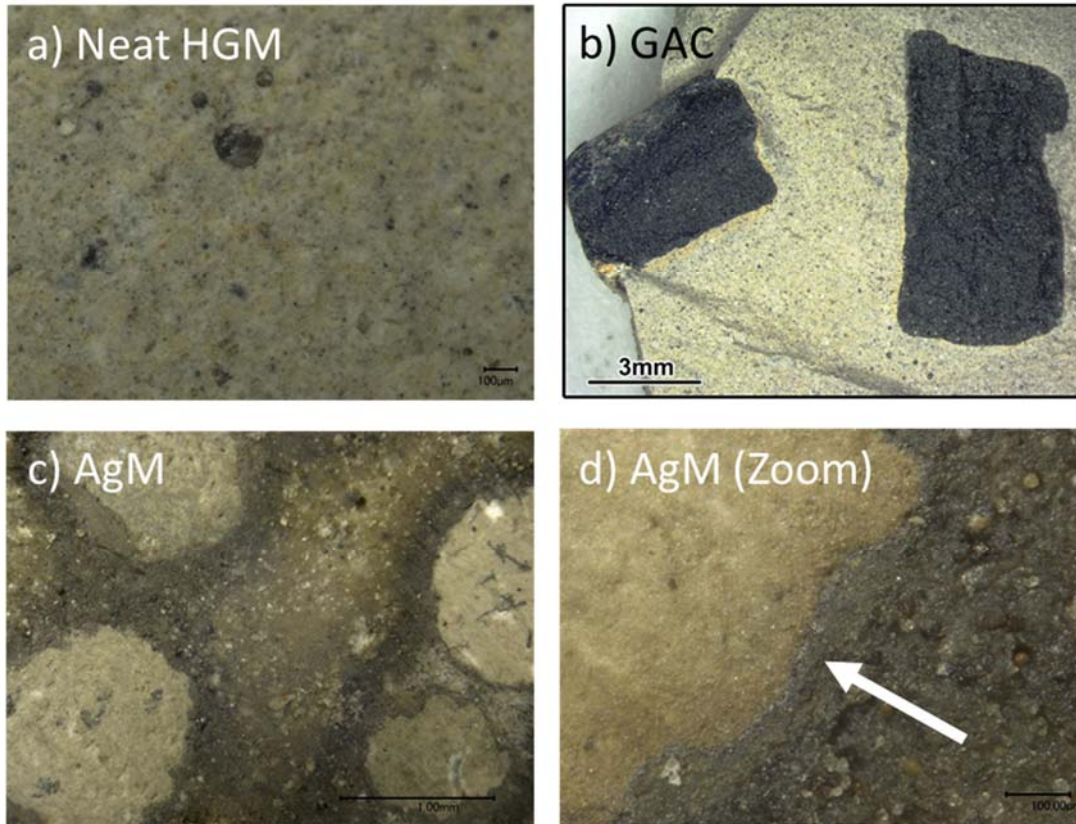


**Figure 5-7** - Optical images of HGM-5 a) Test Batch 1 the neat grout, b) Test Batch 3 with GAC added, c) Test Batch 5 with AgM added and d) magnified view of the image in c). The white arrow indicating a possible region of Ag.

The Cast Stone stabilized samples from test batches 2, 4 and 6 were also imaged and shown in . There appeared to be good adhesion between the hardened grout matrix and the particles for both the GAC (Figure 5-8 - Optical images of Cast Stone a) Test Batch 2 the neat grout, b) Test Batch 4 with GAC added, c) Test Batch 6 with AgM added b) and for the AgM, (Figure 5-8 c). A reaction ring was again observed around the AgM particles.

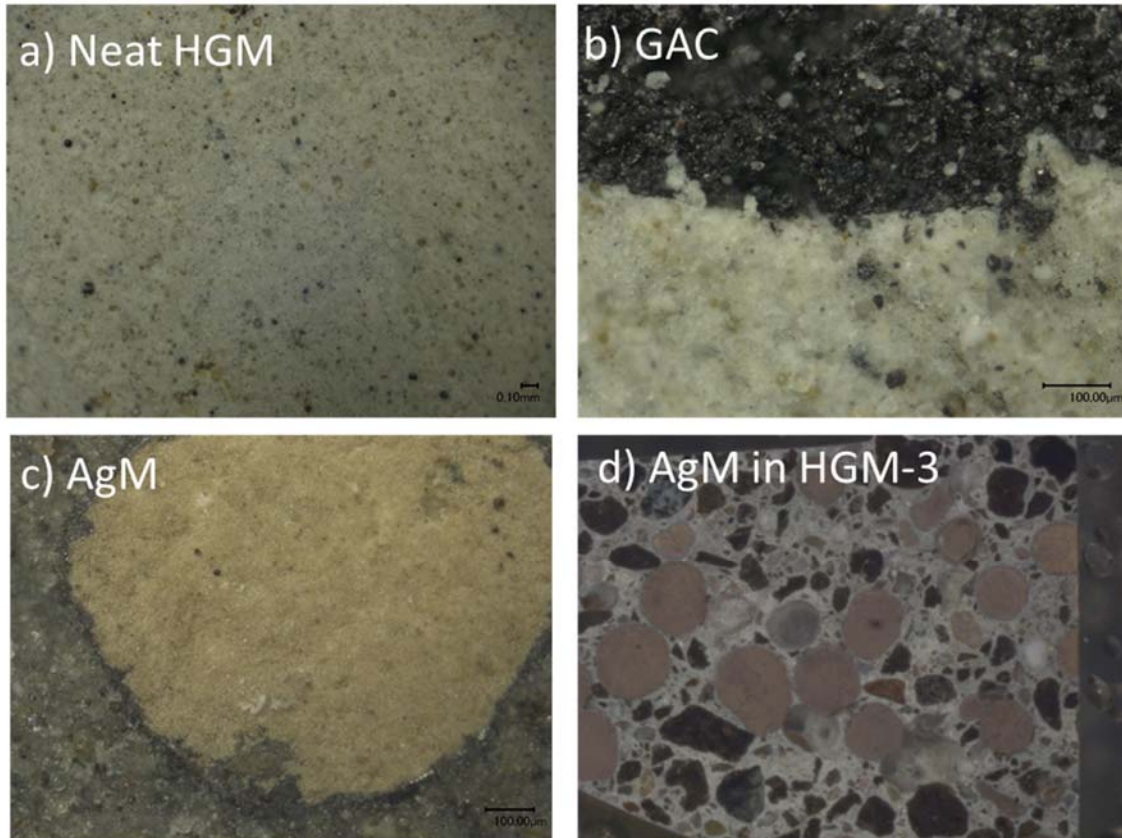


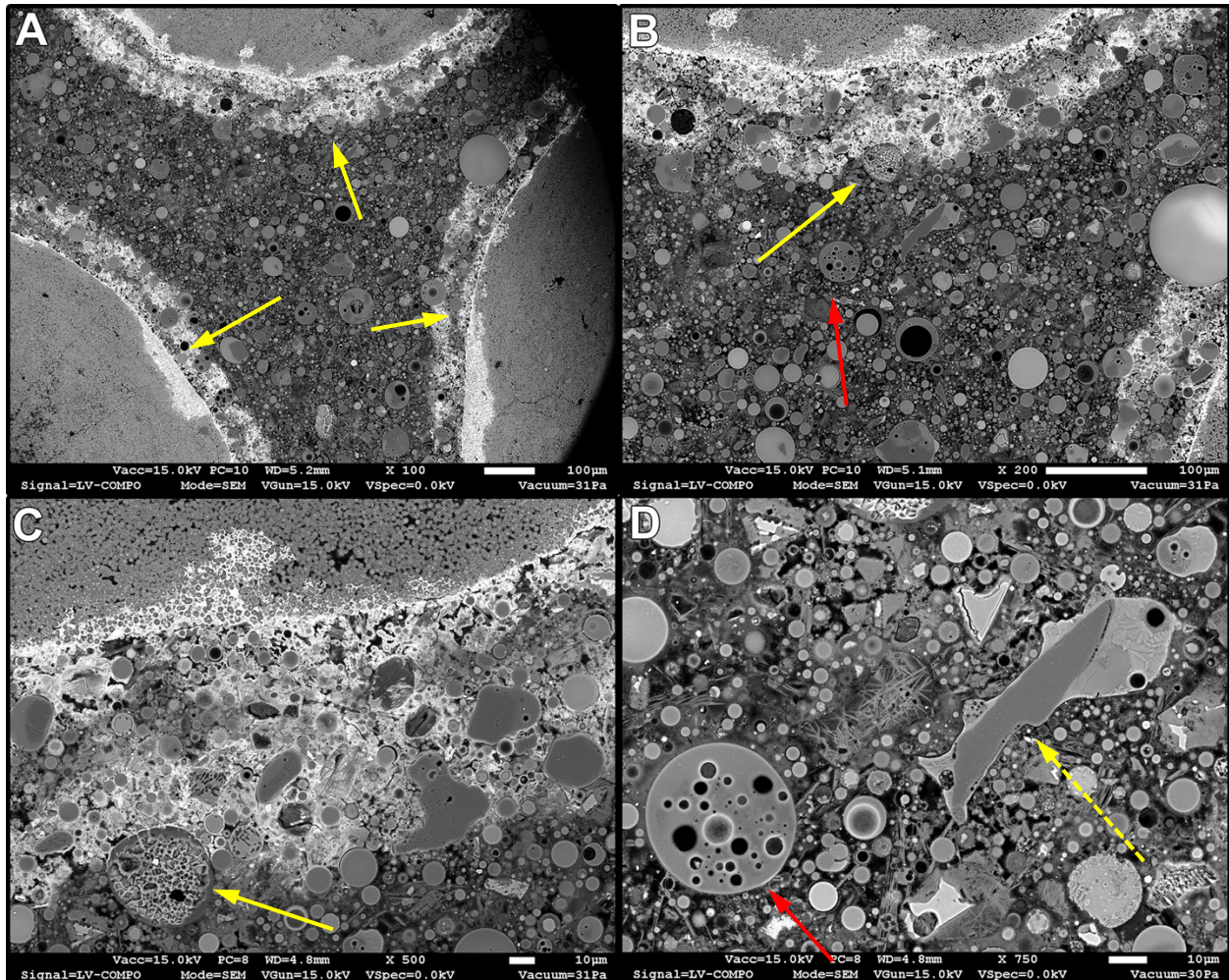
**Figure 5-8** - Optical images of Cast Stone a) Test Batch 2 the neat grout, b) Test Batch 4 with GAC added, c) Test Batch 6 with AgM added and d) HGM-3 with AgM added

### 5.6.3 SEM/EDS

SEM/EDS were used to analyze the interface between the GAC/AgM and the hardened matrix of their host waste form. As the interface between the particle and the hardened grout matrix is the first region of migration of potential contaminants, identifying the final nature of this interface can help direct formulation selection.

#### 5.6.3.1 Stabilized Silver Mordenite

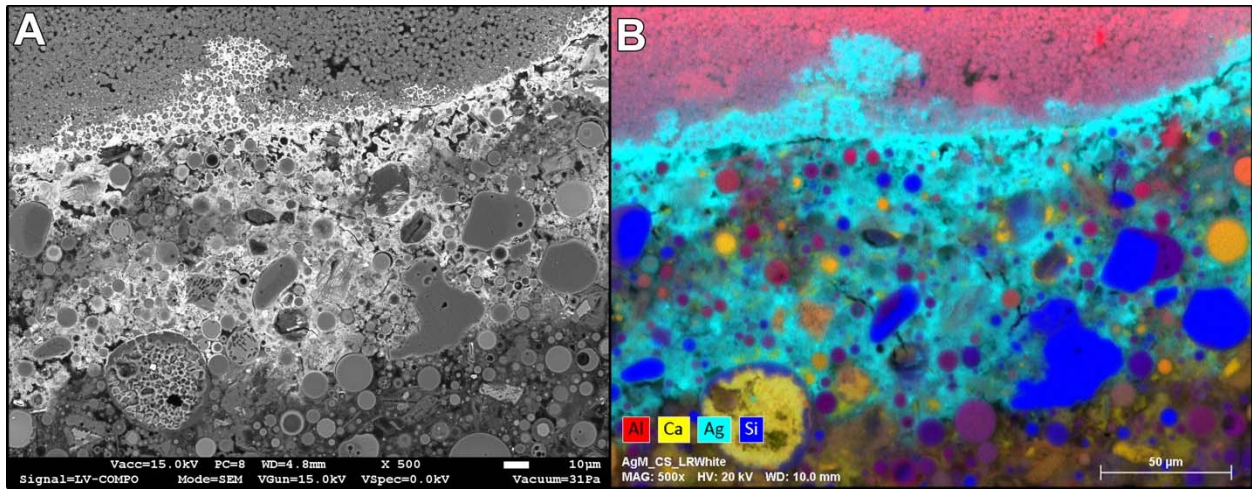
The interaction between AgM and the two cured grout matrices was examined by analyzing polished cross-section specimens using SEM and EDS. The specimens were prepared by vacuum impregnating them with a low-viscosity epoxy (L.R. White hard resin). After curing, the specimens were polished with SiC papers and diamond suspensions with successively finer abrasives. Specific regions of interest were the interface between the AgM granules and the hardened grout matrix, as well as the hydrating particles of OPC, FA and BFS. The major finding in both systems was that a layer of Ag was observed at the interface between the AgM and the hardened paste, which may serve as a barrier for iodine migration. Ag is a RCRA-listed element and its release needs to be minimal. This Ag inventory was not observed to be present in the hardened paste beyond the Ag-layer, thus its migration from the waste form may be limited.



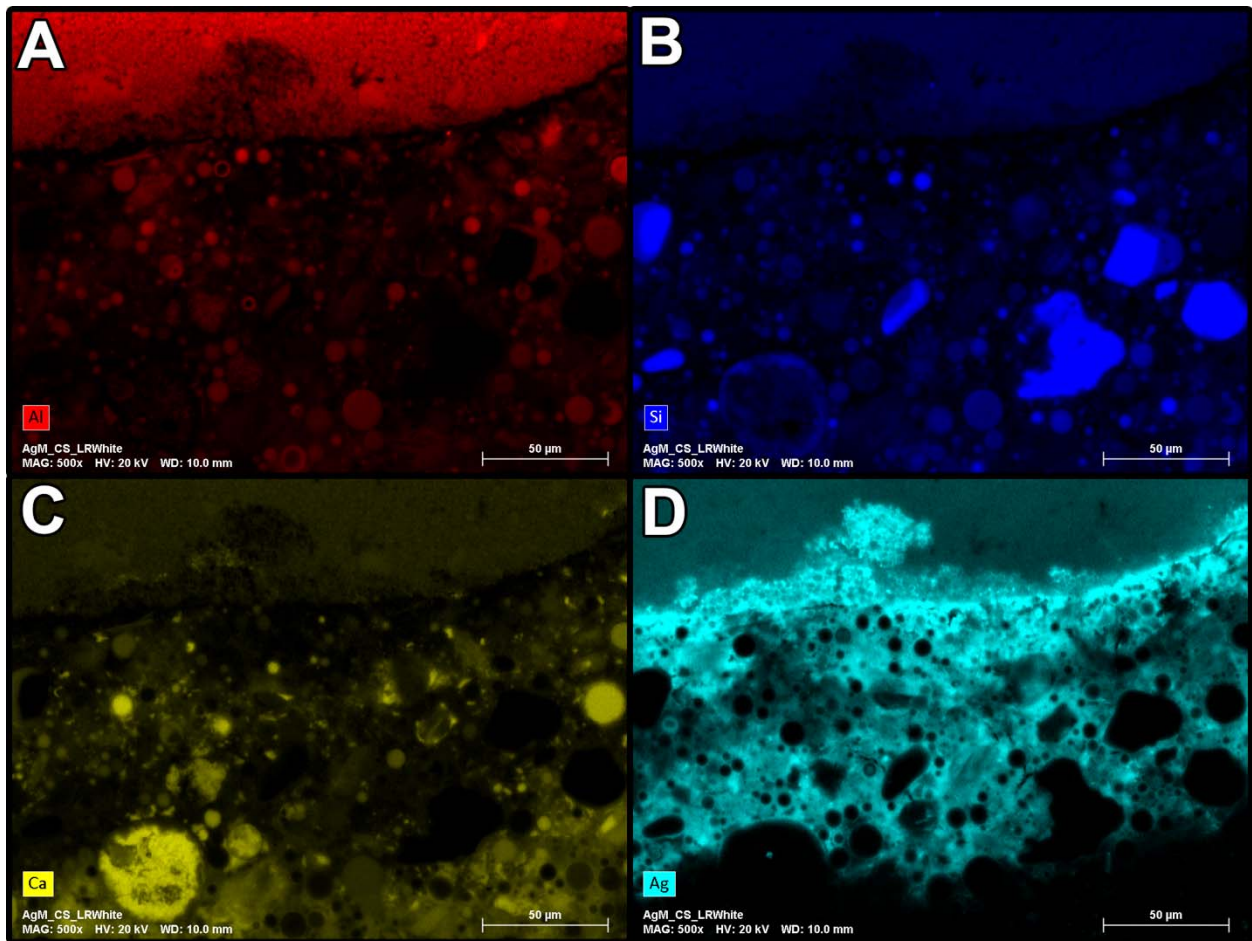
**Figure 5-9** - Collage of SEM BSE micrographs of AgM granules (arrowed) in the Cast Stone Matrix from Test Batch 6. Successively higher magnifications of the AgM-Cast Stone interface are shown in A-C; D is a higher magnification micrograph of the Cast Stone matrix; the red arrow points to a spherical fly ash particle (imaged in both panel B and D) and the dashed arrow to a slag particle.

Figure 5-9 is a collage of related micrographs showing the microstructure of a sample taken from test batch 6 with the AgM stabilized within hardened Cast Stone matrix. The three large, round, light-gray structures at the perimeter of Figure 5-9 A are AgM granules. The micrographs were taken in BSE mode, where brightness is a function of average atomic number. The porous circular feature that was arrowed in Figure 5-9 B and D is a fly ash particle, and the angular particle pointed out by the dashed arrow in Figure 5-9 D is a slag particle. The bright region around the AgM particles correlated to the reaction ring observed in the optical images, in Figure 5-7 c and Figure 5.9 c.

AgM in Cast Stone was examined using EDS to determine the spatial distribution of elements in the specimen at the AgM:hardened grout matrix interface. The BSE micrographs in Figure 5-10 show that there is substantial gray scale contrast in this region, indicating that there was a significant variation in composition. Thus, EDS was used to identify the elements present that were causing the variation in contrast.



**Figure 5-10** - SEM BSE (A) micrograph and elemental EDS dot map (B) showing the interface between an AgM granule and Cast Stone



**Figure 5-11** - SEM EDS elemental maps showing the spatial distributions of Al, Si, Ca, and Ag for AgM in Cast Stone. The intensity of the color is an indication of the relative concentration. (Note: The field of view is the same as shown in Figure 5.9)

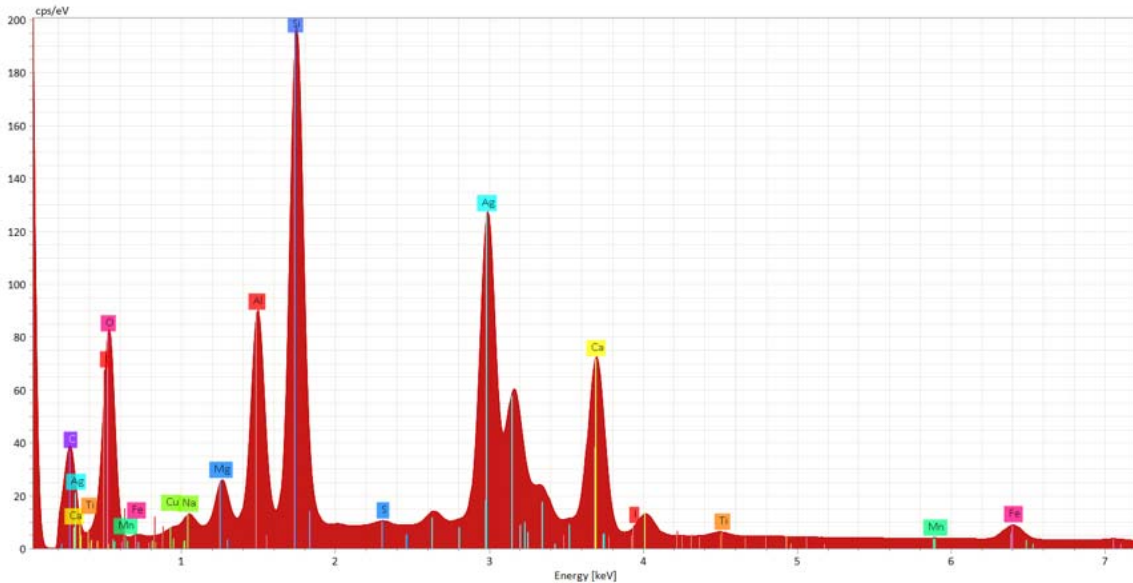


**Figure 5-12** - EDS sum spectrum of AgM in Cast Stone extracted from the EDS dot map in Figure 5.10 B

Figure 5-10 shows an SEM BSE micrograph and the corresponding EDS elemental dot map of the same region. Individual elemental maps from this region are shown in Figure 5-11. The sum spectrum obtained by summing the individual EDS spectra at each pixel is shown in Figure 5-12. Thus, in Figure 5-11 B, areas that are bright blue have a high Si content (e.g., probably fly ash). The brighter white features at the interface of the AgM granule and the Cast Stone matrix in Figure 5-10 A correlates to the cyan colored area for Ag in Figure 5-10 B. Thus, the EDS analysis showed that the Ag from the AgM granule had migrated into the adjacent matrix, possibly from the AgM partaking in hydration reactions. The reaction front observed near the AgM is similar to the hydration rings around fly ash particles from the same sample, shown in Figure 5-13.

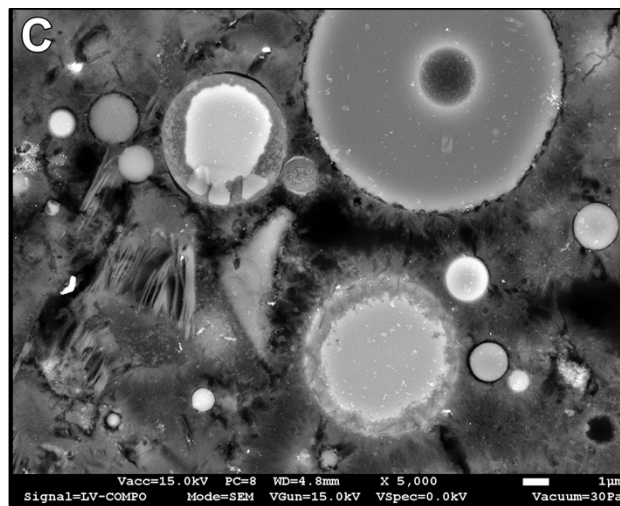


**Figure 5-13** - SEM BSE micrograph of fly ash particles in the AgM-Cast Stone sample from test batch 6 showing the hydration progress around the fly ash

AgM granules were also incorporated into HGM-5. This material was also examined by SEM and EDS to characterize its microstructure and microchemistry. Selected micrographs are shown in Figure 5-14. There were some differences in the microstructure of the AgM granules in HGM-5 as compared to AgM in Cast Stone. There did not appear to be as much diffusion of silver from the AgM granules into the

cement matrix in HGM-5 as compared to Cast Stone. This observation is based on the difference in the thickness of the white boundary area around the AgM granules in Figure 5-9 (Cast Stone) as compared to Figure 5-14 (HGM-5).

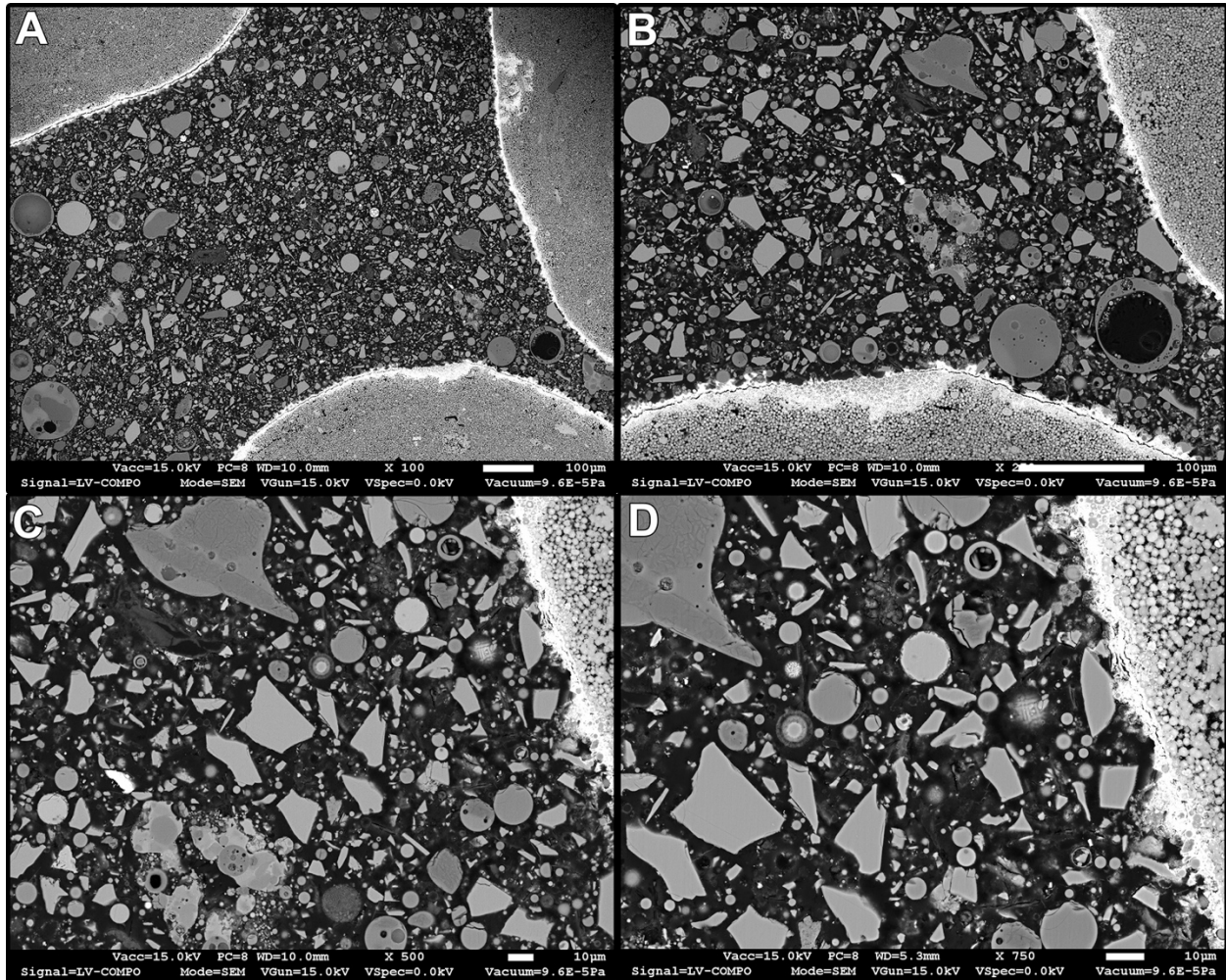


**Figure 5-14** - Collage of SEM BSE micrographs showing the same region with AgM particles (seen in the top, bottom and right of image A) in the cured HGM-5 Matrix at A) 100×, B) 250×, C) 500× and D) 750× magnification. The AgM granules are the very large light-gray features at the edges of the micrographs.

EDS analysis was done at the interface of an AgM granule and the HGM-5 matrix. The BSE micrograph and associated EDS elemental dot map is shown in Figure 5-15 and the individual elemental maps for Al, Si, Ca, and Ag are shown in Figure 5-16. The Ag once again was observed to migrate into the HGM-5 matrix, although not to the same extent as the Cast Stone. The analysis was done qualitatively, so it is not possible from this data set to make a quantitative comparison regarding the concentration of Ag in the granules for the two different specimens.

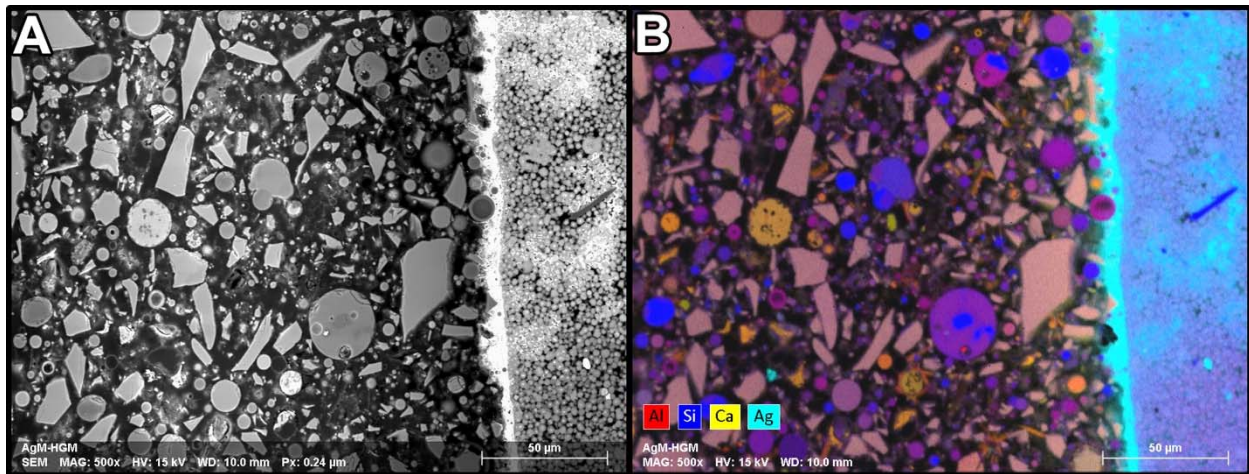


**Figure 5-15** - SEM BSE (A) and EDS elemental dot map (B) of an AgM granule in HGM-5 matrix

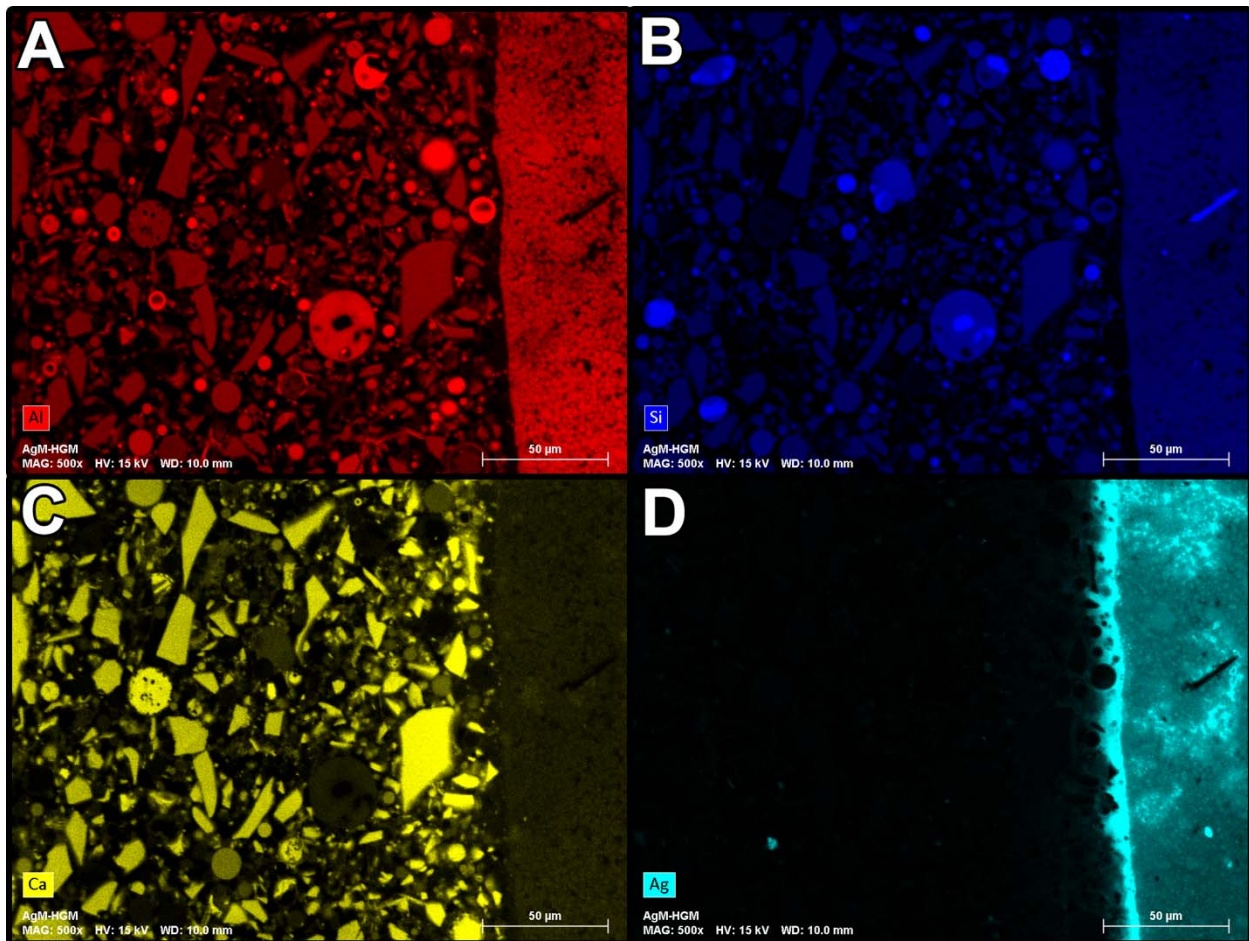


**Figure 5-16** - SEM EDS elemental maps showing the spatial distributions of Al, Si, Ca, and Ag for AgM in HGM-5. The intensity of the color is an indication of the relative concentration. (NOTE: The field of view is the same as shown in the Figure 5.14 EDS elemental dot map.

The sum spectrum from the EDS elemental dot map for AgM in HGM-5 is shown in Figure 5-17. The peak heights for the different elements show relative differences in concentration.

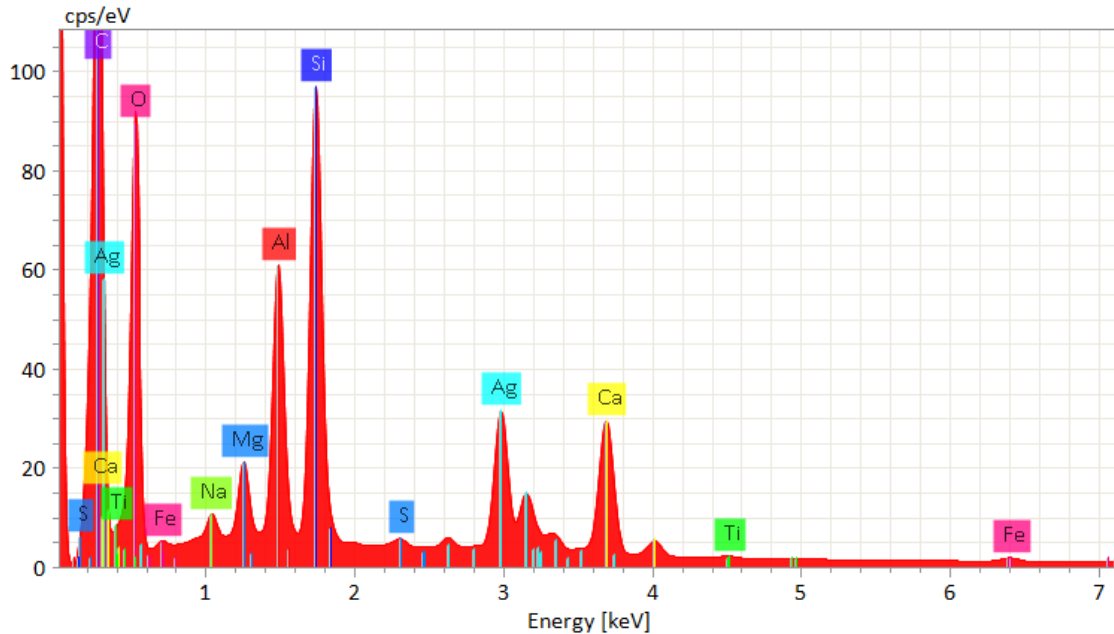


**Figure 5-17** - EDS sum spectrum of AgM in HGM-5 extracted from the EDS dot map in Figure 5-15.

### 5.6.3.2 GAC in Cast Stone

Microstructural and microchemical analysis using SEM and EDS was done on samples from Test Batch 4 for the GAC stabilized in Cast Stone. Because the contrast in BSE micrographs is a function of average atomic number, the GAC particles appear darker due to their higher carbon content than the matrix which is comprised of heavier elements. A collage of SEM-BSE micrographs of GAC particles in the matrix is shown in Figure 5-18. Based on the micrographs, it appears that GAC again shows good adherence to the matrix as no large voids were observed between the GAC particles (bottom of the micrograph, indicated with a white arrow) and the matrix. The small (<1  $\mu\text{m}$ ) cracks observed (red arrow) are associated with incompletely or unreacted starting materials (e.g. fly ash) and are postulated to have formed during dehydration of the sample. It is interesting to note that the hydration product tendrils that were observed in the AgM-containing samples were not observed in the imaged areas from the GAC-containing sample. The microstructure of the GAC appears much more continuous and seems to lack the pore and void space seen in the AgM particles.

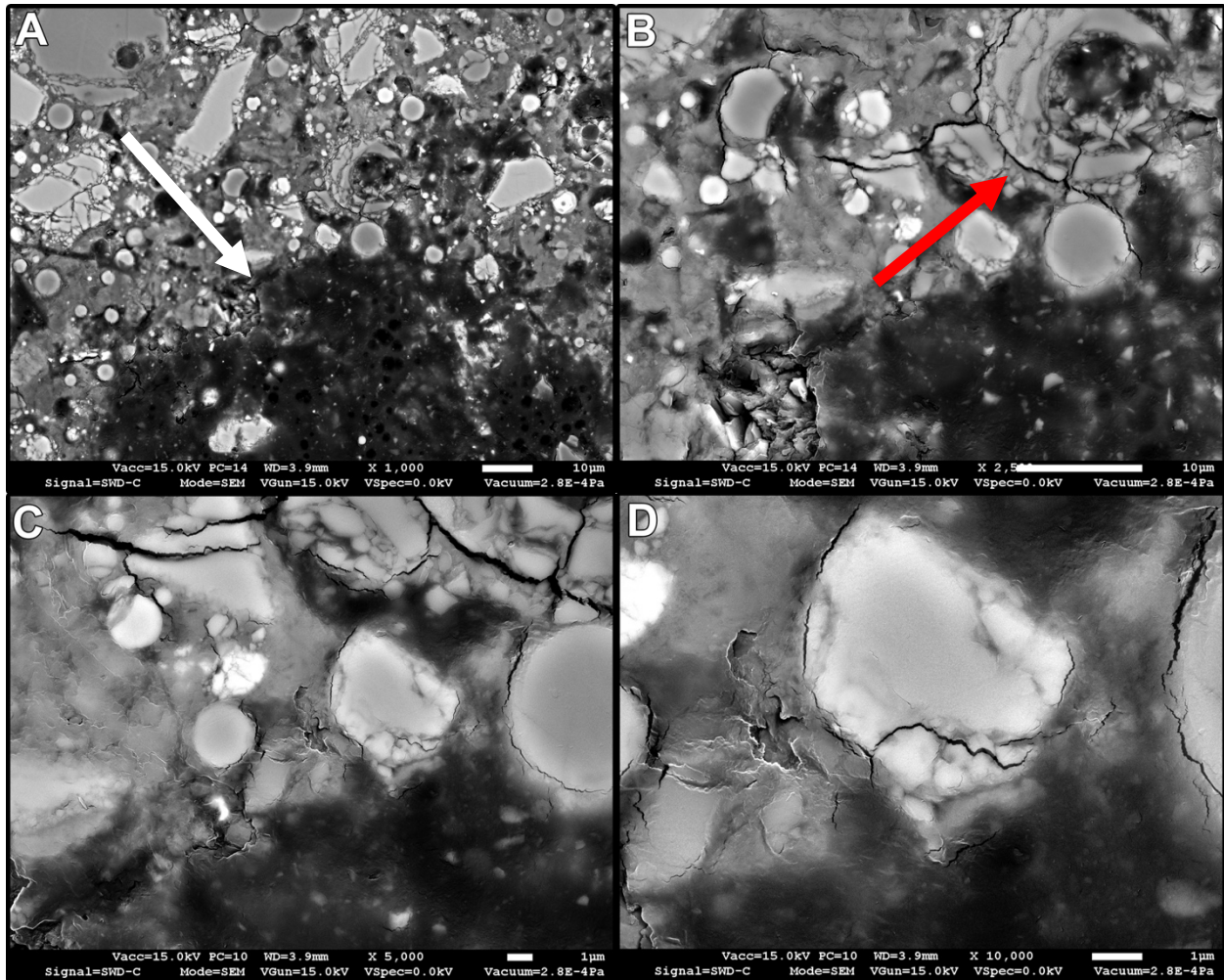


**Figure 5-18** - Higher magnification SEM BSE micrographs showing the interface between GAC and the Cast Stone matrix at A) 1000 ×, B) 2500 ×, C) 5000 × and D) 10000× magnification. The GAC is the dark region at the bottom of the micrographs denoted with the white arrow. The red arrow denotes cracking around the unreacted particles in the paste (e.g. fly ash).

SEM EDS analysis of GAC in Cast Stone mix was performed to determine the elemental distribution in the specimen. The results are shown in Figure 5-19. The elemental dot map clearly shows that the black regions are high in carbon, and thus correspond to the GAC.

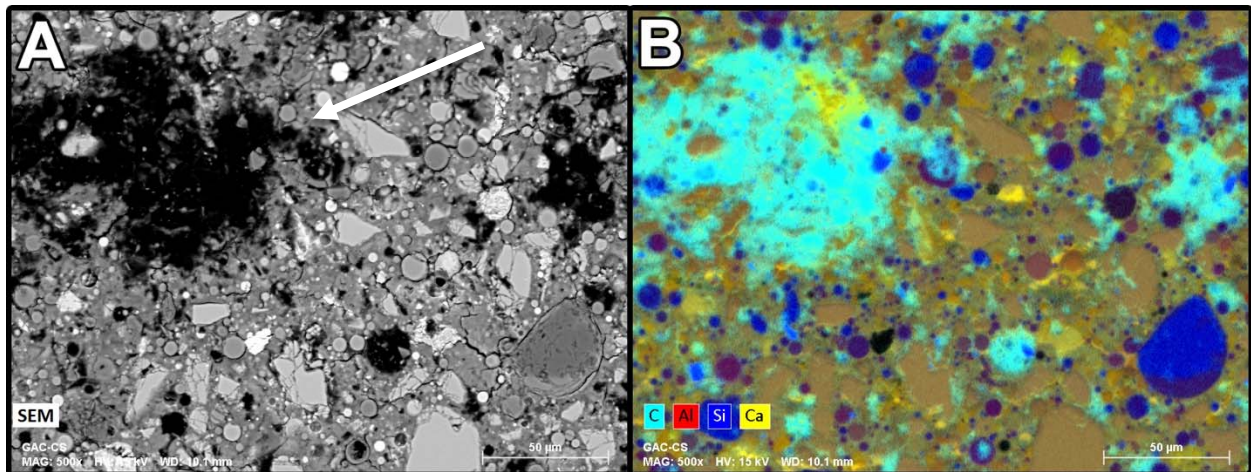


**Figure 5-19** - SEM BSE micrograph (A) of GAC in Cast Stone and (B) the associated EDS elemental dot map from the same area. The GAC particle is marked with a white arrow.

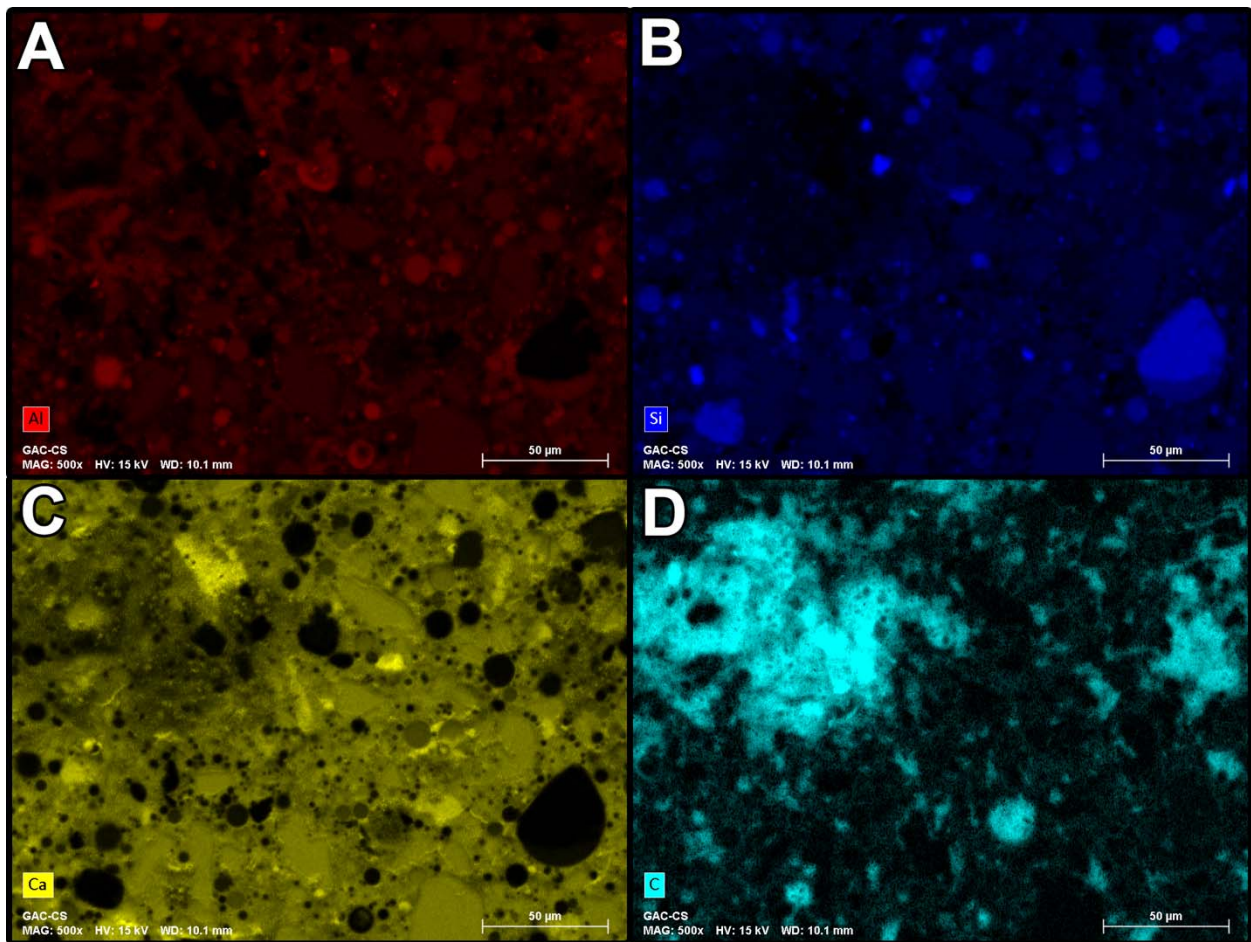


**Figure 5-20** - EDS elemental maps showing the spatial distributions of Al, Si, Ca, and C for GAC in Cast Stone. The intensity of the color is an indication of the relative concentration. (NOTE: The field of view is the same as shown in Figure 5.18 elemental dot map.)

Figure 5-20 shows the individual elemental maps for Al, Si, Ca, and C that were used to create the composite map in Figure 5-19. Figure 5-21 shows the sum spectrum extracted from the EDS elemental dot map. The major elements present in the specimen were C, Si, Ca, and Al, with minor elements being Mg and Na. The trace elements were S, K, Fe, and Ti.

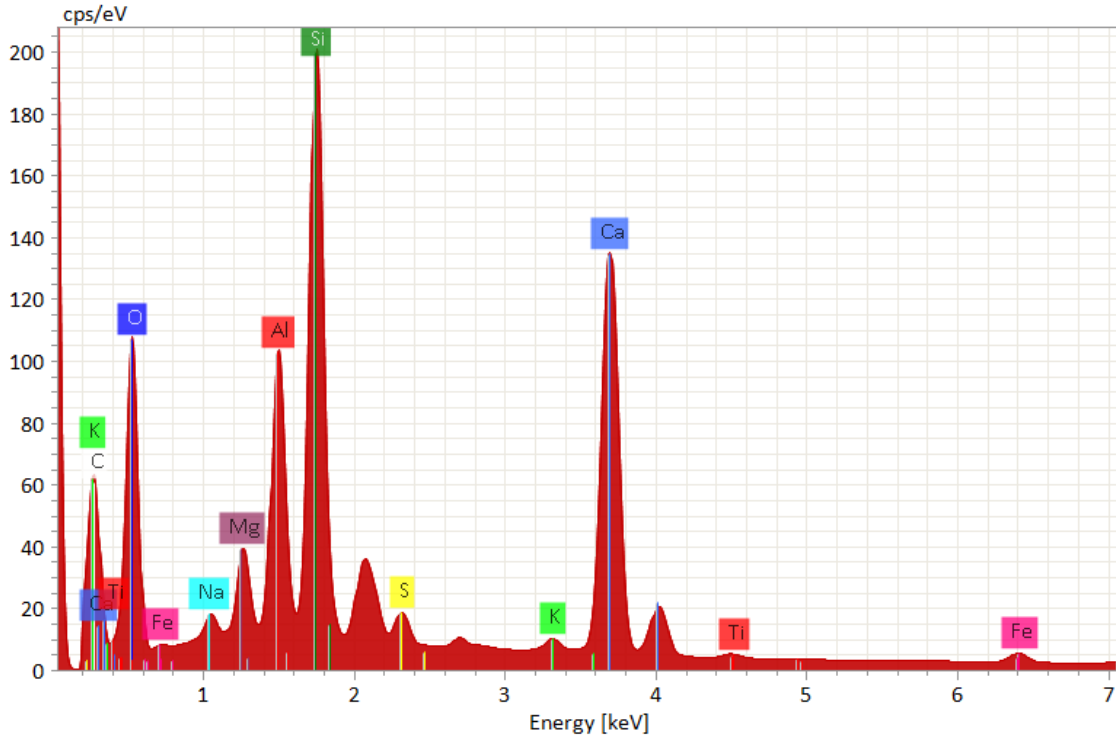


**Figure 5-21.** EDS sum spectrum of AgM in HGM-5 extracted from the EDS dot map in Figure 5.19.

### 5.6.3.3 GAC in Hanford Grout Mix 5

The microstructure and micro-chemistry of GAC incorporated into HGM-5 was imaged. SEM BSE micrographs showing the interface between GAC and HGM-5 matrix are shown in Figure 5-22. Epoxy from the impregnation step filled the cracks and pore space in the specimen. Selected epoxy filled voids are pointed out with arrows. Because the epoxy has a high carbon content, it has a similar gray scale shade as the GAC.

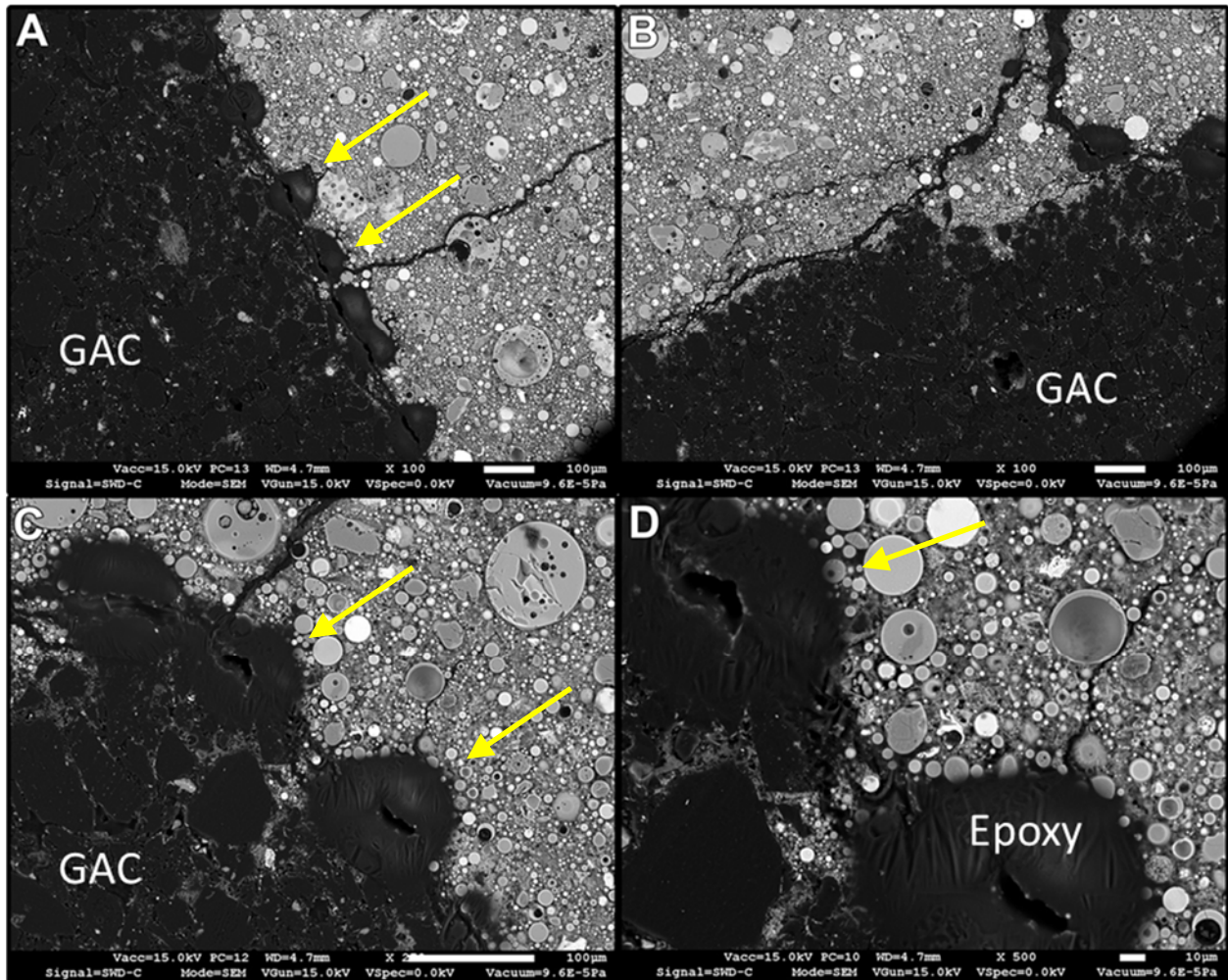
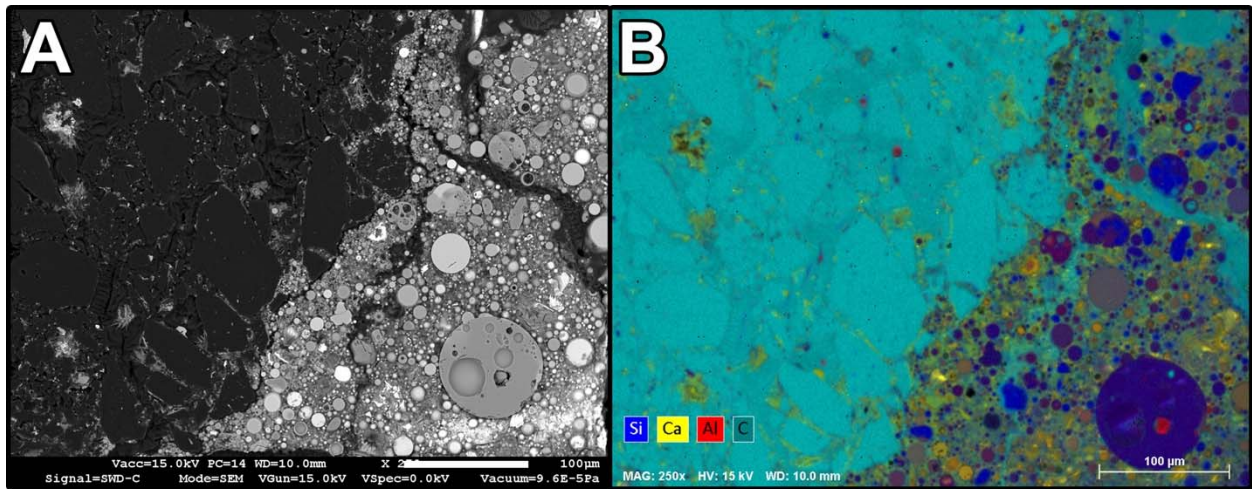


**Figure 5-22.** SEM BSE micrographs from a polished cross-section of GAC in HGM-5. Note: The black spherical shapes (yellow arrows) at the interface were pores that filled with epoxy. A large GAC particle is in the lower left of the image.

The GAC was composed of numerous graphitic grains ranging in size from 10 – 100  $\mu\text{m}$  along with a variety of secondary phase particles. SEM EDS analysis of GAC in HGM-5 was performed to determine the elemental composition and distribution elements in the specimen. An SEM BSE micrograph and the associated EDS elemental dot map from the same region are shown Figure 5-23. The elemental dot map clearly shows that the black regions are high in carbon, and that the bright features in the GAC granule are composed of other elements.



SEM BSE (A) and EDS elemental dot map (B) of granulated activated carbon (GAC) in Handford Grout Mix 5.

**Figure 5-23.** SEM BSE micrograph (A) of GAC in HGM-5 and the associated EDS elemental dot map from the same area (B)

Figure 5-24 shows the sum spectrum extracted from the EDS elemental dot map. The major elements in present in the specimen were C, Si, Ca, and Al, with minor elements being Mg and Na. The trace elements were S, K, Fe, and Ti. These were the same elements as observed for GAC in Cast Stone, Figure 5-21.

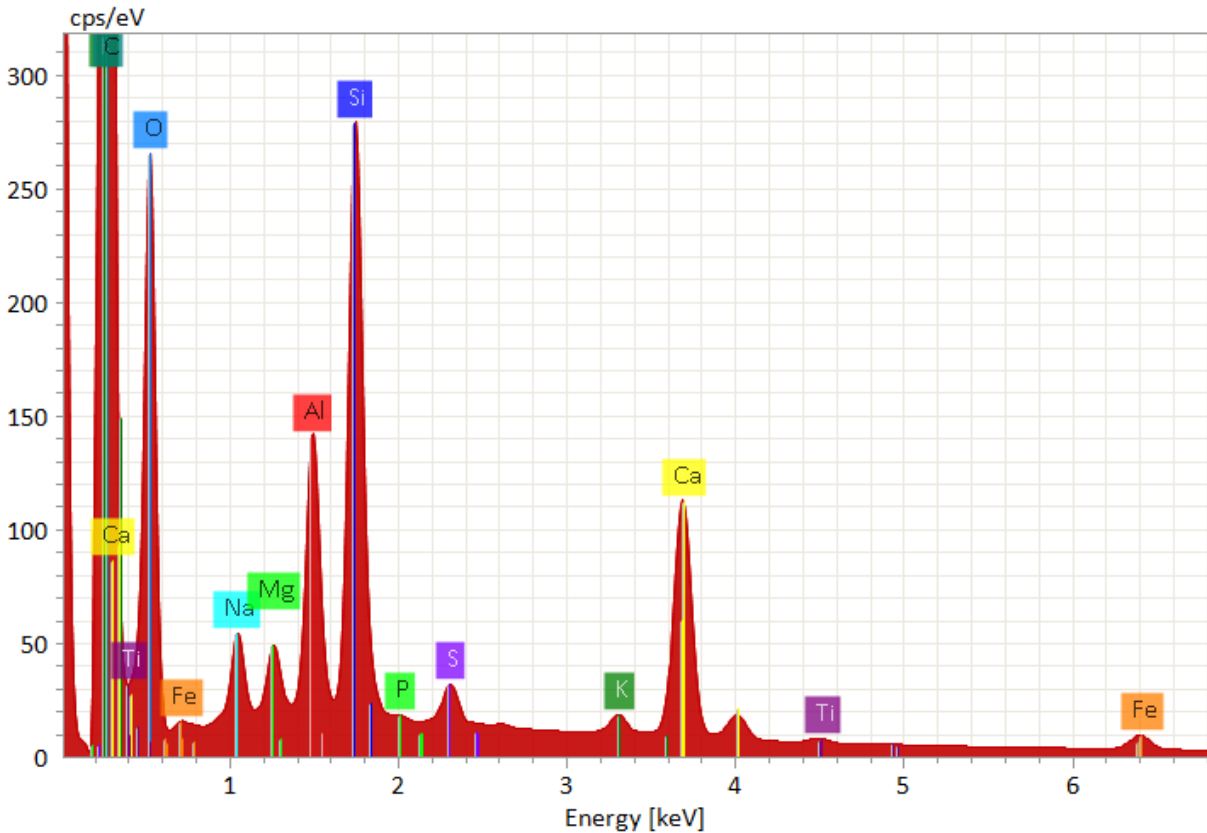


**Figure 5-24.** EDS sum spectrum of GAC in HGM-5 extracted from the EDS elemental map in Figure 5.22.

Selected individual elemental maps for Al, Si, Ca, and C are shown in Figure 5-25. These maps were used to create the composite map shown in Figure 5-23. The relative intensity of the colors in Figure 5-23 are correlated to the concentration of that element. However, for the purpose of emphasizing the spatial distribution of the elements in this field of view, the color intensities in Figure 5-25 were increased. Thus, the color intensities in that figure are not representative of concentration.

The differentiation of epoxy from the GAC was not readily apparent in the carbon elemental map by itself. Thus, the epoxy was differentiated from the GAC using the sulfur signal, image not shown.

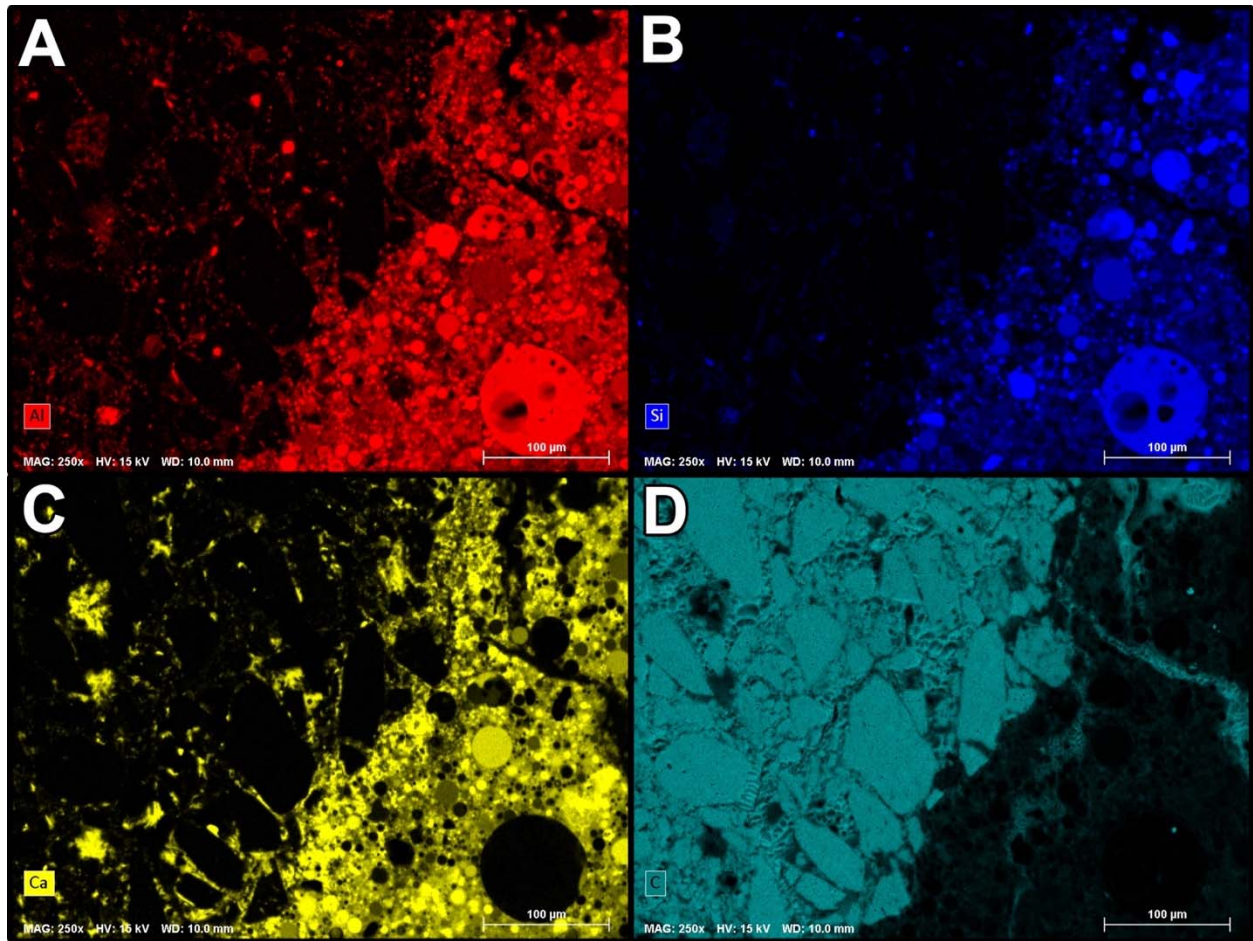


**Figure 5-25.** SEM EDS elemental maps showing the spatial distributions of Al, Si, Ca, and C for GAC in HGM-5. The intensity of the colors was intensified to illustrate where the elements were located in relation to each other; the intensity is NOT correlated to concentration. (Note: The field of view is the same as shown in Figure 5.22.

#### 5.6.3.4 GAC in Hanford Grout Mix 3

The microstructure and micro-chemistry of GAC incorporated into HGM-3 was imaged. SEM BSE micrographs showing the interface between GAC and HGM-5 matrix are shown in Figure 5-26. The GAC particle is in the upper right portion of the micrographs. The interface between the HGM-3 matrix and the GAC was similar to the other formulations with only small voids present. However, the matrix crystalline phases do integrate with the GAC particles as shown in Figure 5-26 B at high resolution.

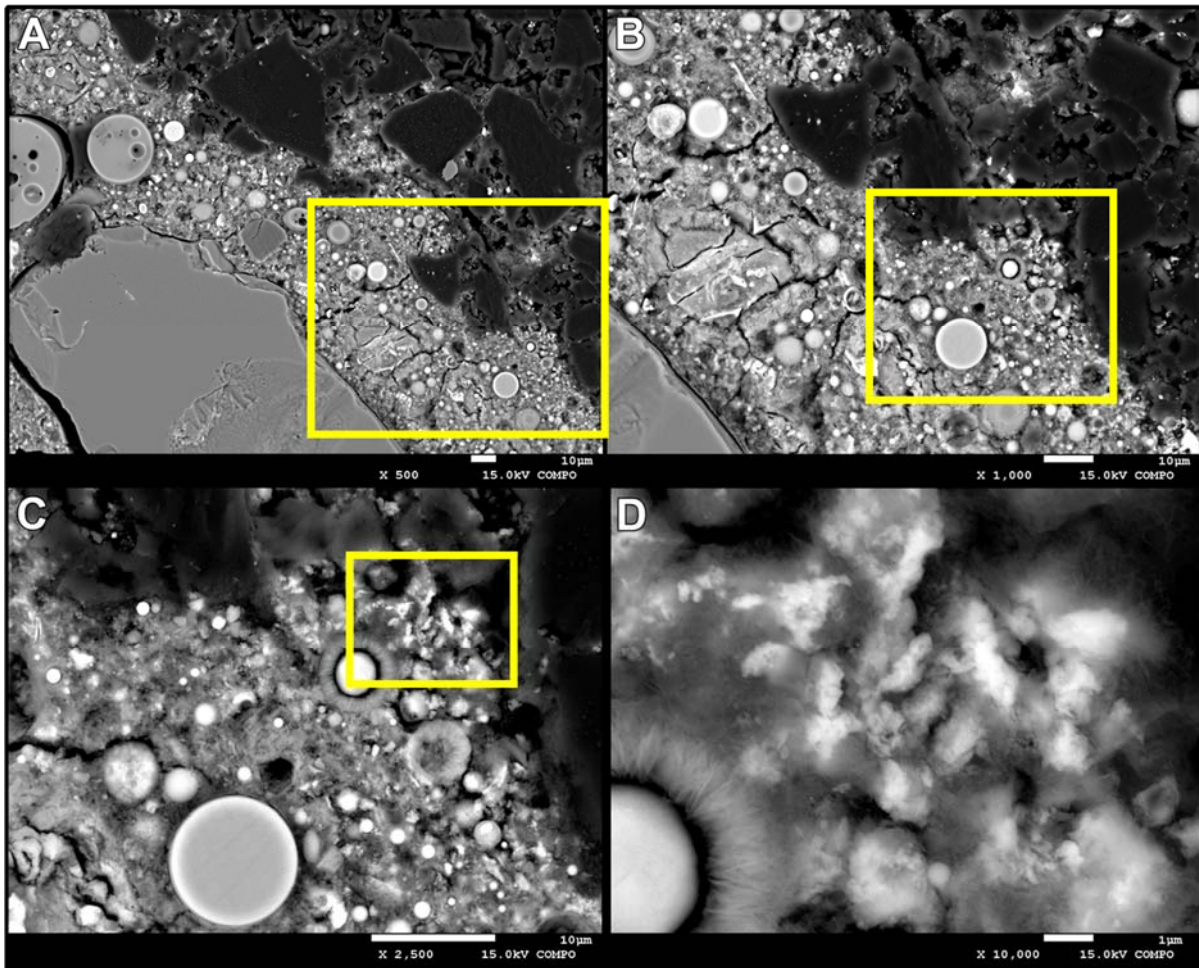


Figure 5-26 - SEM BSE micrographs of increasing magnification from a polished cross-section of GAC in HGM-3. (Note: The GAC is the black area in the upper right of the micrographs. The yellow box in the micrographs highlights the region that is magnified in the subsequent image).

Figure 5-27 shows the sum spectrum extracted from the EDS elemental dot map. Again, the major components were C, Si, Ca, and Al as was the case for the same elements in the other formulations.

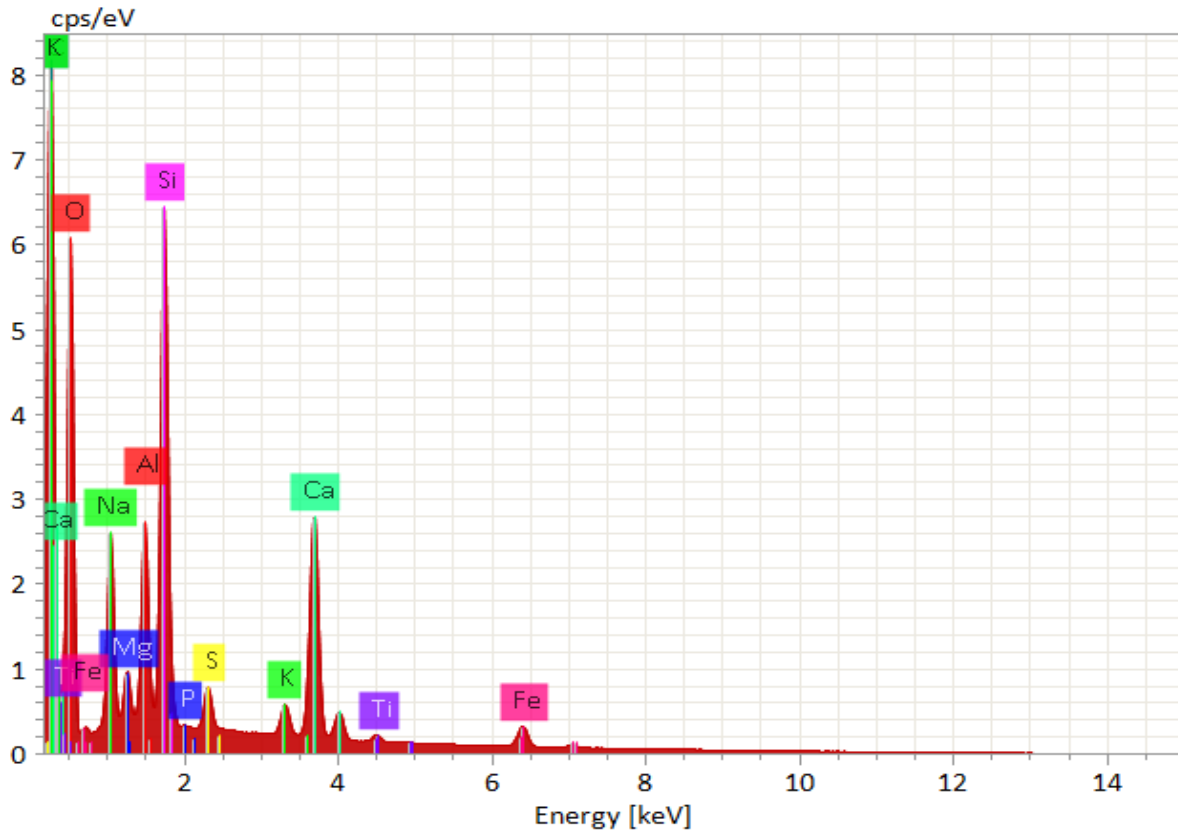


Figure 5-27 - EDS sum spectrum of GAC in HGM-5 extracted from the EDS elemental map in Figure 5.27.

Selected individual elemental maps for Al, Si, Ca, and C are shown in Figure 5-28 and for the purpose of emphasizing the spatial distribution of the elements in this field of view, the color intensities were increased. There is some small migration of the grout into the pore spaces of the GAC as evidenced by the Al and Si isolations in the C rich region (GAC particle, top left).

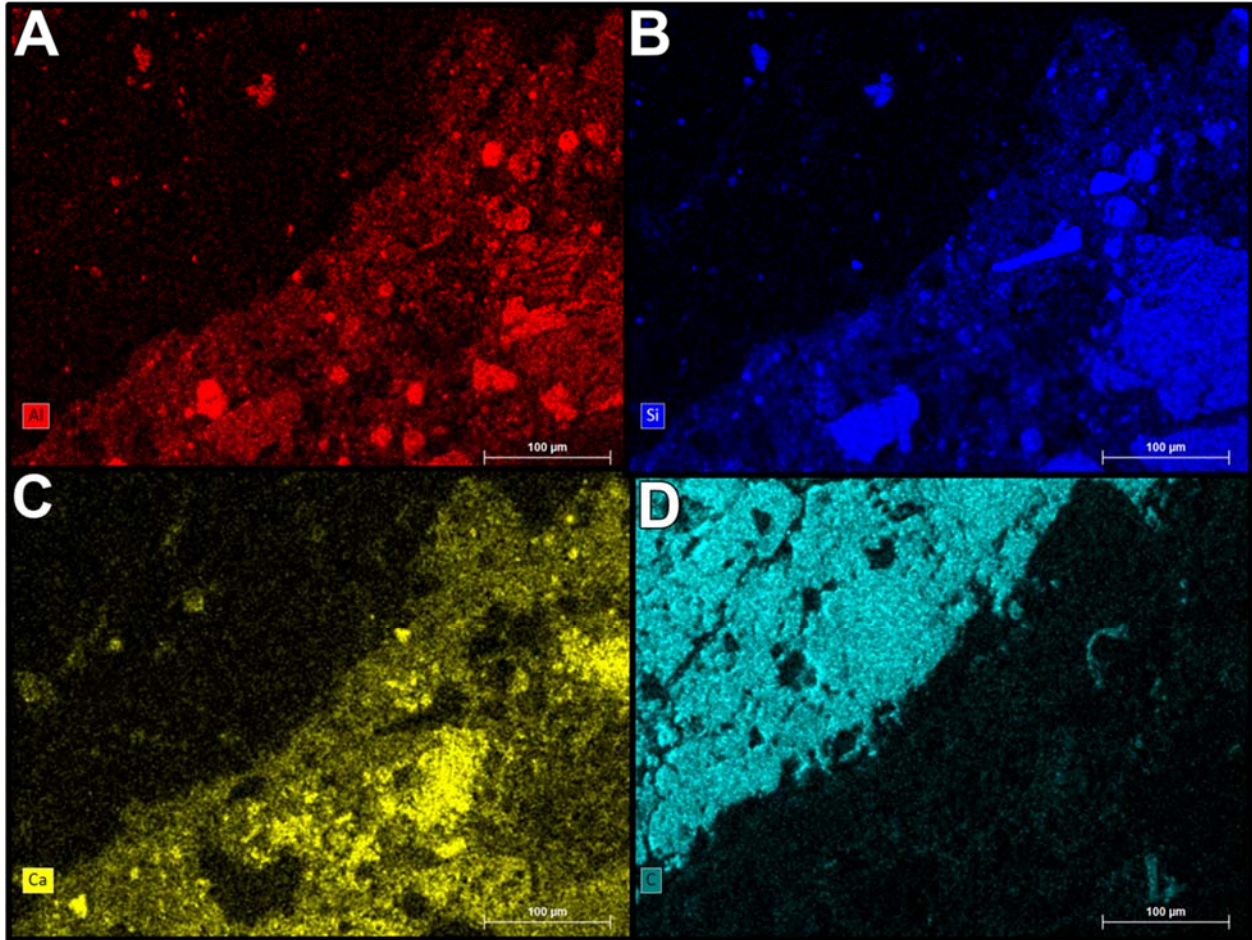


Figure 5-28 - SEM EDS elemental maps showing the spatial distributions of Al, Si, Ca, and C for GAC in HGM-3. The intensity of the colors was intensified to illustrate where the elements were located in relation to each other; the intensity is NOT correlated to concentration.

### 5.6.3.5 AgM in Hanford Grout Mix 3

The microstructure and micro-chemistry of AgM incorporated into HGM-3 was imaged. SEM BSE micrographs showing the interface between AgM and HGM-3 matrix are shown in Figure 5-29. The AgM is in the lower left portion of the micrographs. The interface between the HGM-3 matrix and the AgM again appears to show an enrichment layer of Ag, confirmed in the elemental maps shown in Figure 5-30.

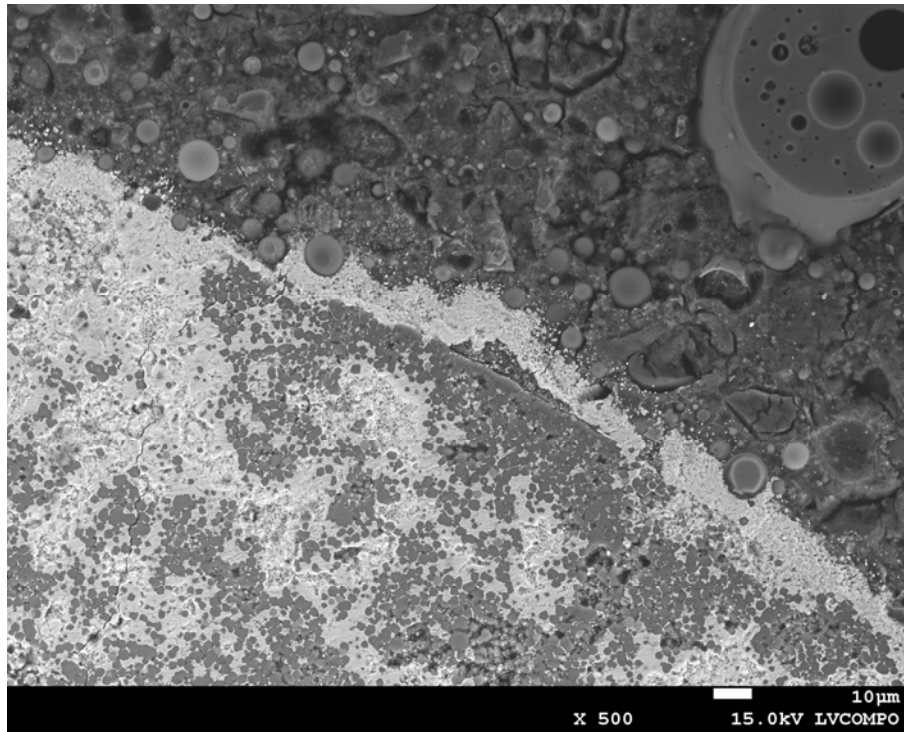


Figure 5-29 - SEM BSE micrographs of the AgM in HGM-3. (Note: The AgM is the region in the bottom left of the image.)

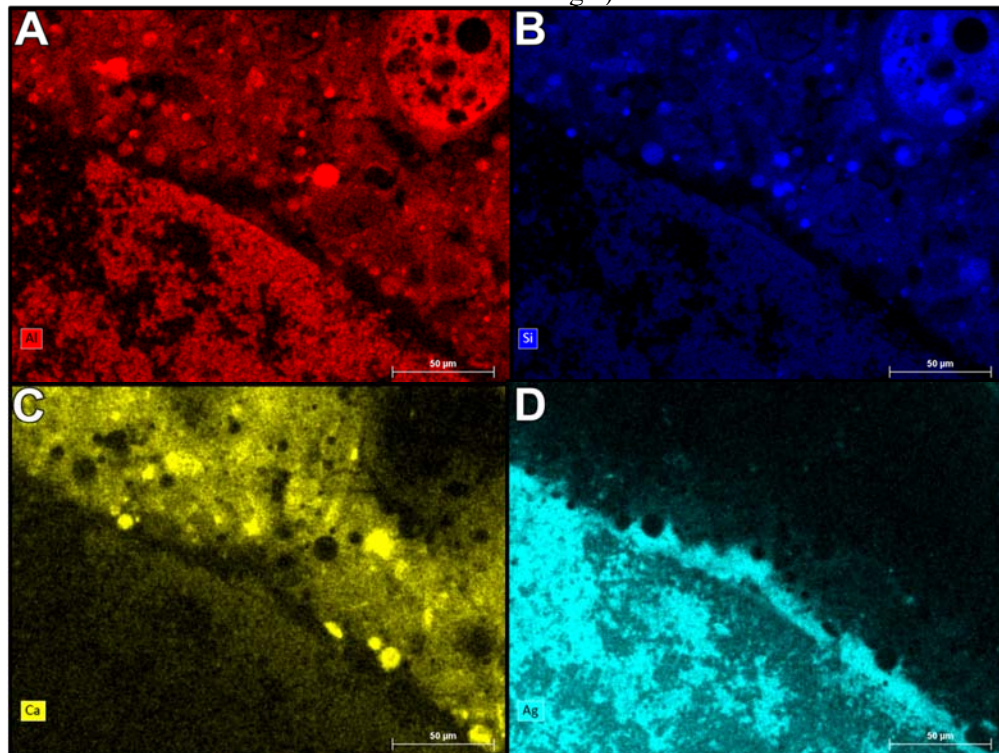
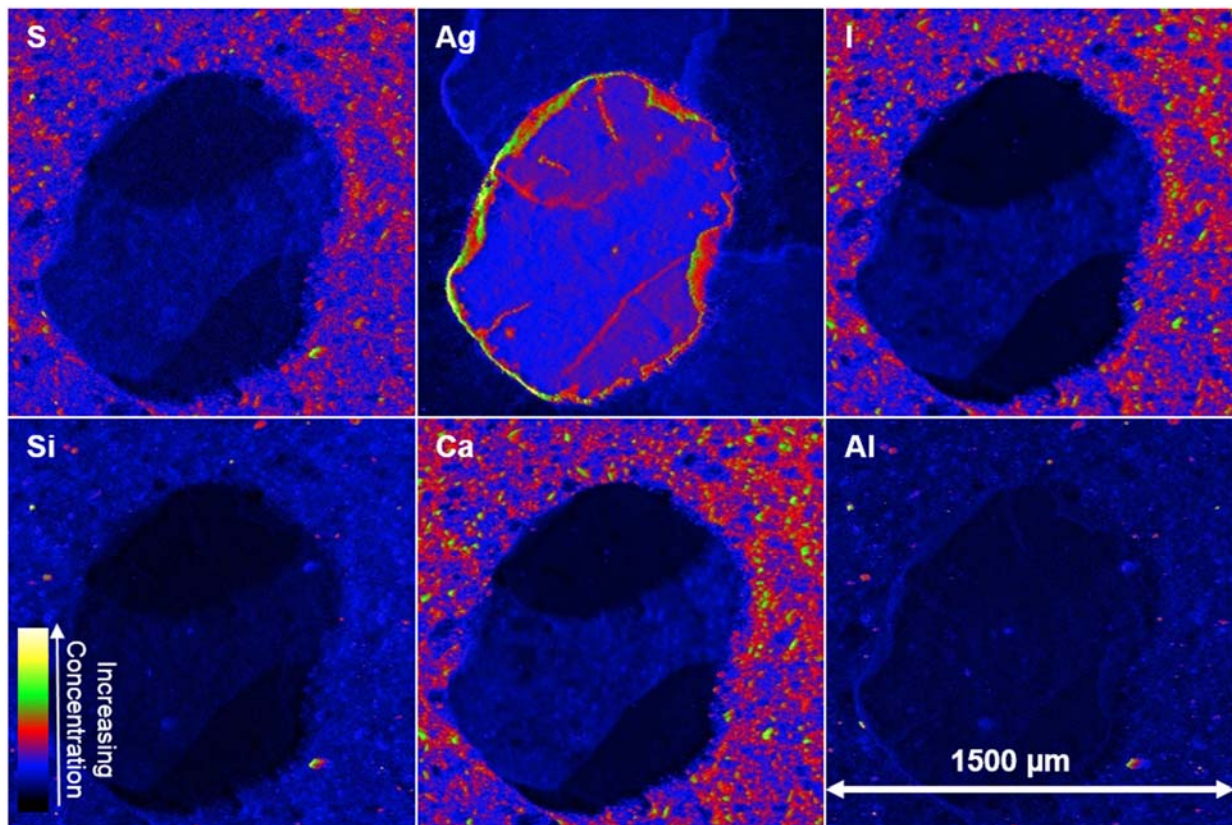


Figure 5-30 - SEM EDS elemental maps showing the spatial distributions of Al, Si, Ca, and C for AgM in HGM-3. The intensity of the colors was intensified to illustrate where the elements were located in relation to each other; the intensity is NOT correlated to concentration.

#### 5.6.4 Microprobe X-ray Fluorescence ( $\mu$ XRF) Mapping

Using  $\mu$ XRF to map major elements found in the SSW containing grout samples, e.g. S, Si, Ca and Al, in addition to Ag and I, the distribution of these elements was investigated in an attempt to better understand the interfacial region between AgM and the hardened grout matrix. Two fragments of a single Cast Stone specimen were analyzed, specifically over a  $1500\ \mu\text{m} \times 1500\ \mu\text{m}$  area in each sample. The elemental  $\mu$ XRF maps collected from each region are shown in Figure 5-31 and Figure 5-32. Immediately apparent from both sampled regions is the regions of Ag that do not contain I as the Ag is present in large excess. Furthermore, in Figure 5-31 the AgM is centered in the image, though X-ray penetration depth reveals two additional circular AgM beads beneath. Regardless of this overlap, there appears to exist a void within the boundary of each bead or an area that lacks primary elements S, Si, Ca, and Al, as indicated by the colorless region in these element maps. This observation would support breakdown of the AgM zeolite backbone and redistribution of the elements elsewhere in the grout matrix. Similarly, in a secondary region shown in Figure 5-32, a distinct void between a AgM bead containing primarily Ag and the other elements exists. In both Figure 5-31 and Figure 5-32, iodine appears to associate with Ca; however, due to the proximity of the I LIII fluorescence line to the Ca K fluorescence line and that Ca concentrations overwhelm that of iodine by orders of magnitude, this positive signal in the iodine maps is likely residual Ca and would require further investigation to resolve. These results show once again Ag enrichment at the AgM particle : hardened grout matrix interface.



**Figure 5-31** -  $\mu$ XRF maps for S, Ag, I, Si, Ca, and Al distributed within a specimen fragment taken from Cast Stone impregnated with iodine contacted AgM and leached in DIW.. Brighter areas indicate higher concentrations of the element of interest. The concentration gradient (color scale) is specific to individual elements.

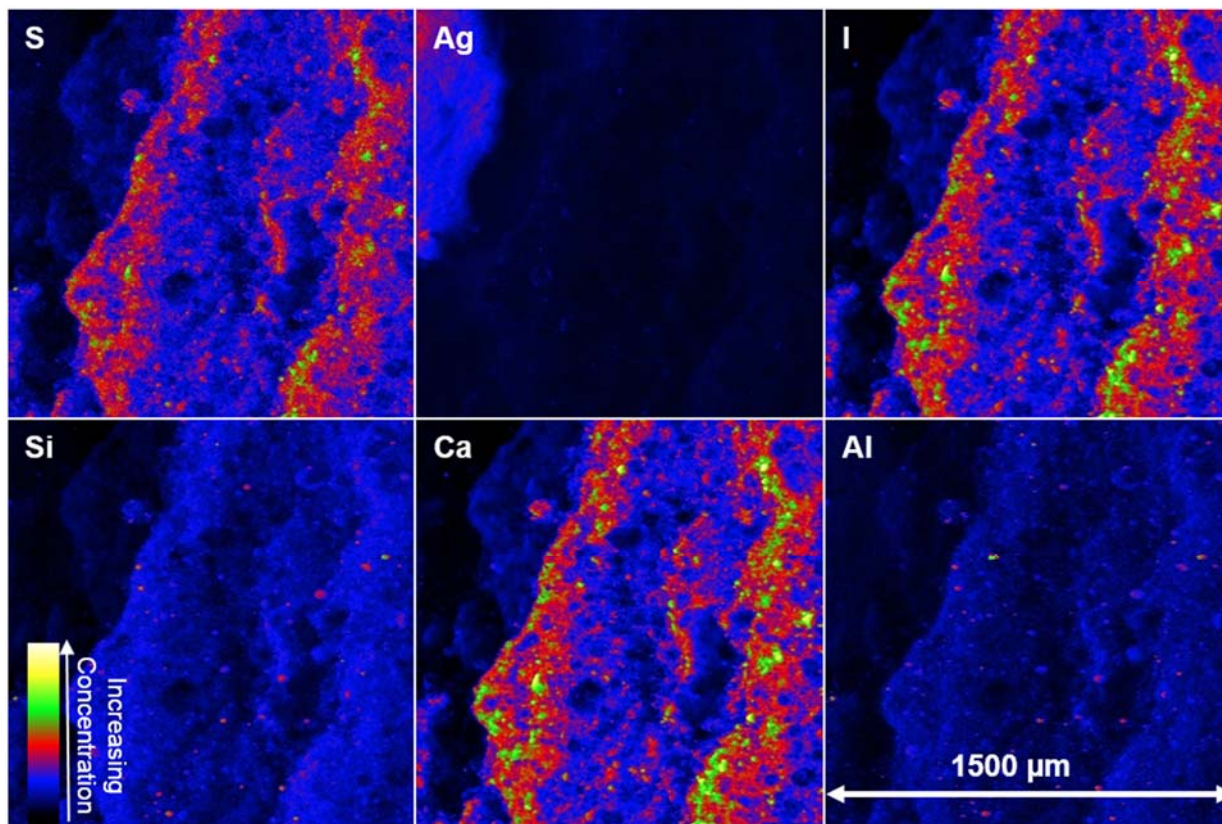


**Figure 5-32** -  $\mu$ XRF maps for S, Ag, I, Si, Ca, and Al distributed within a second fragment taken from Cast Stone impregnated with iodine contacted AgM and leached in DIW.. Brighter areas indicate higher concentrations of the element of interest. The concentration gradient (color scale) is specific to individual elements.

To supplement the  $\mu$ XRF maps identification of iodine within the immobilized AgM samples was pursued using TOF-SIMS. Two samples were analyzed for each formulation: HGM5-AgM-1 that was leached in DIW, Section 7.0, and removed from solution after 90 cumulative days of leaching and HGM5-AgM-4 that was leached in VZPW for  $\sim$ 2 years of cumulative leaching then for Cast Stone a sample after 90 day leaching in VZPW and  $\sim$ 2 years leaching in DIW. Cross sections of the samples were prepared and the interface between the AgM particle and the matrix was imaged with TOF-SIMS, Figure 5-33. The iodine maps presented show the iodine is clearly present on the AgM particle with only a miniscule iodine signal from the matrix. This helps support the excellent leach resistance of iodine from the AgM-HGM5 system in Section 7.0.

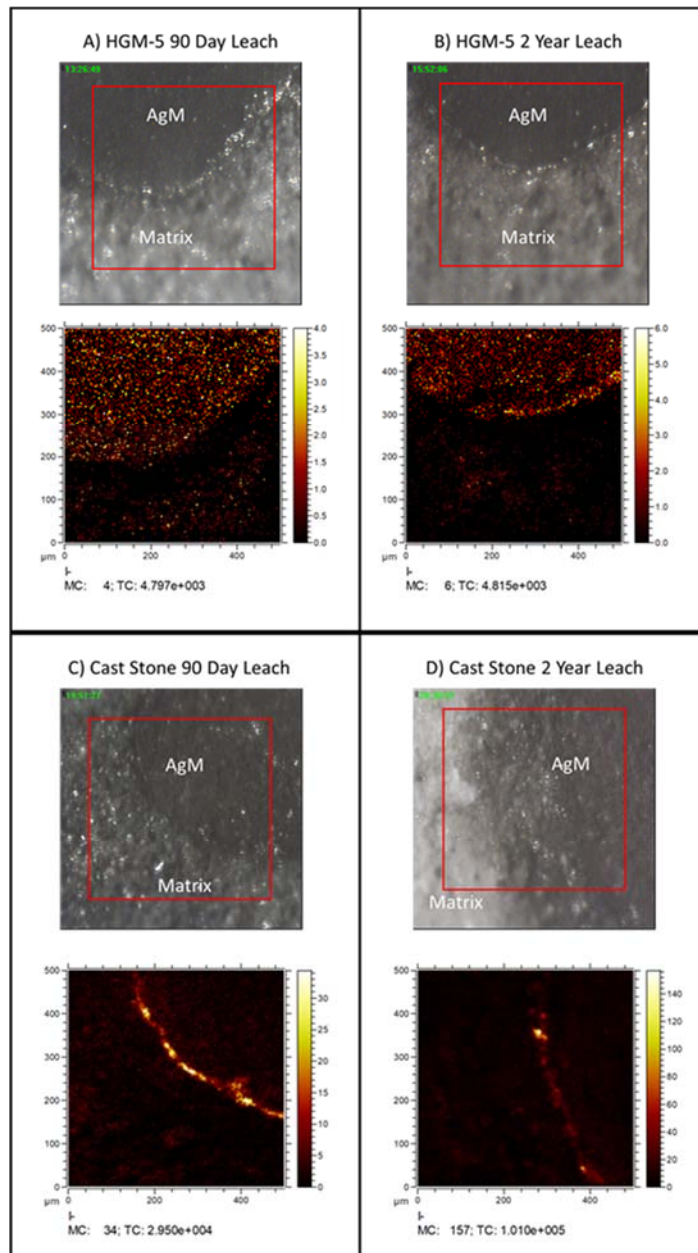


Figure 5-33 – TOF-SIMS iodine images of HGM5-AgM samples after A) 90 day leaching in DIW and B) 2 year leaching in VZPW and Cast Stone-AgM samples after C) 90 day leaching in VZPW and D) 2 year leaching in DIW. Brighter regions correspond to high concentrations of iodine.

## 6.0 Technetium, Iodine, and Mercury Sorption and Desorption Behavior

Sorption processes are generally quantified by measuring the distribution coefficient ( $K_d$ ), which, for the purposes of this discussion, is defined as the ratio of the concentration of a species sorbed (i.e., adsorbed, precipitated and co-precipitated or incorporated) by a solid surface to the concentration that remains in the aqueous phase. For reference, a completely non-sorbing species has a  $K_d$  value of zero mL/g, whereas a completely sorbed species would have an infinitely large  $K_d$ . For contaminants with low  $K_d$  values, small changes in the  $K_d$  value can cause relatively large changes transport modeling where a retardation factor ( $R_f$ ) is used. The  $R_f$  is a value that quantifies how rapidly a chemical species can move relative to the rate of ground-water movement, as the contaminant is transported through the media of interest. The retardation factor can be calculated as follows:

$$R_f = 1 + \left(\frac{\rho b}{\eta_e}\right) K_d \quad (6.1)$$

where:

$R_f$  = retardation factor (unitless)

$\rho b$  = porous media bulk density (mass/length<sup>3</sup>)

$\eta_e$  = effective porosity of the media at saturation (percent)

This means that a small uncertainty in the  $K_d$  value can result in a relatively large uncertainty in models that employ the  $K_d$  concept. The  $K_d$  value for a given analyte and solid material may be dependent on a number of factors including: the concentration and oxidation state of the species, the chemistry of the contacting solution (e.g., ionic strength and composition), pH- $E_h$  relationships, and the properties of the geological material (e.g., ion exchange capacity, presence of organic matter, mineralogy, and particle size distribution) (Kaplan et al. 2000). The  $K_d$  concept employed in the present report ignores the mechanism responsible for partitioning of the sorbate between the solid and aqueous phase and represents the “net effect” of all mechanisms responsible for partitioning into the solid phase. Other geochemical reactions (e.g., solubility-precipitation, colloid facilitated migration, and redox) impact contaminant migration but are not examined in these batch sorption tests. However, the empirically derived  $K_d$  data help in the understanding of bulk behaviors and can be easily accommodated in computer models.

This section provides results from batch sorption  $K_d$  and batch desorption  $K_d$  for the waste materials GAC, AgM, HEPA, and the neat grouts (Cast Stone and HGM-5) in simulated pore waters of both grout mixes. The pore water solutions are spiked with an analyte(s) which partitions between the solid and solution. Determining  $K_d$  values for a variety of analytes and waste materials in site-specific conditions was a major recommendation from the 2016 SSW data package (Flach et al. 2016). For that reason, this series of tests was performed so that more representative  $K_d$  values can be used in future maintenance of the IDF PA. In addition, this new set of tests with  $I^-$  and  $IO_3^-$  are especially important as  $IO_3^-$  has been found to be a major iodine species in the Hanford site subsurface (Zhang et al. 2013). However, recent experiments by Kaplan et al. (2019) have shown that leached grout mixes spiked with iodate and left to cure for 2 months show that little to no iodate are present. Because the two species are coupled and likely to interact differently with various materials so understanding those interactions is important to better capture likely iodine release behavior in the disposal environment. Organo-iodine is also a species that is relatively important but identification of the exact organo-iodine species that might be present is beyond the scope of this work. For that reason, no organo-iodine  $K_d$  tests are presented here.

## 6.1 Sorption/Desorption Characteristics of Secondary Waste Materials

### 6.1.1 Tests to Determine Equilibrium Time

The initial tests were conducted to determine the amount of time required to reach a steady-state analyte concentration in solution. Results are provided in Appendix A. In general, tests reached a steady state after the first five days of contact time. A few solid/solutions combinations resulted in no measurable analyte sorption. However, even if there was no removal by the solid waste material, the analyte/waste material combination was tested in triplicate. Most of the  $K_d$  values were within experimental uncertainty of the results calculated from the triplicate tests. However, four of the tests resulted in values that were outside of the standard deviation of the set of triplicate tests and those differences will be discussed in Section 6.2.

### 6.1.2 Sorption and Desorption $K_d$ Values

The experimentally determined mean sorption  $K_d$  values and the standard deviation of the triplicates tests are provided in Table 6.1. Desorption  $K_d$  values are provided in Table 6.2. The results are discussed in the following subsections.

### 6.1.3 GAC

The capacity of analyte removal by GAC in both pore waters follows  $Hg > Tc > I$ . In both pore waters, the Hg  $K_d$  value is greater than  $10^4$  mL/g. The Hg  $K_d$  is larger for the HGM-5 pore water compared to the Cast Stone pore water but this might be related to the smaller  $[Hg]_{init}$  in the Cast Stone experiments due to Hg precipitation in the Cast Stone pore water solutions. Regardless, the Hg  $K_d$  values demonstrate that on average >99.7% of the initial Hg in solution is transferred to the GAC. In addition, when Hg and I are both present as in the contacting solution, their removal appears to be non-competitive (i.e., the  $K_d$  value does not change when Hg or I are in solution at the same time or when tested individually).

The GAC also removes on average >98.0% of the original Tc from the pore water, however, compared to the Hg values, the relative standard deviation of the triplicate values is large (56% for Cast Stone pore water and 89% for HGM-5 pore water). These large relative standard deviations suggest the form of the GAC pieces, either as the activated cylinders (70% makeup) or as inert particles (30 % makeup), might have an effect on Tc removal. The activated cylinders likely contain S to assist with Hg removal in WTP and sulfide-compounds have been shown to be effective at retaining Tc (Neeway et al. 2016, Asmussen et al. 2018, Pearce et al. 2018). However, the distribution of GAC pieces was not controlled for and further experiments would need to be performed to confirm this hypothesis.

In comparison to Tc and Hg, the removal variability of I or  $IO_3^-$  was much greater between replicates. For example, for GAC removal of I in HGM-5 pore water, the iodine concentration at the end of the each test was measured to be 16.8, 68.5, and 133 ppm in the triplicate test vessels. These large deviations may explain why the iodine  $K_d$  values from the initial tests did not agree with the tests conducted in duplicate. The initial tests, which were conducted at the same solid/solution ratio as the later tests, but used a larger quantity of starting material (2 g), likely had a more representative distribution of GAC particles than the triplicate tests, which used only 0.5 g of the starting material (consisting of 1 to 3 total GAC pieces).

Desorption  $K_d$  values demonstrate whether or not, once sorbed to the waste material surface, the analyte will desorb once exposed to a fresh solution without analyte. A low desorption  $K_d$  value indicates that

most of the analyte is released up on exposure to the fresh solution and a high desorption  $K_d$  value indicates that the analyte material is more likely to remain on the waste material surface. The desorption  $K_d$  values for both iodine species were 0 mg/L, once again highlighting the difficulty of obtaining meaningful  $K_d$  values with the background iodine contained on the starting GAC material but indicating that iodine did not strongly sorb to the GAC in aqueous environments. For systems containing  $I^-$  and Hg, the SSW material releases little of the Hg that sorbed to the surface with desorption  $K_d$  values  $> 10^4$  mL/g. Interestingly, the desorption  $K_d$  for Hg in the HGM-5 pore water was two orders of magnitude lower than the desorption  $K_d$  for Hg in the Cast Stone pore water. Understanding the reasons for this behavior would require further experimentation but may be due to the lower Hg solubility in the Cast Stone pore water (due to the presence of sulfide in solution from the slag component) compared to the HGM-5 pore water. Lastly, the desorption  $K_d$  values for Tc are on the order of  $10^2$  mL/g signifying that roughly 90% of the Tc sorbed by the GAC remained on the solid when fresh solution was introduced to the system.

**Table 6-1 - Sorption  $K_d$  Values for the Specified Combination of Analytes and Waste Materials.**

Pore Water	Waste Material	$K_d$ Value (mL/g)					
		Tc	I	IO <sub>3</sub>	Hg	Hg-I	ALL <sup>(1)</sup>
Cast Stone	GAC <sup>(2)</sup>	$2.3 \pm 1.3 \times 10^3$	$1.0 \pm 0.6 \times 10^2$	$5.2 \pm 6.8 \times 10^0$	$1.0 \pm 0.3 \times 10^4$	Hg: $3.1 \pm 2.1 \times 10^4$	---
						I: $3.9 \pm 4.2 \times 10^2$	
	HEPA	$3.6 \pm 4.8 \times 10^{-1}$	$7.7 \pm 5.8 \times 10^{-2}$	$8.4 \pm 5.0 \times 10^{-1}$	---	---	---
	AgM	$4.3 \pm 2.4 \times 10^0$	$5.8 \pm 4.5 \times 10^4$	$3.5 \pm 1.6 \times 10^0$	---	---	---
Cast Stone	Cast Stone	$1.5 \pm 2.2 \times 10^0$	$2.1 \pm 0.9 \times 10^0$	$2.8 \pm 0.1 \times 10^1$	$1.2 \pm 0.0 \times 10^4$	Hg: $6.2 \pm 0.0 \times 10^4$	Tc: 0
						I: 0	I: $1.2 \pm 0.0 \times 10^1$
							Hg: $7.3 \pm 3.5 \times 10^3$
HGM-5	GAC <sup>(2)</sup>	$2.6 \pm 2.3 \times 10^3$	$1.6 \pm 2.2 \times 10^1$	$2.6 \pm 2.1 \times 10^1$	$1.2 \pm 0.4 \times 10^5$	Hg: $1.1 \pm 0.0 \times 10^5$	---
						I: 0	
	HEPA	$3.2 \pm 4.5 \times 10^{-2}$	$3.9 \pm 3.4 \times 10^{-1}$	0 <sup>(3)</sup>	---	---	---
	AgM	$4.0 \pm 4.2 \times 10^0$	$2.3 \pm 1.0 \times 10^4$	$2.9 \pm 1.3 \times 10^0$	---	---	---
HGM-5	HGM-5	$1.4 \pm 0.7 \times 10^0$	$2.5 \pm 1.4 \times 10^0$	$6.9 \pm 0.4 \times 10^2$	$1.7 \pm 0.2 \times 10^1$	Hg: $2.3 \pm 0.4 \times 10^1$	Tc: $2.0 \pm 2.2 \times 10^{-1}$
						I: $3.6 \pm 0.6 \times 10^1$	I: $2.2 \pm 0.0 \times 10^1$
							Hg: $1.9 \pm 0.1 \times 10^1$

<sup>(1)</sup> These tests labelled "ALL" contained Tc, I and Hg in solution simultaneously.

<sup>(2)</sup> As discussed in the text, the as-received GAC material contained iodine so further tests may be necessary to refine sorption  $K_d$  values with this particular GAC material.

<sup>(3)</sup> A value of zero indicates that the calculated  $K_d$  values was negative (i.e. the measured concentration of the element was greater than the average background concentration. A negative  $K_d$  is the result of analytical uncertainty.)

Notes: "----" indicates that the test was not performed.

**Table 6-2.** Desorption  $K_d$  Values for the Specified Combination of Analyte and Waste Materials

Pore Water	Waste Material	$K_d$ Value (mL/g)					
		Tc	I	IO <sub>3</sub>	Hg	Hg-I	ALL <sup>(1)</sup>
Cast Stone	GAC <sup>(2)</sup>	$1.5 \pm 0.2 \times 10^2$	0 <sup>(3)</sup>	0 <sup>(3)</sup>	$4.4 \pm 4.1 \times 10^2$	Hg: $1.0 \pm 0.5 \times 10^5$ I: $4.3 \pm 0.0 \times 10^0$	---
	HEPA	$3.7 \pm 0.0 \times 10^1$	$1.1 \pm 0.0 \times 10^1$	$1.6 \pm 0.0 \times 10^1$	---	---	---
	AgM	-	$3.0 \pm 1.4 \times 10^5$	$1.4 \pm 0.9 \times 10^3$	---	---	---
	Cast Stone	0 <sup>(3)</sup>	$4.3 \pm 1.7 \times 10^1$	$2.9 \pm 0.9 \times 10^2$	$4.3 \pm 1.0 \times 10^4$	Hg: $2.3 \pm 0.5 \times 10^5$ I: 0	Tc: 0 I: $2.4 \pm 0.5 \times 10^{-1}$ Hg: $1.3 \pm 0.0 \times 10^5$
HGM-5	GAC <sup>(2)</sup>	$1.7 \pm 0.1 \times 10^2$	-	-	$5.1 \pm 1.0 \times 10^4$	Hg: $1.7 \pm 1.1 \times 10^4$ I: 0	---
	HEPA	0 <sup>(3)</sup>	-	-	---	---	---
	AgM	$1.9 \pm 0.5 \times 10^3$	$1.4 \pm 1.1 \times 10^6$	$7.9 \pm 0.2 \times 10^2$	---	---	---
	HGM-5	$7.1 \pm 3.5 \times 10^1$	$1.7 \pm 1.1 \times 10^1$	$5.9 \pm 0.3 \times 10^2$	$5.0 \pm 0.2 \times 10^2$	Hg: $7.2 \pm 0.6 \times 10^2$ I: $6.8 \pm 2.1 \times 10^0$	---
<p><sup>(1)</sup> These tests labelled “ALL” contained Tc, I and Hg in solution simultaneously.</p> <p><sup>(2)</sup> As discussed in the text, the as-received GAC material contained iodine so further tests may be necessary to refine sorption <math>K_d</math> values with this particular GAC material.</p> <p><sup>(3)</sup> A value of zero indicates that the calculated <math>K_d</math> values was negative (i.e. the measured concentration of the element was greater than the average background concentration. A negative <math>K_d</math> is the result of analytical uncertainty.)</p> <p>Note: A “---” indicates that the test was not performed.</p>							

The wide ranges of  $K_d$  for the GAC are likely due to iodine contamination in the GAC material received from the vendor. An additional pore water/GAC batch experiment in the absence of an iodine spike was conducted to see if these mixed results were due to iodine contamination in the GAC. The tests, conducted at a 1:25 solid-to-solution ratio were performed by contacting each pore water solutions with either the individual granular or cylindrical GAC pieces. The iodine release from the inert particles resulted in solution I concentration of  $0.4 \pm 0.2$  ppb for the Cast Stone and HGM-5 pore waters. On the other hand, when the cylindrical active carbon particles were used, the iodine concentrations were  $3.0 \pm 2.0$  ppm and  $21.9 \pm 2.9$  for the Cast Stone and HGM-5 pore water solutions, respectively. In summary, the as-received material was undoubtedly inhomogeneous and this likely caused the large difference in iodine  $K_d$  values from the replicate samples. Future experiments should make an attempt to homogenize the material before testing.

The iodine  $K_d$  values for GAC presented here can be compared to previously obtained values (Flach et al. 2016; Parker et al. 2014; Asmussen et al. 2016b). These  $K_d$  values were obtained with different activated carbon sources, in different types of pore water, in different experimental conditions, and only iodide was studied as the iodine species. Therefore, all reported iodine  $K_d$  values are derived solely from experiments using iodide. Parker et al. (2014) measured  $K_d$  values on six different GAC materials in Hanford groundwater using a 1000 mL/g solution-to-solid ratio, and a contact period of 24 hours. Based on these results, Flach et al. (2016) assigned iodide  $K_d$  values ranging from 20 to 230 mL/g depending on the source. Kuboa et al. (2013) demonstrated that iodide sorption  $K_d$  values decreased with increasing nitrate presence and that iodide could be removed from river water but not from seawater. This effect of ionic strength was also noted by Qafoku et al. (2015) who worked with a silver-impregnated activated carbon source and measured sorption  $K_d$  values in DIW and a 7.8 M Na simulated waste stream at a pH of 13.5. Batch sorption tests were performed for 14 days at a solid-to-solution ratio of 1:100 and three different starting analyte concentrations (0.5, 5, and 10 ppm). The  $\log K_d$  (mL/g) for the activated carbon source was  $\log K_d$  (mL/g) 5.30 in DIW while in the 7.8 M Na simulant the  $\log K_d$  (mL/g) values ranged from 0 to 0.78 for the activated carbon source. Flach et al. (2016) showed a similar impact of ionic strength as they report GAC desorption  $K_d$  values for the iodide from a cement leachate of 320 to 880 mL/g whereas in rain water the values ranged from 58,100 to 132,500 mL/g. So the small  $K_d$  values provided in the present study are likely the result of the relatively high ionic strength of the pore water solutions and are most representative of the anticipated sorption behavior within the pore space of the waste form.

At this point, the mechanism for sorption of iodide on the GAC is unknown. Flach et al. (2016) suggest that it is a relatively weak chemisorption process based on electrostatic attraction between charged iodine species and activated carbon surfaces. This observation was largely based on the effect of ionic strength discussed in the previous paragraph. In addition, surface charge may also influence iodine sorption on GAC. In high pH conditions, the surface is likely negatively charged and would attract cations – i.e., not the anions  $I^-$  or  $IO_3^-$ . Therefore, in order to elucidate the mechanism responsible for iodine a more focused set of experiments, specifically at lower ionic strength and more neutral pH values with both iodine species, would need to be conducted.

#### 6.1.4 Silver Mordenite

The removal of Tc,  $I^-$ , and  $IO_3^-$  by AgM showed almost negligible removal of Tc and  $IO_3^-$  but >99.9% removal of  $I^-$ . In both the Cast Stone and HGM-5 pore waters, the  $K_d$  values for Tc and  $IO_3^-$  were less than 10 mL/g, meaning that less than 10% of the analyte was removed from solution by the solid material. The  $K_d$  values for  $I^-$  in both pore waters were greater than  $10^4$  mL/g. Tc,  $I^-$ , and  $IO_3^-$  all exist as singly charged anions but the differences in removal capacity are likely related to their relative solubilities. The relative  $K_d$  values of the two silver iodide species agree with the relative solubility of the various Ag salts: the  $K_{sp}$  values of  $AgI_{(s)}$  and  $AgIO_{3(s)}$  are on the order of  $10^{-17}$  (Tan et al. 1972) and  $10^{-8}$  (Renier et al. 1956),

respectively, whereas the  $K_{sp}$  of  $\text{AgTcO}_4(\text{cr})$  is  $10^3$  (Guillaumont and Mompean 2003). With a  $k_{sp}$  of  $10^{-17}$ , the expected iodine concentration would be less than 10 nM whereas 360 nM and 490 nM were measured in the Cast Stone and HGM-5 tests, respectively. The higher concentrations of iodine in these tests versus expected values from the literature are likely due to pH effects (Asmussen et al. 2017). We note that the initial test to determine the duration required for equilibrium showed 50% removal of  $\text{IO}_3^-$  and it is unclear why this was the case. The concentration of Ag in solution was not monitored.

Desorption  $K_d$  values were obtained for the AgM tests by adding fresh solution of either Cast Stone or HGM-5 pore water to the system. For Tc and  $\text{IO}_3^-$ , the desorption  $K_d$  values were measured to be  $\sim 10^3$  mL/g or greater signifying that what little Tc and  $\text{IO}_3^-$  that was initially sorbed to the surface remained on the surface after exposure to a fresh solution. The desorption  $K_d$  values for  $\text{I}^-$  are high in both pore waters ( $>10^5$  mL/g) indicating that the AgI formed within the AgM does not readily dissolve when contacted with fresh Cast Stone and HGM-5 pore water systems.

Asmussen et al. (2016b) have also examined the removal of  $\text{I}^-$  from solution by a silver-exchanged zeolite, the same mordenite-based material as this work. They reported maximum sorption  $K_d$  values of  $9.1 \times 10^4$  mL/g in DIW and a minimum value of  $2.4 \times 10^4$  mL/g in a pH 13.5, 7.8 M Na simulated waste stream. Batch sorption tests were performed for 14 days at a solid-to-solution ratio of 1:100 and three different starting analyte concentrations (0.5, 5, and 10 ppm). Thus, the results from Asmussen et al. (2016) suggest that the capacity of  $\text{I}^-$  removal by AgM should not be affected by the relatively high pH and ionic strength of the pore water solutions. In addition, the  $K_d$  values were shown to be independent of whether or not the experiments were conducted in oxic or anoxic conditions.

### 6.1.5 HEPA Filter Media

Flach et al. (2016) did not find any data for analytes of interest sorption/desorption to HEPA filters for the analytes of interest. Thus, to our knowledge, the data collected here are the first set to provide these values. For tests conducted with Cast Stone and HGM-5 pore waters, the  $K_d$  sorption values are  $<1$  mL/g meaning that less than 10% of the analyte was removed from the system at a 1:25 solid-to-solution ratio. However, the relative standard deviations for these values are quite high meaning that these small numbers are likely dominated by analytical uncertainty. Similarly, the desorption  $K_d$  values for the duplicate samples in the Cast Stone pore water fluctuate between 0 and  $\sim 10$  mL/g. However, due to the very small quantity of analytes initially sorbed to the HEPA material, these values are also likely dominated by analytical uncertainty. Because sorption from these tests was so low, the desorption  $K_d$  tests with HGM-5 pore water were not performed.

Because the HEPA filters will come from the off-gas system at WTP, alternative approaches for determining  $K_d$  values would be to 1) collect a used HEPA filter being used for vapor capture of a Tc/I containing stream and subject that material to a desorption  $K_d$  test or 2) add an aliquot of a known amount of Tc to a Tc filter, allow that solution to dry, and then subject the loaded HEPA material to a desorption  $K_d$  test. Because procuring a HEPA sample that has been used in an off-gas system would be difficult, the second approach may be more feasible.

## 6.2 Sorption/Desorption Characteristics of Neat Grouts

The 2016 SSW data package did not contain analyte  $K_d$  values for specific grout formulations as target grout formulations had not yet been identified. Sorption and desorption  $K_d$  values for HGM-5 and Cast Stone show that the Tc and  $\text{I}^-$  sorption  $K_d$  values are consistently smaller than the sorption  $\text{IO}_3^-$  and Hg  $K_d$  values. The sorption  $K_d$  values for Tc were  $1.4 \pm 0.7$  mL/g (HGM-5) and  $1.5 \pm 2.2$  mL/g (Cast Stone) and for  $\text{I}^-$  they were  $2.5 \pm 1.4$  mL/g (HGM-5) and  $2.1 \pm 0.9$  mL/g (Cast Stone), respectively. The calculated

desorption  $K_d$  values are about an order of magnitude higher than the sorption  $K_d$  values for these analyte/ neat grout combinations, but uncertainties on these calculated desorption  $K_d$  values are large due to the very small amount of analyte initially sorbed to the surface.

Both HGM-5 and Cast Stone show some sorption capacity for  $\text{IO}_3^-$  and Hg. For the HGM-5, the  $\text{IO}_3^-$   $K_d$  value of  $6.9 \pm 0.4 \times 10^2$  mL/g is near to the value of  $5.7 \times 10^2$  mL/g obtained after 15 days for the initial test. For Cast Stone, the  $K_d$  value of  $2.8 \pm 0.1 \times 10^1$  mL/g is smaller than that of HGM-5. In addition, HGM-5 and Cast Stone exhibited a desorption  $K_d$  on the order of  $10^2$  mL/g indicating that more than 90% of the  $\text{IO}_3^-$  sorbed to the surface remained on the material after exposure to fresh solution.

On the other hand, a greater amount of Hg is sorbed to Cast Stone than HGM-5. Roughly 40% of the Hg sorbed to HGM-5 whereas Hg concentrations were below the estimated quantitation limit (EQL) in the Cast Stone tests (8.12 ppb or >99.8% removal). This difference was likely due to the presence of sulfide in the slag-containing Cast Stone and the low solubility of  $\text{Hg}_2\text{S}$ . The small desorption  $K_d$  values indicate that the majority of the Hg remains on the neat grout surfaces after exposure to fresh pore water solution.

In conditions where multiple analytes were present in the same system, no interactions were observed, i.e. the  $K_d$  values for the individual analyte tests were similar to analyte  $K_d$  values in the mixed systems.

At this point, no additional information is available to understand the differing interactions of the analytes with the grout materials. This is mostly due to the largely heterogeneous, multi-phase nature of the different grout materials. For instance, it is not known why iodate is more readily removed than iodide but it may be linked to the favorable incorporation of iodate into calcium carbonate minerals (Lawter et al. 2018), although only a small amount of calcite phases was present. This process would be more likely in the high pH/high Ca interstitial pore waters present in the grout materials. However, it is unknown why this process would be more prevalent in the HGM-5 grout compared to the Cast Stone grout. In addition, Hg removal by the grouts also occurs but reasons for this observation remain elusive until more substantial post-reaction characterization studies can be performed.

### 6.3 $K_d$ Summary and Discussion

A test matrix of batch sorption and desorption tests was performed with two grout pore waters (Cast Stone and HGM-5), five solid waste materials (GAC, AgM, HEPA filters, neat Cast Stone, and neat HGM-5), and four different analytes (Tc, I,  $\text{IO}_3^-$ , and Hg). To our knowledge, this is the first full set of tests to provide sorption and desorption  $K_d$  values for these analytes with these materials that are of high importance in Hanford site closure activities. Though the data are informative, for some of the  $K_d$  values are associated with a high uncertainty. This is mainly due to the intrinsic shortcoming of the batch sorption test method that is not well-suited for measuring  $K_d$  values for very low or non-sorbing species (EPA 1999). A specific example of this is seen in Table 6-1 where  $K_d$  values of 0 mL/g were used when the average  $K_d$  value for a set of tests was less than zero – a phenomenon that is caused by analytical uncertainty. A more focused experimental effort would be required to refine the  $K_d$  values for some of the tests with low sorption values. It should also be noted, that no attempt was made to determine in what solid/solution ratios or analytes concentrations these  $K_d$  values would be non-linear. The starting concentration of the analyte should also be varied, ideally to lower concentrations where relative changes in concentrations will be large enough to provide more precise determinations of  $K_d$ . In addition, no attempt was made to monitor the speciation of iodine throughout the experiment, which may also impact the results. Lastly, tests in an inert atmosphere would be required to control for any redox reactions that may have occurred during the present  $K_d$  tests; however the HGM-5 and Cast Stone pore waters provided different redox environments in solution due to the presence of BFS in the Cast Stone.

Of the various solid waste materials, GAC has previously been subjected to the widest range of studies – especially for iodine. However, as indicated by Flach et al. (2016), there was no existing data using site-specific spent-GAC to quantify the tendency for radioiodine to desorb from GAC and it was unknown if iodine oxidation state influences uptake by GAC. Flach et al. (2016) recommended a  $K_d$  value for spent-GAC to have a mean of 600 mL/g and the 95 percentile range be set at 100 to 2000 mL/g. At this point, we cannot recommend a better iodide  $K_d$  value due to the high background of iodine released from the GAC used in this test. Further studies would be needed to either homogenize the GAC material prior to testing or use a radioactive tracer to get more accurate tracking. However, literature evidence would suggest that the iodide  $K_d$  values may be lower due to ionic competition. Tests were also performed with  $\text{IO}_3^-$  and showed that iodate species did not readily adsorb to the GAC. In addition to iodine values, the results presented here are, to our knowledge, the first that report on the interaction of Hg and Tc with GAC. In HGM-5 pore water, the  $K_d$  values for Tc and Hg are  $(2.6 \pm 2.3) \times 10^3$  mL/g and  $(1.2 \pm 0.3) \times 10^3$  mL/g, respectively. In Cast Stone pore water, the  $K_d$  values for Tc and Hg are  $(2.3 \pm 1.3) \times 10^3$  mL/g and  $(1.0 \pm 0.3) \times 10^4$  mL/g, respectively.

Flach et al. (2016) also provided a best estimate  $K_d$  value for the Ag-zeolite of 1000 mL/g with a minimum value of 100 and a maximum value of 10,000 mL/g. The authors noted that no  $K_d$  values for iodide desorption from Ag-zeolite were available. The data from the present test show that for iodide as the dominant iodine species, the maximum value is more realistic. However, in the case of iodate very little was removed from solution ( $K_d$  of  $<5$  mL/g). Therefore, the  $K_d$  value is highly dependent on iodine speciation and before a total iodine  $K_d$  value can be selected, knowledge of iodine speciation at the site must be considered. Lastly, the calculated sorption  $K_d$  value of with AgM is  $(4.3 \pm 2.4)$  mL/g in Cast Stone pore water and  $(4.0 \pm 4.2)$  mL/g in HGM-5 pore water.

Sorption of analytes to HEPA filter material was also examined in this set of batch sorption tests. However, as noted previously, batch sorption tests may not be an optimal method to quantify accurate  $K_d$  values with HEPA filters because low sorption  $K_d$  values are difficult to measure with this method and this subsequently results in difficulty in obtaining accurate desorption  $K_d$  values. Flach et al. (2016) recommended best estimate  $K_d$  values of 3 mL/g with a minimum of 0.5 mL/g and maximum of 30 mL/g for Hg, a value of 0 mL/g with a minimum of 0 mL/g and maximum of 0.2 mL/g for iodide, and values of 0 mL/g with a minimum of 0 mL/g and maximum of 0 mL/g for Tc. The results in this work, which were conducted with both iodide and iodate, support these low values. However, because small changes in the  $K_d$  value for analyte with low  $K_d$  values can cause relatively large changes in contaminant transport calculation, further refinement of these desorption  $K_d$  values are needed.

Lastly, experiments with neat grouts showed that very little Tc or I are sorbed by the grouts but Hg and  $\text{IO}_3^-$  showed some sorption to the grouts. The Hg sorption  $K_d$  with Cast Stone was greater than the Hg sorption  $K_d$  with HGM-5 whereas the  $\text{IO}_3^-$  sorption  $K_d$  of HGM-5 was greater than the  $\text{IO}_3^-$  sorption  $K_d$  of Cast Stone. Once sorbed to the neat grout surface, these contaminants were sparingly released when contacted with fresh pore water solution. To fully understand the sorption capability of the neat grout materials, the mechanism for these sorption and immobilization processes should be identified.

For reference, summary tables comparing the  $K_d$  values for iodine species (Table 6.3), Tc (Table 6.4) and Hg (Table 6.5) are presented below.

**Table 6-3.** Comparison of Iodine Species Sorption and Desorption Distribution Coefficients ( $K_d$ ), mL/g

	IDF PA Data Package	Iodide Sorption $K_d$	Iodide Desorption $K_d$	Iodate Sorption $K_d$	Iodate Desorption $K_d$	Organic I Desorption $K_d$
Grouts						
<b>Oxidizing</b>	HGM-5	$2.5 \pm 1.4$	$17 \pm 11$	$690 \pm 40$	$590 \pm 30$	
	Nichols et al. 2018 Mix 1 <sup>a</sup>	$3.03 \pm 0.23$	$6.14 \pm 0.07$	$3.06 \pm 0.16$	$30.62 \pm 0.17$	$32.28 \pm 1.15$
	Flach et al. 2016 Max <sup>b</sup>	10				
	Best	4				
	Min	0				
<b>Reducing</b>	Cast Stone	$2.1 \pm 0.9$	$43 \pm 17$	$2.8 \pm 0.1$	$290 \pm 90$	
	Nichols et al. 2018 Mix 13 <sup>a</sup>	$2.33 \pm 0.10$	$7.50 \pm 0.10$	$2.80 \pm 0.30$	$121.78 \pm 9.54$	$42.07 \pm 2.47$
	Flach et al. 2016 Max <sup>c</sup>	0				
	Best	0				
	Min	0				
Waste Materials						
<b>GAC</b>	HGM-5 Pore Water	$16 \pm 22$	-	$26 \pm 21$	-	
	Cast Stone Pore Water	$100 \pm 60$	$0.0 \pm 0.0$	$5.2 \pm 6.8$	$0.0 \pm 0.0$	
	Flach et al. 2016 Max <sup>d</sup>	2000				
	Best	600				
	Min	100				
<b>AgM</b>	HGM-5 Pore Water	$2.3 \pm 1.0 \times 10^4$	$1.4 \pm 1.1 \times 10^6$	$2.9 \pm 1.3$	$790 \pm 020$	
	Cast Stone Pore Water	$5.8 \pm 4.5 \times 10^4$	$3.0 \pm 1.4 \times 10^5$	$3.5 \pm 1.6$	$1.4 \pm 0.9 \times 10^3$	
<b>HEPA Filter Media</b>	HGM-5 Pore Water	$0.39 \pm 0.34$	-	$0.0 \pm 0.0$	-	
	Cast Stone Pore Water	$0.077 \pm 0.058$	$11 \pm 0.0$	$0.84 \pm 0.50$	$16 \pm 0.0$	
	Flach et al. 2016 Max <sup>e</sup>	0.2				
	Best	0				
	Min	0				

<sup>a</sup> Nichols et al. 2018. Table 16 and Table 18, <sup>b</sup> Flach et al. 2016. Table 8-4, <sup>c</sup> Flach et al. 2016. Table 8-5, <sup>d</sup> Flach et al. 2016. Table 8-7, <sup>e</sup> Flach et al. 2016. Table 8-8

**Table 6-4.** Comparison of Technetium Sorption and Desorption Distribution Coefficients ( $K_d$ ), mL/g

		IDF PA Data Package	Tc Sorption $K_d$	Tc Desorption $K_d$
<b>Grouts</b>				
<b>Oxidizing</b>	HGM-5		$1.4 \pm 0.7$	$7.1 \pm 3.5$
	Nichols et al. 2018 Mix 1 <sup>a</sup>		$2.39 \pm 0.50$	-
	Flach et al. 2016 Max <sup>b</sup>	2		
	Best	0.8		
	Min	0		
<b>Reducing</b>	Cast Stone		$1.5 \pm 2.2^*$	$0.0 \pm 0.0$
	Nichols et al. 2018 Mix 13 <sup>a</sup>		$2.59 \pm 0.90$	-
	Flach et al. 2016 Max <sup>c</sup>	2000		
	Best	1000		
	Min	100		
<b>Waste Materials</b>				
<b>GAC</b>	HGM-5 Pore Water		$2.6 \pm 2.3 \times 10^3$	$170 \pm 10$
	Cast Stone Pore Water		$2.3 \pm 1.3 \times 10^3$	$150 \pm 20$
<b>AgM</b>	HGM-5 Pore Water		$4.0 \pm 4.2$	$1.9 \pm 0.5 \times 10^3$
	Cast Stone Pore Water		$4.0 \pm 4.2$	-
<b>HEPA Filter Media</b>	HGM-5 Pore Water		$0.32 \pm 0.045$	$0.0 \pm 0.0$
	Cast Stone Pore Water		$0.36 \pm 0.48$	$37 \pm 0.0$
	Flach et al. 2016 Max <sup>d</sup>	0		
	Best	0		
	Min	0		
<sup>a</sup> Nichols et al. 2018. Section 4.2, <sup>b</sup> Flach et al. 2016. Table 8-4, <sup>c</sup> Flach et al. 2016. Table 8-5. <sup>d</sup> Flach et al. 2016. Table 8-8				
*Note: the $K_d$ values for Tc to the neat grouts represent the sorption of Tc to the grout. In the 2017 IDF PA the $K_d$ values used for reducing grout were selected to represent the ability of a reducing grout to sequester Tc by reducing it from its mobile oxidized form to an immobile low solubility state. In this experimental design the Tc is most likely not reduced during the test.				

**Table 6-5.** Comparison of Mercury Sorption and Desorption Distribution Coefficients ( $K_d$ ), mL/g

		<b>IDF PA Data Package</b>	<b>Hg Sorption <math>K_a</math></b>	<b>Hg Desorption <math>K_a</math></b>
Grouts				
<b>Oxidizing</b>	HGM-5		$17 \pm 2$	$500 \pm 20$
	Flach et al. 2016 Max <sup>a</sup>	600		
	Best	300		
	Min	30		
<b>Reducing</b>	Cast Stone		$1.2 \pm 0.0 \times 10^4$	$4.3 \pm 1.0 \times 10^4$
	Flach et al. 2016 Max <sup>b</sup>	1000		
	Best	500		
	Min	50		
Waste Materials				
<b>GAC</b>	HGM-5 Pore Water		$1.2 \pm 0.4 \times 10^5$	$5.1 \pm 1.0 \times 10^4$
	Cast Stone Pore Water		$1.0 \pm 0.3 \times 10^4$	$440 \pm 410$

<sup>a</sup> Flach et al. 2016. Table 8-4  
<sup>b</sup> Flach et al. 2016. Table 8-5

## 7.0 EPA Method 1315 Leach Testing of Stabilized GAC and Ag-Mordenite

### 7.1 Iodide Loading

Prior to fabrication of the monolith samples, the GAC and AgM were first loaded with iodide in aqueous batch contact experiments. For the GAC contact, DDI ( $> 18.2 \text{ M}\Omega\cdot\text{cm}$ , conforming to ASTM Type I standards, ASTM D1193-06(2018)) was spiked to a concentration of  $6335 \pm 162 \mu\text{g/L}$  of iodide, and following contact with 300 g of GAC, the resulting concentration was  $238 \pm 2 \mu\text{g/L}$  of iodide. This gave an iodide loading of  $20 \mu\text{g I/g GAC}$ . For the AgM the DDI was spiked to  $119500 \pm 2121 \mu\text{g/L}$ . After contact with 600 g of AgM, the resulting concentration was  $310 \pm 19 \mu\text{g/L}$  of iodide. The resulting loading of iodide to the AgM was  $199 \mu\text{g I/g AgM}$ . Both the GAC and AgM were dried in an open atmosphere for 24 h prior to fabrication of the monoliths, but both materials still retained water. The GAC had a final water content of 16 wt% and the AgM had a water content of 35 wt%. This mass of water was taken into account for the volume of material added in waste form fabrication. A heat treatment to dry the GAC and AgM was not used to avoid any loss of iodide.

### 7.2 EPA Method 1315

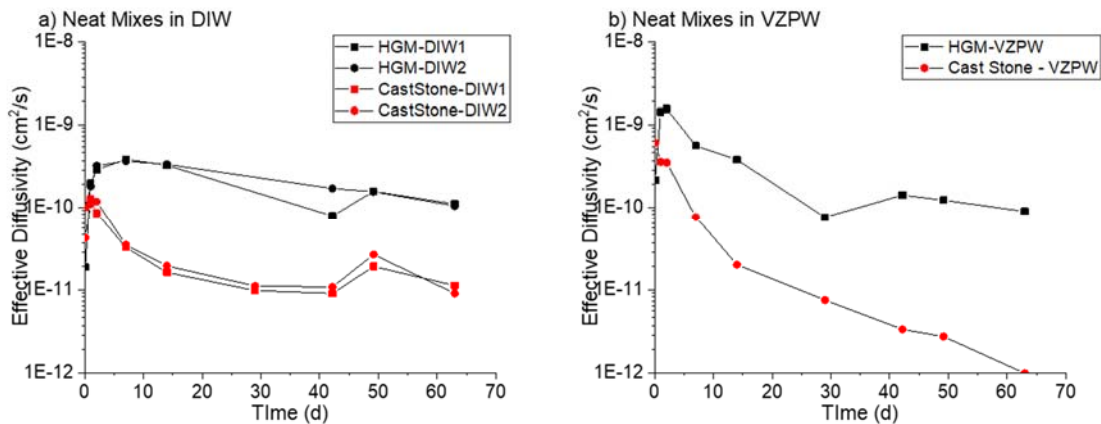
EPA Method 1315 (EPA 2013) was used for leach testing the monoliths using two solutions, building deionized water (DIW) and a synthetic vadose zone pore water (VZPW) (both solutions were open to the atmosphere, and no de-aeration was carried out). The VZPW simulant recipe is shown in Table 7.1. The recipe is based on several direct measurements of actual VZPW removed from Hanford formation sediments from a borehole in the 200 E Area where the IDF is located. Several hundred grams of field moist sediment were removed from core liners drilled into uncontaminated Hanford formation sediments using a cable tool drive barreling. Field moist sediments were placed in special holders and ultra-centrifuged for several hours. Small volumes of VZPW passed through the sediment and collected at the bottom of the holders in small sampling cups. When approximately 30 mL to 50 mL of VZPW was collected from each sediment sample, it was immediately filtered through  $0.45 \mu\text{m}$  membrane filters and analyzed for chemical composition. The pore water characterizing results from two depths (48.5 and 82.5 ft. below ground surface) from borehole C4124; 299-E26.22 (Brown et al. 2006) were averaged and the cation amounts charge balanced using primarily bicarbonate with minor amounts of nitrate, fluoride and sulfate. Although Si is present at  $\sim 23 \text{ ppm}$  in the actual pore waters, it was not added to the simulant recipe to limit precipitation. Reagents were added in the order given in Table 7.1 to the corresponding volume of DIW.

**Table 7-1 - Vadose Zone Pore Water Recipe Listed in Order of Addition of Each Component**

Order	VZPW Recipe			
	Molarity (mol/L)	Reagents	MW (g/mol)	g/L
1	0.012	CaSO <sub>4</sub> •2H <sub>2</sub> O	172.17	2.07
2	0.0017	NaCl	58.44	0.10
3	0.0004	NaHCO <sub>3</sub>	84.01	0.03
4	0.0034	NaNO <sub>3</sub>	84.99	0.29
5	0.0026	MgSO <sub>4</sub>	120.37	0.31
6	0.0024	MgCl <sub>2</sub> •6H <sub>2</sub> O	203.31	0.49
7	0.0007	KCl	74.55	0.05

Adjust pH to 7.0 (± 0.2) with sodium hydroxide or sulfuric acid dependent on initial pH.

The observed diffusivities ( $D_{obs}$ ) for iodide from the neat mixes (Test Batches 1 and 2) (HGM-5 and Cast Stone) are shown in Figure 7-1. Plots of log cumulative release vs log time are available in Appendix E. Duplicate monoliths were leached in DIW whereas only a single sample from Test Batch 1 and 2 was leached in VZPW due to sample availability. In DIW (Figure 7-1 a), the HGM-5 samples measured a peak iodide observed diffusivity of  $3.8 \times 10^{-10}$  cm<sup>2</sup>/s at 7 d and a 28 d to 63 d average of  $1.3 \times 10^{-10}$  cm<sup>2</sup>/s. The Cast Stone samples measured a peak iodide observed diffusivity of  $1.1 \times 10^{-10}$  cm<sup>2</sup>/s at 2 d before ending with a 28 to 63 d average of  $1.3 \times 10^{-11}$  cm<sup>2</sup>/s. In VZPW (Figure 7-1b), the HGM-5 again had a higher iodide observed diffusivity with a  $1.8 \times 10^{-10}$  cm<sup>2</sup>/s average between 28 and 63 d, compared with the Cast Stone sample, which continually decreased in iodide observed diffusivity giving an average of  $3.6 \times 10^{-12}$  cm<sup>2</sup>/s between 28 and 63 d. The iodide observed diffusivity values for the Cast Stone are within range of those previously measured for iodide containing Cast Stone (Westsik et al. 2013, Serne et al. 2015).



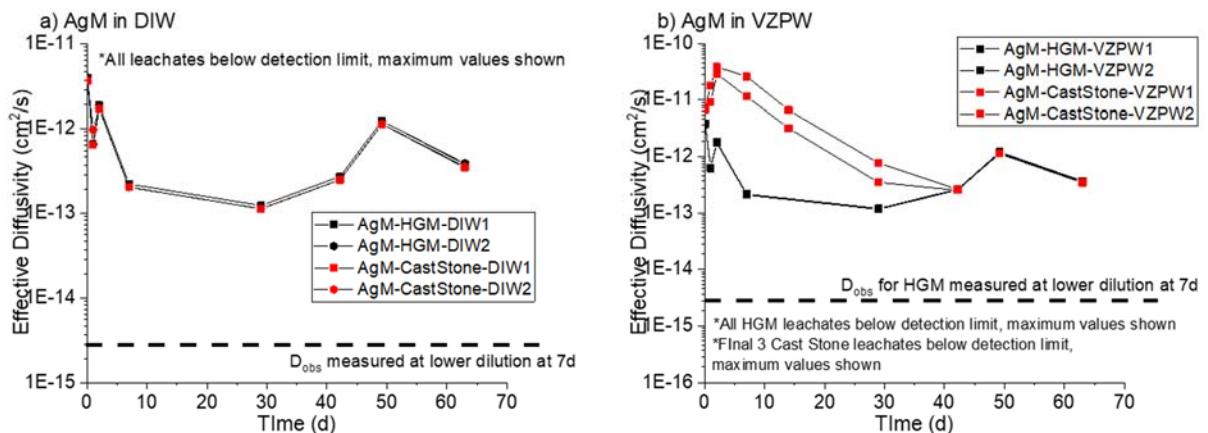
**Figure 7-1.** The Iodide Observed Diffusivities for the Two Neat Mixes, HGM-5 and Cast Stone, following Leach Testing in (a) DIW and (b) VZPW

Figure 7-2 displays the iodide observed diffusivities from the stabilized AgM samples from Test Batches 5 and 6. For tests in DIW (Figure 7-2a), no measurable iodide was found in the collected leachates for both the HGM-5 and Cast Stone samples. *The observed diffusivities presented are maximum values calculated using the instrument detection limit for the ICP-MS iodide method (1.26 µg/L).* The 28 to

63-d average of the maximum iodide observed diffusivity was  $5.0 \times 10^{-13} \text{ cm}^2/\text{s}$ . For comparison purposes, the 7-d sample was analyzed at a lower dilution (achieving a detection limit of  $0.126 \mu\text{g}/\text{L}$ ), and no iodide was measurable. This indicates that the observed diffusivities may be lower than  $3 \times 10^{-15} \text{ cm}^2/\text{s}$ , which was the observed diffusivity calculated using the lower detection limit value.

In tests in VZPW (Figure 7-2b), the HGM-5 leachates also did not contain measurable iodide, and the observed diffusivities displayed were again calculated using the instrument detection limit ( $1.26 \mu\text{g}/\text{L}$ ). The 20 to 63-d *maximum* iodide observed diffusivity for the HGM-5 was  $4.9 \times 10^{-13} \text{ cm}^2/\text{s}$ . The 7-d sample was analyzed with a lower dilution (achieving an instrument detection limit of  $0.126 \mu\text{g}/\text{L}$ ), and iodide was not detected. This measurement indicates that the iodide observed diffusivity for stabilized AgM in HGM-5 may be as low as  $2.7 \times 10^{-15} \text{ cm}^2/\text{s}$ . The Cast Stone AgM samples on the other hand, had measurable iodide in the leachates for intervals  $< 42$  d. The highest iodide observed diffusivity measured  $3.8 \times 10^{-11} \text{ cm}^2/\text{s}$  at the 2-d interval and steadily decreased to an average of  $5.7 \times 10^{-13} \text{ cm}^2/\text{s}$  between the 28 to 63 d intervals. The leachate from the final three intervals did not have measurable iodide. The reasoning for measurable iodide being present in the VZPW leachates and not the DIW leachates is not known, The main difference between the two systems being the pH difference in the leachate (DIW  $\sim 12$  and VZPW  $\sim 10.8$ ) and the migrating species from the VZPW into the monoliths (e.g.  $\text{CO}_3^{2-}$ ,  $\text{SO}_4^{2-}$ ) and it is unknown if either of these lead to the difference in iodide release.

The difference in iodide retention between the HGM-5 and Cast Stone samples likely arises from the presence of BFS in the Cast Stone formulation. The iodide was held on the AgM as AgI, and the BFS has two possible methods of destabilizing this AgI. The BFS generated a reducing environment within the cured waste form, which can lead to reduction of the  $\text{Ag}^+$  to  $\text{Ag}^0$  of the AgI, and in turn, release the iodide. This process was shown in a recent study of AgI stability in reducing grouts (Kaplan et al. 2018). Secondly, the BFS contains sulfur which can displace the iodide from the Ag, leading to iodide release, as was shown for LAW Cast Stone (Asmussen et al. 2017). These interference mechanisms are not possible in the oxidized, sulfur-free HGM-5 formulation.



**Figure 7-2.** The Iodide Observed Diffusivities for the HGM-5 and Cast Stone Mixes Used to Stabilize AgM following Leach Testing in a) DIW and b) VZPW. In DIW, all leachate concentrations were below the instrument detection limit used. In the VZPW, all HGM-5 leachates and the final three Cast Stone leachates were below the instrument detection limit. In these cases, the values shown represent a maximum observed diffusivity possible based on the detection limit value ( $1.26 \mu\text{g}/\text{L}$ ). The 7-d sample was analyzed as a lower dilution ( $0.126 \mu\text{g}/\text{L}$ ) and was also a non-detect, and the corresponding diffusivity is shown as the dotted line.

The iodide observed diffusivities for the stabilized GAC leach tests are shown in Figure 7-3. All values are corrected to account for total iodide present on the GAC. As seen in Section 5.0, all iodide in the GAC can be easily leached and thus was available to leach from the waste form. In DIW (Figure 7-3a), the observed diffusivities for the HGM-5 and Cast Stone samples were similar. For HGM-5, the highest iodide observed diffusivity measured was  $3.0 \times 10^{-9} \text{ cm}^2/\text{s}$  at 2 d, and at 63 d, the average diffusivity from the two samples was  $6.4 \times 10^{-10} \text{ cm}^2/\text{s}$ . For the Cast Stone, a maximum iodide observed diffusivity of  $6.1 \times 10^{-9} \text{ cm}^2/\text{s}$  was measured at 2 d, and an average iodide observed diffusivity of  $6.8 \times 10^{-10} \text{ cm}^2/\text{s}$  was measured at 63 d. In VZPW (Figure 7-3b), the average iodide observed diffusivity at the 63-d interval was  $3.9 \times 10^{-10} \text{ cm}^2/\text{s}$  for the HGM-5 samples and  $5.6 \times 10^{-10} \text{ cm}^2/\text{s}$  for the Cast Stone samples. These iodide observed diffusivities are comparable to those previously measured in iodide containing waste forms Asmussen et al. 2016a, Serne et al. 2015, Westsik et al. 2013, Crawford et al. 2017).

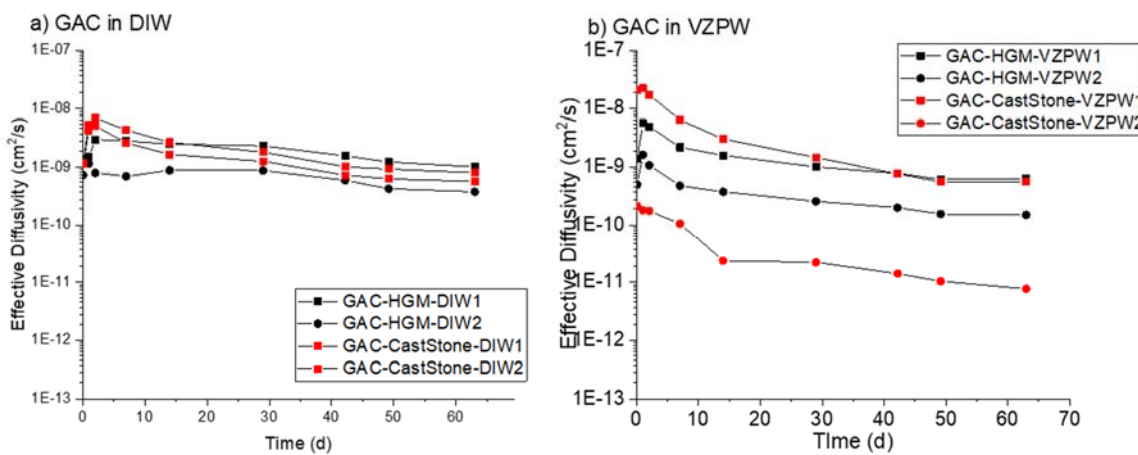


**Figure 7-3.** The Iodide Observed Diffusivities for the HGM-5 and Cast Stone Mixes Used to Stabilize GAC following Leach Testing in a) DIW and b) VZPW. The iodide observed diffusivities were calculated to account for the leachable iodide nominally present in the GAC.

### 7.3 Leach Testing Discussion and Summary

In the SSW data package used for the 2017 IDF PA (Flach et al. 2016), values were suggested for the effective diffusivities to be used to represent non-sorbing species in stabilized SSW. The values were based on available effective/observed diffusivity data on freely leachable species (e.g.,  $\text{NO}_3^-$ ,  $\text{NO}_2^-$ ,  $\text{Cl}^-$ ) from cementitious materials. Non-sorbing diffusivity values were suggested for three material types: grout, paste and mortar. Stabilized non-debris waste was suggested to behave most like a mortar. The laboratory  $D_{\text{obs}}$  values measure the ability of the waste form to retain its contaminant inventory in saturated leaching tests, the effective diffusivity ( $D_e$ ) values used in the PA represent the waste form contaminant retention in disposal.  $D_e$  and  $D_{\text{obs}}$  are very similar to one another (Serne et al. 2015).  $D_e$  is determined through adjustment of an apparent diffusion coefficient ( $D_a$ ), which is the diffusivity value for a non-sorbing species, by a retardation factor,  $R_f$ . If the species is also non-sorbing, the  $D_e$  and  $D_a$  will be similar as the  $R_f$  will be close to 1. If the species is sorbing or retained in the waste form by a separate process (e.g. redox), then the  $R_f$  will be large and lead to a smaller  $D_e$ , and in turn lower release. This relationship is shown in Equation 7.1.

$$D_e = \frac{D_a}{R_f} \quad (7.1)$$

where:

$R_f$  = retardation factor

$D_e$  = effective diffusion coefficient (cm<sup>2</sup>/s)

$D_a$  = apparent diffusion coefficient (cm<sup>2</sup>/s)

A comparison between the non-sorbing effective diffusivities for SSW and iodide observed diffusivities from the present work is given in Table 7-2. The comparison to make is if the  $D_{obs}$  is smaller than the  $D_e$  in the data package, the iodine is more strongly held within the waste form. The optimistic effective diffusivity for a non-sorbing species reported in the data package for mortar was  $6.3 \times 10^{-9}$  cm<sup>2</sup>/s. No measurement of a  $D_{obs}$  for a mobile species was performed for the samples as there was no artificial source of a mobile species beside iodide in the samples (e.g. Na, K, NO<sub>3</sub>). Commonly, the Na/NO<sub>3</sub> will be added through the liquid simulant used in fabrication and that inventory solely used to determine the initial concentration. Fly ash contains Na and K, more so than slag and cement, and these values were reported previously (Westsik et al. 2013). However, it is unknown what fraction of this inventory in the solid material is leachable. Thus, the solid inventory has been ignored in previous testing efforts and was not used for a  $D_{obs}$  calculation in this work. The Na concentration in the leachates was measured for select samples with DIW as the leachant. Example plots of log cumulative Na release vs log time for Na can be found in Appendix E. The neat HGM-5 and Cast Stone and the GAC containing samples were within the EPA Method 1315 guideline of a slope of  $0.5 \pm 0.15$ . These slopes relate to a diffusive process for Na release, as has been reported previously. The slopes of the AgM containing samples were above this range. The origin is unknown but could be due to the mordenite slowing release of the Na. With the similarity of the neat grout, it is suggested that the geometric average for Na release from Cast Stone given in Cantrell et al. 2015 ( $5.8 \times 10^{-9}$  cm<sup>2</sup>/s) be used for a comparative mobile species  $D_{obs}$ .

This mobile effective diffusivity of both the mortar in the SSW data package (Flach et al. 2016) and the suggested value above were comparable to the iodide observed diffusivities for the GAC in both the HGM-5 and Cast Stone.

Using the average observed diffusivity from the 28-d through the 63-d interval, the iodide observed diffusivities for GAC stabilized in HGM-5 was  $1.1 \times 10^{-9}$  cm<sup>2</sup>/s in DIW and  $4.8 \times 10^{-10}$  cm<sup>2</sup>/s in VZPW. When stabilized in Cast Stone, the iodide observed diffusivities were  $9.7 \times 10^{-10}$  cm<sup>2</sup>/s in DIW and  $4.3 \times 10^{-10}$  cm<sup>2</sup>/s in VZPW. The assumption that stabilized GAC waste forms behave similarly to an aggregate-containing mortar appears to be valid based on these results.

For the AgM stabilized in HGM-5, the iodide observed diffusivity could only be determined as a conservative maximum value of  $5.0 \times 10^{-13}$  cm<sup>2</sup>/s in DIW and  $4.6 \times 10^{-13}$  cm<sup>2</sup>/s in VZPW. A conservative maximum iodide observed diffusivity was also only possible for the AgM stabilized in Cast Stone in DIW ( $4.9 \times 10^{-13}$  cm<sup>2</sup>/s). In VZPW the 28 – 63 d interval average observed diffusivity was  $5.7 \times 10^{-13}$  cm<sup>2</sup>/s with larger values measured at the shorter time intervals. The AgM is capable of stabilizing the iodide within the waste form, through the formation of AgI. In the non-slag containing, oxidized grout (HGM-5) the AgI remains stable, and although conservative observed diffusivities were reported, much lower observed diffusivities are likely more realistic. In slag-containing grout (Cast Stone), either the reducing conditions or the presence of sulfur led to destabilization of the AgI and measurable iodide concentrations in the leachate. The observed iodide diffusivities for the AgM in Cast Stone were far lower than that of an aggregate containing mortar. Based on these observations, it is suggested that a non-reducing grout be used for stabilization of AgM.

**Table 7-2.** A comparison between the suggested effective diffusivity values for a mobile species from the 2017 IDF PA Data Packages for SSW and the iodine observed diffusivities from this work. The values from this work listed are the average 28 d – 63 d. ***Italicized and bolded values represent maximum values because measurements of the iodine concentrations in the leachates were below detection limits.***

Effective/Observed Diffusion Coefficient (cm <sup>2</sup> /s)	Grout (cm <sup>2</sup> /s)	Paste (cm <sup>2</sup> /s)	Mortar (cm <sup>2</sup> /s)	Neat Oxidized Grout (cm <sup>2</sup> /s)	Neat Reduced Grout (cm <sup>2</sup> /s)	GAC in Oxidized Grout (HGM-5) (cm <sup>2</sup> /s)	GAC in Slag Containing (Cast Stone) (cm <sup>2</sup> /s)	AgM in Oxidized Grout (HGM-5) (cm <sup>2</sup> /s)	AgM in Slag Containing (Cast Stone) (cm <sup>2</sup> /s)
Pessimistic Value <sup>1</sup>	8.1×10 <sup>-7</sup>	8.2×10 <sup>-7</sup>	4.7×10 <sup>-7</sup>	-	-	-	-	-	-
Best Estimate <sup>1</sup>	3.0×10 <sup>-8</sup>	2.9×10 <sup>-8</sup>	5.4×10 <sup>-8</sup>	-	-	-	-	-	-
Optimistic Value <sup>1</sup>	1.1×10 <sup>-9</sup>	1.0×10 <sup>-9</sup>	6.3×10 <sup>-9</sup>	-	-	-	-	-	-
This Work DIW	-	-	-	1.3×10 <sup>-10</sup>	1.3×10 <sup>-10</sup>	1.1×10 <sup>-9</sup>	9.7×10 <sup>-11</sup>	<b>5.0×10<sup>-13</sup></b>	<b>4.6×10<sup>-13</sup></b>
This Work VZPW	-	-	-	1.8×10 <sup>-10</sup>	3.6×10 <sup>-12</sup>	4.8×10 <sup>-10</sup>	4.3×10 <sup>-10</sup>	<b>4.9×10<sup>-13</sup></b>	5.7×10 <sup>-13</sup>
LAW Cast Stone <sup>2</sup>	5.7×10 <sup>-9</sup>	-	-	-	-	-	-	-	-

<sup>1</sup> Flach et al. 2016

<sup>2</sup> Cantrell et al. 2016

## 8.0 Summary

In summary, the work presented in this report provides data needs to fill knowledge and data gaps related to the performance of stabilized SSW in grout. Two grout formulations were investigated to compare an oxidized grout (FA+OPC, similar to Hanford grout mix 5) and a reduced grout (FA+OPC+BFS, similar to the formulation used to fabricate Cast Stone waste forms). Specifically, findings were presented related to: 1) provide the sorption/desorption data on key contaminants (technetium, iodide, iodate, mercury) expected to be found in Hanford SSW (GAC, AgM, HEPA) in simulated grout pore water conditions; (2) the leaching behavior of iodide from stabilized/blended GAC/AgM in oxidizing and reducing grout; (3) measure physical properties of two grout mixes to stabilize GAC/AgM upon curing; and (4) provide additional data on candidate grout mixes to immobilize SSW.

The testing involved evaluation of the fresh grout properties (flowability, set time, free liquids, and heat of hydration), cured grout properties (compressive strength, saturated hydraulic conductivity, and water characteristic curve), the interaction between the GAC/AgM and cured grout matrix (microscopy and imaging), the sorption/desorption of Tc, iodide, iodate, and mercury species to SSW materials and the grouts (ASTM C1733-17 to determine the distribution coefficient,  $K_d$ ), and leach testing (EPA Method 1315).

The major findings of this work are given below.

- *GAC/AgM Stabilization*: both grout mixes were able to incorporate and suspend the GAC and AgM. Distribution of the particulates of both materials was mostly homogenous based on results of cross section imaging and XCT. Optical microscopy and SEM results indicated that the GAC was well adhered to the hardened grout matrix for both formulations. Imaging of the AgM showed a reaction region was observed between the particles and the hardened grout matrix. Using EDS this region was found to contain Ag that had migrated from the AgM to the grout matrix. The AgM likely participated, partially, in hydration reactions during curing.
- *Sorption/Desorption*:
  - *Iodide*: The  $K_d$  for iodide sorption to the oxidized grout (HGM-5) was  $2.5 \pm 1.4$  mL/g, which was comparable to the data package “best” value (Flach et al. 2016). The reduced grout (Cast Stone) had a nonzero value,  $2.1 \pm 0.9$  mL/g, different from the zero  $K_d$  in the data package. For sorption to the GAC material itself, the measured  $K_d$  values ( $16 \pm 2.2$  mL/g in reduced grout pore water and  $100 \pm 60$  mL/g in the oxidized grout pore water) were lower than the data package values. This difference was likely a result of the high ionic competition in the grout pore water, which was supported by literature available on GAC sorption with iodide. Iodide  $K_d$  values for the sorption to AgM were extremely high ( $> 2 \times 10^4$  mL/g), with little desorption observed. The HEPA filter media had a nonzero  $K_d$  for iodide, although it was  $< 1$  mL/g.
  - *Iodate*: Iodate  $K_d$  values were not included in the SSW data package (Flach et al. 2016), but were included in this work due to minimal knowledge of iodine speciation throughout the WTP flowsheet and identification of the prevalence of iodate in the Hanford subsurface. Iodate  $K_d$ s were comparable to iodide in all material cases except for a larger  $K_d$  ( $2.6 \pm 2.1 \times 10^1$  mL/g) measured for the GAC in HGM-5 pore water.
  - *Technetium*: The  $K_d$  values for sorption of Tc to the oxidized grout ( $1.4 \pm 0.7$  mL/g) were similar to the SSW data package values (Flach et al. 2016). For the reduced grout, the measured values ( $1.5 \pm 2.2$  mL/g) were lower than the SSW data package values; however, this was a result of the test method used, in which a cured reducing grout was added to the solution, and was likely unable to reduce the Tc to its lower oxidation state. The reduced-grout data package values assume Tc is added to the waste form from the time of curing, where the Tc can be reduced

directly. A high measured  $K_d$  value for Tc sorption to GAC ( $2.3 \pm 1.3 \times 10^3$  mL/g) suggests promise for GAC to be used as a Tc barrier material, while nonzero  $K_d$  values were measured for the AgM (4.0 – 4.3 mL/g) and HEPA filter media (0.32 – 0.36 mL/g).

- *Mercury*: The  $K_d$  values for sorption of Hg to the oxidized grout ( $1.7 \pm 0.2 \times 10^1$  mL/g) were slightly below the minimum value used in the SSW data package (Flach et al. 2016). The  $K_d$  was higher in the tests with the reduced grout ( $1.2 \pm 0.0 \times 10^4$  mL/g) compared with the data package value. In addition, the measured  $K_d$  was higher for sorption to the GAC ( $1.0 \pm 0.3 \times 10^4$  mL/g) than that in the data package.
- *Leaching*: The iodide observed diffusivity ( $D_{obs}$ ) values in both DIW ( $1.3 \pm 0.2 \times 10^{-10}$  cm<sup>2</sup>/s for the HGM-5 and  $1.3 \pm 0.1 \times 10^{-11}$  cm<sup>2</sup>/s for the Cast Stone, 28 d to 63 d average) and simulated Hanford VZPW ( $1.8 \pm 0.3 \times 10^{-10}$  cm<sup>2</sup>/s for the HGM-5 and  $3.6 \times 10^{-12}$  cm<sup>2</sup>/s for the Cast Stone, 28 d to 63 d average) were comparable to the optimistic  $D_e$  value for both grout and paste suggested in the SSW data package (Flach et al. 2016), an expected result as iodide is anticipated to have low sorption to the grout and measured to be low in this work. For the stabilized GAC in oxidized (HGM-5,  $1.1 \times 10^{-9}$  cm<sup>2</sup>/s) and reduced (Cast Stone,  $9.7 \times 10^{-10}$  cm<sup>2</sup>/s) grout, the iodide observed diffusivities were below the optimistic value reported for a mortar in the SSW data package ( $6.3 \times 10^{-9}$  cm<sup>2</sup>/s). This suggests that iodide is only slightly bound by the GAC in the waste form. These values may be further decreased through use of a low porosity/permeable grout such as UHPC. The stabilized AgM grout samples in the oxidized system (HGM-5) did not produce measurable iodide in the leachates, and only maximum  $D_{obs}$  values ( $< 5.0 \times 10^{-13}$  cm<sup>2</sup>/s) could be reported. These  $D_{obs}$  values are more than four orders of magnitude lower than the mobile species effective diffusivities listed in the SSW data package for a mortar. In the reduced grout, some measurable iodide was present in the leachates due to reactants (e.g. sulfur) present in the reduced grout. It is suggested that an oxidized grout system be used to immobilize AgM.
- *Fresh Properties*: The grouts prepared, similar formulations to HGM-5 and Cast Stone, had similar fresh properties (flowability, set time, heat of hydration) to those in previous reports where down-selections to these formulations were performed (Nichols et al. 2017).
- *Cured Properties*: Compressive strength values for the neat grouts were comparable to previous work. Upon the introduction of GAC to the grout (up to 30 wt%), the compressive strength decreased, as had been expected; however, it still met projected waste acceptance criteria limits.
- *Hydraulic Properties*: The saturated hydraulic conductivity ( $K_{sat}$ ) and van Genuchten parameters of the neat grouts were similar to those suggested in the SSW data package and reported elsewhere (Flach et al. 2016). Upon addition of GAC or AgM to the grout, the  $K_{sat}$  values ranged from  $(5.7 \pm 3.9) \times 10^{-9}$  cm/s –  $(5.8 \pm 2.8) \times 10^{-10}$  cm/s for Cast Stone, HGM-5 and HGM-3. The reported hydraulic conductivity value range can be used in an updated IDF PA calculation for SSW. The origin of the high  $K_{sat}$  values measured in FY18 at 30 vol% GAC loading are still unknown and the values within this revision supersede the prior release. Recent grout simulations in the IDF have shown that orders of magnitude increase in  $K_{sat}$  only correlate to  $\approx 2 \times$  increase in contaminant release, thus the  $K_{sat}$  range reported herein is unlikely to significantly influence contaminant release from SSW waste forms in the IDF (Asmussen et al. 2019). The need for a consensus method or test suite to evaluate hydraulic conductivity of nuclear waste form/barrier cementitious materials and associated precision and bias is again evident.

The data presented in this report can be used in future updates of the IDF PA related to SSW and can be used to inform grout formulation selection for SSW disposal. Negative variances between the data package values and measured values in this report were found in several cases listed below along with suggestions for confirmatory testing:

- **the  $K_d$  for sorption of Tc to reduced grout was lower than the data package value.** This difference was likely due to the nature of the batch test used. The data package  $K_d$  for Tc was selected to account for the reducing capacity of the grout (from the slag) when the Tc is added to grout from the beginning. In this test, the Tc was unlikely to be reduced in the dilute environment. The diffusivity of Tc from the oxidized vs. reduced grouts should be compared in future work or extrapolated from previous slag containing-grout development work for saltstone.
- **the  $K_d$  measured for sorption of iodide to GAC was measured to be lower than the data package value.** The data package value used iodide  $K_d$  values from neutral pH environments with low salt concentrations. Results from this work indicated that in the presence competitive anionic species iodide  $K_d$  values for sorption to the GAC decreased. These findings are supported by previous examples in the literature. pH may also influence sorption in the alkaline grout pore water due to as increasing alkalinity will generate a negative surface charge that can repel anions such as iodide and iodate. The leaching data supports iodide sorption behavior to GAC as iodide  $D_{obs}$  from GAC containing grout was much larger than AgM containing grout.

## 9.0 References

ANSI/ANS—American National Standards Institute/American Nuclear Society. 1992. *Solid Radioactive Waste Processing System for Light-Water-Cooled Reactor Plants*; Appendix B - Testing for Free Liquids in Solidified Matrices. ANSI/ANS-55.1, La Grange Park, IL.

Asmussen RM, AR Lawter, JR Stephenson, ME Bowden, NM Washton, JJ Neeway, Y Du, CI Pearce, RE Clayton, SA Saslow, et al. 2016a. *Getter Incorporation into Cast Stone and Solid State Characterizations*. PNNL-25577 Rev. 0; RPT-SLAW-003 Rev A, Pacific Northwest National Laboratory, Richland, WA.

Asmussen RM, JJ Neeway, AJ Lawter, A Wilson, and N Qafoku. 2016b. “Silver-based getters for <sup>129</sup>I removal from low-activity waste.” *Radiochimica Acta* 104(12): 905.913. doi: 10.1515/ract-2016.2598.

Asmussen RM, CI Pearce, AR Lawter, BW Miller, JJ Neeway, B Lawler, GL Smith, RJ Serne, DJ Swanberg, and N Qafoku. 2017. “Preparation, performance and mechanism of Tc and I getters in cementitious waste forms.” *Proceedings of Waste Management Symposium 2017*, 17124.

Asmussen RM, CI Pearce, BW Miller, AR Lawter, JJ Neeway, WW Lukens, ME Bowden, MA Miller, EC Buck, and RJ Serne. 2018. “Getters for improved technetium containment in cementitious waste forms.” *Journal of Hazardous Materials* 341:238-247.

Asmussen RM, Y Fang, G Tartakovsky, X Song, JH Westsik Jr., and GL Smith. 2019. Performance Metric for Cementitious Waste Form Inventory Release in the Integrated Disposal Facility. PNNL-28992 Rev. 0. Pacific Northwest National Laboratory, Richland, WA.

ASTM C39 / C39M-18, Standard Test Method for Compressive Strength of Cylindrical Concrete Specimens, ASTM International, West Conshohocken, PA, 2018, [www.astm.org](http://www.astm.org)

ASTM C191-13, Standard Test Methods for Time of Setting of Hydraulic Cement by Vicat Needle, ASTM International, West Conshohocken, PA, 2013, [www.astm.org](http://www.astm.org)

ASTM C642-13, Standard Test Method for Density, Absorption, and Voids in Hardened Concrete, ASTM International, West Conshohocken, PA, 2013, [www.astm.org](http://www.astm.org)

ASTM C1679-17, Standard Practice for Measuring Hydration Kinetics of Hydraulic Cementitious Mixtures Using Isothermal Calorimetry, ASTM International, West Conshohocken, PA, 2017, [www.astm.org](http://www.astm.org)

ASTM C1733-17a, Standard Test Method for Distribution Coefficients of Inorganic Species by the Batch Method, ASTM International, West Conshohocken, PA, 2017, [www.astm.org](http://www.astm.org)

ASTM D1193-06(2018), Standard Specification for Reagent Water, 2018, ASTM International, West Conshohocken, PA, 2018, [www.astm.org](http://www.astm.org)

ASTM D5084-16a, Standard Test Methods for Measurement of Hydraulic Conductivity of Saturated Porous Materials Using a Flexible Wall Permeameter, ASTM International, West Conshohocken, PA, 2016, [www.astm.org](http://www.astm.org)

ASTM D6103 / D6103M-17, Standard Test Method for Flow Consistency of Controlled Low Strength Material (CLSM), ASTM International, West Conshohocken, PA, 2017, [www.astm.org](http://www.astm.org)

Brown, CF, RJ Serne, BN Bjornstad, DG Horton, DC Lanigan, RE Clayton, MM Valenta, TS Vickerman, IV Kutnyakov and KN Geiszler. 2006. "Characterization of Vadose Zone Sediments Below the C Tank Farm: Borehole C4297 and RCRA Borehole 299-E26.22." *PNNL-15503, Rev. 1* Pacific Northwest National Laboratory (PNNL), Richland, WA (US).

Brown E, DJ Swanberg, JRK Surman, and K Williams. 2017. *Benchmarking of DFLAW Solid Secondary Wastes and Processes with UK/Europe Counterparts*. Washington River Protection Solutions, Richland, WA.

Cantrell KJ, JH Westsik, RJ Serne, W Um, and AD Cozzi. 2016. *Secondary Waste Cementitious Waste Form Data Package for the Integrated Disposal Facility Performance Assessment*. PNNL-25194, Pacific Northwest National Laboratory, Richland, WA. Accessed February 13, 2019, at [https://www.pnnl.gov/main/publications/external/technical\\_reports/PNNL-25194.pdf](https://www.pnnl.gov/main/publications/external/technical_reports/PNNL-25194.pdf).

Cozzi AD and DJ McCabe. 2016. *Phase I Testing Results of Immobilization of WTP Effluent Management Facility Evaporator Bottoms Core Simulant*. SRNL-STI-2016.00675, Savannah River National Laboratory, Aiken, SC. Accessed May 26, 2017, at <http://sti.srs.gov/fulltext/SRNL-STI-2016.00675.pdf>.

Crawford C, A Cozzi, K Hill, and A Ramsey. 2017. *Analysis of Hanford Cast Stone Supplemental LAW using Composition Adjusted SRS Tank 50 Salt Solution*. SRNL-STI-2016-00619, Savannah River Site (SRS), Aiken, SC.

EPA—U.S. Environmental Protection Agency. 1999. "Understanding Variation in Partition Coefficient,  $K_d$ , Values: Volume I." The  $K_d$  Model, Methods of Measurement, and Application of Chemical Reaction Codes. EPA 402-R-99-004A, U.S. Environmental Protection Agency, Washington, D.C. Prepared by KM Krupka, DI Kaplan, G Whelan, RJ Serne, and SV Mattigod at Pacific Northwest National Laboratory, Richland, WA.

EPA—U.S. Environmental Protection Agency. 2004. "Paint Filter Liquid Test." EPA Method 9095A. In *Test Methods for Evaluating Solid Waste: Physical/Chemical Methods*. EPA SW 846, U.S. Environmental Protection Agency, Washington, D.C. [www.epa.gov/sites/production/files/2015.12/documents/9095b\\_0.pdf](http://www.epa.gov/sites/production/files/2015.12/documents/9095b_0.pdf)

EPA—U.S. Environmental Protection Agency. 2013. *Method 1315, Revision 0 – Mass Transfer Rates of Constituents in Monolithic or Compacted Granular Materials Using a Semi-Dynamic Tank Leaching Procedure*. U.S. Environmental Protection Agency, Washington, D.C.

Flach GP, DI Kaplan, RL Nichols, RR Seitz, and RJ Serne. 2016. *Solid Secondary Waste Data Package Supporting Hanford Integrated Disposal Facility Performance Assessment*. SRNL-STI-2016.00175, Rev. 0, Savannah River National Laboratory, Aiken, SC.

Guillaumont R, Mompean FJ. 2003. Update on the chemical thermodynamics of uranium, neptunium, plutonium, americium and technetium. Amsterdam: Elsevier

Harbour JR, TB Edwards, EK Hansen, and WJ Williams. 2005. *Variability Study for Saltstone*. WSRC-TR-2005.00447, Rev. 0, Savannah River National Laboratory, Aiken, SC.

Jubin RT, TR Watkins, SH Bruffey, JA Jordan, and ML Parks. 2017. *Hot Isostatic Pressing of Engineered Forms of I-AgZ*; ORNL/TM-2017/707; Other: NTRD-MRWFD-2016.000412 United States

10.2172/1415914 Other: NTRD-MRWFD-2016.000412 ORNL English, Oak Ridge National Laboratory, Oak Ridge, TN, p Medium: ED; Size: 57 p.

Jury WA and R Horton. 2004. *Soil Physics*, 6<sup>th</sup> ed. John Wiley and Sons, Inc., Hoboken, NJ.

Kaplan DI, SV Mattigod, KE Parker, and G Iversen. 2000. *Experimental Work in Support of the <sup>129</sup>I Disposal Special Analysis*. WSRC-TR-2000-00283, Rev. 0, Westinghouse Savannah River Company, Aiken, SC.

Kaplan DI, K Price, J Seaman, D Li, P Lin, C Xu, K Schwehr, K Tanaka, T Ohnuki, and P Santschi. "Radioiodine Speciation Impact on Ag-Activated Carbon Immobilization in Cementitious Environments." 2018. In *Proceedings of Goldschmidt*, Boston, MA, p. 1231.

Kuboa T, S Fukutani, T Ohta, and Y Mahara. 2013. "Removal of radioactive cesium, strontium, and iodine from natural waters using bentonite, zeolite, and activated carbon." *Journal of Radioanalytical and Nuclear Chemistry* 296: 981–984.

Lawter AR, WL Garcia, RK Kukkadapu, O Qafoku, ME Bowden, SA Saslow, and NP Qafoku. 2018. "Technetium and iodine aqueous species immobilization and transformations in the presence of strong reductants and calcite-forming solutions: Remedial action implications." *Science of the Total Environment* 636: 588-595.

Neeway JJ, RM Asmussen, AR Lawter, ME Bowden, WW Lukens, D Sarma, BJ Riley, MG Kanatzidis, and NP Qafoku. 2016. "Removal of TcO<sub>4</sub>– from representative nuclear waste streams with layered potassium metal sulfide materials." *Chemistry of Materials* 28:3976.3983.

Nichols RL, KL Dixon, and DL Kaplan. 2018. *Stabilization of Spherical Resorcinol Resin – Maintenance of the Hanford Integrated Disposal Performance Assessment FY2018*. SRNL-STI-2018-00342, Savannah River National Laboratory, Aiken, SC.

Nichols RL, RR Seitz, and KL Dixon. 2017. *Solid Secondary Waste Testing for Maintenance of the Hanford Integrated Disposal Facility Performance Assessment – FY 2017*. SRNL-STI-2016.00564, Rev. 0, Savannah River National Laboratory, Aiken, SC.

Parker KE, EC Golovich, and DM Wellman. 2014. *Iodine Adsorption on Ion-Exchange Resins and Activated Carbons–Batch Testing*. PNNL-23730 or RPT-DVZ-AFRI-021, Rev. 0. Pacific Northwest Laboratory, Richland, WA.

Pearce CI, JP Icenhower, RM Asmussen, PG Tratnyek, KM Rosso, WW Lukens, and NP Qafoku. 2018. "Technetium Stabilization in Low-Solubility Sulfide Phases: A Review." *Earth and Space Chemistry* 2:532-547.

Pease III LF, SK Fiskum, HA Colburn, and PP Schonewill. 2019. *Cesium Ion Exchange with Crystalline Silicotitanate Literature Review*. PNNL-28343, Pacific Northwest National Laboratory, Richland, WA. Accessed February 13, 2019, at <https://www.osti.gov/servlets/purl/1466215>.

Qafoku N, JJ Neeway, AR Lawter, TG Levitskaia, RJ Serne, JH Westsik, and M Snyder. 2015. *Technetium and Iodine Getters to Improve Cast Stone Performance*. PNNL-23282, Rev. 1, Pacific Northwest National Laboratory, Richland, WA.

Ramirez AJ. 2008. *Hanford Site Solid Waste Acceptance Criteria*. HNF-EP-0063, Rev. 14, Fluor Federal Services, Inc., Richland, WA. Accessed May 31, 2017, at [http://www.hanford.gov/files.cfm/WAC\\_HNF-EP-0063\\_%20CurrentRv.pdf](http://www.hanford.gov/files.cfm/WAC_HNF-EP-0063_%20CurrentRv.pdf).

Renier JJ, Martin Jr DS. 1956 The Solubility of Silver Iodate in Iodate Solutions. Iodate Complexes of Silver. *Journal of the American Chemical Society*. 78:1833-1837.

Santschi PH, C Xu, S Zhang, YF Ho, HP Li, KA Schwehr, and DI Kaplan. 2012. *Laboratory Results on Iodine (<sup>129</sup>I and <sup>127</sup>I) Speciation, Transformation and Mobility in Hanford Groundwater, Suspended Particles and Sediments*. SRNL-STI-2012-00592, Savannah River National Laboratory, Aiken, SC.

Saslow SA, W Um, RL Russell, BD Williams, RM Asmussen, T Varga, O Qafoku, BJ Riley, AR Lawter, MV Snyder, SR Baum, and II Leavy. 2018. *Effluent Management Facility Evaporator Bottoms: Waste Streams Formulation and Waste Form Qualification Testing*. PNNL-26570, Rev. 1. Pacific Northwest National Laboratory, Richland, WA.

Scheele RD, CF Wend, WC Buchmiller, AE Kozelisky, and RL Sell. 2002. *Preliminary Evaluation of Spent Silver Mordenite Disposal Forms Resulting from Gaseous Radioiodine Control at Hanford's Waste Treatment Plan*. PNWD-3225, WTP-RPT-039, Rev. 0. Pacific Northwest National Laboratory, Richland, WA.

Seitz RR. 2017. *Examples of Disposition Alternatives for Solid Secondary Waste*. SRNL-STI-2017-00508, Savannah River National Laboratory, Aiken, SC.

Serne RJ, DC Lanigan, JH Westsik, BD Williams, HB Jung, G Wang. 2015. *Extended Leach Testing of Simulated LAW Cast Stone Monoliths*. PNNL-24297 Rev 1, Pacific Northwest National Laboratory, Richland, Washington. Accessed February 13, 2019, at [https://www.pnnl.gov/main/publications/external/technical\\_reports/PNNL-24297.pdf](https://www.pnnl.gov/main/publications/external/technical_reports/PNNL-24297.pdf).

Siskind B and MG Cowgill. 1992. *Technical Justifications for the Tests and Criteria in the Waste Form Technical Position Appendix on Cement Stabilization*. BNL-NUREG-47121, Brookhaven National Laboratory, Upton, NY.

Tan ZC, Vought RC, Pontius RB. 1972 Determination of solubility product constants of some 1: 1 silver salts of thiols by direct competition with silver iodide. *Analytical Chemistry*. 44:411-413.

Taylor WJ. 2010. *Hanford Facility RCRA Permit Modification Notification Form Part III*. U.S. Department of Energy - Office of River Protection, Richland, WA. Accessed February 15, 2019, at <https://pdw.hanford.gov/arpir/pdf.cfm?accession=0084162>.

Washington River Protection Solutions. 2018. "2017 Integrated Disposal Facility Performance Assessment" RPP-RPT-59958, Rev.1. Richland, WA.

Westsik Jr. JH, GF Piepel, MJ Lindberg, PG Heasler, TM Mercier, RL Russell, AD Cozzi, WE Daniel, RE Eibling, EK Hansen, MR Reigal, and DJ Swanberg. 2013. *Supplemental Immobilization of Hanford Low-Activity Waste: Cast Stone Screening Tests*. PNNL-22747, SRNL-STI-2013-00465, Rev. 0, Pacific Northwest National Laboratory, Richland, WA and Savannah River National Laboratory, Aiken, SC.

Zhang S, C Xu, D Creeley, Y-F Ho, H-P Li, R Grandbois, KA Schwehr, DI Kaplan, CM Yeager, D Wellman and PH Santschi (2013) Iodine-129 and Iodine-127 Speciation in Groundwater at the Hanford Site, U.S.: Iodate Incorporation into Calcite. *Environmental Science & Technology* 47, 9635-9642.

## **Appendix A**

### **Scanning Electron Micrographs of GAC and AgM Materials**

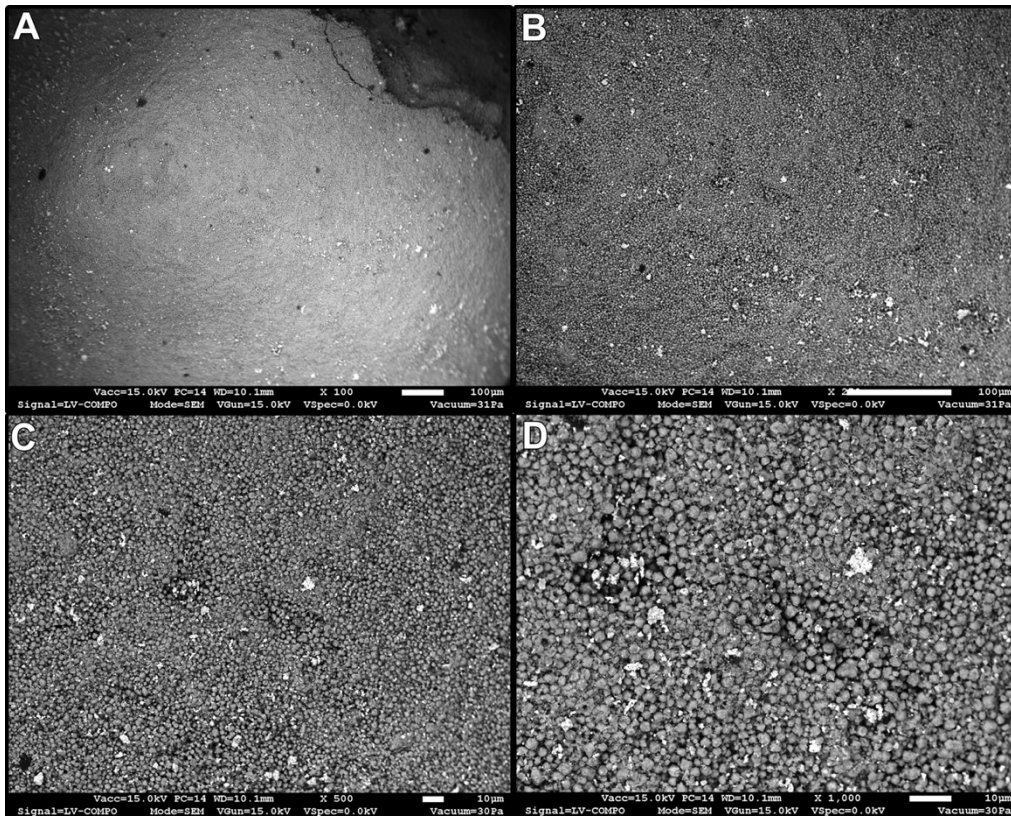
# Appendix A

## Scanning Electron Micrographs of GAC and AgM Materials

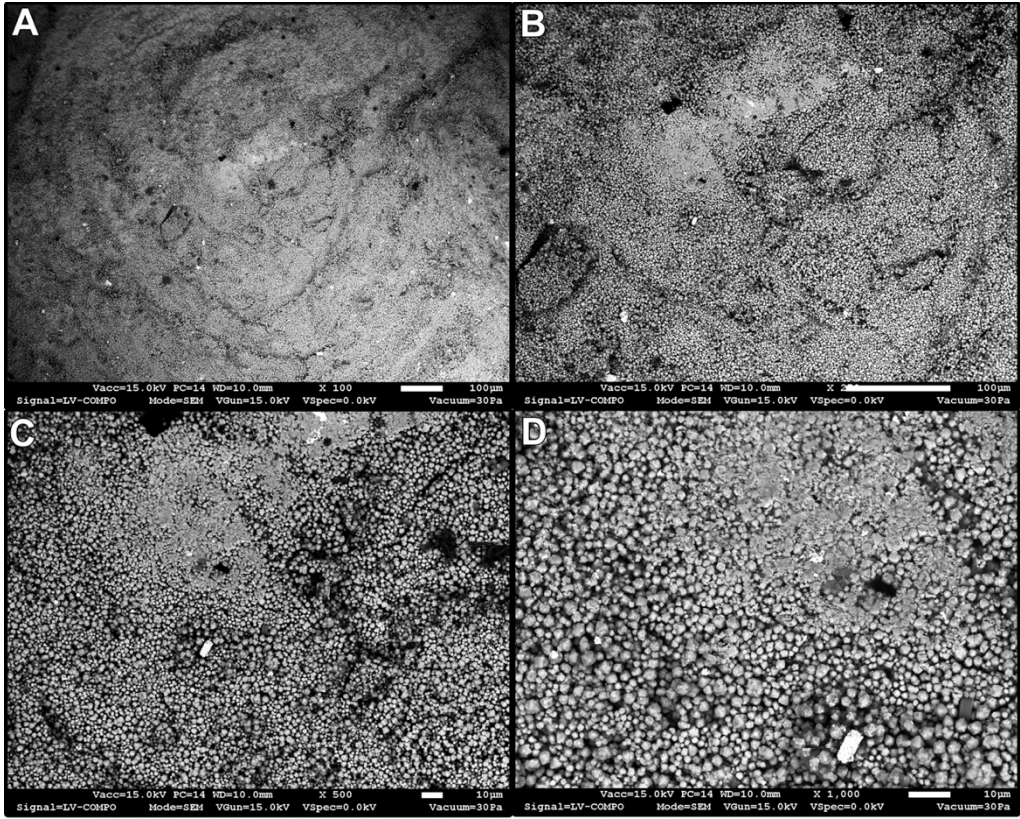
This appendix provides additional electron microscopy images characterizing the SSW materials (GAC and AgM) and the hardened pastes when used to stabilize the materials.

### A.1 As-Received Silver Mordenite

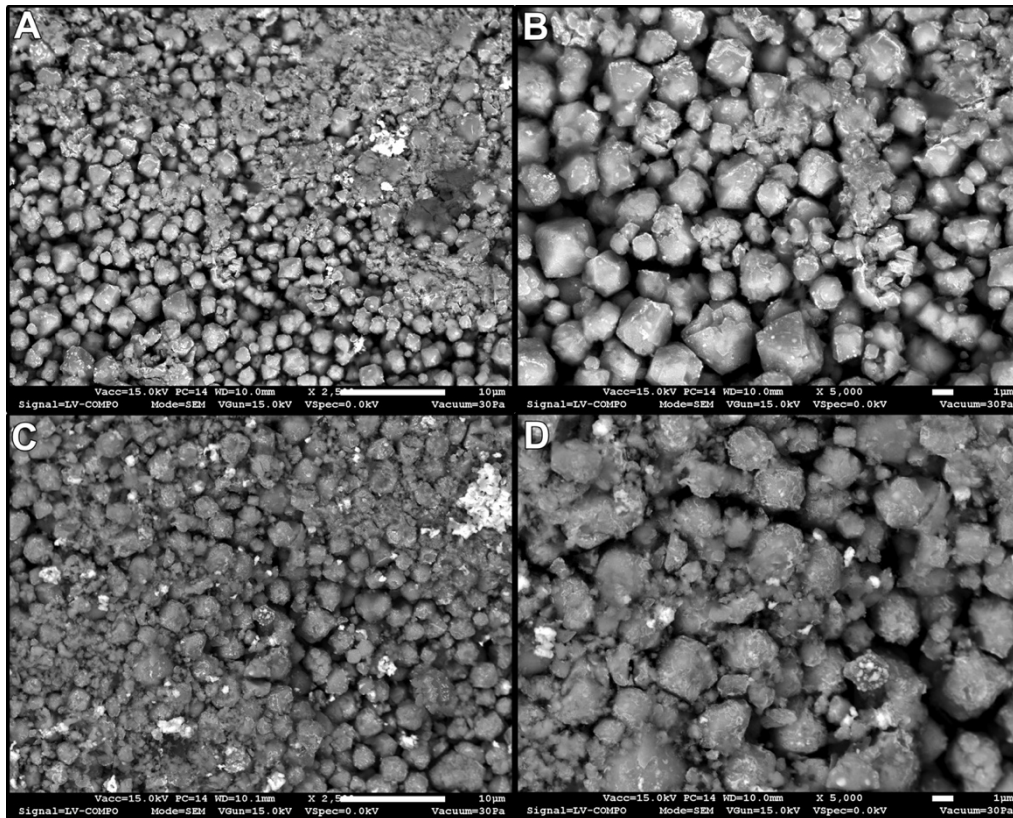
Specimens of as-received silver mordenite (AgM) were examined using SEM and EDS to better understand the microstructure and the elemental components present in the as-received material. The granules were imaged un-coated, in LV mode, using a BSE detector. The contrast in the micrographs was a function of differences in average atomic number - higher average atomic number phases are brighter than lower. The AgM consisted of granules that were approximately 1-2 mm in diameter. The granules were examined by looking at their un-modified, native surface (Figure A.1) as well as at fracture surfaces (Figure A.2). A side-by-side series of micrographs is shown in Figure A.3. There were no obvious differences in appearance between the native and fractured surfaces. The granules themselves were composed of much smaller particles that ranged in size from approximately 0.8 – 3.5  $\mu\text{m}$  in diameter.



**Figure A.1.** Collage of SEM Micrographs from the Native Surface of AgM Granules

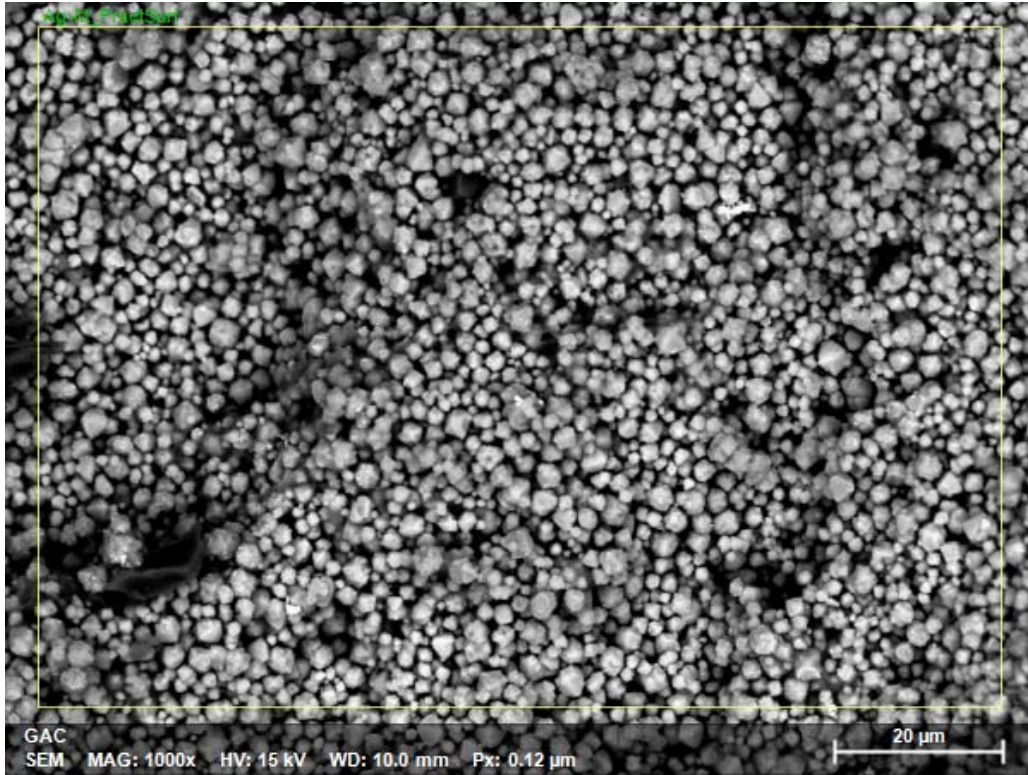


**Figure A.2.** Collage of SEM Micrographs from a Fractured Surface of a AgM Granule

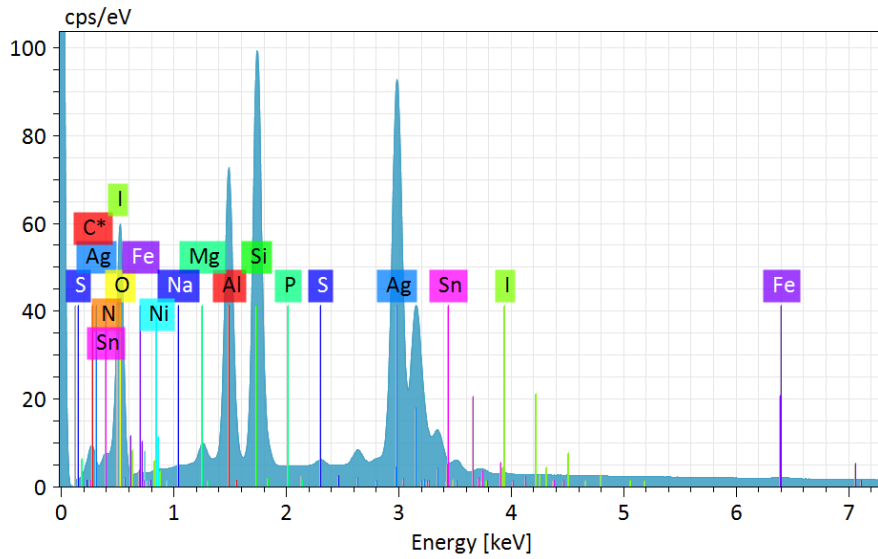


**Figure A.3.** Collage of SEM Micrographs of AgM Comparing the Native Surface (A & B), to the Fracture Surface (C & D)

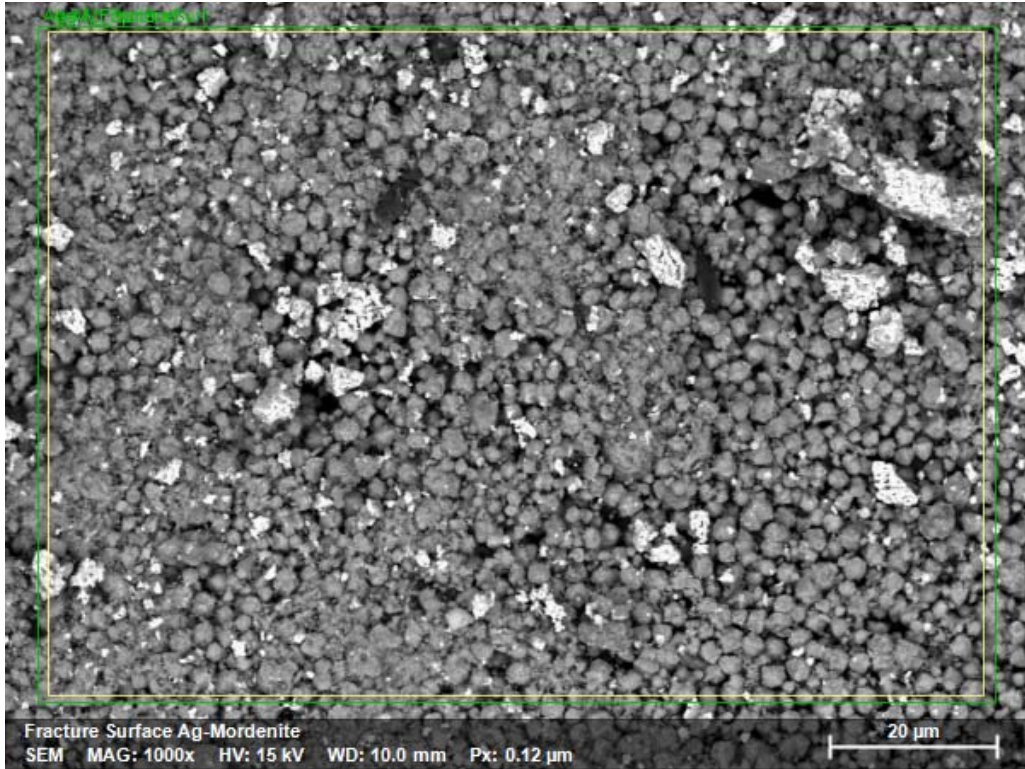
The elemental composition of the AgM granules was evaluated by collecting EDS spectra from a fracture surface of an AgM granule. Two different fields of view were evaluated; each was approximately  $120 \mu\text{m} \times 90 \mu\text{m}$ . SEM micrographs and the associated EDS spectra for the two regions analyzed are shown in Figure A.4 – Figure A.7.



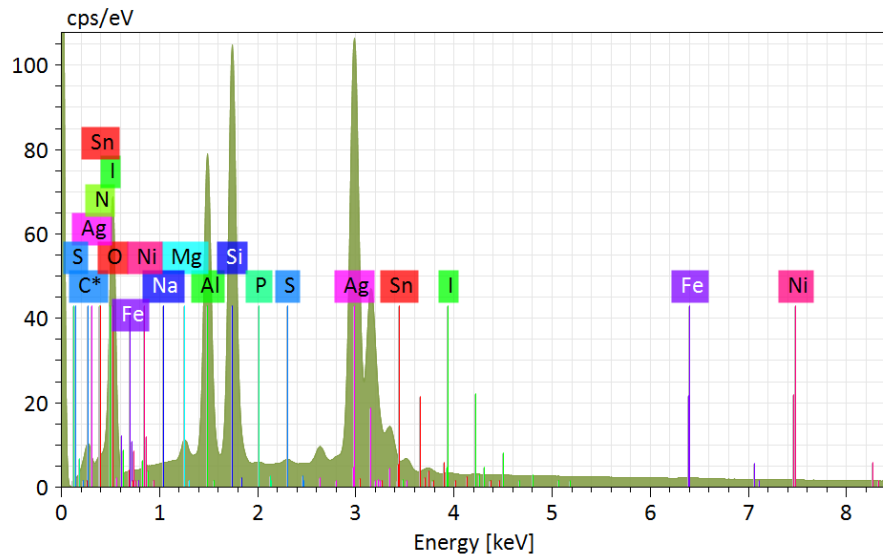
**Figure A.4.** SEM Micrograph from a Fractured AgM Granule. This was field of view #1 used to collect the EDS spectra from the AgM granule.



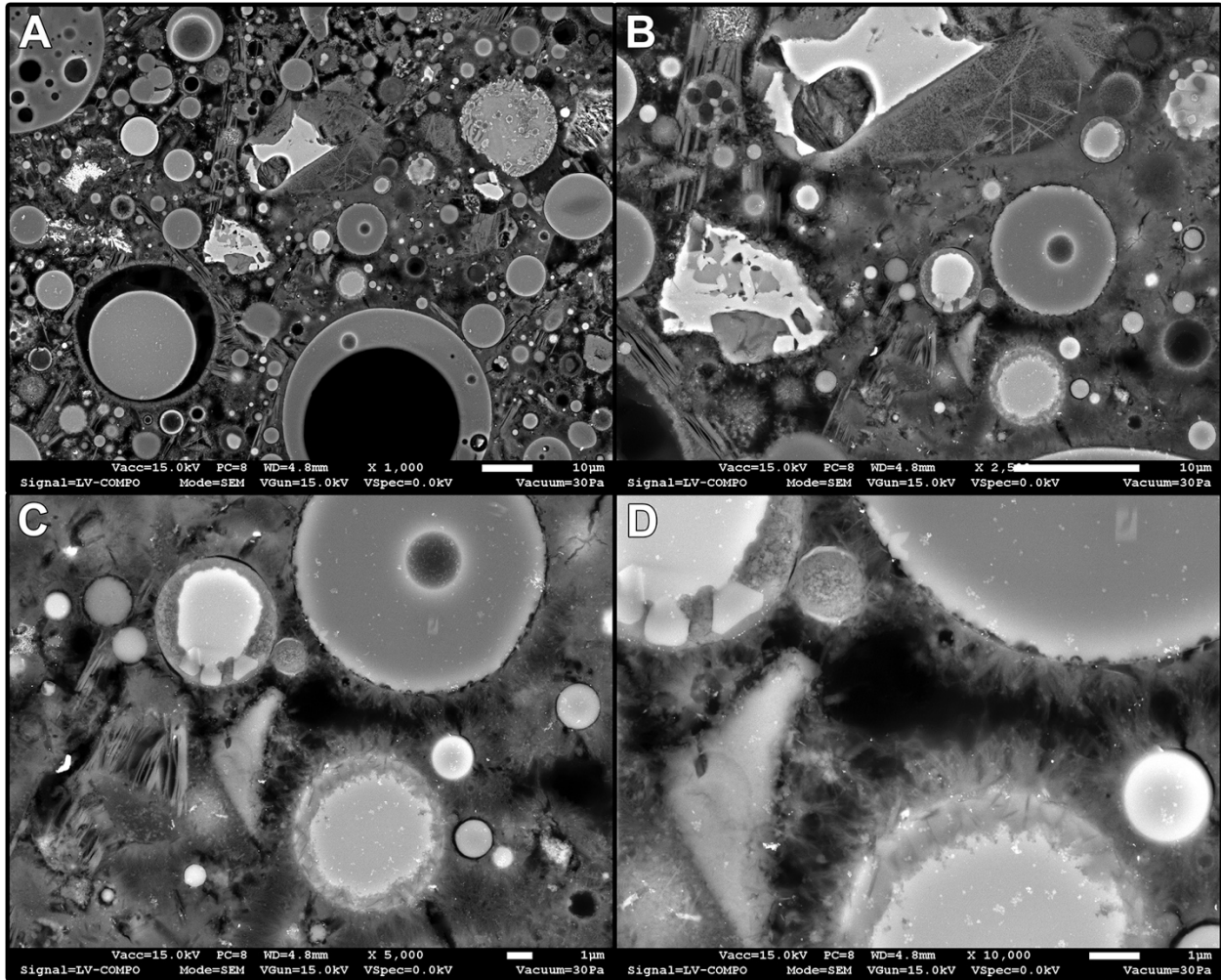
**Figure A.5.** EDS Spectrum from a Fractured AgM Granule Region #1



**Figure A.6.** SEM Micrograph from a Fractured AgM Granule. This was field of view #2 used to collect the EDS spectra from the AgM granule.

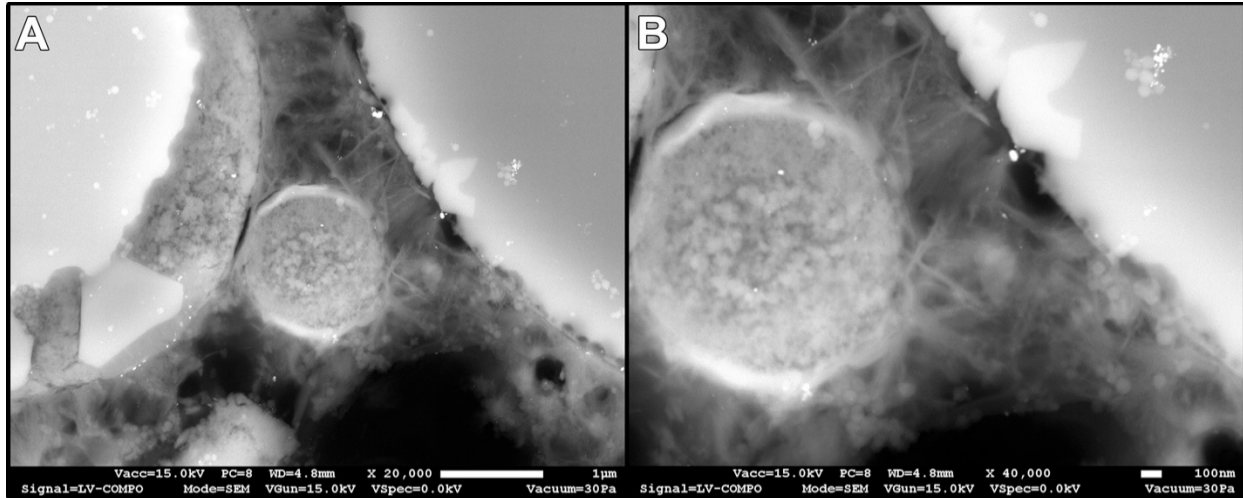


**Figure A.7.** EDS Spectrum from a Fractured AgM Granule Region #2



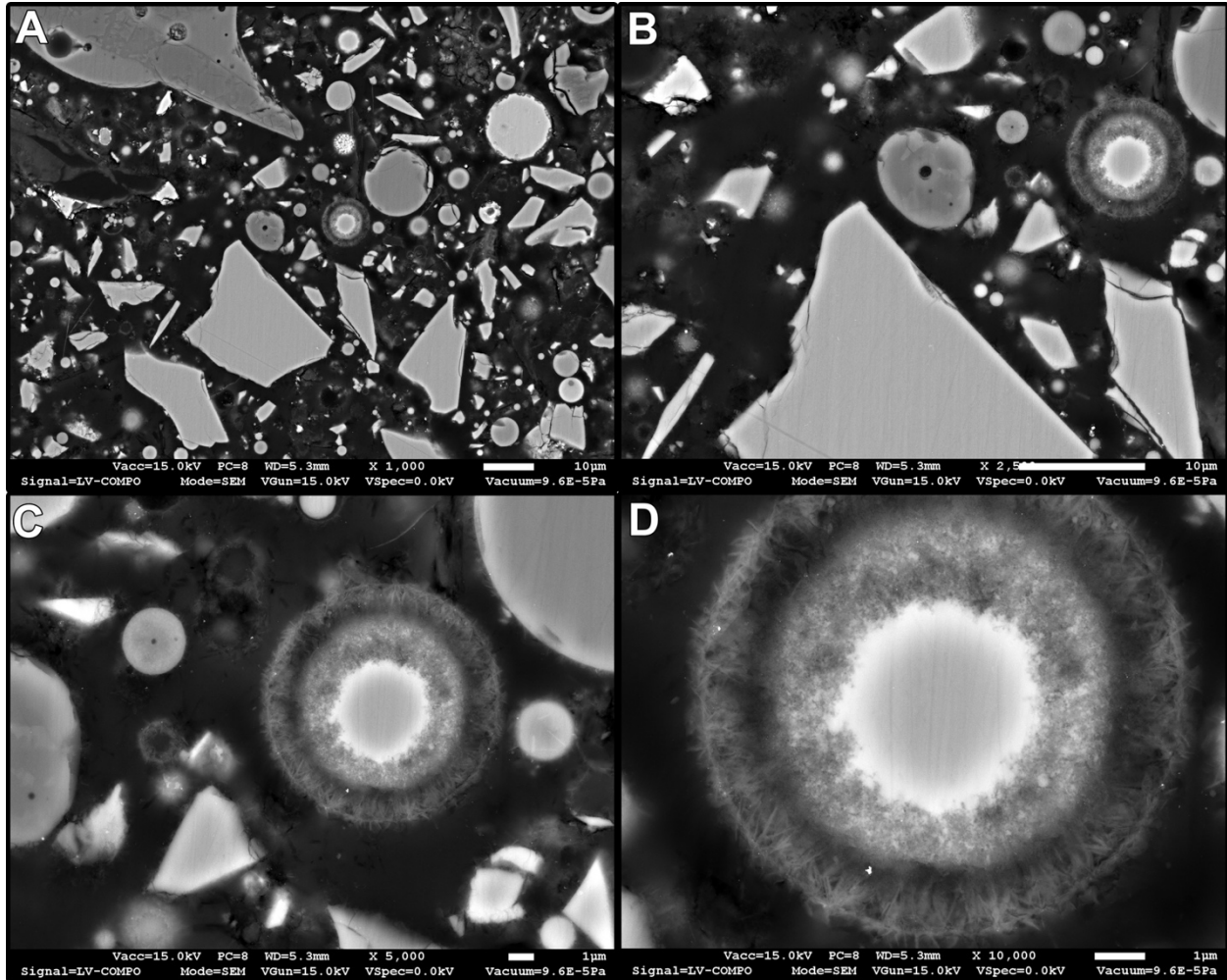
**Figure A.8.** SEM BSE micrographs from a specimen of AgM in CS. The circular particles were fly ash; the medium gray wavy features around the perimeter of the fly ash particles are hydration products. The bright, angular features in “B” were blast furnace slag particles.

Figure A.8 is a collage of SEM BSE micrographs at successively higher magnifications. The purpose of this set of micrographs is to illustrate the hydration reactions occurring between fly ash, BFS, and cement grains. The spherical particles are fly ash, which have a high silica content; the bright angular particles are slag. The tendrils extending from the fly ash into the pore space are hydration products that result from caustic reactions between  $\text{Ca}(\text{OH})_2$  (from the dissolved Portland cement grains) and the silica in silica fume. Figure A.9 shows an even higher magnification view of reacted silica fume. Note that the small particle is almost completely reacted, while the larger particle only has a partially reacted outer rind.



**Figure A.9.** High Magnification SEM BSE Micrographs of Hydration in AgM-Cast Stone Compositated Waste Form

In terms of hydration reactions, hydrated fly ash particles and cement grains were identified in Figure A.10 and Figure A.11. Not as many particles seemed to have reacted in the HGM-5 as compared to the Cast Stone specimen (Figure A.8 and Figure A.9). But, the particles that did react in HGM-5 seemed to be fully reacted, yet not as fully inter-connected with other hydrating particles as in the Cast Stone specimen.



**Figure A.10.** SEM BSE Micrographs Showing the Hydration Reaction Interface Around a Fly Ash Particle in the HGM-5

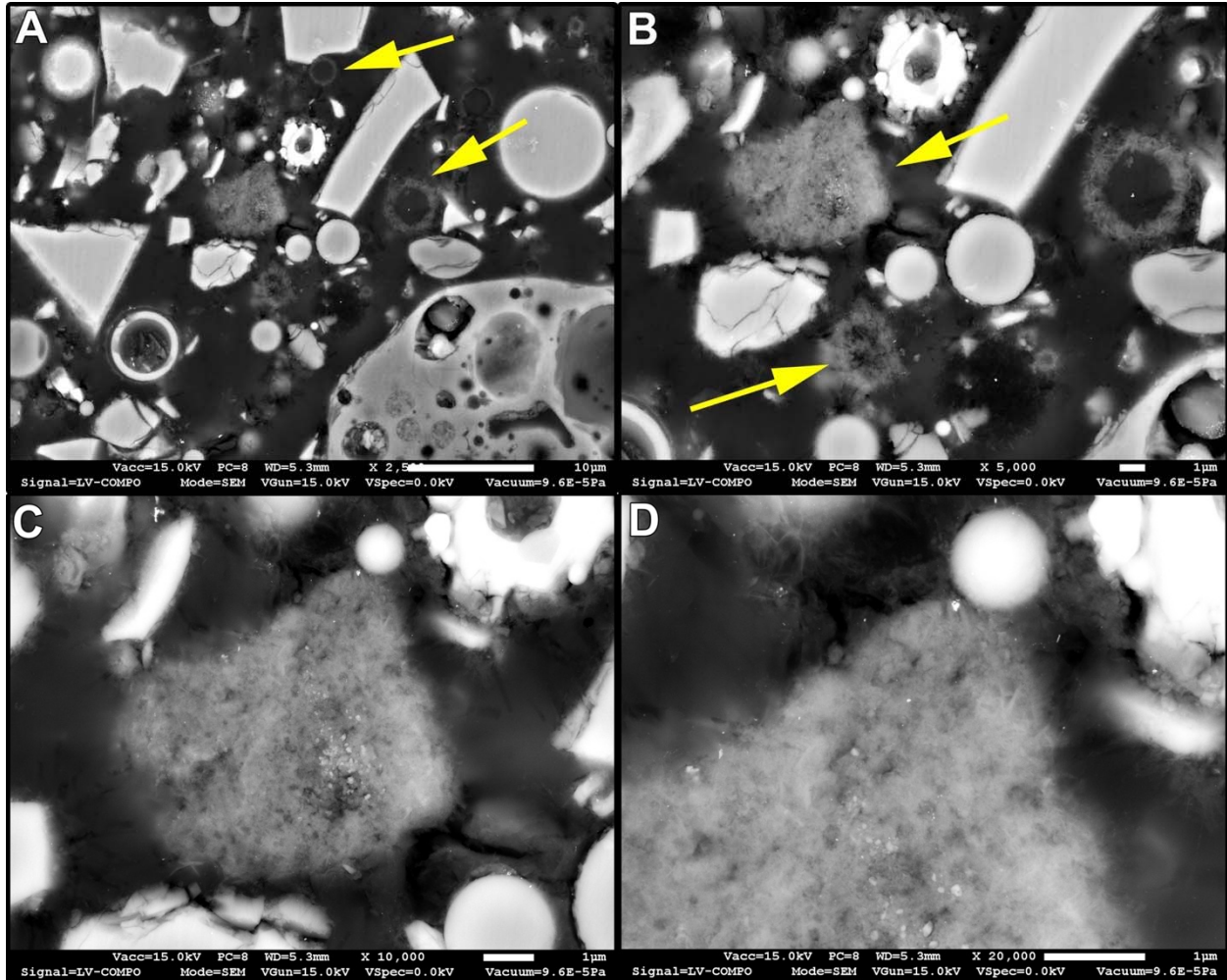


**Figure A.11.** SEM BSE Micrographs Showing Hydration Reactions Around Fly Ash Particles (A) and Cement Grains (B – D) in HGM-5

## A.2 As-Received GAC

GAC was another material that was incorporated into grout. A collage of SEM BSE micrographs from the fracture surface of as-received GAC are shown in Figure A.12. The material had a rough texture at a 10 micron length scale and the texture looked like the material fractured in a brittle manner. There were a large number of secondary phases and particles that were embedded in the GAC. The variation in contrast in the BSE micrographs indicated that the second phase inclusions/particles had a higher atomic number than the carbon matrix.

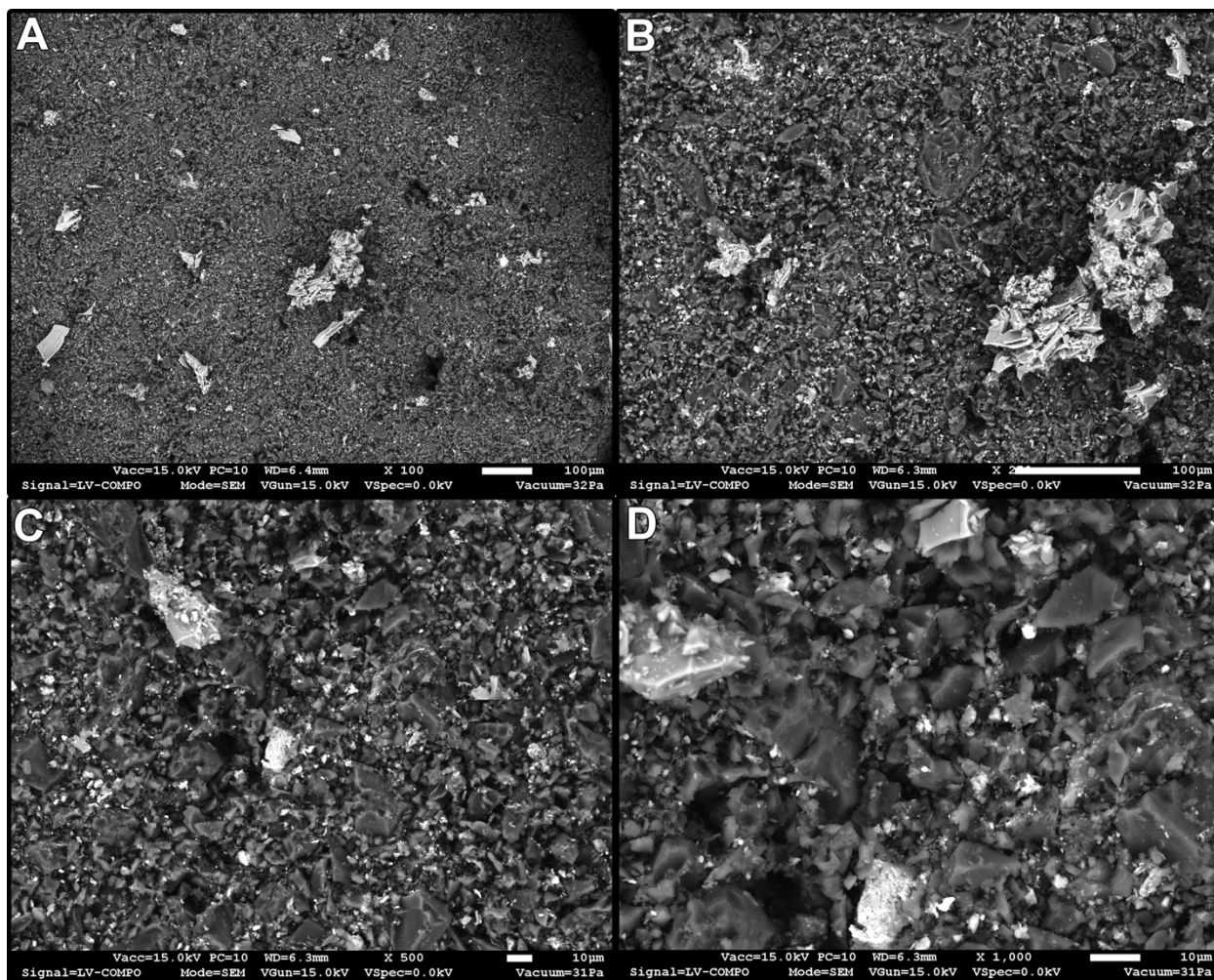


**Figure A.12.** SEM BSE Micrographs from a Fractured Surface of As-Received GAC

EDS analysis was done to determine the elemental composition of the GAC. The area analyzed is shown in Figure A.13 and the EDS spectrum from that area is shown in Figure A.14. Because carbon was the dominant peak, the y-axis was scaled to emphasize the other elements present in the sample, and the carbon peak is off-scale. The other elements present included S, Si, Na, O, Al, as minor phases and Ca, Mg, I, and Fe as trace constituents. It is important to point out that there is a strong overlap between the  $K_B$  peak for Ca and the L-lines for I. Typically, the overlap is so strong, that it is very difficult to discern the presence of I if the concentration of Ca is substantially greater than I. However, for this sample, there was sufficient I present so that it could be detected.



**Figure A.13.** Area of Analysis on the Fracture Surface of a GAC Granule where the EDS Spectrum was Collected

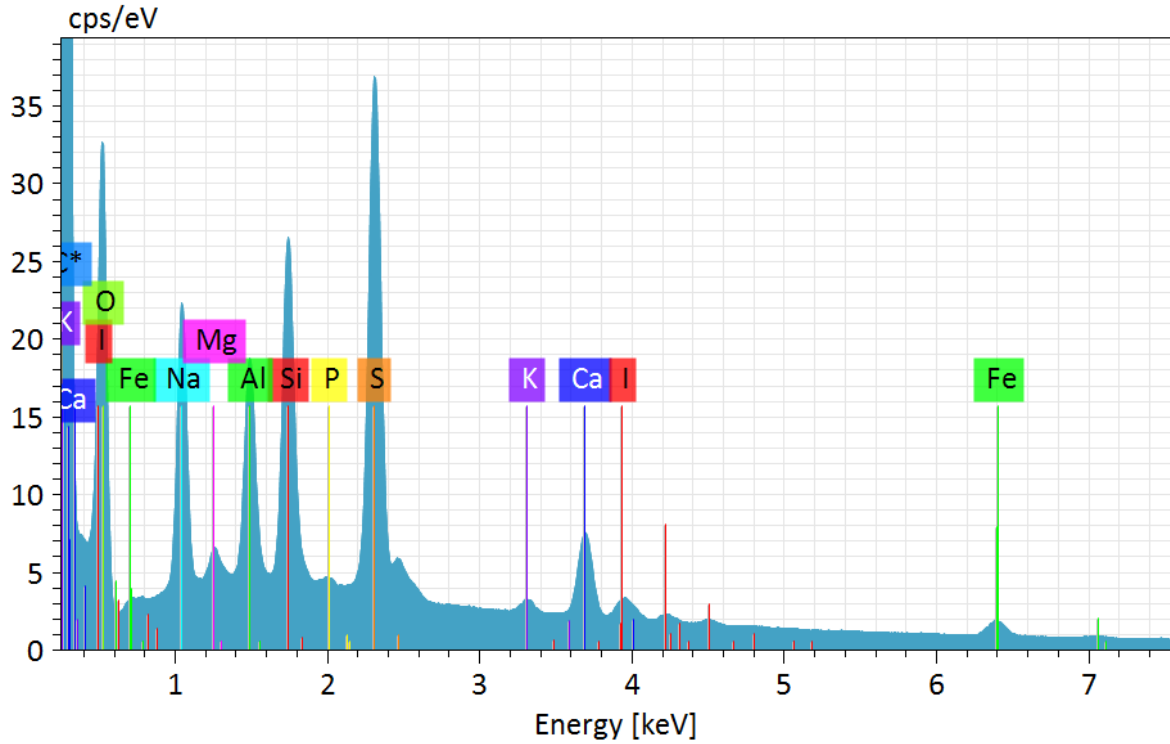


**Figure A.14.** EDS Spectrum of GAC from the Field of View Shown in Figure A.13.

A collage of low magnification micrographs is shown in Figure A.15. The intent was to find pieces of GAC and observe the interface between the GAC and the Cast Stone. However, the GAC pieces apparently broke and were crushed during processing the Cast Stone-GAC mixture. Thus, the GAC pieces that were found were quite small in comparison to their original size.

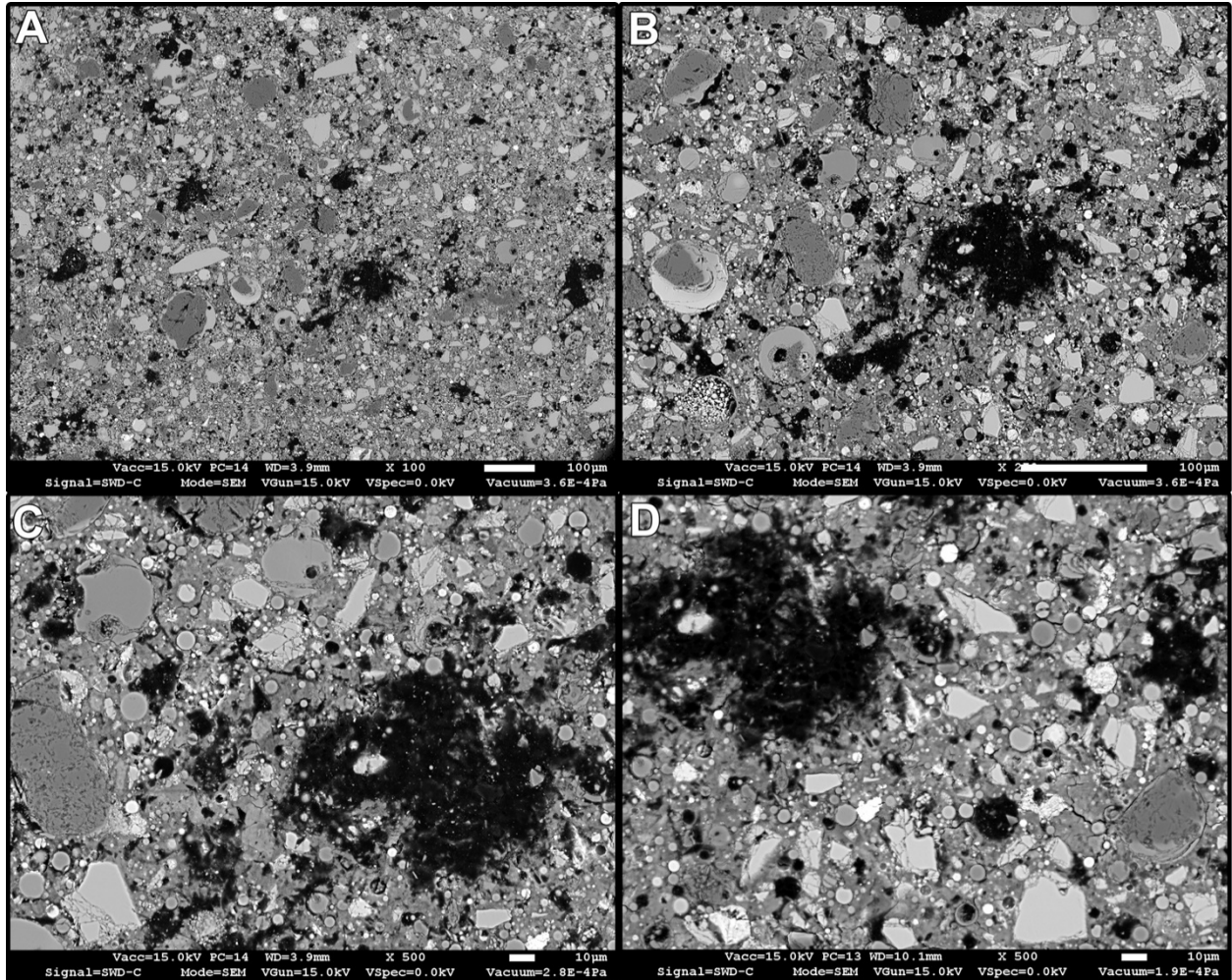


**Figure A.15.** SEM BSE Micrographs of GAC Mixed in with Cast Stone Matrix. The dark features are GAC.

**Appendix B**  
**Initial  $K_d$  Tests**

## Appendix B

### Initial $K_d$ Tests

<b>Solid Material:</b>	GAC	
<b>Pore Water:</b>	HGM-5	
<b>Contaminant:</b>	I <sup>-</sup>	
<b>Mass of Solid Material:</b>	2.01	g
<b>Mass of Pore Water:</b>	49.30	g
<b>[I]<sub>blank</sub>:</b>	56400	ug/L

Interval #	Total Time, days	Iodine (ug/L)	Volume (mL)	$K_d$ (mL/g)
1	1.0	93400	49.30	0.00E+00
2	2.0	91000	48.80	0.00E+00
3	5.1	90700	48.30	0.00E+00
4	6.3	92200	47.80	0.00E+00
5	7.0	89700	47.30	0.00E+00
6	8.0	92700	46.80	0.00E+00
7	9.1	91800	46.30	0.00E+00
8	12.2	93100	45.80	0.00E+00
9	13.1	93000	45.30	0.00E+00
10	15.0	92000	44.80	0.00E+00

<b>Solid Material:</b>	AgM	
<b>Pore Water:</b>	HGM-5	
<b>Contaminant:</b>	I <sup>-</sup>	
<b>Mass of Solid Material:</b>	2.00	g
<b>Mass of Pore Water:</b>	50.57	g
<b>[I]<sub>blank</sub>:</b>	56400	ug/L

Interval #	Total Time, days	Iodine (ug/L)	Volume (mL)	$K_d$ (mL/g)
1	1.0	310	50.57	4.57E+03
2	2.0	85.9	50.07	1.64E+04
3	5.1	20.8	49.57	6.71E+04
4	6.3	9.0	49.07	1.54E+05
5	7.0	9.9	48.57	1.38E+05
6	8.0	10.5	48.07	1.29E+05
7	9.1	23.6	47.57	5.68E+04
8	12.2	40.2	47.07	3.30E+04
9	13.1	43.9	46.57	2.99E+04
10	15.0	51.7	46.07	2.51E+04

<b>Solid Material:</b>	HEPA	
<b>Pore Water:</b>	HGM-5	
<b>Contaminant:</b>	IO <sub>3</sub> <sup>-</sup>	
<b>Mass of Solid Material:</b>	2.04	g
<b>Mass of Pore Water:</b>	49.13	g
<b>[I]<sub>blank</sub>:</b>	36000	ug/L

Interval #	Total Time, days	Iodine (ug/L)	Volume (mL)	<i>K<sub>d</sub></i> (mL/g)
1	1.0	33700	49.13	1.64E+00
2	2.0	33400	48.63	1.85E+00
3	5.1	33900	48.13	1.46E+00
4	6.3	33900	47.63	1.45E+00
5	7.0	34000	47.13	1.36E+00
6	8.0	35300	46.63	4.53E-01
7	9.1	35200	46.13	5.14E-01
8	12.2	34900	45.63	7.05E-01
9	13.1	36400	45.13	0.00E+00
10	15.0	35200	44.63	4.97E-01

<b>Solid Material:</b>	HEPA	
<b>Pore Water:</b>	HGM-5	
<b>Contaminant:</b>	I <sup>-</sup>	
<b>Mass of Solid Material:</b>	2.00	g
<b>Mass of Pore Water:</b>	49.62	g
<b>[I]<sub>blank</sub>:</b>	56400	ug/L

Interval #	Total Time, days	Iodine (ug/L)	Volume (mL)	<i>K<sub>d</sub></i> (mL/g)
1	1.0	48700	49.62	3.91E+00
2	2.0	47900	49.12	4.35E+00
3	5.1	47000	48.62	4.85E+00
4	6.3	48200	48.12	4.08E+00
5	7.0	47200	47.62	4.63E+00
6	8.0	48500	47.12	3.83E+00
7	9.1	48800	46.62	3.62E+00
8	12.2	48900	46.12	3.53E+00
9	13.1	48900	45.62	3.49E+00
10	15.0	49400	45.12	3.19E+00

<b>Solid Material:</b>	HGM-5	
<b>Pore Water:</b>	HGM-5	
<b>Contaminant:</b>	I <sup>-</sup>	
<b>Mass of Solid Material:</b>	2.00	g
<b>Mass of Pore Water:</b>	49.53	g
<b>[I]<sub>blank</sub>:</b>	56400	ug/L

Interval #	Total Time, days	Iodine (ug/L)	Volume (mL)	<i>K<sub>d</sub></i> (mL/g)
1	1.0	39700	49.53	1.04E+01
2	2.0	39200	49.03	1.08E+01
3	5.1	38000	48.53	1.18E+01
4	6.3	38700	48.03	1.10E+01
5	7.0	38300	47.53	1.12E+01
6	8.0	39900	47.03	9.73E+00
7	9.1	39800	46.53	9.71E+00
8	12.2	39300	46.03	1.00E+01
9	13.1	40000	45.53	9.34E+00
10	15.0	40800	45.03	8.61E+00

<b>Solid Material:</b>	AgM	
<b>Pore Water:</b>	HGM-5	
<b>Contaminant:</b>	IO <sub>3</sub> <sup>-</sup>	
<b>Mass of Solid Material:</b>	2.00	g
<b>Mass of Pore Water:</b>	50.11	g
<b>[I]<sub>blank</sub>:</b>	36000	ug/L

Interval #	Total Time, days	Iodine (ug/L)	Volume (mL)	<i>K<sub>d</sub></i> (mL/g)
1	1.0	26700	50.11	8.74E+00
2	2.0	23000	49.61	1.40E+01
3	5.1	19400	49.11	2.10E+01
4	6.3	19600	48.61	2.04E+01
5	7.0	18800	48.11	2.20E+01
6	8.0	19800	47.61	1.95E+01
7	9.1	19600	47.11	1.97E+01
8	12.2	18600	46.61	2.18E+01
9	13.1	18900	46.11	2.09E+01
10	15.0	18700	45.61	2.11E+01

<b>Solid Material:</b>	GAC	
<b>Pore Water:</b>	HGM-5	
<b>Contaminant:</b>	IO <sub>3</sub> <sup>-</sup>	
<b>Mass of Solid Material:</b>	2.01	g
<b>Mass of Pore Water:</b>	50.74	g
<b>[I]<sub>blank</sub>:</b>	36000	ug/L

Interval #	Total Time, days	Iodine (ug/L)	Volume (mL)	K <sub>d</sub> (mL/g)
1	1.0	26400	50.74	9.20E+00
2	2.0	27700	50.24	7.51E+00
3	5.1	31900	49.74	3.19E+00
4	6.3	31300	49.24	3.69E+00
5	7.0	29100	48.74	5.76E+00
6	8.0	32000	48.24	3.01E+00
7	9.1	37500	47.74	0.00E+00
8	12.2	36300	47.24	0.00E+00
9	13.1	39900	46.74	0.00E+00
10	15.0	37800	46.24	0.00E+00

<b>Solid Material:</b>	HGM-5	
<b>Pore Water:</b>	HGM-5	
<b>Contaminant:</b>	IO <sub>3</sub> <sup>-</sup>	
<b>Mass of Solid Material:</b>	1.99	g
<b>Mass of Pore Water:</b>	49.17	g
<b>[I]<sub>blank</sub>:</b>	36000	ug/L

Interval #	Total Time, days	Iodine (ug/L)	Volume (mL)	K <sub>d</sub> (mL/g)
1	1.0	6730	49.17	1.07E+02
2	2.0	4210	48.67	1.84E+02
3	5.1	1820	48.17	4.54E+02
4	6.3	2520	47.67	3.18E+02
5	7.0	1460	47.17	5.60E+02
6	8.0	2040	46.67	3.90E+02
7	9.1	2360	46.17	3.30E+02
8	12.2	1580	45.67	4.99E+02
9	13.1	1520	45.17	5.14E+02
10	15.0	1370	44.67	5.67E+02

<b>Solid Material:</b>	GAC	
<b>Pore Water:</b>	HGM-5	
<b>Contaminant:</b>	Hg	
<b>Mass of Solid Material:</b>	2.02	
<b>Mass of Pore Water:</b>	49.46	
<b>[Hg]<sub>blank</sub>:</b>	52200	ug/L

Interval #	Total Time, days	Mercury (ug/L)	Volume (mL)	<i>K<sub>d</sub></i> (mL/g)
1	1.0	2170	49.46	5.65E+02
2	2.0	2740	48.96	4.38E+02
3	5.1	4280	48.46	2.69E+02
4	6.3	4500	47.96	2.52E+02
5	7.0	2170	47.46	5.42E+02
6	8.0	2840	46.96	4.04E+02
7	9.1	8980	46.46	1.11E+02
8	12.2	750	45.96	1.56E+03
9	13.1	387	45.46	3.02E+03
10	15.0	<162	44.96	>7.2E+03

<b>Solid Material:</b>	HGM-5	
<b>Pore Water:</b>	HGM-5	
<b>Contaminant:</b>	Hg	
<b>Mass of Solid Material:</b>	2.03	g
<b>Mass of Pore Water:</b>	49.73	g
<b>[Hg]<sub>blank</sub>:</b>	52200	ug/L

Interval #	Total Time, days	Mercury (ug/L)	Volume (mL)	<i>K<sub>d</sub></i> (mL/g)
1	1.0	37100	49.73	9.98E+00
2	2.0	40000	49.23	7.41E+00
3	5.1	37200	48.73	9.69E+00
4	6.3	36700	48.23	1.00E+01
5	7.0	36700	47.73	9.94E+00
6	8.0	21400	47.23	3.35E+01
7	9.1	28600	46.73	1.90E+01
8	12.2	31600	46.23	1.49E+01
9	13.1	29400	45.73	1.75E+01
10	15.0	26700	45.23	2.13E+01

<b>Solid Material:</b>	HGM-5	
<b>Pore Water:</b>	HGM-5	
<b>Contaminant:</b>	Tc-99	
<b>Mass of Solid Material:</b>	2.01	g
<b>Mass of Pore Water:</b>	49.10	g
<b>[Tc]<sub>blank</sub>:</b>	69700	ug/L

Interval #	Total Time, days	Tc-99 (ug/L)	Volume (mL)	$K_d$ (mL/g)
1	1.0	52700	49.10	7.89E+00
2	1.9	50600	48.60	9.14E+00
3	5.0	51500	48.10	8.47E+00
4	6.1	52300	47.60	7.89E+00
5	7.1	47800	47.10	1.08E+01
6	8.3	63400	46.60	2.31E+00
7	9.0	69900	46.10	0.00E+00
8	12.1	73200	45.60	0.00E+00
9	13.2	71400	45.10	0.00E+00
10	15.0	74100	44.60	0.00E+00

<b>Solid Material:</b>	AgM	
<b>Pore Water:</b>	HGM-5	
<b>Contaminant:</b>	Tc-99	
<b>Mass of Solid Material:</b>	2.01	g
<b>Mass of Pore Water:</b>	49.80	g
<b>[Tc]<sub>blank</sub>:</b>	69700	ug/L

Interval #	Total Time, days	Tc-99 (ug/L)	Volume (mL)	$K_d$ (mL/g)
1	1.0	50200	49.80	9.61E+00
2	1.9	48700	49.30	1.06E+01
3	5.0	52300	48.80	8.07E+00
4	6.1	52300	48.30	7.98E+00
5	7.1	49100	47.80	9.96E+00
6	8.3	80000	47.30	0.00E+00
7	9.0	76500	46.80	0.00E+00
8	12.1	82900	46.30	0.00E+00
9	13.2	77800	45.80	0.00E+00
10	15.0	76100	45.30	0.00E+00

<b>Solid Material:</b>	GAC	
<b>Pore Water:</b>	HGM-5	
<b>Contaminant:</b>	Tc-99	
<b>Mass of Solid Material:</b>	2.02	g
<b>Mass of Pore Water:</b>	49.81	g
<b>[Tc]<sub>blank</sub>:</b>	69700	ug/L

Interval #	Total Time, days	Tc-99 (ug/L)	Volume (mL)	$K_d$ (mL/g)
1	1.0	19700	49.81	6.26E+01
2	1.9	21100	49.31	5.62E+01
3	5.0	29400	48.81	3.31E+01
4	6.1	28600	48.31	3.44E+01
5	7.1	25300	47.81	4.15E+01
6	8.3	27800	47.31	3.53E+01
7	9.0	30900	46.81	2.91E+01
8	12.1	34000	46.31	2.41E+01
9	13.2	36100	45.81	2.11E+01
10	15.0	32400	45.31	2.58E+01

<b>Solid Material:</b>	HEPA	
<b>Pore Water:</b>	HGM-5	
<b>Contaminant:</b>	Tc-99	
<b>Mass of Solid Material:</b>	2.01	g
<b>Mass of Pore Water:</b>	50.92	g
<b>[Tc]<sub>blank</sub>:</b>	69700	ug/L

Interval #	Total Time, days	Tc-99 (ug/L)	Volume (mL)	$K_d$ (mL/g)
1	1.0	50600	50.92	9.57E+00
2	1.9	41100	50.42	1.75E+01
3	5.0	53700	49.92	7.41E+00
4	6.1	46200	49.42	1.25E+01
5	7.1	52200	48.92	8.17E+00
6	8.3	73200	48.42	0.00E+00
7	9.0	80500	47.92	0.00E+00
8	12.1	42400	47.42	1.52E+01
9	13.2	66100	46.92	1.27E+00
10	15.0	77500	46.42	0.00E+00

## **Appendix C**

### **Sorption $K_d$**

## Appendix C

### Sorption $K_d$

Test ID	Spike	Bottle Number	Mass of Solution	Mass of Solid Material	Total Time, Days	[x] (x = I <sup>-</sup> or IO <sub>3</sub> <sup>-</sup> ) ug/L	[Hg] ug/L	[Tc] ug/L
			Measured (g)	Measured (g)				
No Solid-CS-Tc	Tc	1	12.4797	-	12.17	NA	NA	62800
		2	12.4751	-	12.17	NA	NA	67400
		3	12.5034	-	12.17	NA	NA	66300
					<i>average:</i>	---	---	65500
					<i>stdev:</i>	---	---	1961
No Solid-CS-I	Iodide	1	12.51	-	9.99	48000	NA	NA
		2	12.51	-	9.99	47700	NA	NA
		3	12.50	-	9.99	47900	NA	NA
					<i>average:</i>	47867	---	---
					<i>stdev:</i>	125	---	---
No Solid-CS-IO <sub>3</sub>	Iodate	1	12.44	-	9.98	33800	NA	NA
		2	12.43	-	9.98	35500	NA	NA
		3	12.45	-	9.98	36000	NA	NA
					<i>average:</i>	35100	---	---
					<i>stdev:</i>	942	---	---
No Solid-CS-Hg	Hg	1	12.40	-	9.95	NA	2900	NA
		2	12.42	-	9.95	NA	4310	NA
		3	12.37	-	9.95	NA	4520	NA
					<i>average:</i>	---	3910	---
					<i>stdev:</i>	---	719	---

C.1

C2

Test ID	Spike	Bottle Number	Mass of Solution	Mass of Solid Material	Total Time, Days	[x] (x = I <sup>-</sup> or IO <sub>3</sub> <sup>-</sup> ) ug/L	[Hg] ug/L	[Tc] ug/L
			Measured (g)	Measured (g)				
No Solid-CS-Hg-I	Hg-I	1	12.47	-	11.79	37700	18200	NA
		2	12.41	-	11.79	38000	20700	NA
		3	12.36	-	11.79	39200	21400	NA
					<i>average:</i>	38300	20100	---
					<i>stdev:</i>	648	1374	---
No Solid-CS-ALL	ALL	1	12.4665	-	12.21	72300	8630	53500
		2	12.4741	-	12.21	73100	8020	51200
		3	12.4687	-	12.21	73900	8160	56600
					<i>average:</i>	73100	8270	53767
					<i>stdev:</i>	653	261	2213
No Solid-HGM-5.Tc	Tc	1	12.4908	-	12.19	NA	NA	56400
		2	12.4845	-	12.19	NA	NA	72900
		3	12.4956	-	12.19	NA	NA	78500
					<i>average:</i>	---	---	69267
					<i>stdev:</i>	---	---	9381
No Solid-HGM-5.I	Iodide	1	12.43	-	9.97	48200	NA	NA
		2	12.47	-	9.97	48700	NA	NA
		3	12.47	-	9.97	47500	NA	NA
					<i>average:</i>	48133	---	---
					<i>stdev:</i>	492	---	---
No Solid-HGM-5.IO <sub>3</sub>	Iodate	1	12.43	-	9.97	34200	NA	NA
		2	12.46	-	9.97	34700	NA	NA
		3	12.54	-	9.97	34900	NA	NA
					<i>average:</i>	34600	---	---
					<i>stdev:</i>	294	---	---

Test ID	Spike	Bottle Number	Mass of Solution	Mass of Solid Material	Total Time, Days	[x] (x = I <sup>-</sup> or IO <sub>3</sub> <sup>-</sup> ) ug/L	[Hg] ug/L	[Tc] ug/L
			Measured (g)	Measured (g)				
No Solid-HGM-5.Hg	Hg	1	12.40	-	9.96	NA	56300	NA
		2	12.41	-	9.96	NA	54500	NA
		3	12.36	-	9.96	NA	53300	NA
					<i>average:</i>	---	54700	---
					<i>stdev:</i>	---	1233	---
No Solid-HGM-5.Hg-I	Hg-I	1	12.48	-	11.83	43100	38300	NA
		2	12.55	-	11.83	42200	38000	NA
		3	12.48	-	11.83	41500	38500	NA
					<i>average:</i>	42267	38267	---
					<i>stdev:</i>	655	205	---
No Solid-HGM-5.ALL	ALL	1	12.4667	-	12.20	73700	35400	57600
		2	12.4571	-	12.20	66200	35200	53400
		3	12.4852	-	12.20	73000	36200	50700
					<i>average:</i>	70967	35600	53900
					<i>stdev:</i>	3383	432	2839

C.3

**ADSORPTION  $K_d$**

Test ID	Spike	Bottle Number	Mass of Solution Measured (g)	Mass of Solid Material Measured (g)	Total Time Days	[x] (x = I <sup>-</sup> or IO <sub>3</sub> <sup>-</sup> ) ug/L	[Hg] ug/L <sup>(a)</sup>	[Tc] ug/L	$K_d$ (I <sup>-</sup> or IO <sub>3</sub> <sup>-</sup> )	$K_d$ (Hg)	$K_d$ (Tc)
GAC-CS-Tc	Tc	1	12.4613	0.5085	12.11	NA	NA	2990	---	---	5.12E+02
		2	12.4654	0.4973	12.11	NA	NA	468	---	---	3.48E+03
		3	12.4786	0.4992	12.11	NA	NA	580	---	---	2.80E+03
									average:	---	---
								stdev:	---	---	1.27E+03
GAC-CS-I	Iodide	1	12.47	0.5090	10.00	5680	NA	NA	1.82E+02	---	---
		2	12.46	0.4918	10.00	14400	NA	NA	5.89E+01	---	---
		3	12.44	0.5023	10.72	13600	NA	NA	6.24E+01	---	---
									average:	1.01E+02	---
								stdev:	5.72E+01	---	---
GAC-CS-IO <sub>3</sub>	Iodate	1	12.50	0.5048	10.09	80100	NA	NA	0.00E+00	---	---
		2	12.52	0.5096	10.09	34000	NA	NA	7.95E-01	---	---
		3	12.50	0.5027	10.80	22000	NA	NA	1.48E+01	---	---
									average:	5.20E+00	---
								stdev:	6.80E+00	---	---
GAC-CS-Hg	Hg	1	12.40	0.5017	10.78	NA	8.12	NA	---	1.19E+04	---
		2	12.50	0.4922	10.78	NA	15.6	NA	---	6.34E+03	---
		3	12.51	0.4995	10.78	NA	8.12	NA	---	1.20E+04	---
									average:	---	1.01E+04
								stdev:	---	2.65E+03	---
GAC-CS-No Spike	No Spike	1	12.49	0.4952	11.00	NA	NA	NA	---	---	---
		2	12.56	0.5089	11.00	NA	NA	NA	---	---	---
		3	12.44	0.4993	11.00	NA	NA	NA	---	---	---
									average:	---	---
								stdev:	---	---	---

C.4

ADSORPTION  $K_d$

Test ID	Spike	Bottle Number	Mass of Solution Measured (g)	Mass of Solid Material Measured (g)	Total Time Days	[x] (x = I <sup>-</sup> or IO <sub>3</sub> <sup>-</sup> ) ug/L	[Hg] ug/L <sup>(a)</sup>	[Tc] ug/L	$K_d$ (I <sup>-</sup> or IO <sub>3</sub> <sup>-</sup> )	$K_d$ (Hg)	$K_d$ (Tc)
GAC-CS-Hg-I	Hg -I	1	12.43	0.4992	10.82	940	8.12	NA	9.90E+02	6.16E+04	---
		2	12.44	0.5002	10.82	10800	35.5	NA	6.33E+01	1.41E+04	---
		3	12.47	0.5029	10.82	6140	26.9	NA	1.30E+02	1.85E+04	---
								average:	3.94E+02	3.14E+04	---
								stdev:	4.22E+02	2.14E+04	---
GAC-HGM-5.Tc	Tc	1	12.4599	0.4917	12.17	NA	NA	2670	---	---	6.32E+02
		2	12.4718	0.5017	12.17	NA	NA	1300	---	---	1.30E+03
		3	12.4705	0.5000	12.17	NA	NA	297	---	---	5.79E+03
								average:	---	---	2.57E+03
								stdev:	---	---	2.29E+03
GAC-HGM-5.I	Iodide	1	12.49	0.5018	10.05	133000	NA	NA	0.00E+00	---	---
		2	12.44	0.4931	10.05	16800	NA	NA	4.71E+01	---	---
		3	12.46	0.4940	10.05	68500	NA	NA	0.00E+00	---	---
								average:	1.57E+01	---	---
								stdev:	2.22E+01	---	---
GAC-HGM-5.IO <sub>3</sub>	Iodate	1	12.45	0.5059	10.02	30400	NA	NA	3.40E+00	---	---
		2	12.43	0.4960	10.02	19000	NA	NA	2.06E+01	---	---
		3	12.46	0.5028	10.77	11000	NA	NA	5.32E+01	---	---
								average:	2.57E+01	---	---
								stdev:	2.06E+01	---	---
GAC-HGM-5.Hg	Hg	1	12.42	0.5024	10.84	NA	11.0	NA	---	1.23E+05	---
		2	12.36	0.5076	10.84	NA	8.12	NA	---	1.64E+05	---
		3	12.41	0.4981	10.84	NA	17.6	NA	---	7.74E+04	---
								average:	---	1.21E+05	---
								stdev:	---	3.54E+04	---
GAC-HGM-5.No Spike	No Spike	1	12.53	0.4966	11.03	NA	NA	NA	---	---	---
		2	12.47	0.4993	11.03	NA	NA	NA	---	---	---
		3	12.48	0.4981	11.03	NA	NA	NA	---	---	---
								average:	---	---	---
								stdev:	---	---	---

**ADSORPTION  $K_d$**

Test ID	Spike	Bottle Number	Mass of Solution Measured (g)	Mass of Solid Material Measured (g)	Total Time Days	[x] (x = I <sup>-</sup> or IO <sub>3</sub> <sup>-</sup> ) ug/L	[Hg] ug/L <sup>(a)</sup>	[Tc] ug/L	$K_d$ (I <sup>-</sup> or IO <sub>3</sub> <sup>-</sup> )	$K_d$ (Hg)	$K_d$ (Tc)
GAC-HGM-5.Hg-I	Hg-I	1	12.54	0.4963	10.95	46400	10.2	NA	0.00E+00	9.48E+04	---
		2	12.45	0.5075	10.95	143000	8.12	NA	0.00E+00	1.16E+05	---
		3	12.50	0.5011	10.95	75700	8.55	NA	0.00E+00	1.12E+05	---
									<i>average:</i>	0.00E+00	1.07E+05
								<i>stdev:</i>	0.00E+00	9.03E+03	---
HEPA-CS-Tc	Tc	1	12.4223	0.5077	12.16	NA	NA	70900	---	---	0.00E+00
		2	12.4310	0.5031	12.16	NA	NA	65400	---	---	3.78E-02
		3	12.4678	0.4941	12.16	NA	NA	62900	---	---	1.04E+00
									<i>average:</i>	---	---
								<i>stdev:</i>	---	---	4.83E-01
HEPA-CS-I	Iodide	1	12.48	0.5039	11.86	48000	NA	NA	0.00E+00	---	---
		2	12.48	0.4903	11.86	47700	NA	NA	8.89E-02	---	---
		3	12.49	0.4936	11.86	47600	NA	NA	1.42E-01	---	---
									<i>average:</i>	7.69E-02	---
								<i>stdev:</i>	5.85E-02	---	---
HEPA-CS-IO <sub>3</sub>	Iodate	1	12.48	0.5051	11.88	33600	NA	NA	1.10E+00	---	---
		2	12.56	0.4980	11.88	34900	NA	NA	1.45E-01	---	---
		3	12.49	0.4971	10.00	33400	NA	NA	1.28E+00	---	---
									<i>average:</i>	8.42E-01	---
								<i>stdev:</i>	4.98E-01	---	---
HEPA-CS-No Spike	No Spike	1	12.55	0.5059	12.09	NA	NA	NA	---	---	---
		2	12.57	0.5048	12.09	NA	NA	NA	---	---	---
		3	12.46	0.5046	12.09	NA	NA	NA	---	---	---
									<i>average:</i>	---	---
								<i>stdev:</i>	---	---	---

C.6

ADSORPTION  $K_d$

Test ID	Spike	Bottle Number	Mass of Solution Measured (g)	Mass of Solid Material Measured (g)	Total Time Days	[x] (x = I <sup>-</sup> or IO <sub>3</sub> <sup>-</sup> ) ug/L	[Hg] ug/L <sup>(a)</sup>	[Tc] ug/L	$K_d$ (I <sup>-</sup> or IO <sub>3</sub> <sup>-</sup> )	$K_d$ (Hg)	$K_d$ (Tc)
HEPA-HGM-5.Tc	Tc	1	12.4464	0.4956	12.15	NA	NA	73100	---	---	0.00E+00
		2	12.4665	0.4980	12.15	NA	NA	69700	---	---	0.00E+00
		3	12.4741	0.5066	12.15	NA	NA	69000	---	---	9.52E-02
									average:	---	---
								stdev:	---	---	4.49E-02
HEPA-HGM-5.I	Iodide	1	12.44	0.4955	11.88	48800	NA	NA	0.00E+00	---	---
		2	12.45	0.4948	11.88	47500	NA	NA	3.35E-01	---	---
		3	12.48	0.4946	11.88	46600	NA	NA	8.30E-01	---	---
									average:	3.89E-01	---
								stdev:	3.41E-01	---	---
HEPA-HGM-5.IO <sub>3</sub>	Iodate	1	12.47	0.5014	11.88	34800	NA	NA	0.00E+00	---	---
		2	12.46	0.4995	11.88	35000	NA	NA	0.00E+00	---	---
		3	12.47	0.5076	11.88	36200	NA	NA	0.00E+00	---	---
									average:	0.00E+00	---
								stdev:	0.00E+00	---	---
HEPA-HGM-5.No Spike	No Spike	1	12.46	0.4981	12.03	NA	NA	NA	---	---	---
		2	12.46	0.5023	12.03	NA	NA	NA	---	---	---
		3	12.50	0.4995	10.16	NA	NA	NA	---	---	---
									average:	---	---
								stdev:	---	---	---
AgM-CS-Tc	Tc	1	12.4633	0.4976	12.13	NA	NA	57100	---	---	3.68E+00
		2	12.4605	0.4920	12.13	NA	NA	61300	---	---	1.74E+00
		3	12.4889	0.5000	10.91	NA	NA	50400	---	---	7.48E+00
									average:	---	---
								stdev:	---	---	2.39E+00
AgM-CS-I	Iodide	1	12.50	0.5003	11.00	10.1	NA	NA	1.18E+05	---	---
		2	12.53	0.5051	11.00	28.1	NA	NA	4.22E+04	---	---
		3	12.49	0.4900	10.96	98.8	NA	NA	1.23E+04	---	---
									average:	5.76E+04	---
								stdev:	4.47E+04	---	---

ADSORPTION  $K_d$

Test ID	Spike	Bottle Number	Mass of Solution Measured (g)	Mass of Solid Material Measured (g)	Total Time Days	[x] (x = I <sup>-</sup> or IO <sub>3</sub> <sup>-</sup> ) ug/L	[Hg] ug/L <sup>(a)</sup>	[Tc] ug/L	$K_d$ (I <sup>-</sup> or IO <sub>3</sub> <sup>-</sup> )	$K_d$ (Hg)	$K_d$ (Tc)
AgM-CS-IO <sub>3</sub>	Iodate	1	12.46	0.5001	9.98	33400	NA	NA	1.27E+00	---	---
		2	12.47	0.4951	9.98	29900	NA	NA	4.38E+00	---	---
		3	12.50	0.4900	10.94	29500	NA	NA	4.84E+00	---	---
								average:	3.50E+00	---	---
								stdev:	1.59E+00	---	---
AgM-CS-No Spike	No Spike	1	12.49	0.5041	11.11	NA	NA	NA	---	---	---
		2	12.47	0.4915	11.11	NA	NA	NA	---	---	---
		3	12.45	0.4999	11.11	NA	NA	NA	---	---	---
								average:	---	---	---
								stdev:	---	---	---
AgM-HGM-5.Tc	Tc	1	12.4876	0.4923	12.18	NA	NA	64000	---	---	2.09E+00
		2	12.4591	0.5065	12.18	NA	NA	75400	---	---	0.00E+00
		3	12.4511	0.51	10.91	NA	NA	49400	---	---	9.82E+00
								average:	---	---	3.97E+00
								stdev:	---	---	4.22E+00
AgM-HGM-5.I	Iodide	1	12.90	0.5004	10.95	80	NA	NA	1.55E+04	---	---
		2	12.47	0.4997	10.95	76	NA	NA	1.59E+04	---	---
		3	12.40	0.5	10.95	32	NA	NA	3.78E+04	---	---
								average:	2.31E+04	---	---
								stdev:	1.04E+04	---	---
AgM-HGM-5.IO <sub>3</sub>	Iodate	1	12.46	0.4943	10.95	32900	NA	NA	1.30E+00	---	---
		2	12.42	0.5016	10.95	29300	NA	NA	4.48E+00	---	---
		3	12.40	0.5	10.96	31000	NA	NA	2.88E+00	---	---
								average:	2.89E+00	---	---
								stdev:	1.30E+00	---	---
AgM-HGM-5.No Spike	No Spike	1	12.47	0.4929	11.16	NA	NA	NA	---	---	---
		2	12.45	0.4945	10.17	NA	NA	NA	---	---	---
		3	12.51	0.5	10.96	NA	NA	NA	---	---	---
								average:	---	---	---
								stdev:	---	---	---

**ADSORPTION  $K_d$**

Test ID	Spike	Bottle Number	Mass of Solution Measured (g)	Mass of Solid Material Measured (g)	Total Time Days	[x] (x = I <sup>-</sup> or IO <sub>3</sub> <sup>-</sup> ) ug/L	[Hg] ug/L <sup>(a)</sup>	[Tc] ug/L	$K_d$ (I <sup>-</sup> or IO <sub>3</sub> <sup>-</sup> )	$K_d$ (Hg)	$K_d$ (Tc)
CS-CS-Tc	Tc	1	12.5269	0.4992	12.15	NA	NA	70000	---	---	0.00E+00
		2	12.4564	0.4984	12.15	NA	NA	69200	---	---	0.00E+00
		3	12.4682	0.497	12.15	NA	NA	55400	---	---	4.57E+00
									average:	---	---
								stdev:	---	---	2.16E+00
CS-CS-I	Iodide	1	12.53	0.4945	11.03	44900	NA	NA	1.67E+00	---	---
		2	12.50	0.5041	11.03	42200	NA	NA	3.33E+00	---	---
		3	12.49	0.5041	10.04	45600	NA	NA	1.23E+00	---	---
									average:	2.08E+00	---
								stdev:	9.03E-01	---	---
CS-CS-IO <sub>3</sub>	Iodate	1	12.44	0.5052	11.02	16600	NA	NA	2.74E+01	---	---
		2	12.46	0.5048	11.02	16800	NA	NA	2.69E+01	---	---
		3	12.48	0.498	11.02	16400	NA	NA	2.86E+01	---	---
									average:	2.76E+01	---
								stdev:	7.02E-01	---	---
CS-CS-Hg	Hg	1	12.42	0.4981	11.00	NA	8.12	NA	---	1.20E+04	---
		2	12.42	0.5025	11.00	NA	8.12	NA	---	1.19E+04	---
		3	12.43	0.4982	11.00	NA	8.12	NA	---	1.20E+04	---
									average:	---	1.19E+04
								stdev:	---	5.12E+01	---
CS-CS-No Spike	No Spike	1	12.44	0.5020	11.26	NA	NA	NA	---	---	---
		2	12.48	0.5013	11.26	NA	NA	NA	---	---	---
		3	12.46	0.504	11.26	NA	NA	NA	---	---	---
									average:	---	---
								stdev:	---	---	---
CS-CS-Hg-I	Hg -I	1	12.4300	0.4933	11.03	42000	8.12	NA	0.00E+00	6.23E+04	---
		2	12.4200	0.4958	11.03	---	---	NA	---	---	---
		3	12.4600	0.4988	11.03	42000	8.12	NA	0.00E+00	6.18E+04	---
									average:	0.00E+00	6.21E+04
								stdev:	0.00E+00	2.69E+02	---
CS-CS-ALL	ALL	1	12.4649	0.5055	12.20	48900	16.6	56800	1.22E+01	1.23E+04	0.00E+00
		2	12.4756	0.5061	12.20	48100	41.7	68000	1.28E+01	4.86E+03	0.00E+00

C9

ADSORPTION  $K_d$

Test ID	Spike	Bottle Number	Mass of Solution Measured (g)	Mass of Solid Material Measured (g)	Total Time Days	[x] (x = I <sup>-</sup> or IO <sub>3</sub> <sup>-</sup> ) ug/L	[Hg] ug/L <sup>(a)</sup>	[Tc] ug/L	$K_d$ (I <sup>-</sup> or IO <sub>3</sub> <sup>-</sup> )	$K_d$ (Hg)	$K_d$ (Tc)
		3	12.4728	0.4976	12.20	48800	42.5	55300	1.25E+01	4.85E+03	0.00E+00
								average:	1.25E+01	7.33E+03	0.00E+00
								stdev:	2.49E-01	3.49E+03	0.00E+00
HGM-5.HGM-5.Tc	Tc	1	12.4494	0.5012	12.20	NA	NA	66600	---	---	9.95E-01
		2	12.4707	0.4969	12.20	NA	NA	63100	---	---	2.45E+00
		3	12.4743	0.5046	12.20	NA	NA	67000	---	---	8.36E-01
								average:	---	---	1.43E+00
								stdev:	---	---	7.28E-01
HGM-5.HGM-5.I	Iodide	1	12.48	0.4925	11.09	41100	NA	NA	4.34E+00	---	---
		2	12.49	0.4948	11.09	46000	NA	NA	1.17E+00	---	---
		3	12.47	0.5061	11.09	44700	NA	NA	1.89E+00	---	---
								average:	2.47E+00	---	---
								stdev:	1.35E+00	---	---
HGM-5.HGM-5.IO <sub>3</sub>	Iodate	1	12.40	0.4988	11.90	1230	NA	NA	6.74E+02	---	---
		2	12.43	0.503	11.90	1260	NA	NA	6.54E+02	---	---
		3	12.48	0.5082	11.90	1100	NA	NA	7.48E+02	---	---
								average:	6.92E+02	---	---
								stdev:	4.03E+01	---	---
HGM-5.HGM-5.Hg	Hg	1	12.38	0.4995	11.08	NA	32200	NA	---	1.73E+01	---
		2	12.40	0.4984	11.08	NA	34600	NA	---	1.45E+01	---
		3	12.42	0.5036	11.08	NA	31600	NA	---	1.80E+01	---
								average:	---	1.66E+01	---
								stdev:	---	1.55E+00	---
HGM-5.HGM-5.No Spike	No Spike	1	12.43	0.5061	11.28	NA	NA	NA	---	---	---
		2	12.48	0.5077	10.20	NA	NA	NA	---	---	---
		3	12.48	0.5000	10.20	NA	NA	NA	---	---	---
								average:	---	---	---
								stdev:	---	---	---

C.10

**ADSORPTION  $K_d$**

Test ID	Spike	Bottle Number	Mass of Solution Measured (g)	Mass of Solid Material Measured (g)	Total Time Days	[x] (x = I <sup>-</sup> or IO <sub>3</sub> <sup>-</sup> ) ug/L	[Hg] ug/L <sup>(a)</sup>	[Tc] ug/L	$K_d$ (I <sup>-</sup> or IO <sub>3</sub> <sup>-</sup> )	$K_d$ (Hg)	$K_d$ (Tc)
HGM-5.HGM-5.Hg-I	Hg -I	1	12.4900	0.4939	11.19	36300	18200	NA	4.16E+00	2.79E+01	---
		2	12.5300	0.5081	11.19	36600	20700	NA	3.82E+00	2.09E+01	---
		3	12.4700	0.5048	11.19	38000	21400	NA	2.77E+00	1.95E+01	---
								<i>average:</i>	3.58E+00	2.28E+01	---
								<i>stdev:</i>	5.89E-01	3.67E+00	---
HGM-5.HGM-5.ALL	ALL	1	12.4498	0.5088	12.21	37100	18200	54100	2.37E+01	0.00E+00	0.00E+00
		2	12.4114	0.5012	12.21	38100	20700	52800	2.27E+01	0.00E+00	4.53E-01
		3	12.4772	0.5027	12.21	38200	21400	53700	2.27E+01	0.00E+00	3.08E-02
								<i>average:</i>	2.31E+01	0.00E+00	1.61E-01
								<i>stdev:</i>	4.87E-01	0.00E+00	2.07E-01

**Appendix D**  
**Desorption  $K_d$**

## Appendix D Desorption $K_d$

### DESORPTION $K_d$

Test ID	Spike	Bottle Number	Mass of Solution	Mass of Solid Material	Total Time, Days	[x] (x = I <sup>-</sup> or IO <sub>3</sub> <sup>-</sup> ) ug/L	[Hg] ug/L <sup>(a)</sup>	[Tc] ug/L	$K_d$ (I <sup>-</sup> or IO <sub>3</sub> <sup>-</sup> )	$K_d$ (Hg)	$K_d$ (Tc)
			Measured (g)	Measured (g)							
GAC-CS-Tc desorb	Tc	1	12.5161	0.6765	13.94	NA	NA	9970	NA	NA	1.29E+02
		2	12.4440	0.6759	13.94	NA	NA	8030	NA	NA	1.78E+02
								<i>average:</i>	---	---	1.54E+02
								<i>stdev:</i>	---	---	2.44E+01
GAC-CS-I desorb	Iodide	1	15.3081	0.6126	13.97	41500	NA	NA	0	NA	NA
		2	16.6489	0.6624	13.97	30000	NA	NA	0	NA	NA
								<i>average:</i>	---	---	---
								<i>stdev:</i>	---	---	---
GAC-CS-IO <sub>3</sub> desorb	Iodate	1	16.2688	0.6503	13.96	71600	NA	NA	0	NA	NA
		2	16.4185	0.6566	13.96	27200	NA	NA	0	NA	NA
								<i>average:</i>	---	---	---
								<i>stdev:</i>	---	---	---
GAC-CS-Hg desorb	Hg	1	15.4301	0.6028	13.96	NA	1530	NA	NA	3.23E+01	NA
		2	14.5003	0.5772	13.96	NA	113	NA	NA	8.46E+02	NA
								<i>average:</i>	---	4.39E+02	---
								<i>stdev:</i>	---	4.07E+02	---
GAC-CS-Hg-I desorb	Hg -I	1	12.7801	0.5111	13.97	31100	3.19	NA	4.31E+00	1.57E+05	NA
		2	15.3832	0.6149	13.97	43200	9.61	NA	0	5.19E+04	NA
								<i>average:</i>	4.31E+00	1.04E+05	---
								<i>stdev:</i>	0.00E+00	5.25E+04	---
GAC--HGM-5.Tc	Tc	1	12.4549	0.7087	13.92	NA	NA	8160	NA	NA	1.82E+02
		2	12.4454	0.6664	13.92	NA	NA	9180	NA	NA	1.59E+02
								<i>average:</i>	---	---	1.70E+02
								<i>stdev:</i>	---	---	1.12E+01
GAC--HGM-5.I	Iodide	1			0.00		NA	NA	#DIV/0!	NA	NA
		2			0.00		NA	NA	#DIV/0!	NA	NA

D.1

DESORPTION  $K_d$

Test ID	Spike	Bottle Number	Mass of Solution	Mass of Solid Material	Total Time, Days	[x] (x = I <sup>-</sup> or IO <sub>3</sub> <sup>-</sup> ) ug/L	[Hg] ug/L <sup>(a)</sup>	[Tc] ug/L	$K_d$ (I <sup>-</sup> or IO <sub>3</sub> <sup>-</sup> )	$K_d$ (Hg)	$K_d$ (Tc)
			Measured (g)	Measured (g)							
								average:	---	---	---
								stdev:	---	---	---
GAC--HGM-5.IO <sub>3</sub>	Iodate	1			0.00		NA	NA	#DIV/0!	NA	NA
		2			0.00		NA	NA	#DIV/0!	NA	NA
								average:	---	---	---
								stdev:	---	---	---
GAC-H-HGM-5GM5.Hg	Hg	1	16.8267	0.6733	13.99	NA	32.7	NA	NA	4.13E+04	NA
		2	16.1277	0.6430	13.99	NA	21.7	NA	NA	6.13E+04	NA
								average:	---	5.13E+04	---
								stdev:	---	1.00E+04	---
GAC-H-HGM-5GM5.Hg-I	Hg-I	1	15.70	0.6182	9.99	15200	161	NA	0	5.97E+03	NA
		2	16.43	0.6577	9.99	74000	33.9	NA	0	2.77E+04	NA
								average:	---	1.68E+04	---
								stdev:	---	1.08E+04	---
HEPA-CS-Tc	Tc	1	12.4350	1.1002	13.93	NA	NA	2440	NA	NA	0
		2	12.4043	1.3511	13.93	NA	NA	3300	NA	NA	3.77E+01
								average:	---	---	3.77E+01
								stdev:	---	---	0.00E+00
HEPA-CS-I	Iodide	1	22.7952	0.9115	14.01	960	NA	NA	0	NA	NA
		2	20.4273	0.8178	14.01	820	NA	NA	1.06E+01	NA	NA
								average:	1.06E+01	---	---
								stdev:	0.00E+00	---	---
HEPA-CS-IO <sub>3</sub>	Iodate	1	25.7997	1.0318	14.02	890	NA	NA	1.61E+01	NA	NA
		2	21.0910	0.8433	14.02	540	NA	NA	0	NA	NA
								average:	1.61E+01	---	---
								stdev:	0.00E+00	---	---
HEPA--HGM-5.Tc	Tc	1	12.4535	1.0711	13.92	NA	NA	2330	---	---	0
		2	12.4436	1.2025	13.92	NA	NA	2680	---	---	0
								average:	---	---	---
								stdev:	---	---	---

D 2

DESORPTION  $K_d$

Test ID	Spike	Bottle Number	Mass of Solution	Mass of Solid Material	Total Time, Days	[x] (x = I <sup>-</sup> or IO <sub>3</sub> <sup>-</sup> ) ug/L	[Hg] ug/L <sup>(a)</sup>	[Tc] ug/L	$K_d$ (I <sup>-</sup> or IO <sub>3</sub> <sup>-</sup> )	$K_d$ (Hg)	$K_d$ (Tc)
			Measured (g)	Measured (g)							
HEPA-HGM-5.I	Iodide	1			0.00		NA	NA	---	---	---
		2			0.00		NA	NA	---	---	---
								average:	---	---	---
								stdev:	---	---	---
HEPA-HGM-5.IO <sub>3</sub>	Iodate	1			0.00		NA	NA	---	---	---
		2			0.00		NA	NA	---	---	---
								average:	---	---	---
								stdev:	---	---	---
AgM-CS-Tc	Tc	1	12.4273	0.6850	13.90	NA	NA	94.8	NA	NA	2.42E+03
		2	12.4520	0.6806	13.90	NA	NA	94.3	NA	NA	1.35E+03
								average:	---	---	1.89E+03
								stdev:	---	---	5.35E+02
AgM-CS-I	Iodide	1	16.1693	0.6462	13.99	4.11	NA	NA	2.91E+05	NA	NA
		2	13.2036	0.5203	13.99	0.46	NA	NA	2.58E+06	NA	NA
								average:	1.44E+06	---	---
								stdev:	1.14E+06	---	---
AgM-CS-IO <sub>3</sub>	Iodate	1	15.8277	0.6323	13.99	64	NA	NA	7.72E+02	NA	NA
		2	16.6991	0.6682	13.99	169	NA	NA	8.03E+02	NA	NA
								average:	7.87E+02	---	---
								stdev:	1.56E+01	---	---
AgM-HGM-5.Tc	Tc	1			0.00	NA	NA		---	---	---
		2			0.00	NA	NA		---	---	---
								average:	---	---	---
								stdev:	---	---	---
AgM-HGM-5.I	Iodide	1	16.9398	0.6768	14.07	7.51	NA	NA	1.60E+05	---	---
		2	18.3950	0.7350	14.07	2.71	NA	NA	4.44E+05	---	---
								average:	3.02E+05	---	---
								stdev:	1.42E+05	---	---

DESORPTION  $K_d$

Test ID	Spike	Bottle Number	Mass of Solution	Mass of Solid Material	Total Time, Days	[x] (x = I <sup>-</sup> or IO <sub>3</sub> <sup>-</sup> ) ug/L	[Hg] ug/L <sup>(a)</sup>	[Tc] ug/L	$K_d$ (I <sup>-</sup> or IO <sub>3</sub> <sup>-</sup> )	$K_d$ (Hg)	$K_d$ (Tc)
			Measured (g)	Measured (g)							
AgM-HGM-5.IO <sub>3</sub>	Iodate	1	17.5456	0.7033	14.08	370	NA	NA	2.31E+03	---	---
		2	17.7136	0.7082	14.08	1440	NA	NA	5.76E+02	---	---
								average:	1.44E+03	---	---
								stdev:	8.66E+02	---	---
CS-CS-Tc	Tc	1	12.4220	0.5936	13.92	NA	NA	1210	NA	NA	0
		2	12.4392	0.6184	13.92	NA	NA	1180	NA	NA	0
								average:	---	---	---
								stdev:	---	---	---
CS-CS-I	Iodide	1	15.7693	0.6305	13.98	1520	NA	NA	2.57E+01	NA	NA
		2	13.0721	0.5236	13.98	1660	NA	NA	5.97E+01	NA	NA
								average:	4.27E+01	---	---
								stdev:	1.70E+01	---	---
CS-CS-IO <sub>3</sub>	Iodate	1	15.3099	0.6126	13.97	1100	NA	NA	3.87E+02	NA	NA
		2	15.6409	0.3256	13.97	1950	NA	NA	1.98E+02	NA	NA
								average:	2.92E+02	---	---
								stdev:	9.47E+01	---	---
CS-CS-Hg	Hg	1	14.2859	0.5708	14.07	NA	2.93	NA	NA	3.32E+04	NA
		2	14.3570	0.5751	14.07	NA	1.82	NA	NA	5.30E+04	NA
								average:	---	4.31E+04	---
								stdev:	---	9.89E+03	---
CS-CS-Hg-I	Hg -I	1	14.1491	0.5670	13.96	1530	2.93	NA	0	1.73E+05	NA
		2	14.2679	0.5665	13.96	1400	1.82	NA	0	2.77E+05	---
								average:	---	2.25E+05	---
								stdev:	---	5.19E+04	---
CS-CS-ALL	ALL	1	12.4532	0.6298	13.91		1.62	1390		1.26E+05	0
		2	12.4274	0.6386	13.91		1.62	1270		1.25E+05	0
								average:	---	1.25E+05	---
								stdev:	---	2.09E+02	---

D.4

DESORPTION  $K_d$

Test ID	Spike	Bottle Number	Mass of Solution	Mass of Solid Material	Total Time, Days	[x] (x = I <sup>-</sup> or IO <sub>3</sub> <sup>-</sup> ) ug/L	[Hg] ug/L <sup>(a)</sup>	[Tc] ug/L	$K_d$ (I <sup>-</sup> or IO <sub>3</sub> <sup>-</sup> )	$K_d$ (Hg)	$K_d$ (Tc)
			Measured (g)	Measured (g)							
HGM-5.-HGM-5.Tc	Tc	1	12.4818	0.5664	13.94	NA	NA	1240	NA	NA	3.55E+01
		2	12.4657	0.5820	13.94	NA	NA	1260	NA	NA	1.06E+02
								average:	---	---	7.09E+01
								stdev:	---	---	3.54E+01
HGM-5.-HGM-5.I	Iodide	1	14.6013	0.5837	13.97	5150	NA	NA	6.44E+00	NA	NA
		2	14.8334	0.5938	13.97	1100	NA	NA	2.73E+01	NA	NA
								average:	1.69E+01	---	---
								stdev:	1.05E+01	---	---
HGM-5.-HGM-5.IO <sub>3</sub>	Iodate	1	14.5071	0.5678	13.97	1270	NA	NA	6.24E+02	NA	NA
		2	13.7092	0.5485	13.97	1410	NA	NA	5.57E+02	NA	NA
								average:	5.91E+02	---	---
								stdev:	3.36E+01	---	---
HGM-5.-HGM-5.Hg	Hg	1	13.71	0.5424	9.98	NA	1040	NA	NA	5.11E+02	NA
		2	14.33	0.5569	9.98	NA	988	NA	NA	4.82E+02	NA
								average:	---	4.96E+02	---
								stdev:	---	1.50E+01	---
HGM-5.-HGM-5.Hg-I	Hg -I	1	13.86	0.5490	9.98	4730	628	NA	4.69E+00	7.83E+02	NA
		2	13.51	0.5231	9.98	3960	627	NA	8.97E+00	6.65E+02	NA
								average:	6.83E+00	7.24E+02	---
								stdev:	2.14E+00	5.90E+01	---
CS-CS-ALL	ALL	1			0.00						
		2			0.00						
								average:	---	---	---
								stdev:	---	---	---

D.5

## **Appendix E**

### **EPA 1315 Leach Test Data**

# Appendix E

## EPA 1315 Leach Test Data

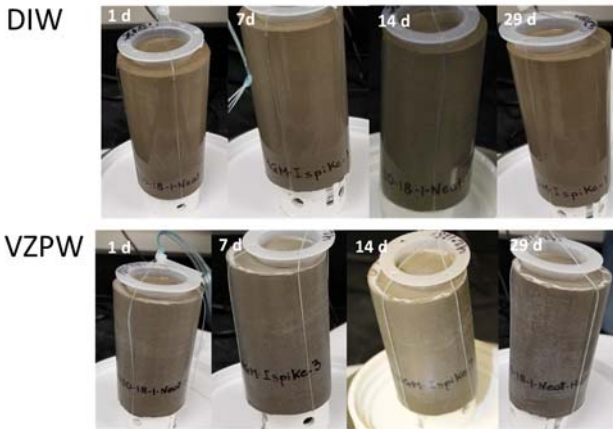


Figure E. 1 - Images showing the progress of Test Batch 1 (Neat HGM-5) during EPA Method 1315 Leach Testing



Figure E. 2 - Images showing the progress of Test Batch 2 (Neat Cast Stone) during EPA Method 1315 Leach Testing



Figure E. 3 - Images showing the progress of Test Batch 3 (GAC in HGM-5) during EPA Method 1315 Leach Testing



Figure E. 4 - Images showing the progress of Test Batch 4 (GAC in Cast Stone) during EPA Method 1315 Leach Testing

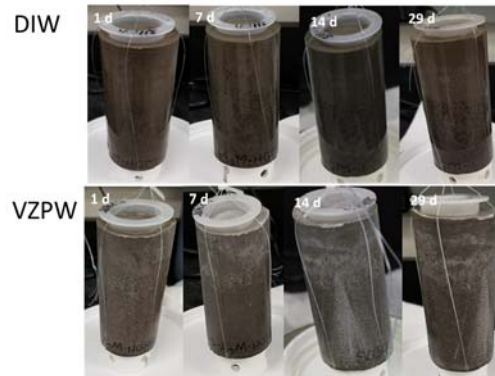


Figure E. 5 - Images showing the progress of Test Batch 5 (AgM in HGM-5) during EPA Method 1315 Leach Testing



Figure E. 6 - Images showing the progress of Test Batch 6 (AgM in Cast Stone) during EPA Method 1315 Leach Testing

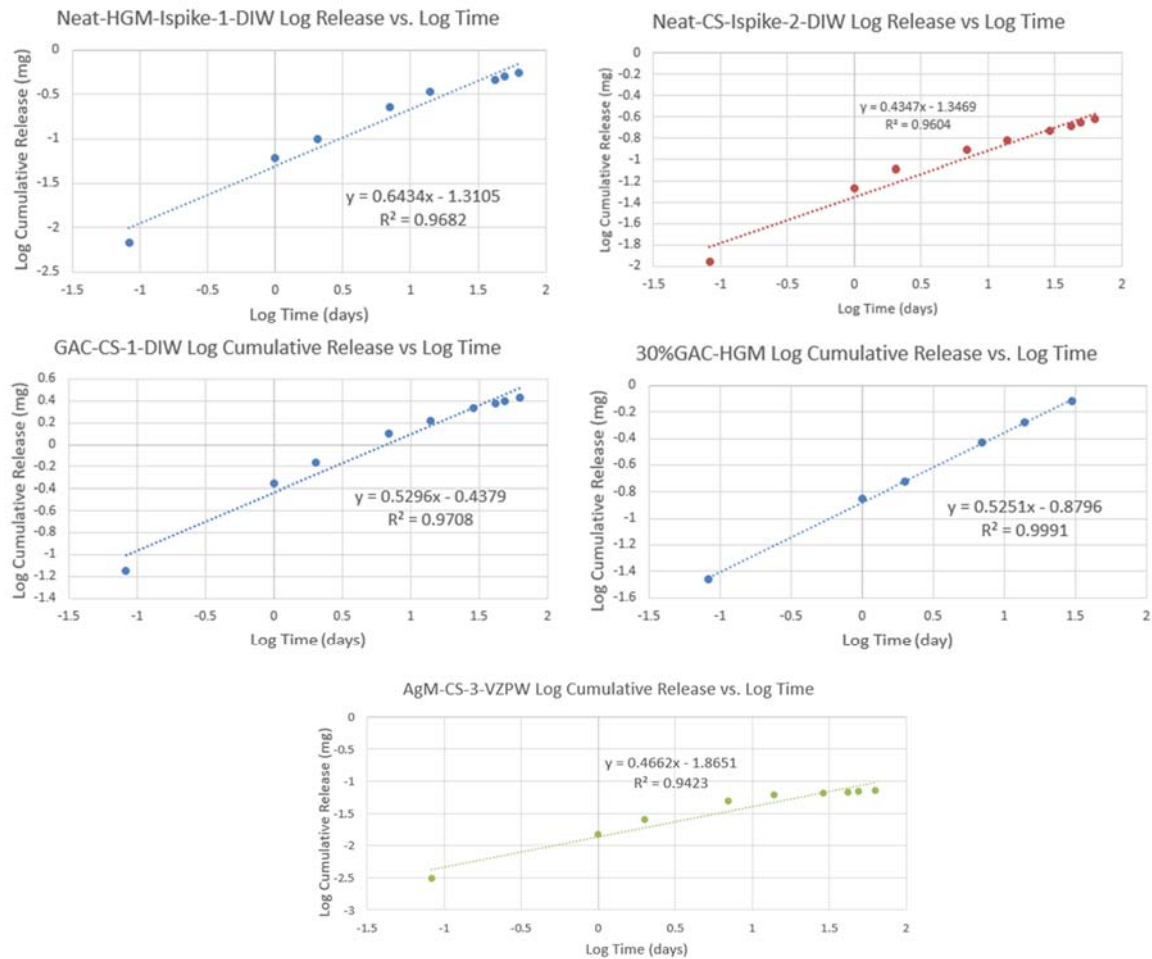


Figure E. 7 - Representative plots of Log cumulative release vs log time for the EPA Method 1315 tests. All plots gave a slope between  $0.5 \pm 50\%$ , confirming diffusive release from the waste form. The results for AgM in HGM-5 are not shown as no measurable analyte was present in the leachates.

Table E. 1 - Summary of slopes produced from log cumulative release vs log time plots from EPA Method 1315 tests. N/A are given for samples where no detectable I was present in the leachates.

Test Batch	Sample	Slope
1 - Neat HGM5	DIW1	0.64
	DIW2	0.52
	VZPW1	0.49
2-Neat - CS	DIW1	0.37
	DIW2	0.44
	VZPW1	0.28
3-GAC-HGM5	DIW1	0.34
	DIW2	0.36
	VZPW1	0.42
	VZPW2	0.45
4-GAC-CS	DIW1	0.53
	DIW2	0.5
	VZPW1	0.37
	VZPW2	0.37
5-AgM-HGM5	DIW1	N/A
	DIW2	N/A
	VZPW1	N/A
	VZPW2	N/A
6-AgM-CS	DIW1	N/A
	DIW2	N/A
	VZPW1	0.47
	VZPW2	0.43

Table E.2 Cumulative Fraction of I Leached for Samples in EPA Method 1315 Testing after 63 Days.

<b>Batch</b>	<b>Sample</b>	<b>Leachant</b>	<b>% Leached at 63 d</b>
1	1	DIW	3.5
	2	DIW	3.2
	3	VZPW	4.8
2	1	DIW	1.4
	2	DIW	1.4
	3	VZPW	1.8
3	1	DIW	12.7
	2	DIW	7.6
	3	VZPW	11.3
	4	VZPW	5.6
4	1	DIW	14.8
	2	DIW	12.2
	3	VZPW	18.9
	4	VZPW	2.1
5	1	DIW	0.2
	2	DIW	0.2
	3	VZPW	0.2
	4	VZPW	0.2
6	1	DIW	0.2
	2	DIW	0.2
	3	VZPW	0.6
	4	VZPW	0.5

Table E. 3 - Summary of slopes produced from log cumulative Na release vs log time plots from EPA Method 1315 tests. VZPW were not used due to Na being present in the background.

<b>Test Batch</b>	<b>Sample</b>	<b>Slope</b>
Neat-HGM	DIW 1	0.55
	DIW 2	0.52
AgM-HGM	DIW 1	0.69
	DIW 2	0.68
GAC-HGM	DIW 1	0.52
	DIW 2	0.47
Neat-CS	DIW 1	0.4
	DIW 2	0.43
AgM-CS	DIW 1	0.76
	DIW 2	0.79
GAC-CS	DIW 1	0.56
	DIW 2	0.53

Table E.4 EPA Method 1315 Leach Test Data for the HGM-5 Neat Batch

		Experiment Start		7/10/18 10:30											
Name	I (µg/L)	Interval Begin	Sampling Date	ti (min)	ti-1 (min)	Monolith mass (g)	Monolith Dry Mass (g)	Surface Area (cm <sup>2</sup> )	Solution Volume (mL)	Mti (mg/m <sup>2</sup> )	p (kg/m <sup>3</sup> )	Co (mg/kgmo)	Dobs (m <sup>2</sup> /s)	Dobs (cm <sup>2</sup> /s)	
Neat-HGM-Ispike-1-DIW-2h	4.00	7/10/18 10:30	07/10/2018 12:30:00	120	0	350.8	283.4464	185.949346	1673.53	3.60E-01	1.55E+03	5.62E+01	1.86E-15	1.86E-11	
Neat-HGM-Ispike-1-DIW-1d	32.1	07/10/2018 12:30:00	07/11/2018 10:30:00	1440	120	350.8	283.4464	185.949346	1673.50	2.89E+00	1.55E+03	5.62E+01	1.97E-14	1.97E-10	
Neat-HGM-Ispike-1-DIW-2d	23.3	07/11/2018 10:30:00	07/12/2018 11:30:00	2940	1440	350.8	283.4464	185.949346	1673.56	2.10E+00	1.55E+03	5.62E+01	2.86E-14	2.86E-10	
Neat-HGM-Ispike-1-DIW-7d	76.7	07/12/2018 11:30:00	07/17/2018 10:30:00	10080	2940	350.8	283.4464	185.949346	1673.53	6.90E+00	1.55E+03	5.62E+01	3.84E-14	3.84E-10	
Neat-HGM-Ispike-1-DIW-14d	63.6	07/17/2018 10:30:00	07/24/2018 10:47:00	20177	10080	350.8	283.4464	185.949346	1673.51	5.72E+00	1.55E+03	5.62E+01	3.25E-14	3.25E-10	
No Sample Collected	0	07/24/2018 10:47:00	8/8/18 10:30	41760	20177	350.8	283.4464	185.949346	N/A	N/A	N/A	N/A	N/A	N/A	
Neat-HGM-Ispike-1-DIW-42d	78.4	07/24/2018 10:47:00	08/21/2018 14:45:00	60735	20177	350.8	283.4464	185.949346	1673.54	7.06E+00	1.55E+03	5.62E+01	7.86E-15	7.86E-11	
Neat-HGM-Ispike-1-DIW-49d	20.8	08/21/2018 14:45:00	08/28/2018 14:25:00	70795	60735	350.8	283.4464	185.949346	1673.52	1.87E+00	1.55E+03	5.62E+01	1.56E-14	1.56E-10	
Neat-HGM-Ispike-1-DIW-63d	31.6	08/28/2018 14:25:00	09/11/2018 14:30:00	90960	70795	350.8	283.4464	185.949346	1673.51	2.84E+00	1.55E+03	5.62E+01	1.10E-14	1.10E-10	
		Experiment Start		7/10/2018 10:30:00 AM											
Name	I (µg/L)	Interval Begin	Sampling Date	ti (min)	ti-1 (min)	Monolith mass (g)	Monolith Dry Mass (g)	Surface Area (cm <sup>2</sup> )	Solution Volume (mL)	Mti (mg/m <sup>2</sup> )	p (kg/m <sup>3</sup> )	Co (mg/kgmo)	Dobs (m <sup>2</sup> /s)	Dobs (cm <sup>2</sup> /s)	
Neat-HGM-Ispike-2-DIW-2h	9.50	7/10/2018 10:30:00 AM	07/10/2018 12:30:00	120	0	335.79	271.31832	179.5042022	1615.49	8.55E-01	1.55E+03	5.62E+01	1.05E-14	1.05E-10	
Neat-HGM-Ispike-2-DIW-1d	30.7	07/10/2018 12:30:00	07/11/2018 10:30:00	1440	120	335.79	271.31832	179.5042022	1615.50	2.76E+00	1.55E+03	5.62E+01	1.80E-14	1.80E-10	
Neat-HGM-Ispike-2-DIW-2d	24.7	07/11/2018 10:30:00	07/12/2018 11:30:00	2940	1440	335.79	271.31832	179.5042022	1615.44	2.22E+00	1.55E+03	5.62E+01	3.21E-14	3.21E-10	
Neat-HGM-Ispike-2-DIW-7d	74.8	07/12/2018 11:30:00	07/17/2018 10:30:00	10080	2940	335.79	271.31832	179.5042022	1615.53	6.73E+00	1.55E+03	5.62E+01	3.65E-14	3.65E-10	
Neat-HGM-Ispike-2-DIW-14d	64.5	07/17/2018 10:30:00	07/24/2018 10:50:00	20180	10080	335.79	271.31832	179.5042022	1615.54	5.81E+00	1.55E+03	5.62E+01	3.34E-14	3.34E-10	
No Sample Collected	0	07/24/2018 10:50:00	8/8/2018 10:30:00 AM	41760	20180	335.79	271.31832	179.5042022	N/A	N/A	N/A	N/A	N/A	N/A	
Neat-HGM-Ispike-2-DIW-42d	46.5	8/8/2018 10:30:00 AM	08/21/2018 14:55:00	60745	41760	335.79	271.31832	179.5042022	1615.48	4.18E+00	1.55E+03	5.62E+01	1.70E-14	1.70E-10	
Neat-HGM-Ispike-2-DIW-49d	20.7	08/21/2018 14:55:00	08/28/2018 14:25:00	70795	60745	335.79	271.31832	179.5042022	1615.48	1.86E+00	1.55E+03	5.62E+01	1.55E-14	1.55E-10	
Neat-HGM-Ispike-2-DIW-63d	30.8	08/28/2018 14:25:00	09/11/2018 14:30:00	90960	70795	335.79	271.31832	179.5042022	1615.51	2.77E+00	1.55E+03	5.62E+01	1.05E-14	1.05E-10	
		Experiment Start		7/10/18 10:30											
Name	I (µg/L)	Interval Begin	Sampling Date	ti (min)	ti-1 (min)	Monolith mass (g)	Monolith Dry Mass (g)	Surface Area (cm <sup>2</sup> )	Solution Volume (mL)	Mti (mg/m <sup>2</sup> )	p (kg/m <sup>3</sup> )	Co (mg/kgmo)	Dobs (m <sup>2</sup> /s)	Dobs (cm <sup>2</sup> /s)	
Neat-HGM-Ispike-3-VZPW-2h	13.9	7/10/18 10:30	07/10/2018 12:30:00	120	0	337.17	272.43336	177.7632161	1599.91	1.25E+00	1.59E+03	5.62E+01	2.14E-14	2.14E-10	
Neat-HGM-Ispike-3-VZPW-1d	88.5	07/10/2018 12:30:00	07/11/2018 10:30:00	1440	120	337.17	272.43336	177.7632161	1599.90	7.97E+00	1.59E+03	5.62E+01	1.43E-13	1.43E-09	
Neat-HGM-Ispike-3-VZPW-2d	55.5	07/11/2018 10:30:00	07/12/2018 11:30:00	2940	1440	337.17	272.43336	177.7632161	1599.95	5.00E+00	1.59E+03	5.62E+01	1.55E-13	1.55E-09	
Neat-HGM-Ispike-3-VZPW-7d	94.5	07/12/2018 11:30:00	07/17/2018 10:30:00	10080	2940	337.17	272.43336	177.7632161	1599.90	8.51E+00	1.59E+03	5.62E+01	5.58E-14	5.58E-10	
Neat-HGM-Ispike-3-VZPW-14d	70.3	07/17/2018 10:30:00	07/24/2018 10:53:00	20183	10080	337.17	272.43336	177.7632161	1599.91	6.33E+00	1.59E+03	5.62E+01	3.79E-14	3.79E-10	
Neat-HGM-Ispike-3-VZPW-28d	47.0	07/24/2018 10:53:00	08/08/2018 10:30:00	41760	20183	337.17	272.43336	177.7632161	1599.93	4.23E+00	1.59E+03	5.62E+01	7.58E-15	7.58E-11	
Neat-HGM-Ispike-3-VZPW-42d	43.3	08/08/2018 10:30:00	08/21/2018 14:45:00	60735	41760	337.17	272.43336	177.7632161	1599.92	3.90E+00	1.59E+03	5.62E+01	1.41E-14	1.41E-10	
Neat-HGM-Ispike-3-VZPW-49d	18.8	08/21/2018 14:45:00	08/28/2018 14:25:00	70795	60735	337.17	272.43336	177.7632161	1599.93	1.69E+00	1.59E+03	5.62E+01	1.22E-14	1.22E-10	
Neat-HGM-Ispike-3-VZPW-63d	29.1	08/28/2018 14:25:00	09/11/2018 14:30:00	90960	70795	337.17	272.43336	177.7632161	1599.91	2.62E+00	1.59E+03	5.62E+01	8.94E-15	8.94E-11	

Table E.5 EPA Method 1315 Leach Test Data for the Cast Stone Neat Batch

Experiment Start														
Name	l (µg/L)	Interval Begin	Sampling Date	ti (min)	ti-1 (min)	Monolith mass (g)	Monolith Dry Mass (g)	Surface Area (cm <sup>2</sup> )	Solution Volume (mL)	Mti (mg/m <sup>2</sup> )	ρ (kg/m <sup>3</sup> )	Co (mg/kgmono)	Dobs (m <sup>2</sup> /s)	Dobs (cm <sup>2</sup> /s)
Neat-CS-Ispike-1-DIW-2h	10.3	7/10/18 10:30	07/10/2018 12:30:00	120	0	331.3	217.0015	184.7573242	1662.81	0.93	1204.11	80.01	1.01E-14	1.01E-10
Neat-CS-Ispike-1-DIW-1d	28.3	07/10/2018 12:30:00	07/11/2018 10:30:00	1440	120	331.3	217.0015	184.7573242	1662.80	2.55	1204.11	80.01	1.26E-14	1.26E-10
Neat-CS-Ispike-1-DIW-2d	14.0	07/11/2018 10:30:00	07/12/2018 11:30:00	2940	1440	331.3	217.0015	184.7573242	1662.81	1.26	1204.11	80.01	8.45E-15	8.45E-11
Neat-CS-Ispike-1-DIW-7d	24.5	07/12/2018 11:30:00	07/17/2018 10:30:00	10080	2940	331.3	217.0015	184.7573242	1662.86	2.21	1204.11	80.01	3.22E-15	3.22E-11
Neat-CS-Ispike-1-DIW-14d	15.6	07/17/2018 10:30:00	07/24/2018 10:30:00	20160	10080	331.3	217.0015	184.7573242	1662.83	1.40	1204.11	80.01	1.61E-15	1.61E-11
Neat-CS-Ispike-1-DIW-28d	18.2	07/24/2018 10:30:00	08/08/2018 10:30:00	41760	20160	331.3	217.0015	184.7573242	1662.80	1.64	1204.11	80.01	9.73E-16	9.73E-12
Neat-CS-Ispike-1-DIW-42d	11.8	08/08/2018 10:30:00	08/21/2018 14:55:00	60745	41760	331.3	217.0015	184.7573242	1662.81	1.06	1204.11	80.01	8.97E-16	8.97E-12
Neat-CS-Ispike-1-DIW-49d	9.10	08/21/2018 14:55:00	08/29/2018 14:30:00	72240	60745	331.3	217.0015	184.7573242	1662.84	0.82	1204.11	80.01	1.90E-15	1.90E-11
Neat-CS-Ispike-1-DIW-63d	10.2	08/29/2018 14:30:00	09/11/2018 14:30:00	90960	72240	331.3	217.0015	184.7573242	1673.51	0.92	1204.11	80.01	1.12E-15	1.12E-11
Experiment Start														
7/10/2018 10:30:00 AM														
Name	l (µg/L)	Interval Begin	Sampling Date	ti (min)	ti-1 (min)	Monolith mass (g)	Monolith Dry Mass (g)	Surface Area (cm <sup>2</sup> )	Solution Volume (mL)	Mti (mg/m <sup>2</sup> )	ρ (kg/m <sup>3</sup> )	Co (mg/kgmono)	De (m <sup>2</sup> /s)	De (cm <sup>2</sup> /s)
Neat-CS-Ispike-2-DIW-2h	6.70	7/10/2018 10:30:00 AM	07/10/2018 12:30:00	120	0	327.63	214.59765	182.5262504	1642.70	0.60	1211.59	80.01	4.22E-15	4.22E-11
Neat-CS-Ispike-2-DIW-1d	26.6	07/10/2018 12:30:00	07/11/2018 10:30:00	1440	120	327.63	214.59765	182.5262504	1642.70	2.39	1211.59	80.01	1.10E-14	1.10E-10
Neat-CS-Ispike-2-DIW-2d	16.6	07/11/2018 10:30:00	07/12/2018 11:30:00	2940	1440	327.63	214.59765	182.5262504	1642.74	1.49	1211.59	80.01	1.17E-14	1.17E-10
Neat-CS-Ispike-2-DIW-7d	25.6	07/12/2018 11:30:00	07/17/2018 10:30:00	10080	2940	327.63	214.59765	182.5262504	1642.71	2.30	1211.59	80.01	3.47E-15	3.47E-11
Neat-CS-Ispike-2-DIW-14d	17.2	07/17/2018 10:30:00	07/24/2018 10:30:00	20160	10080	327.63	214.59765	182.5262504	1642.72	1.55	1211.59	80.01	1.93E-15	1.93E-11
Neat-CS-Ispike-2-DIW-28d	19.5	07/24/2018 10:30:00	08/08/2018 10:30:00	41760	20160	327.63	214.59765	182.5262504	1642.72	1.75	1211.59	80.01	1.10E-15	1.10E-11
Neat-CS-Ispike-2-DIW-42d	13.0	08/08/2018 10:30:00	08/21/2018 14:55:00	60745	41760	327.63	214.59765	182.5262504	1642.73	1.17	1211.59	80.01	1.08E-15	1.08E-11
Neat-CS-Ispike-2-DIW-49d	9.50	08/21/2018 14:55:00	08/28/2018 14:30:00	70800	60745	327.63	214.59765	182.5262504	1642.73	0.85	1211.59	80.01	2.65E-15	2.65E-11
Neat-CS-Ispike-2-DIW-63d	10.2	08/28/2018 14:30:00	09/11/2018 14:30:00	90960	70800	327.63	214.59765	182.5262504	1615.51	0.90	1211.59	80.01	9.00E-16	9.00E-12
Experiment Start														
7/10/18 10:30														
Name	l (µg/L)	Interval Begin	Sampling Date	ti (min)	ti-1 (min)	Monolith mass (g)	Monolith Dry Mass (g)	Surface Area (cm <sup>2</sup> )	Solution Volume (mL)	Mti (mg/m <sup>2</sup> )	ρ (kg/m <sup>3</sup> )	Co (mg/kgmono)	De (m <sup>2</sup> /s)	De (cm <sup>2</sup> /s)
Neat-CS-Ispike-3-VZPW-2h	25.0	7/10/18 10:30	07/10/2018 12:30:00	120	0	329.59	215.88145	185.15	1666.30	2.25	1191.93	80.01	6.07E-14	6.07E-10
Neat-CS-Ispike-3-VZPW-1d	47.3	07/10/2018 12:30:00	07/11/2018 10:30:00	1440	120	329.59	215.88145	185.15	1666.31	4.26	1191.93	80.01	3.58E-14	3.58E-10
Neat-CS-Ispike-3-VZPW-2d	28.2	07/11/2018 10:30:00	07/12/2018 11:30:00	2940	1440	329.59	215.88145	185.15	1666.38	2.54	1191.93	80.01	3.50E-14	3.50E-10
Neat-CS-Ispike-3-VZPW-7d	37.2	07/12/2018 11:30:00	07/17/2018 10:30:00	10080	2940	329.59	215.88145	185.15	1666.36	3.35	1191.93	80.01	7.57E-15	7.57E-11
Neat-CS-Ispike-3-VZPW-14d	17.2	07/17/2018 10:30:00	07/24/2018 10:30:00	20160	10080	329.59	215.88145	185.15	1666.34	1.55	1191.93	80.01	1.99E-15	1.99E-11
Neat-CS-Ispike-3-VZPW-28d	15.8	07/24/2018 10:30:00	08/08/2018 10:30:00	41760	20160	329.59	215.88145	185.15	1666.32	1.42	1191.93	80.01	7.48E-16	7.48E-12
Neat-CS-Ispike-3-VZPW-42d	7.10	08/08/2018 10:30:00	08/21/2018 14:50:00	60740	41760	329.59	215.88145	185.15	1666.28	0.64	1191.93	80.01	3.32E-16	3.32E-12
Neat-CS-Ispike-3-VZPW-49d	3.00	08/21/2018 14:50:00	08/28/2018 14:30:00	70800	60740	329.59	215.88145	185.15	1666.25	0.27	1191.93	80.01	2.72E-16	2.72E-12
Neat-CS-Ispike-3-VZPW-63d	3.40	08/28/2018 14:30:00	09/11/2018 14:30:00	90960	70800	329.59	215.88145	185.15	1599.91	0.29	1191.93	80.01	9.85E-17	9.85E-13

Table E.6 EPA Method 1315 Leach Test Data for the HGM-5 containing GAC

Experiment Start														
Name	l (µg/L)	Interval Begin	Sampling Date	ti (min)	ti-1 (min)	Monolith mass (g)	Monolith Dry Mass (g)	Surface Area (cm2)	Solution V	Mti (mg/n	p (kg/m3)	Co (mg/kgmon	Dobs (m2/s)	Dobs (cm2/s)
7/10/18 10:30														
GAC-HGM-1-DIW-2h	42.9	7/10/18 10:30	07/10/2018 12:30:00	120	0	345.22	278.94	191.40	1722.60	3.86	1476.95	70.98	1.48E-13	1.48E-09
GAC-HGM-1-DIW-1d	114	07/10/2018 12:30:00	07/11/2018 10:30:00	1440	120	345.22	278.94	191.40	1722.60	10.26	1476.95	70.98	1.72E-13	1.72E-09
GAC-HGM-1-DIW-2d	97.4	07/11/2018 10:30:00	07/12/2018 11:30:00	2940	1440	345.22	278.94	191.40	1722.66	8.77	1476.95	70.98	3.46E-13	3.46E-09
GAC-HGM-1-DIW-7d	268	07/12/2018 11:30:00	07/17/2018 10:30:00	10080	2940	345.22	278.94	191.40	1722.60	24.12	1476.95	70.98	3.25E-13	3.25E-09
GAC-HGM-1-DIW-14d	227	07/17/2018 10:30:00	07/24/2018 10:30:00	20160	10080	345.22	278.94	191.40	1722.62	20.43	1476.95	70.98	2.87E-13	2.87E-09
GAC-HGM-1-DIW-28d	328	07/24/2018 10:30:00	08/08/2018 10:30:00	41760	20160	345.22	278.94	191.40	1722.62	29.52	1476.95	70.98	2.67E-13	2.67E-09
GAC-HGM-1-DIW-42d	182	08/08/2018 10:30:00	08/21/2018 14:45:00	60735	41760	345.22	278.94	191.40	1722.61	16.38	1476.95	70.98	1.80E-13	1.80E-09
GAC-HGM-1-DIW-49d	75.3	08/21/2018 14:45:00	08/28/2018 14:30:00	70800	60735	345.22	278.94	191.40	1722.65	6.78	1476.95	70.98	1.42E-13	1.42E-09
GAC-HGM-1-DIW-63d	122	08/28/2018 14:30:00	09/11/2018 10:30:00	90720	70800	345.22	278.94	191.40	1722.62	10.98	1476.95	70.98	1.16E-13	1.16E-09
Experiment Start														
7/10/2018 10:30:00 AM														
Name	l (µg/L)	Interval Begin	Sampling Date	ti (min)	ti-1 (min)	Monolith mass (g)	Monolith Dry Mass (g)	Surface Area (cm2)	Solution V	Mti (mg/n	p (kg/m3)	Co (mg/kgmon	De (m2/s)	De (cm2/s)
7/10/2018 10:30:00 AM														
GAC-HGM-2-DIW-2h	32.6	7/10/2018 10:30:00 AM	07/10/2018 12:30:00	120	0	355.33	287.11	194.62	1751.60	2.93	1487.65	70.98	8.42E-14	8.42E-10
GAC-HGM-2-DIW-1d	101	07/10/2018 12:30:00	07/11/2018 10:30:00	1440	120	355.33	287.11	194.62	1751.60	9.09	1487.65	70.98	1.33E-13	1.33E-09
GAC-HGM-2-DIW-2d	50.7	07/11/2018 10:30:00	07/12/2018 11:30:00	2940	1440	355.33	287.11	194.62	1751.66	4.56	1487.65	70.98	9.23E-14	9.23E-10
GAC-HGM-2-DIW-7d	134	07/12/2018 11:30:00	07/17/2018 10:30:00	10080	2940	355.33	287.11	194.62	1751.60	12.06	1487.65	70.98	8.01E-14	8.01E-10
GAC-HGM-2-DIW-14d	136	07/17/2018 10:30:00	07/24/2018 10:30:00	20160	10080	355.33	287.11	194.62	1751.60	12.24	1487.65	70.98	1.02E-13	1.02E-09
GAC-HGM-2-DIW-28d	203	07/24/2018 10:30:00	08/08/2018 10:30:00	41760	20160	355.33	287.11	194.62	1751.61	18.27	1487.65	70.98	1.01E-13	1.01E-09
GAC-HGM-2-DIW-42d	113	08/08/2018 10:30:00	08/21/2018 14:45:00	60735	41760	355.33	287.11	194.62	1751.60	10.17	1487.65	70.98	6.85E-14	6.85E-10
GAC-HGM-2-DIW-49d	44.5	08/21/2018 14:45:00	08/28/2018 14:30:00	70800	60735	355.33	287.11	194.62	1751.59	4.01	1487.65	70.98	4.88E-14	4.88E-10
GAC-HGM-2-DIW-63d	75.0	08/28/2018 14:30:00	09/11/2018 10:30:00	90720	70800	355.33	287.11	194.62	1751.59	6.75	1487.65	70.98	4.34E-14	4.34E-10
Experiment Start														
7/10/18 10:30														
Name	l (µg/L)	Interval Begin	Sampling Date	ti (min)	ti-1 (min)	Monolith mass (g)	Monolith Dry Mass (g)	Surface Area (cm2)	Solution V	Mti (mg/n	p (kg/m3)	Co (mg/kgmon	De (m2/s)	De (cm2/s)
7/10/18 10:30														
GAC-HGM-3-VZPW-2h	45.4	7/10/18 10:30	07/10/2018 12:30:00	120	0	360.28	291.11	195.11	1756.00	4.09	1505.75	70.98	1.59E-13	1.59E-09
GAC-HGM-3-VZPW-1d	227	07/10/2018 12:30:00	07/11/2018 10:30:00	1440	120	360.28	291.11	195.11	1756.00	20.43	1505.75	70.98	6.56E-13	6.56E-09
GAC-HGM-3-VZPW-2d	128	07/11/2018 10:30:00	07/12/2018 11:30:00	2940	1440	360.28	291.11	195.11	1755.98	11.52	1505.75	70.98	5.74E-13	5.74E-09
GAC-HGM-3-VZPW-7d	241	07/12/2018 11:30:00	07/17/2018 10:30:00	10080	2940	360.28	291.11	195.11	1756.00	21.69	1505.75	70.98	2.53E-13	2.53E-09
GAC-HGM-3-VZPW-14d	185	07/17/2018 10:30:00	07/24/2018 10:30:00	20160	10080	360.28	291.11	195.11	1756.01	16.65	1505.75	70.98	1.84E-13	1.84E-09
GAC-HGM-3-VZPW-28d	221	07/24/2018 10:30:00	08/08/2018 10:30:00	41760	20160	360.28	291.11	195.11	1756.01	19.89	1505.75	70.98	1.17E-13	1.17E-09
GAC-HGM-3-VZPW-42d	131	08/08/2018 10:30:00	08/21/2018 14:45:00	60735	41760	360.28	291.11	195.11	1756.00	11.79	1505.75	70.98	8.99E-14	8.99E-10
GAC-HGM-3-VZPW-49d	54.3	08/21/2018 14:45:00	08/28/2018 14:30:00	70800	60735	360.28	291.11	195.11	1756.02	4.89	1505.75	70.98	7.10E-14	7.10E-10
GAC-HGM-3-VZPW-63d	98.6	08/28/2018 14:30:00	09/11/2018 10:30:00	90720	70800	360.28	291.11	195.11	1756.04	8.87	1505.75	70.98	7.32E-14	7.32E-10
Experiment Start														
7/10/18 10:30														
Name	l (µg/L)	Interval Begin	Sampling Date	ti (min)	ti-1 (min)	Monolith mass (g)	Monolith Dry Mass (g)	Surface Area (cm2)	Solution V	Mti (mg/n	p (kg/m3)	Co (mg/kgmon	De (m2/s)	De (cm2/s)
7/10/18 10:30														
GAC-HGM-4-VZPW-2h	27.4	7/10/18 10:30	07/10/2018 12:30:00	120	0	362.24	292.69	194.83	1753.51	2.47	1512.86	70.98	5.75E-14	5.75E-10
GAC-HGM-4-VZPW-1d	122	07/10/2018 12:30:00	07/11/2018 10:30:00	1440	120	362.24	292.69	194.83	1753.51	10.98	1512.86	70.98	1.88E-13	1.88E-09
GAC-HGM-4-VZPW-2d	59.7	07/11/2018 10:30:00	07/12/2018 11:30:00	2940	1440	362.24	292.69	194.83	1753.58	5.37	1512.86	70.98	1.24E-13	1.24E-09
GAC-HGM-4-VZPW-7d	113	07/12/2018 11:30:00	07/17/2018 10:30:00	10080	2940	362.24	292.69	194.83	1753.58	10.17	1512.86	70.98	5.51E-14	5.51E-10
GAC-HGM-4-VZPW-14d	90.2	07/17/2018 10:30:00	07/24/2018 10:30:00	20160	10080	362.24	292.69	194.83	1753.54	8.12	1512.86	70.98	4.33E-14	4.33E-10
GAC-HGM-4-VZPW-28d	112	07/24/2018 10:30:00	08/08/2018 10:30:00	41760	20160	362.24	292.69	194.83	1753.52	10.08	1512.86	70.98	2.97E-14	2.97E-10
GAC-HGM-4-VZPW-42d	66.7	08/08/2018 10:30:00	08/21/2018 14:45:00	60735	41760	362.24	292.69	194.83	1753.46	6.00	1512.86	70.98	2.31E-14	2.31E-10
GAC-HGM-4-VZPW-49d	27.4	08/21/2018 14:45:00	08/28/2018 14:30:00	70800	60735	362.24	292.69	194.83	1753.49	2.47	1512.86	70.98	1.79E-14	1.79E-10
GAC-HGM-4-VZPW-63d	48.2	08/28/2018 14:30:00	09/11/2018 10:30:00	90720	70800	362.24	292.69	194.83	1753.51	4.34	1512.86	70.98	1.73E-14	1.73E-10

Table E.7 EPA Method 1315 Leach Test Data for the Cast Stone containing GAC

Experiment Start 7/10/18 11:30														
Name	I (µg/L)	Interval Begin	Sampling Date	ti (min)	ti-1 (min)	Monolith mass (g)	Monolith Dry Mass (g)	Surface Area (cm <sup>2</sup> )	Solution Volume (mL)	Mti (mg/m <sup>2</sup> )	ρ (kg/m <sup>3</sup> )	Co (mg/kgmono)	Dobs (m <sup>2</sup> /s)	Dobs (cm <sup>2</sup> /s)
GAC-CS-1-DIW-2h	40.9	7/10/18 11:30	07/10/2018 13:30:00	120	0	318.45	257.3076	190.83	1717.4	3.68	1366.80	71.03	1.568E-13	1.568E-09
GAC-CS-1-DIW-1d	214	07/10/2018 13:30:00	07/11/2018 11:30:00	1440	120	318.45	257.3076	190.83	1717.37	19.26	1366.80	71.03	7.0696E-13	7.0696E-09
GAC-CS-1-DIW-2d	145	07/11/2018 11:30:00	07/12/2018 12:00:00	2910	1440	318.45	257.3076	190.83	1717.36	13.05	1366.80	71.03	9.2409E-13	9.2409E-09
GAC-CS-1-DIW-7d	332	07/12/2018 12:00:00	07/17/2018 11:30:00	10080	2910	318.45	257.3076	190.83	1717.34	29.88	1366.80	71.03	5.7447E-13	5.7447E-09
GAC-CS-1-DIW-14d	233	07/17/2018 11:30:00	07/24/2018 11:30:00	20160	10080	318.45	257.3076	190.83	1717.42	20.97	1366.80	71.03	3.531E-13	3.531E-09
GAC-CS-1-DIW-28d	288	07/24/2018 11:30:00	08/08/2018 11:30:00	41760	20160	318.45	257.3076	190.83	1717.42	25.92	1366.80	71.03	2.3987E-13	2.3987E-09
GAC-CS-1-DIW-42d	145	08/08/2018 11:30:00	08/21/2018 14:45:00	60675	41760	318.45	257.3076	190.83	1717.42	13.05	1366.80	71.03	1.3426E-13	1.3426E-09
GAC-CS-1-DIW-49d	64.9	08/21/2018 14:45:00	08/28/2018 14:30:00	70740	60675	318.45	257.3076	190.83	1717.4	5.84	1366.80	71.03	1.2274E-13	1.2274E-09
GAC-CS-1-DIW-63d	109	08/28/2018 14:30:00	09/11/2018 14:30:00	90900	70740	318.45	257.3076	190.83	1717.39	9.81	1366.80	71.03	1.0588E-13	1.0588E-09
Experiment Start 7/10/2018 11:30:00 AM														
Name	I (µg/L)	Interval Begin	Sampling Date	ti (min)	ti-1 (min)	Monolith mass (g)	Monolith Dry Mass (g)	Surface Area (cm <sup>2</sup> )	Solution Volume (mL)	Mti (mg/m <sup>2</sup> )	ρ (kg/m <sup>3</sup> )	Co (mg/kgmono)	Dobs (m <sup>2</sup> /s)	Dobs (cm <sup>2</sup> /s)
GAC-CS-2-DIW-2h	40.4	7/10/2018 11:30:00 AM	07/10/2018 13:30:00	120	0	323.51	261.39608	192.02	1728.2	3.64	1378.59	71.03	1.504E-13	1.504E-09
GAC-CS-2-DIW-1d	193	07/10/2018 13:30:00	07/11/2018 11:30:00	1440	120	323.51	261.39608	192.02	1728.25	17.37	1378.59	71.03	5.6534E-13	5.6534E-09
GAC-CS-2-DIW-2d	125	07/11/2018 11:30:00	07/12/2018 12:00:00	2910	1440	323.51	261.39608	192.02	1728.22	11.25	1378.59	71.03	6.7517E-13	6.7517E-09
GAC-CS-2-DIW-7d	260	07/12/2018 12:00:00	07/17/2018 11:30:00	10080	2910	323.51	261.39608	192.02	1728.26	23.40	1378.59	71.03	3.464E-13	3.464E-09
GAC-CS-2-DIW-14d	185	07/17/2018 11:30:00	07/24/2018 11:30:00	20160	10080	323.51	261.39608	192.02	1728.23	16.65	1378.59	71.03	2.1883E-13	2.1883E-09
GAC-CS-2-DIW-28d	242	07/24/2018 11:30:00	08/08/2018 11:30:00	41760	20160	323.51	261.39608	192.02	1728.23	21.78	1378.59	71.03	1.665E-13	1.665E-09
GAC-CS-2-DIW-42d	124	08/08/2018 11:30:00	08/21/2018 14:45:00	60675	41760	323.51	261.39608	192.02	1728.2	11.16	1378.59	71.03	9.6522E-14	9.6522E-10
GAC-CS-2-DIW-49d	53.9	08/21/2018 14:45:00	08/28/2018 14:30:00	70740	60675	323.51	261.39608	192.02	1728.2	4.85	1378.59	71.03	8.3225E-14	8.3225E-10
GAC-CS-2-DIW-63d	92.5	08/28/2018 14:30:00	09/11/2018 14:30:00	90900	70740	323.51	261.39608	192.02	1728.18	8.33	1378.59	71.03	7.4962E-14	7.4962E-10
Experiment Start 7/10/18 11:30														
Name	I (µg/L)	Interval Begin	Sampling Date	ti (min)	ti-1 (min)	Monolith mass (g)	Monolith Dry Mass (g)	Surface Area (cm <sup>2</sup> )	Solution Volume (mL)	Mti (mg/m <sup>2</sup> )	ρ (kg/m <sup>3</sup> )	Co (mg/kgmono)	Dobs (m <sup>2</sup> /s)	Dobs (cm <sup>2</sup> /s)
GAC-CS-3-VZPW-2h	173	7/10/18 11:30	07/10/2018 13:30:00	120	0	324.69	262.34952	192.45	1732.1	15.57	1377.31	71.03	2.7631E-12	2.7631E-08
GAC-CS-3-VZPW-1d	441	07/10/2018 13:30:00	07/11/2018 11:30:00	1440	120	324.69	262.34952	192.45	1732.16	39.69	1377.31	71.03	2.9573E-12	2.9573E-08
GAC-CS-3-VZPW-2d	230	07/11/2018 11:30:00	07/12/2018 12:00:00	2910	1440	324.69	262.34952	192.45	1732.13	20.70	1377.31	71.03	2.2902E-12	2.2902E-08
GAC-CS-3-VZPW-7d	408	07/12/2018 12:00:00	07/17/2018 11:30:00	10080	2910	324.69	262.34952	192.45	1732.12	36.72	1377.31	71.03	8.5459E-13	8.5459E-09
GAC-CS-3-VZPW-14d	251	07/17/2018 11:30:00	07/24/2018 11:30:00	20160	10080	324.69	262.34952	192.45	1732.1	22.59	1377.31	71.03	4.0358E-13	4.0358E-09
GAC-CS-3-VZPW-28d	261	07/24/2018 11:30:00	08/08/2018 11:30:00	41760	20160	324.69	262.34952	192.45	1732.09	23.49	1377.31	71.03	1.9402E-13	1.9402E-09
GAC-CS-3-VZPW-42d	127	08/08/2018 11:30:00	08/21/2018 14:45:00	60675	41760	324.69	262.34952	192.45	1732.12	11.43	1377.31	71.03	1.0144E-13	1.0144E-09
GAC-CS-3-VZPW-49d	50.7	08/21/2018 14:45:00	08/28/2018 14:30:00	70740	60675	324.69	262.34952	192.45	1732.14	4.56	1377.31	71.03	7.3779E-14	7.3779E-10
GAC-CS-3-VZPW-63d	91.9	08/28/2018 14:30:00	09/11/2018 14:30:00	90900	70740	324.69	262.34952	192.45	1732.12	8.27	1377.31	71.03	7.4135E-14	7.4135E-10
Experiment Start 7/10/18 11:30														
Name	I (µg/L)	Interval Begin	Sampling Date	ti (min)	ti-1 (min)	Monolith mass (g)	Monolith Dry Mass (g)	Surface Area (cm <sup>2</sup> )	Solution Volume (mL)	Mti (mg/m <sup>2</sup> )	ρ (kg/m <sup>3</sup> )	Co (mg/kgmono)	Dobs (m <sup>2</sup> /s)	Dobs (cm <sup>2</sup> /s)
GAC-CS-4-VZPW-2h	18.2	7/10/18 11:30	07/10/2018 13:30:00	120	0	333.07	269.12056	190.52	1714.6	1.64	1431.61	71.03	2.8301E-14	2.8301E-10
GAC-CS-4-VZPW-1d	41.3	07/10/2018 13:30:00	07/11/2018 11:30:00	1440	120	333.07	269.12056	190.52	1714.59	3.72	1431.61	71.03	2.4001E-14	2.4001E-10
GAC-CS-4-VZPW-2d	24.1	07/11/2018 11:30:00	07/12/2018 12:00:00	2910	1440	333.07	269.12056	190.52	1714.61	2.17	1431.61	71.03	2.327E-14	2.327E-10
GAC-CS-4-VZPW-7d	54.2	07/12/2018 12:00:00	07/17/2018 11:30:00	10080	2910	333.07	269.12056	190.52	1714.59	4.88	1431.61	71.03	1.3956E-14	1.3956E-10
GAC-CS-4-VZPW-14d	22.9	07/17/2018 11:30:00	07/24/2018 11:30:00	20160	10080	333.07	269.12056	190.52	1714.62	2.06	1431.61	71.03	3.1089E-15	3.1089E-11
GAC-CS-4-VZPW-28d	33.3	07/24/2018 11:30:00	08/08/2018 11:30:00	41760	20160	333.07	269.12056	190.52	1714.62	3.00	1431.61	71.03	2.923E-15	2.923E-11
GAC-CS-4-VZPW-42d	17.9	08/08/2018 11:30:00	08/21/2018 14:45:00	60675	41760	333.07	269.12056	190.52	1714.61	1.61	1431.61	71.03	1.8649E-15	1.8649E-11
GAC-CS-4-VZPW-49d	7.2	08/21/2018 14:45:00	08/28/2018 14:30:00	70740	60675	333.07	269.12056	190.52	1714.6	0.65	1431.61	71.03	1.3769E-15	1.3769E-11
GAC-CS-4-VZPW-63	11.2	08/28/2018 14:30:00	09/11/2018 14:30:00	90900	70740	333.07	269.12056	190.52	1714.59	1.01	1431.61	71.03	1.019E-15	1.019E-11

Table E.8 EPA Method 1315 Leach Test Data for the HGM-5 Containing AgM

Experiment Start 7/10/18 11:30														
Name	l (µg/L)	Interval Begin	Sampling Date	ti (min)	ti-1 (min)	Monolith mass	Monolith Dry Mass (g)	Surface Area (cm <sup>2</sup> )	Solution Volume (mL)	Mti (mg/m <sup>2</sup> )	ρ (kg/m <sup>3</sup> )	Co (mg/kgmon)	Dobs (m <sup>2</sup> /s)	Dobs (cm <sup>2</sup> /s)
AgM-HGM-1-DIW-2h	1.26	7/10/18 11:30	07/10/2018 13:30:00	120	0	352.03	214.7383	189.31	1703.81	0.11	1149.53	51.73	3.96761E-16	3.96761E-12
AgM-HGM-1-DIW-1d	1.26	07/10/2018 13:30:00	07/11/2018 11:30:00	1440	120	352.03	214.7383	189.31	1703.83	0.11	1149.53	51.73	6.53464E-17	6.53464E-13
AgM-HGM-1-DIW-2d	1.26	07/11/2018 11:30:00	07/12/2018 12:00:00	2910	1440	352.03	214.7383	189.31	1703.80	0.11	1149.53	51.73	1.86047E-16	1.86047E-12
AgM-HGM-1-DIW-7d	1.26	07/12/2018 12:00:00	07/17/2018 11:30:00	10080	2910	352.03	214.7383	189.31	1703.83	0.11	1149.53	51.73	2.20627E-17	2.20627E-13
AgM-HGM-1-DIW-14d	0.126	07/17/2018 11:30:00	07/24/2018 11:30:00	20160	10080	352.03	214.7383	189.31	1703.84	0.01	1149.53	51.73	2.75306E-19	2.75306E-15
AgM-HGM-1-DIW-28d	1.26	07/24/2018 11:30:00	08/08/2018 11:30:00	41760	20160	352.03	214.7383	189.31	1703.81	0.11	1149.53	51.73	1.22406E-17	1.22406E-13
AgM-HGM-1-DIW-42d	1.26	08/08/2018 11:30:00	08/21/2018 14:45:00	60675	41760	352.03	214.7383	189.31	1703.79	0.11	1149.53	51.73	2.70281E-17	2.70281E-13
AgM-HGM-1-DIW-49d	1.26	08/21/2018 14:45:00	08/28/2018 14:30:00	70740	60675	352.03	214.7383	189.31	1703.80	0.11	1149.53	51.73	1.23343E-16	1.23343E-12
AgM-HGM-1-DIW-63d	1.26	08/28/2018 14:30:00	09/11/2018 14:30:00	90900	70740	352.03	214.7383	189.31	1703.79	0.11	1149.53	51.73	3.77223E-17	3.77223E-13
Experiment Start 7/10/2018 11:30:00 AM														
Name	l (µg/L)	Interval Begin	Sampling Date	ti (min)	ti-1 (min)	Monolith mass	Monolith Dry Mass (g)	Surface Area (cm <sup>2</sup> )	Solution Volume (mL)	Mti (mg/m <sup>2</sup> )	ρ (kg/m <sup>3</sup> )	Co (mg/kgmon)	Dobs (m <sup>2</sup> /s)	Dobs (cm <sup>2</sup> /s)
AgM-HGM-2-DIW-2h	1.26	7/10/2018 11:30:00	07/10/2018 13:30:00	120	0	353.01	215.3361	189.87	1708.80	0.11	1148.99	51.73	3.97106E-16	3.97106E-12
AgM-HGM-2-DIW-1d	1.26	07/10/2018 13:30:00	07/11/2018 11:30:00	1440	120	353.01	215.3361	189.87	1708.83	0.11	1148.99	51.73	6.5404E-17	6.5404E-13
AgM-HGM-2-DIW-2d	1.26	07/11/2018 11:30:00	07/12/2018 12:00:00	2910	1440	353.01	215.3361	189.87	1708.82	0.11	1148.99	51.73	1.86216E-16	1.86216E-12
AgM-HGM-2-DIW-7d	1.26	07/12/2018 12:00:00	07/17/2018 11:30:00	10080	2910	353.01	215.3361	189.87	1708.83	0.11	1148.99	51.73	2.20822E-17	2.20822E-13
AgM-HGM-2-DIW-14d	0.126	07/17/2018 11:30:00	07/24/2018 11:30:00	20160	10080	353.01	215.3361	189.87	1708.81	0.01	1148.99	51.73	2.75539E-19	2.75539E-15
AgM-HGM-2-DIW-28d	1.26	07/24/2018 11:30:00	08/08/2018 11:30:00	41760	20160	353.01	215.3361	189.87	1708.81	0.11	1148.99	51.73	1.22514E-17	1.22514E-13
AgM-HGM-2-DIW-42d	1.26	08/08/2018 11:30:00	08/21/2018 14:45:00	60675	41760	353.01	215.3361	189.87	1708.83	0.11	1148.99	51.73	2.70532E-17	2.70532E-13
AgM-HGM-2-DIW-49d	1.26	08/21/2018 14:45:00	08/28/2018 14:30:00	70740	60675	353.01	215.3361	189.87	1708.83	0.11	1148.99	51.73	1.23456E-16	1.23456E-12
AgM-HGM-2-DIW-63d	1.26	08/28/2018 14:30:00	09/11/2018 10:30:00	90660	70740	353.01	215.3361	189.87	1708.79	0.11	1148.99	51.73	3.86166E-17	3.86166E-13
Experiment Start 7/10/18 11:30														
Name	l (µg/L)	Interval Begin	Sampling Date	ti (min)	ti-1 (min)	Monolith mass	Monolith Dry Mass (g)	Surface Area (cm <sup>2</sup> )	Solution Volume (mL)	Mti (mg/m <sup>2</sup> )	ρ (kg/m <sup>3</sup> )	Co (mg/kgmon)	Dobs (m <sup>2</sup> /s)	Dobs (cm <sup>2</sup> /s)
AgM-HGM-3-VZPW-2h	1.26	7/10/18 11:30	07/10/2018 13:30:00	120	0	361.06	220.2466	192.25	1730.31	0.11	1158.26	51.73	3.90816E-16	3.90816E-12
AgM-HGM-3-VZPW-1d	1.26	07/10/2018 13:30:00	07/11/2018 11:30:00	1440	120	361.06	220.2466	192.25	1730.35	0.11	1158.26	51.73	6.43687E-17	6.43687E-13
AgM-HGM-3-VZPW-2d	1.26	07/11/2018 11:30:00	07/12/2018 12:00:00	2910	1440	361.06	220.2466	192.25	1730.35	0.11	1158.26	51.73	1.8327E-16	1.8327E-12
AgM-HGM-3-VZPW-7d	1.26	07/12/2018 12:00:00	07/17/2018 11:30:00	10080	2910	361.06	220.2466	192.25	1730.35	0.11	1158.26	51.73	2.17326E-17	2.17326E-13
AgM-HGM-3-VZPW-14d	0.126	07/17/2018 11:30:00	07/24/2018 11:30:00	20160	10080	361.06	220.2466	192.25	1730.33	0.01	1158.26	51.73	2.71178E-19	2.71178E-15
AgM-HGM-3-VZPW-28d	1.26	07/24/2018 11:30:00	08/08/2018 11:30:00	41760	20160	361.06	220.2466	192.25	1730.33	0.11	1158.26	51.73	1.20575E-17	1.20575E-13
AgM-HGM-3-VZPW-42d	1.26	08/08/2018 11:30:00	08/21/2018 14:45:00	60675	41760	361.06	220.2466	192.25	1730.32	0.11	1158.26	51.73	2.6624E-17	2.6624E-13
AgM-HGM-3-VZPW-49d	1.26	08/21/2018 14:45:00	08/28/2018 14:30:00	70740	60675	361.06	220.2466	192.25	1730.30	0.11	1158.26	51.73	1.21495E-16	1.21495E-12
AgM-HGM-3-VZPW-63d	1.26	08/28/2018 14:30:00	09/11/2018 14:30:00	90900	70740	361.06	220.2466	192.25	1730.30	0.11	1158.26	51.73	3.71575E-17	3.71575E-13
Experiment Start 7/10/18 11:30														
Name	l (µg/L)	Interval Begin	Sampling Date	ti (min)	ti-1 (min)	Monolith mass	Monolith Dry Mass (g)	Surface Area (cm <sup>2</sup> )	Solution Volume (mL)	Mti (mg/m <sup>2</sup> )	ρ (kg/m <sup>3</sup> )	Co (mg/kgmon)	Dobs (m <sup>2</sup> /s)	Dobs (cm <sup>2</sup> /s)
AgM-HGM-4-VZPW-2h	1.26	7/10/18 11:30	07/10/2018 13:30:00	120	0	349.69	213.3109	185.42	1668.79	0.11	1180.05	51.73	3.76495E-16	3.76495E-12
AgM-HGM-4-VZPW-1d	1.26	07/10/2018 13:30:00	07/11/2018 11:30:00	1440	120	349.69	213.3109	185.42	1668.75	0.11	1180.05	51.73	6.20042E-17	6.20042E-13
AgM-HGM-4-VZPW-2d	1.26	07/11/2018 11:30:00	07/12/2018 12:00:00	2910	1440	349.69	213.3109	185.42	1668.76	0.11	1180.05	51.73	1.7654E-16	1.7654E-12
AgM-HGM-4-VZPW-7d	1.26	07/12/2018 12:00:00	07/17/2018 11:30:00	10080	2910	349.69	213.3109	185.42	1668.76	0.11	1180.05	51.73	2.09346E-17	2.09346E-13
AgM-HGM-4-VZPW-14d	0.126	07/17/2018 11:30:00	07/24/2018 11:30:00	20160	10080	349.69	213.3109	185.42	1668.80	0.01	1180.05	51.73	2.61238E-19	2.61238E-15
AgM-HGM-4-VZPW-28d	1.26	07/24/2018 11:30:00	08/08/2018 11:30:00	41760	20160	349.69	213.3109	185.42	1668.83	0.11	1180.05	51.73	1.1616E-17	1.1616E-13
AgM-HGM-4-VZPW-42d	1.26	08/08/2018 11:30:00	08/21/2018 14:45:00	60675	41760	349.69	213.3109	185.42	1668.81	0.11	1180.05	51.73	2.56487E-17	2.56487E-13
AgM-HGM-4-VZPW-49d	1.26	08/21/2018 14:45:00	08/28/2018 14:30:00	70740	60675	349.69	213.3109	185.42	1668.82	0.11	1180.05	51.73	1.17048E-16	1.17048E-12
AgM-HGM-4-VZPW-63d	1.26	08/28/2018 14:30:00	09/11/2018 10:30:00	90660	70740	349.69	213.3109	185.42	1668.88	0.11	1180.05	51.73	3.66166E-17	3.66166E-13

Table E.9 EPA Method 1315 Leach Test Data for the Cast Stone Containing AgM

Experiment Start														
Name	I (µg/L)	Interval Begin	Sampling Date	ti (min)	ti-1 (min)	Monolith mass (g)	Monolith Dry Mass (g)	Surface Area (cm <sup>2</sup> )	Solution Volume (mL)	Mti (mg/m <sup>2</sup> )	ρ (kg/m <sup>3</sup> )	Co (mg/kgmono)	Dobs (m <sup>2</sup> /s)	Dobs (cm <sup>2</sup> /s)
AgM-CS-1-DIW-2h	1.26	7/10/18 11:30	07/10/2018 13:30:00	120	0	323.72	243.76116	183.29	1649.61	0.11	1364.30	45.53	3.6355E-16	3.6355E-12
AgM-CS-1-DIW-1d	1.30	07/10/2018 13:30:00	07/11/2018 11:30:00	1440	120	323.72	243.76116	183.29	1649.67	0.12	1364.30	45.53	6.3741E-17	6.3741E-13
AgM-CS-1-DIW-2d	1.26	07/11/2018 11:30:00	07/12/2018 12:00:00	2910	1440	323.72	243.76116	183.29	1649.66	0.11	1364.30	45.53	1.7048E-16	1.7048E-12
AgM-CS-1-DIW-7d	1.26	07/12/2018 12:00:00	07/17/2018 11:30:00	10080	2910	323.72	243.76116	183.29	1649.64	0.11	1364.30	45.53	2.0216E-17	2.0216E-13
AgM-CS-1-DIW-14d	0.126	07/17/2018 11:30:00	07/24/2018 11:30:00	20160	10080	323.72	243.76116	183.29	1649.64	0.01	1364.30	45.53	2.5226E-19	2.5226E-15
AgM-CS-1-DIW-28d	1.26	07/24/2018 11:30:00	08/08/2018 11:30:00	41760	20160	323.72	243.76116	183.29	1649.61	0.11	1364.30	45.53	1.1216E-17	1.1216E-13
AgM-CS-1-DIW-42d	1.26	08/08/2018 11:30:00	08/21/2018 14:45:00	60675	41760	323.72	243.76116	183.29	1649.62	0.11	1364.30	45.53	2.4766E-17	2.4766E-13
AgM-CS-1-DIW-49d	1.26	08/21/2018 14:45:00	08/28/2018 14:30:00	70740	60675	323.72	243.76116	183.29	1649.64	0.11	1364.30	45.53	1.1302E-16	1.1302E-12
AgM-CS-1-DIW-63d	1.26	08/28/2018 14:30:00	09/11/2018 14:30:00	90900	70740	323.72	243.76116	183.29	1649.62	0.11	1364.30	45.53	3.4566E-17	3.4566E-13
Experiment Start														
Name	I (µg/L)	Interval Begin	Sampling Date	ti (min)	ti-1 (min)	Monolith mass (g)	Monolith Dry Mass (g)	Surface Area (cm <sup>2</sup> )	Solution Volume (mL)	Mti (mg/m <sup>2</sup> )	ρ (kg/m <sup>3</sup> )	Co (mg/kgmono)	Dobs (m <sup>2</sup> /s)	Dobs (cm <sup>2</sup> /s)
AgM-CS-2-DIW-2h	1.26	7/10/2018 11:30:00	07/10/2018 13:30:00	120	0	325.59	245.16927	184.27	1658.42	0.11	1362.53	45.53	3.6448E-16	3.6448E-12
AgM-CS-2-DIW-1d	1.60	07/10/2018 13:30:00	07/11/2018 11:30:00	1440	120	325.59	245.16927	184.27	1658.37	0.14	1362.53	45.53	9.6791E-17	9.6791E-13
AgM-CS-2-DIW-2d	1.26	07/11/2018 11:30:00	07/12/2018 12:00:00	2910	1440	325.59	245.16927	184.27	1658.34	0.11	1362.53	45.53	1.709E-16	1.709E-12
AgM-CS-2-DIW-7d	1.26	07/12/2018 12:00:00	07/17/2018 11:30:00	10080	2910	325.59	245.16927	184.27	1658.42	0.11	1362.53	45.53	2.0267E-17	2.0267E-13
AgM-CS-2-DIW-14d	0.126	07/17/2018 11:30:00	07/24/2018 11:30:00	20160	10080	325.59	245.16927	184.27	1658.42	0.01	1362.53	45.53	2.529E-19	2.529E-15
AgM-CS-2-DIW-28d	1.26	07/24/2018 11:30:00	08/08/2018 11:30:00	41760	20160	325.59	245.16927	184.27	1658.40	0.11	1362.53	45.53	1.1245E-17	1.1245E-13
AgM-CS-2-DIW-42d	1.26	08/08/2018 11:30:00	08/21/2018 14:45:00	60675	41760	325.59	245.16927	184.27	1658.40	0.11	1362.53	45.53	2.4829E-17	2.4829E-13
AgM-CS-2-DIW-49d	1.26	08/21/2018 14:45:00	08/28/2018 14:30:00	70740	60675	325.59	245.16927	184.27	1658.41	0.11	1362.53	45.53	1.1331E-16	1.1331E-12
AgM-CS-2-DIW-63d	1.26	08/28/2018 14:30:00	09/11/2018 10:30:00	90660	70740	325.59	245.16927	184.27	1658.40	0.11	1362.53	45.53	3.5444E-17	3.5444E-13
Experiment Start														
Name	I (µg/L)	Interval Begin	Sampling Date	ti (min)	ti-1 (min)	Monolith mass (g)	Monolith Dry Mass (g)	Surface Area (cm <sup>2</sup> )	Solution Volume (mL)	Mti (mg/m <sup>2</sup> )	ρ (kg/m <sup>3</sup> )	Co (mg/kgmono)	Dobs (m <sup>2</sup> /s)	Dobs (cm <sup>2</sup> /s)
AgM-CS-3-VZPW-2h	1.80	7/10/18 11:30	07/10/2018 13:30:00	120	0	332.25	250.18425	187.14	1684.20	0.16	1364.38	45.53	7.4179E-16	7.4179E-12
AgM-CS-3-VZPW-1d	6.90	07/10/2018 13:30:00	07/11/2018 11:30:00	1440	120	332.25	250.18425	187.14	1684.19	0.62	1364.38	45.53	1.7952E-15	1.7952E-11
AgM-CS-3-VZPW-2d	6.00	07/11/2018 11:30:00	07/12/2018 12:00:00	2910	1440	332.25	250.18425	187.14	1684.18	0.54	1364.38	45.53	3.8648E-15	3.8648E-11
AgM-CS-3-VZPW-7d	14.3	07/12/2018 12:00:00	07/17/2018 11:30:00	10080	2910	332.25	250.18425	187.14	1684.16	1.29	1364.38	45.53	2.6032E-15	2.6032E-11
AgM-CS-3-VZPW-14d	6.47	07/17/2018 11:30:00	07/24/2018 11:30:00	20160	10080	332.25	250.18425	187.14	1684.21	0.58	1364.38	45.53	6.65E-16	6.65E-12
AgM-CS-3-VZPW-28d	3.30	07/24/2018 11:30:00	08/08/2018 11:30:00	41760	20160	332.25	250.18425	187.14	1684.19	0.30	1364.38	45.53	7.6919E-17	7.6919E-13
AgM-CS-3-VZPW-42d	1.30	08/08/2018 11:30:00	08/21/2018 14:45:00	60675	41760	332.25	250.18425	187.14	1684.20	0.12	1364.38	45.53	2.6359E-17	2.6359E-13
AgM-CS-3-VZPW-49d	1.26	08/21/2018 14:45:00	08/28/2018 14:30:00	70740	60675	332.25	250.18425	187.14	1684.23	0.11	1364.38	45.53	1.13E-16	1.13E-12
AgM-CS-3-VZPW-63d	1.26	08/28/2018 14:30:00	09/11/2018 14:30:00	90900	70740	332.25	250.18425	187.14	1684.20	0.11	1364.38	45.53	3.4559E-17	3.4559E-13
Experiment Start														
Name	I (µg/L)	Interval Begin	Sampling Date	ti (min)	ti-1 (min)	Monolith mass (g)	Monolith Dry Mass (g)	Surface Area (cm <sup>2</sup> )	Solution Volume (mL)	Mti (mg/m <sup>2</sup> )	ρ (kg/m <sup>3</sup> )	Co (mg/kgmono)	Dobs (m <sup>2</sup> /s)	Dobs (cm <sup>2</sup> /s)
AgM-CS-4-VZPW-2h	1.70	7/10/18 11:30	07/10/2018 13:30:00	120	0	335.84	252.88752	190.04	1710.41	0.15	1347.30	45.53	6.7862E-16	6.7862E-12
AgM-CS-4-VZPW-1d	4.90	07/10/2018 13:30:00	07/11/2018 11:30:00	1440	120	335.84	252.88752	190.04	1710.40	0.44	1347.30	45.53	9.2854E-16	9.2854E-12
AgM-CS-4-VZPW-2d	5.10	07/11/2018 11:30:00	07/12/2018 12:00:00	2910	1440	335.84	252.88752	190.04	1710.44	0.46	1347.30	45.53	2.8641E-15	2.8641E-11
AgM-CS-4-VZPW-7d	9.40	07/12/2018 12:00:00	07/17/2018 11:30:00	10080	2910	335.84	252.88752	190.04	1710.51	0.85	1347.30	45.53	1.1539E-15	1.1539E-11
AgM-CS-4-VZPW-14d	4.43	07/17/2018 11:30:00	07/24/2018 11:30:00	20160	10080	335.84	252.88752	190.04	1710.41	0.40	1347.30	45.53	3.1975E-16	3.1975E-12
AgM-CS-4-VZPW-28d	2.20	07/24/2018 11:30:00	08/08/2018 11:30:00	41760	20160	335.84	252.88752	190.04	1710.42	0.20	1347.30	45.53	3.5064E-17	3.5064E-13
AgM-CS-4-VZPW-42d	1.26	08/08/2018 11:30:00	08/21/2018 14:45:00	60675	41760	335.84	252.88752	190.04	1710.43	0.11	1347.30	45.53	2.5397E-17	2.5397E-13
AgM-CS-4-VZPW-49d	1.26	08/21/2018 14:45:00	08/28/2018 14:30:00	70740	60675	335.84	252.88752	190.04	1710.41	0.11	1347.30	45.53	1.1589E-16	1.1589E-12
AgM-CS-4-VZPW-63d	1.26	08/28/2018 14:30:00	09/11/2018 14:30:00	90900	70740	335.84	252.88752	190.04	1710.50	0.11	1347.30	45.53	3.5449E-17	3.5449E-13

**Distribution List**

**Washington River Protection Solutions**

DJ Swanberg  
EE Brown  
JR Vitali  
RB Mabrouki  
RS Skeen  
KP Lee (Orano)  
DJ Reid  
RM Yanochko

**Office of River Protection**

DM Smith  
GL Pyles  
EN Diaz

**Savannah River National Laboratory**

DI Kaplan  
RL Nichols  
CA Langton  
RR Seitz  
R Wyras

**Pacific Northwest National Laboratory**

RM Asmussen  
SA Saslow  
AL Fujii Yamagata  
GL Smith  
JJ Neeway  
BR Johnson  
CR Lonergan  
BD Williams  
VV Gervasio  
JV Ryan  
JV Crum  
SN Kerisit  
BP Parruzot  
CB Bonham  
DM Wellman  
DK Peeler  
Project File  
Information Release

\*All distribution will be made electronically



**Pacific  
Northwest**  
NATIONAL LABORATORY

[www.pnnl.gov](http://www.pnnl.gov)

902 Battelle Boulevard  
P.O. Box 999  
Richland, WA 99352  
1-888-375-PNNL (7665)

---

U.S. DEPARTMENT OF  
**ENERGY**